ACCELERATED CREEP TESTING FOR HIGH TEMPERATURE DESIGN

Thesis submitted at the University of Leicester
in partial fulfilment of the requirements for
the degree of Doctor of Philosophy

by

Wayne Ronald Smith
Department of Engineering
University of Leicester

June 2021

Declaration

All sentences or passages quoted in this project dissertation from other people's work have been specifically acknowledged by clear cross referencing to author, work and page(s). I understand that failure to do this amounts to plagiarism and will be considered grounds for failure in this module and the degree examination as a whole.

Name: Wayne Ronald Smith

Signed:

Date: 30th June 2021

Abstract

Components in-service at temperature are most likely designed with a creep strain limit achieved in a time frame as end of life criteria. In applying a negligible limit of 0.2% creep strain at 200kh recent work within European Standards has found the traditional 'rule-of-thumb' that ferritic martensitic (F/M) materials do not creep below 375°C, and austenitic materials below 425°C may not be the case. Creep testing is normally carried out at temperatures well above the limits and there is simply no experimental evidence of creep behaviour at temperatures around the limits with little to justify the expensive and extensive long-term creep testing required. This work focuses on the models and techniques available to establish those limits for individual materials.

The recognised creep models available for extrapolation have been found to be limited in their usefulness simply not extrapolating to low enough temperatures or simple not representing the physical reality adequately being unstable at lower stresses. The models that can extrapolate to lower temperatures have been applied to German VDEh and NIMS data sets with results finding the limit is too broad with potential differences of 100°C between C-Mn and Grade 91 steels. The Wilshire model and equations have been reviewed and applied to the NIMS data for Grade 91. The Wilshire equations in their original form appear to provide conservative estimations of the no-creep temperature. An Evans-Wilshire modification is reviewed and found to more appropriate for the Grade 91 material with a no-creep temperature around 410°C at a design reference stress of 2/3 tensile strength at temperature. The use of an artificial neural network confirms the Evans-Wilshire model results for the NIMS data. This work also addresses the gap in experimental data around the limit and provides a methodology for defining the temperature limits. Temperature limits for P265GH, Grade 91 and 316L(N) are presented from both experimental and historical data sets. Finally a novel stress relaxation method has been developed and described to estimate long-term creep properties with limited specialist equipment and skills.

Acknowledgements

Firstly thanks to the staff at GE, Rugby and Westmoreland Mechanical Testing and Research (WMTR), Banbury for their help, assistance and generally putting up with me during a difficult time. I would also like to thank GE and WMTR for their support in the use of their equipment and facilities and members of the European Creep Collaborative Committee (ECCC) for their interest, help and financial support.

I would also like to thank the support staff at the University of Leicester, IMPaCT Centre for Doctoral Training for keeping us on the straight and narrow and the Engineering and Physical Sciences Research Council for their funding of the PhD.

The people without whom this project would not have started - Dr Chris Bullough of GE, Rugby for his enthusiasm and support for the project and wisdom and guidance as Industrial Supervisor and Professor Simon Gill for his unwavering support throughout.

Contents

List of Figures

List of Tables

Nomenclature

$\dot{\varepsilon}$	strain rate
$\dot{\varepsilon}_{min}$	minimum creep rate
$\dot{\varepsilon}_{ss}$	steady state creep rate
σ	stress
$\sigma_{0.2}, \sigma_{0.2\%}$	0.2 percent proof stress at temperature
σ_{TS}	tensile strength at temperature
σ_Y	yield strength at temperature
ε	strain
ε_0	strain on loading
ε_a	anelastic strain
ε_e	elastic strain
$\varepsilon_f, \varepsilon_r, \varepsilon_u$	strain at failure, rupture or ultimate
ε_i	instantaneous plastic strain
ε_{pl}	plastic strain
ε_p	primary strain
ε_r	rupture strain
ε_{ter}	tertiary strain
ε_{tot}	total strain

D	Diffusion coefficient
E	Youngs, Elastic Modulus
G	Shear Modulus
k	Boltzmans constant
M	Monkman-Grant constant
n	stress exponent
Q	activation energy J/mol
Q_{Core}	activation energy for dislocation core or pipe diffusion
Q_{GB}	activation energy for grain boundary diffusion
Q_{SD}	activation energy for self diffusion
Qc	creep activation energy J/mol
R	gas constant 8.314 J.mol degK
Rm	ultimate tensile strength
Rm,T	ultimate tensile strength at temperature T
T	temperature
t	time
$t_{0.2}$	time to 0.2 percent strain (creep or total as specified)
t_f, t_r, t_u	time to failure, rupture or ultimate
T_{NC}	no-creep temperature
T_{NEC}	negligible-creep temperature
t_{NEC}	time to negligible creep (0.2 percent)
Tm	absolute temperature deg K
Zu	rupture elongation

A5	reduction of area at rupture
Au	reduction of area at rupture
CSEF	creep strength enhanced ferritic
ECCC	European Creep Collaboration Committee
GW	Graham-Walles
IPS	Intantaneous 'plastic' strain
LMP	Larson Miller parameter
MB	model bolt
MG	Monkman-Grant
MH4	Manson-Haferd 4 C335 1974 model
MHG	Manson-Haferd Grounes mod.
MHP	Manson-Haferd parameter
MMB	modified model bolt
RT	room temperature
SMCM	simplified minimum committment method
SRT	stress relaxation testing
TTP	time temperature parameter
UTS	ultimate tensile stress
WE	Wilshire Equations
WS	Wilshire-Scharning

List of associated publications

- Bullough C and Smith W and Holmström S. Provision of materials creep properties for design of high temperature plant to EN13445-3. In 1st EPERC International Conference Pressure Equipment Innovation and Safety, 1-3rd April 2019, Rome, pages 84–104, 2019.

- Smith W and Bullough C and Gill S. Determination of no-creep and negligible creep temperatures using accelerated testing methods. In 1st EPERC International Conference Pressure Vessel Safety, 1-3rd April 2019, Rome, pages 105–116, 2019.

- Holmström S., Bullough C., Tonti A., Baylac G., Forot C, Smith W. New Approaches to determine Negligible Creep of Steels for EN13445 CEN/TC 54 Technical Report 2019 Working Group 59 (CREEP)

- Baylac G., Bullough C., Holmström S., Smith W., Tonti A., and Forot C. (2021) New approaches to determine negligible creep, ECCC Conference ECCC-108-NEC, 2021

The effects of the Covid-19 Pandemic on the Project

This project had already suffered significant disruption before the pandemic. The sale of the laboratory by the industrial sponsor meant significant curtailing of creep testing and the lack of equipment for significant periods of time. Traditional stress relaxation testing could not be carried out. This disruption also led to a build up of confirmatory tests to be carried out at the end of the test program - final overall length measurements of the model bolt samples, hardness and microstructural evolution - though the microstructural work was viewed as low priority given the temperature/stress/duration regime under investigation. The pandemic meant these could not be carried out.

Chapter 1

Basic Concepts

1.1 Creep

A stress applied to a metallic material will result in a strain when the service conditions require a load applied over an extended time and elevated temperature creep must be considered. Creep is the irreversible time-dependent plastic deformation of materials and although creep can occur at all temperatures above absolute zero it is generally regarded as significant at temperatures above about 0.4Tm (Tm is the absolute melting temperature) which is when diffusion processes become significant within the lattice. In the case of steels, this is an elevated temperature.

Figure 1.1 shows a typical creep curve plot of strain accumulation with time with a constant load. Since the work of Andrade [5] creep curves have been described by three stages. Following an initial strain on loading to, ε_0, the creep rate decreases during the primary stage (Stage I) due to strain hardening, with contributions from changes in dislocation density and configuration, grain boundary sliding, elastic back stress, sub-grain formation until a minimum is reached at t1. This steady-state creep rate is maintained during the secondary stage (Stage II) from t1 to t2 where the strain hardening is balanced by thermal softening processes such as recovery, recrystallization, strain softening and precipitate overaging. The minimum creep rate is related to the balance caused by deterioration of microstructure but the terms are used interchangeably. During this stage, the dislocation density and arrangement remains essentially constant. At some stage cavities have nucleated and later in the secondary stage creep damage mechanisms become evident with cavity growth and coalescence and necking and the creep rate increases at the onset and accelerates through the tertiary stage (Stage

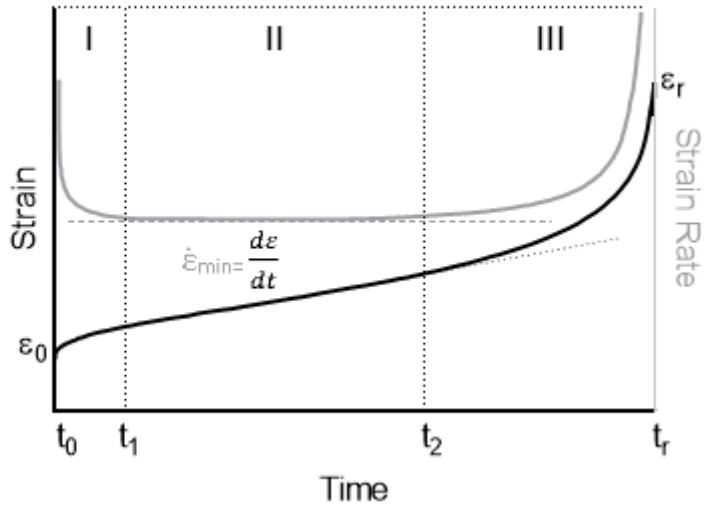

Figure 1.1: A typical steel creep curve at constant load and temperature (log time scale).

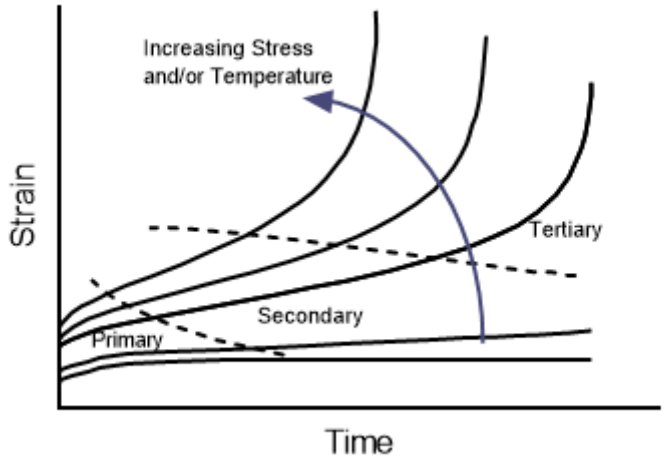

Figure 1.2: Influence of stress and temperature on creep curve shape [16].

III). Recrystallization, precipitate overaging, the coalescence of cracks and necking may be accompanied by grain boundary sliding with the creep rate accelerating until finally, failure occurs with rupture. The final stage is greatly affected by the reduction in cross-sectional area and the dashed line indicates the path when constant stress is maintained instead of a constant load. The shape of the curve and the ease with which the stages can be identified is highly dependent on temperature and stress and relatively small changes in chemical composition [6, 7, 8, 9, 10]

Figure 1.2 shows the typical dependency of a constant load creep plot on temperature and stress. Relatively small changes in stress and temperature can dramatically reduce a

material's performance and expected life. Creep deformation rarely leads to rupture at low stresses and below 0.4Tm. At intermediate temperature (100-450°C for steels [11]) and/or stress some primary creep occurs before strain hardening prevents further slip from taking place and creep strain is negligible. As diffusion increases strain hardening effects are reduced. Deviations from this classical representation occur because of prior deformation or complexities of strengthening mechanisms or phase changes which can appear as inverse primary creep, wavy curves or initial contraction [12, 13, 14, 15]. Many creep-resistant steels show no extended steady-state region and are characterised by a minimum creep rate [9]. Indeed, most of the data in the public domain are time to failure and minimum creep rate with limited time to specific strains [16]. Multiaxial stress will move a curve to the lower left compared to the uniaxial - lowering the rupture strain and time to rupture while torsion will move it to the upper right - increasing both [17]. Creep strain is only the strain subsequent to the initial loading, ε_0 in Figure 1.1 and there are many models available to describe the creep response over the stages; most are phenomenological and some with some physical basis. Under low-temperature conditions (< 0.3T/Tm) where diffusion is slow or strongly strain hardening materials creep is limited to the primary stage known as logarithmic creep (the lower plot in figure 1.2). When secondary creep dominates with a steady-state creep rate the Norton Law [18] provides the basis for the 'power-law' relationships widely used to describe high-temperature creep behaviour [7]. Table 1.1 shows the development of the power-law relation from combination with the Arrhenius type equation [19] with the activation energy, Q, required to cause the imperfection to move (J/mol). The value for Q for many ferritic steels has been reported to be approximately 380 kJ/mol [20]. Orr, Sherby and Dorn [21] introduced the concept that the activation energy for self-diffusion, Q_{SD} and creep, Qc were the same for a number of metals [22] and combined with the Norton Law, provides the power-law relationship with some physical basis. The shear modulus, G is now the generally used divisor justified by approximately identical microstructures at constant stress normalised by modulus [23]. According to Brown and Ashby [24], early versions of the Norton model included a $\sigma 0$ divisor but this was not clearly defined and often omitted or replaced by the Young's Modulus based on creep data by e.g. Sherby *et al.*. Grain boundaries and therefore grain size is important for some of the processes and catered for with d as the grain size and b its exponent. This has been further developed by Mukherjee *et al*. [25] to include lattice diffusion D and the Burger vector.

The values of n and Qc have been shown to be variable with respect to stress and temperature. On a practical level assuming they are quasi-constant to the controlling diffusion mechanism provides the basis to identify dominant creep mechanisms for changes in stress and temperature. Its simplicity makes it the most commonly used function [12]. Plots of log minimum strain rate vs log stress, vs inverse absolute temperature (1/T) and vs log grain size over a stress and temperature range provide the linear gradient stress exponent, n, activation energy, Qc and the grain size exponent respectively from the power-law relationship. The simplification assumes any 'kink' in the plot to a different gradient will identity a mechanism change though changes in n and Qc (stress and temperature-dependent) vary within regimes. Variation is attributed to an internal back stress arising from dislocation configurations, precipitate dispersion and solid-solution effects as such it is required to refer to material-specific values in literature and databases. Power-law breakdown occurs at high stress when the relationship is no longer linear [7].

There is no single constitutive equation to represent the creep deformation characteristics of all materials over their entire temperature range. Many creep constitutive models have been developed to represent the primary, secondary and tertiary stages (Table 1.1) and many of the models in use are derived from these [17].

Table 1.1: Classical representations of primary, secondary and tertiary creep stages [13].

Models	Equation	Ref.
Primary Creep		
Logarithmic	$\varepsilon = \varepsilon_{TOT} - \varepsilon_0 = a\log(1+bt)$	Phillips[26]
Andrade Creep	$\varepsilon = \varepsilon_o + \beta t^{1/3}$	Cottrell [27] [28]
	$\varepsilon = at^{1/3} + ct + dt^{4/3}$	Evans & Wilshire [29]
Power	$\varepsilon = at^b$	Graham and Walles[30]
Exponential	$\varepsilon = a\left(1-\exp^{-bt}\right)$	McVetty[31]
Hyperbolic Sine	$\varepsilon = a\sinh\left(bt^c\right)$	Conway & Mulkinin[32]
Secondary Creep		
Power	$\dot{\varepsilon}_{\min} = A\sigma^n$	Norton[18]
	$\dot{\varepsilon}_{\min} = A\sigma^n + D = D_0 \exp\left(-\frac{Q}{RT}\right)$	
	$\dot{\varepsilon}_{\min} = Aexp\left(-\frac{Q_C}{RT}\right)\left(\frac{\sigma}{G}\right)^n$	
	$\dot{\varepsilon}_{\min} = \frac{A\sigma^n}{d^b}\exp\left(\frac{-Q_c}{RT}\right)\left(\frac{\sigma}{G}\right)^n$	
	$\dot{\varepsilon}_{\min} = \frac{ADGp}{kT}\left(\frac{p}{d}\right)^b\left(\frac{\sigma}{G}\right)^n\exp\left(\frac{-Qc}{RT}\right)$	Mukherjee *et* al.[25]
Exponential	$\dot{\varepsilon}_{\min} = d\exp(e\sigma)$	
Hyperbolic Sine	$\dot{\varepsilon}_{\min} = dsinh(e\sigma)$	Nadai[33]
Tertiary		
Power	$\varepsilon_f = ft^g$	Graham and Walles[30]
Exponential	$\varepsilon_f = f(exp(-gt)-1)$	McHenry[34]
Damage Type	$\dot{\varepsilon}_f = a\sigma^n(1-\omega)^{-q}$where $\dot{\omega} = c\sigma^k(1-\omega)^{-r}$	Kachanov[35], Rabotov[36]
Omega	$\dot{\varepsilon}_f = \dot{\varepsilon}_0 exp(\Omega\varepsilon$	Prager[37]

Design engineers require models to describe the long-term creep behaviour of specified alloys rather than single casts in the primary and secondary deformation range. Remaining life assessment, in contrast, requires the best model to describe a single cast in the secondary

and tertiary regimes. In general specific models are better suited to representing a material creep strain in either the primary/secondary or secondary/tertiary though some can be appropriate for both [38]. A number of the constitutive models listed can be combined to represent the material behaviour over all three stages as simply additive.

$$\varepsilon_{total} = \varepsilon_{primary} + \varepsilon_{secondary} + \varepsilon_{tertiary} \tag{1.1}$$

Alternatively, a secondary model can be extended to the primary and tertiary stages with the introduction of variables to represent e.g. strain hardening, precipitate spacing and cavitation damage as the Dyson & McClean [39] model is an extension of the Nadai model in Table 1.1.

$$\dot{\varepsilon} = Asinh\left[\frac{B(1-H)}{(1-\varphi)(1-\omega)}\right] \tag{1.2}$$

With the components combined in product form rather than additively viewing creep deformation as a single mechanism allows for mechanism interaction [40]. More recently a handful of models have been developed to cover the full creep curve and these will be discussed later.

The instantaneous strain on loading, ε_0 relative to the total plastic strain can be significant, in particular for austenitic steels at low application temperatures in the creep range [17]. ε_0 consists of recoverable and non-recoverable components, ε_e elastic (recoverable on unloading-time independent), ε_{pl} plastic (non-recoverable time-independent) and ε_a anelastic (time dependent recoverable) such that

$$\varepsilon_0 = \varepsilon_{tot} = \varepsilon_e + \varepsilon_{pl} + \varepsilon_a \tag{1.3}$$

It is suggested these occur simultaneously and independently and there is a plastic creep limit stress below which all creep is anelastic whilst above partially anelastic and plastic until eventually creep recovery effects are negligible at higher stresses [41]. The influence of prior monotonic prestrain on creep deformation is not well understood and material-specific, for stainless steels it generally leads to an increase in creep resistance [42] and the opposite for low alloys. The IMechE guidelines [43] excludes data from correlations of ferritic steels with instantaneous plasticity > 0.2% that could influence the subsequent creep behaviour.

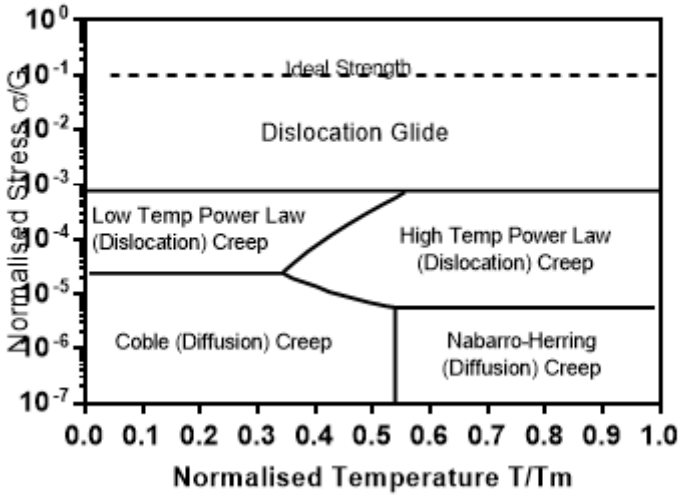

Figure 1.3: Basic deformation mechanism map [7].

1.2 Creep Deformation Mechanisms

A number of mechanisms contribute to the creep deformation at elevated temperatures. During the primary and secondary stages, these are limited to diffusional and dislocation mechanisms Nabarro-Hering Creep (Bulk Volume Diffusion) Coble (Grain Boundary Diffusion) Dislocation Creep controlled by bulk diffusion (high-temperature power-law creep) Dislocation Creep controlled by pipe diffusion along dislocations (low-temperature power-law creep) Dislocation creep mechanisms are often considered the only mechanisms of engineering significance for most applications. It is thought each of the mechanisms is independent and contributes additively to the total creep strain with the highest contributor dependent on the stress and temperature being the controlling mechanism. Above a temperature, dislocations can more easily cross-slip and climb. Ashby [44, 45], developed deformation mechanism maps that show the deformation characteristics over the stress/ temperature domain with the upper-stress limit set by the plastic flow behaviour (Figure 1.3). The boundaries indicate an equal contribution to the overall creep rate. Maps for different grain sizes can be produced and contours for specific creep rates superimposed. Within the creep region, the contribution of each may be determined from the theoretical equations of each process. The maps provide an adequate portrayal of steady-state deformation but in practical situations, the approximation is poor with small strains and primary or transient creep [46].

Table 1.2: Values of n, Qc and b associated with dislocation and diffusional processes (Adapted from [3,9]).

Creep process	Temperature	Stress	n value	Qc value	b value	Comments
High Temp Dislocation	> ∼0.7Tm	Intermediate /high	∼4-6	$\sim Q_{SD}$	0	Little grain size dependence and high stress dependence
Low Temp Dislocation	∼0.4Tm to ∼0.7Tm	Intermediate /high	∼4-6	$\sim Q_{Core}$	0	Little grain size dependence and high stress dependence
High Temp Diffusional (Nabarro-Herring)	>∼0.7Tm	Low	∼1	$\sim Q_{SD}$	2	Weak Stress and moderate grain size dependence
Low Temp Diffusional (Coble)	∼0.4Tm to ∼0.7Tm	Low	∼1	$\sim Q_{GB}$	3	Weak Stress and high grain boundary dependence

As mentioned above the values of n, Qc and b are experimentally measured and compared with the theoretical for different creep mechanisms to identify the dominant mechanism and mechanism changes. Table 1.2 illustrates the relationships between different mechanisms and the creep parameters.

Diffusion along grain boundaries and dislocations is somewhat easier than through the lattice and the activation energy (Qc =$0.5Q_{SD}$) for bulk diffusion is much higher allowing the separation of Nabarro-Herring and Coble creep mechanisms. A stress exponent, n > 7 is indicative of the power-law breakdown [13]. The low stress creep deformation mechanism remains unclear as morphological and compositional changes have a reduced effect on dislocation motion [47]. It is suggested that when $\sigma < \sigma_Y$ essentially the strain on loading is fully elastic, no new dislocations are generated and creep occurs as the result of pre-existing dislocation movement [48].

1.3 Predicting Creep Strain and Failure

For components in service, the material should never enter the tertiary stage where creep rate is unstable, accelerating and creep test data can be scattered. The end of life criteria is most likely to be a strain limit to avoid loss of clearance during service or a ductility limit [17]. Ductility exhaustion is failure when the accumulated strain equals the available ductility. Materials that can accommodate high levels of damage and an extended tertiary stage before failure are described as creep-ductile. Creep-brittle behaviour in contrast shows limited tertiary creep strain with damage quickly propagating to failure. Many potential industrial applications limit the allowable lifetime creep strain to a specific 0.2, 0.5 or 1% which makes the primary creep response of paramount importance making up a large portion of the first 1% creep strain [49] with primary/secondary models more useful at this stage. The selection of alloy steels for components in large power, industrial and petrochemical plants is generally based on 'allowable creep stress' calculated from the tensile stress causing creep rupture or failure at 100,000 or 200,000 hours at the service temperature. The 10^5-hour rupture strength is one of the basic properties used in the establishment of design stresses. Creep strength can also be defined as the stress required to produce a nominal strain 0.1, 0.2 or 0.5% in the same time period [12]. Creep or stress rupture tests are seldom carried out to the in-service timescales and extrapolation of shorter-term tests is required. The main issue, at this stage, is to determine the stress level at which a materials creep behaviour or lifetime should be estimated [50] once it is established creep strain is significant enough to consider. The consideration of nucleation, growth and linking of cavities, the loss of ductility and changes from trans-granular to inter-granular cracking and the damage mechanisms is largely unnecessary at the design stage if the primary objective is for the design life strain to remain significantly below the minimum creep rate. The extrapolation of data should always be carried out with caution when variation in creep strength and microstructural evolution need to be considered. Major drawbacks to extrapolation occur when the assumption that the physical mechanisms controlling behaviour in the extrapolated region are represented by the adopted model is incorrect [51]. The creep rupture strength of creep enhanced ferritic steels (CSEF) is often overestimated [52]; consequently, allowable stresses have been continually reduced once test durations have exceeded 30k hours [53, 54]. Creep rupture data extrapolation has been shown to give reliable results to a factor of x3 in time which was the limit of standard DIN-50118 [55] while good agreement has been achieved with extrapolation up to

x100 with the isostress method [56]. These methods will be described further later in this chapter. The theta model has been used with success for rupture extrapolations of x30 [57] and longer curves [58, 59]. The use of short term data over multiple mechanisms and at different stress levels, some dated and without known levels of initial plasticity may all contribute to the scatter and overestimation. The methods used to extrapolate data are divided into three groups, within these, they vary from entirely empirical to those which attempt to reflect some physical behaviour [12]

- Parametric methods
- Graphical methods - these methods do not appear widely adopted and not described further here.
- Algebraic or Theoretical methods

1.4 Parametric Methods

The method of extrapolation popularised by Larson & Miller [60] is based on the condensing or collapsing of a family of rupture curves at specific temperatures to one overall master curve; the function of time and temperature used to plot the master curve is known as the time-temperature parameter (TTP). This normalising of the time axis allows a master curve to be constructed by performing short term tests at high temperature (accelerated testing). While the Larson-Miller parameter is by far the best known and widely used it is unfortunately not the best and often the worst method tending to provide over-optimistic creep lives [12, 61]. Although the methods are generally explained with reference to creep-rupture time, which has received the most attention because of the drastic consequences, many were originally applied and are used to predict creep strain behaviour [12]. TTP is an analytical means of correlating and extrapolating creep and rupture data and by far the most widely used method for data extrapolation because of its ease of use and the convenience of a single curve to summarise data. The sheer level of literature on this subject demonstrates its importance. The method is based on the simplification of reaction rate theory as increased temperature leads to a reduced time of test or empirical parameters [12]. The conditions imposed on the experimental data by the methods are [62]

- linearity of isostress curves, and

- parallelism or convergence of families of curves

Figure 1.4 provides a summary of a few popular steady-state models for creep rate comparing these conditions where $\sigma 1 < \sigma 2 < \sigma 3$. Of particular note, Manson and Haferd [63] found better linearisation when plotted against temperature rather than the reciprocal. The Larson-Miller C parameter assumes extended isostress lines intersect the vertical axis at 1/T = 0 with a classical value of 20 claimed to be reasonably accurate for most materials but this is no longer accepted [12, 64], and it is often inconsistent for large extrapolations in temperature [65]. Table 1.3 shows others of note. Several functions have a similar functional form covered by Manson's generalised parameter in Table 1.3 as shown in Table 1.4.

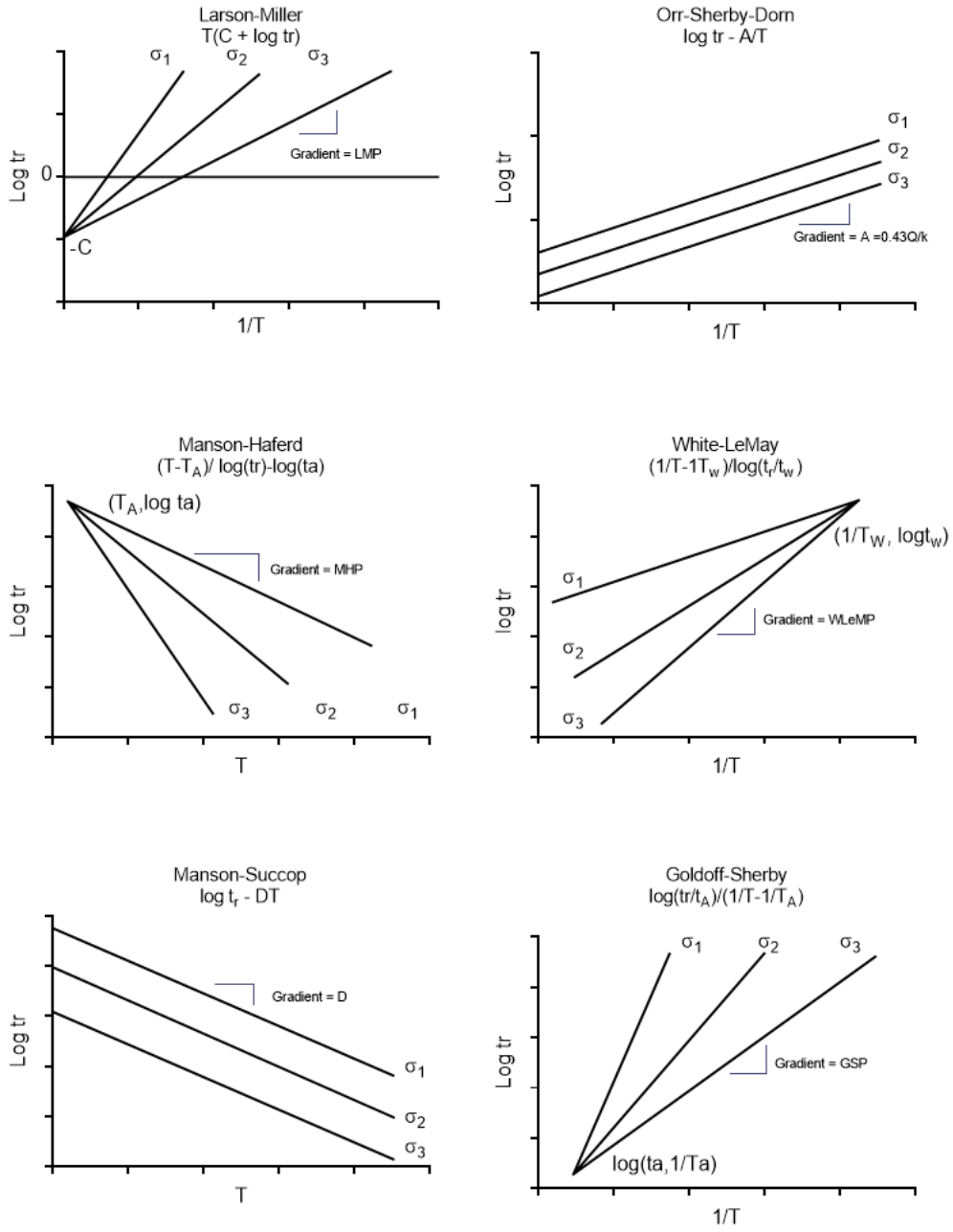

Figure 1.4: Comparison of assumed constant stress vs temperature relationships for the most common parametric models [56,20,59,47] (Adapted from [19]).

By optimising the intersection point, (T_a, t_a) and solving the isostatic lines for the coefficients c_0-c_3 (in Eq. 1.4 and Figure 1.5) from constant temperature and stress data a master curve can be plotted as Figure 1.6 .

$$\log(t_r) = (T - T_a) \cdot \left(c_0 + c_1 \log\sigma + c_2 \log^2\sigma + c_3 \log^3\sigma\right) + \log t_a \qquad (1.4)$$

Table 1.3: Other parameters of note (from [8]).

Name	Expression
Manson-Brown [63]	$\frac{\log t_r - \log t_a}{(T-T_a)^P}$
Graham-Walles [30]	$\sigma^a t_r^b (T-T_a)^c$
Manson [66]	$\frac{\sigma^v \log t_r - \log t_a}{(T-T_a)^w}$

Table 1.4: Variation from Manson's generalised form [8].

Larson-Miller	v=0	w=-1	Ta=0
Manson-Haferd	v=0	w=1	Ta≠0
Manson-Brown	v=0	w≠1	Ta≠0

The values of T_a and t_a(log) at the intersection of the extrapolated isostress lines require best fit to all the data. Manson and Haferd showed that T_a ranged from ∼-18-93°C for most materials and the value of t_a varied appreciably [63]. These values can have a significant effect on the extrapolation of short term data [67].

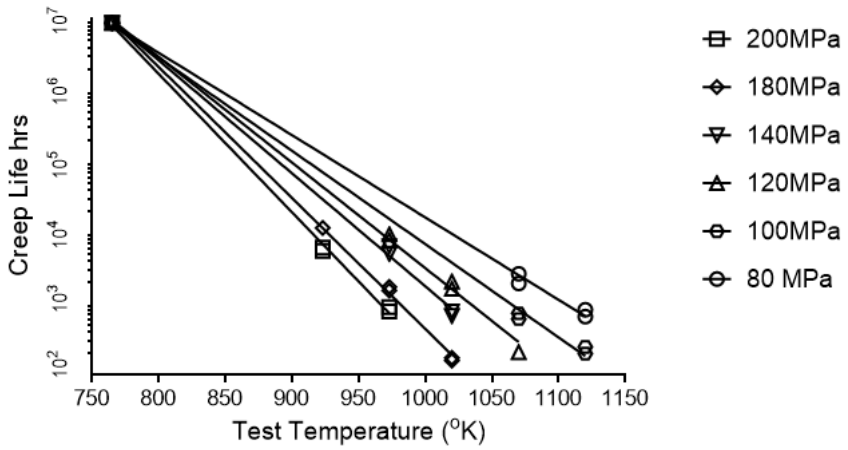

Figure 1.5: An example of an isostatic plot fitting a Manson-Haferd TTP (singular stress/ temperature data points omitted).

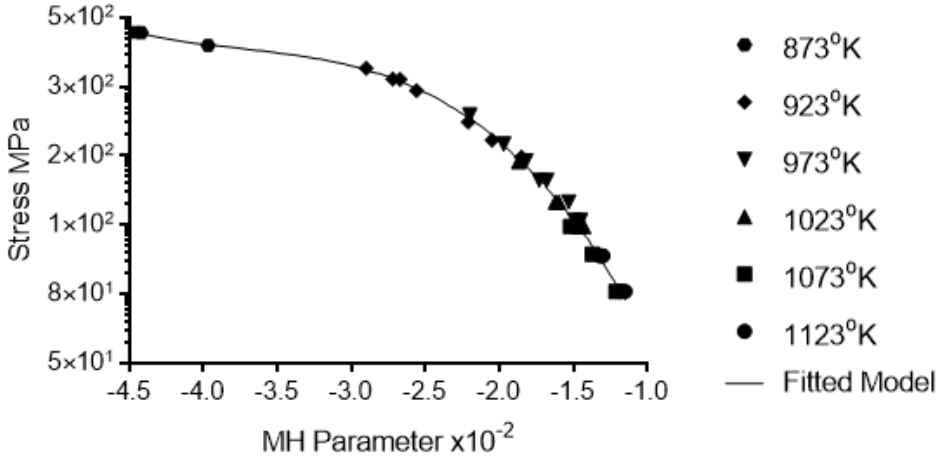

Figure 1.6: Creep life data and the Manson-Haferd master curve for the data in Figure 1.5.

1.5 Algebraic methods

There is little between these and TTP methods. The two of note described as algebraic are the Soviet model [68] and the minimum commitment method (MCM) [69] developed to address extrapolation errors induced by the averaging of constants in TTP methods [62] . Both are included in the standard EN13445 [70] but are less flexible than the TTP methods in application [71]. Figure 1.7 lists the model equations used in EN13445 for the extrapolation of creep rupture strengths this is accompanied by a list of the recommended model and model constants to be used for specific material grades.

Table R-1 — Creep-rupture model equations

MODEL	Code	*COMMENT*
Algebraic models:		
1) Soviet Model 1		
$\log(t_u^*) = \beta_0 + \beta_1.\log(T) + \beta_2.\log(\sigma) + \beta_3/T + \beta_4.\sigma/T$	SM1	
2) Soviet Model 2		
$\log(t_u^*) = \beta_0 + \beta_1.\log(T) + \beta_2.\log(\sigma)/T + \beta_3/T + \beta_4.\sigma/T$	SM2	
3) Minimum Commitment Model		
$\log(t_u^*) = \beta_0 + \beta_1.\log(\sigma) + \beta_2.\sigma + \beta_3.\sigma^2 + \beta_4.T + \beta_5/T$	MC	
TTP models:		
$f(\sigma) = \beta_0 + \beta_1.\log(\sigma) + \beta_2.\log(\sigma)^2 + \beta_3.\log(\sigma)^3 + \beta_4.\log(\sigma)^4$		
a) Mendelson-Roberts-Manson (MRM)		
$\log(t_u^*) = f(\sigma).(T - T_o)^r + \beta_5$		
b) MRM with r = -1		
$\log(t_u^*) = f(\sigma)/(T - T_o) + \beta_5$	MRn	n is order of $f(\sigma)$ polynomial
c) Larson-Miller (MRn with T_o = 0)		
$\log(t_u^*) = f(\sigma)/T + \beta_5$	LMn	n is order of $f(\sigma)$ polynomial
d) Manson-Haferd (MRM with r = 1)		
$\log(t_u^*) = f(\sigma).(T - T_o) + \beta_5$	MHn	n is order of $f(\sigma)$ polynomial
e) Manson-Haferd with T_o = 0		
$\log(t_u^*) = f(\sigma).T + \beta_5$	MH0n	n is order of $f(\sigma)$ polynomial
f) Orr-Sherby-Dorn		
$\log(t_u^*) = f(\sigma) + \beta_5$	OSDn	n is order of $f(\sigma)$ polynomial
t_u^* is time to rupture in h, T is temperature in K, and σ is stress in MPa		

Figure 1.7: EN13445 Annex R [67] Creep Rupture Model Equations.

Many of the models are asymptotic and don't extrapolate to lower temperatures. Models need to represent the physical reality of creep strain accumulation but e.g. the Manson-Haferd can turn back in time when extrapolated outside the data range [72].

1.6 Full Curve models

Much of the historical data does not include full creep curve information let alone instantaneous strain and is generally limited to time to rupture and minimum creep rate and possibly some times to specific strains. Figure 1.8 illustrates the problem of calculating the time to a specific strain, the need to expand on the use of minimum creep rate and the importance of creep curve shape characteristics. All three curves have identical minimum creep rate (mcr), failure strain and time to failure [7].

Table 1.5: Full Creep Curve Models.

Name	Equation	Ref.
Theta (4Θ)	$\varepsilon_c = \varepsilon_t - \varepsilon_o = \theta_1\left(1-e^{-\theta_2 t}\right)+\theta_3\left(e^{\theta_4 t}-1\right)$	[73]
modified Theta (6Θ)	$\varepsilon_c = \theta_1\left(1-e^{-\theta_2 t}\right)+\theta_3\left(e^{\theta_4 t}-1\right)+\theta_5\left(1-e^{-\theta_6 t}\right)$	[74]
Gray & Whittaker	$t(\varepsilon)\exp\left(\frac{-Qc*}{RT}\right) = M(\varepsilon)\left(1-\frac{\sigma}{\sigma_n}\right)^{p(\varepsilon)}$ $M(\varepsilon) = A1\exp\left(-\left(\frac{\varepsilon}{A2}\right)^{-A3}\right)$ $P(\varepsilon) = \frac{A4}{\varepsilon A5\sqrt{2\pi}}\exp\left(-\frac{[In(A6\cdot\varepsilon)]^2}{2A5^2}\right)+A7$	[14]
LCSP	$\log(t_\varepsilon) = \frac{\log(\alpha t_r)+\beta}{1+\left(\frac{\log\varepsilon}{x_0}\right)}\mathrm{P}-\beta$	[75]
Wilshire Equations	$\left(\frac{\sigma}{\sigma_{TS}}\right) = \exp\left\{-k_1\left[t_f\exp\left(\frac{-Q_c^*}{RT}\right)\right]^{u_1}\right\}$ $\left(\frac{\sigma}{\sigma_{TS}}\right) = \exp\left\{-k_3\left[t_\varepsilon\exp\left(\frac{-Q_c^*}{RT}\right)\right]^{u_3}\right\}$	[76]

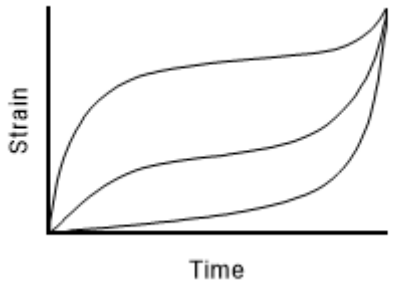

Figure 1.8: Creep curves with identical minimum creep rates, strain at failure and time to failure [3].

While the models above are the accepted methods for creep extrapolation based on their inclusion in the standard EN13445. There have been developments with a limited number of 'full curve' models. These are listed in Table 1.5.

It is suggested the theta model strain-like and rate parameters have linear stress and temperature dependencies that could be used to predict shape change with test conditions [59]. The approach has been used with some success to predict minimum creep rates and time to failure but is poor at predicting low strains (0.05-0.1%) [77] and can be poor fitting whole curves of low ductility materials [74]. Additional parameters have been utilized to represent the relatively short-term anelastic components (sliding relaxation across grain boundaries) [78, 79] and improve the model fit in the early primary stage. The theta models do require failure or extensive tertiary data for calibration. The Gray & Whittaker model [14] was de-

veloped from a database of 181 creep curves of 7 materials from tests from the early 1990s and based on a general shape with the time to a specific strain related to normalised stress by a power relationship. This model could be used with limited times to specific strain data. The LCSP model [75] in contrast uses only two material-specific parameters and the time to failure which is explicitly suggested could from a master curve prediction obtained by Wilshire equations. The Wilshire equations (WE) are a TTP as described above which combine the Monkman-Grant [80] relationship with the power-law model in Table 1.1 using stress normalised by a material strength parameter. The equations can be used to extrapolate either rupture or time to specific strains which makes them particularly appealing. They are reviewed in a later chapter.

1.7 Holmström *et al.*

As part of the European MATTER project, Holmström *et al.* [81, 82, 83, 84, 85] have extrapolated data by applying a rupture time factor (RTF) to a Wilshire model rupture master curve data to provide time to specific strain (0.2%). Utilising the limited time to specific strain data available an RTF of 1000 was calculated and applied to the rupture data for all materials. The results are shown in Figure 1.9 for ferritic/martensitic and Figure 1.10 for austenitic steels. These values indicate that some of these materials could be creeping below the classical 'no creep' temperature of 375°C. Specifically, the non-alloyed ferritic steels looked vulnerable and there is a clear need to further verify this with data available in the public domain and/or experimentally. The classic 'no creep' temperatures 375°C and 425°C appear too broad and there is a requirement for a methodology to derive the 'no creep' and negligible creep temperatures experimentally with accelerated testing. The specific strain form of the Wilshire model has been rearranged to give the negligible creep temperature in Eq. 1.5. A drawback of the approach is that extrapolation beyond the max x3 may be required to define them [84]. The motivation is the simplicity of providing a material-specific 'no creep' temperature (e.g. 0.2% strain at 200k hours) and a negligible creep curve to 0.2% for component lives below the 200k hours limit as in Figure 1.11. The diagram shows the no-creep temperature, T_{NC} as a red dashed line set at the present 'classical' limit of 375°C below which creep is below 0.2% at 200kh and creep design need not be considered. The negligible creep region above is then limited by 0.2% strain at temperature, T_{NEC} where the

significant creep region starts bounded by rupture. The example shown on the diagram is to define a design life - the maximum allowable time in negligible creep (t_{NEC}) at 475C is 3000 hours [85].

$$T_{NEC} = \frac{Q}{R \cdot \ln\left(t_{\varepsilon 0.2\%} \cdot \left[-\frac{1}{k_{e0.2\%}} \ln\left(\frac{\sigma}{R_m}\right)\right]^{-\frac{1}{u_{e0.2\%}}}\right)} \tag{1.5}$$

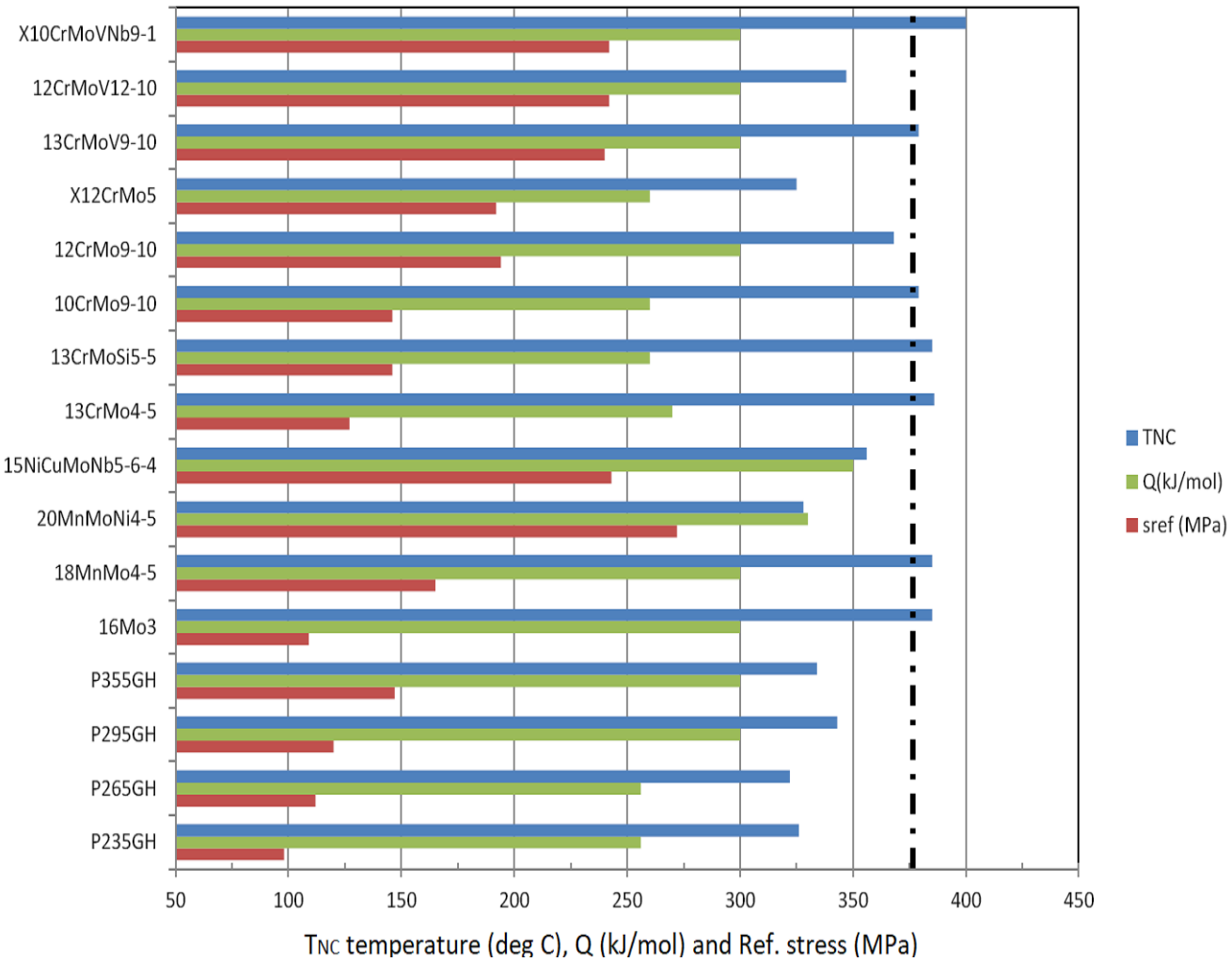

Figure 1.9: T_{NC},σref stress and chosen Q for the ferritic/martensitic steels from EN10028-2. The classical temperature limit of 375°C is given as a dash-dot line [82].

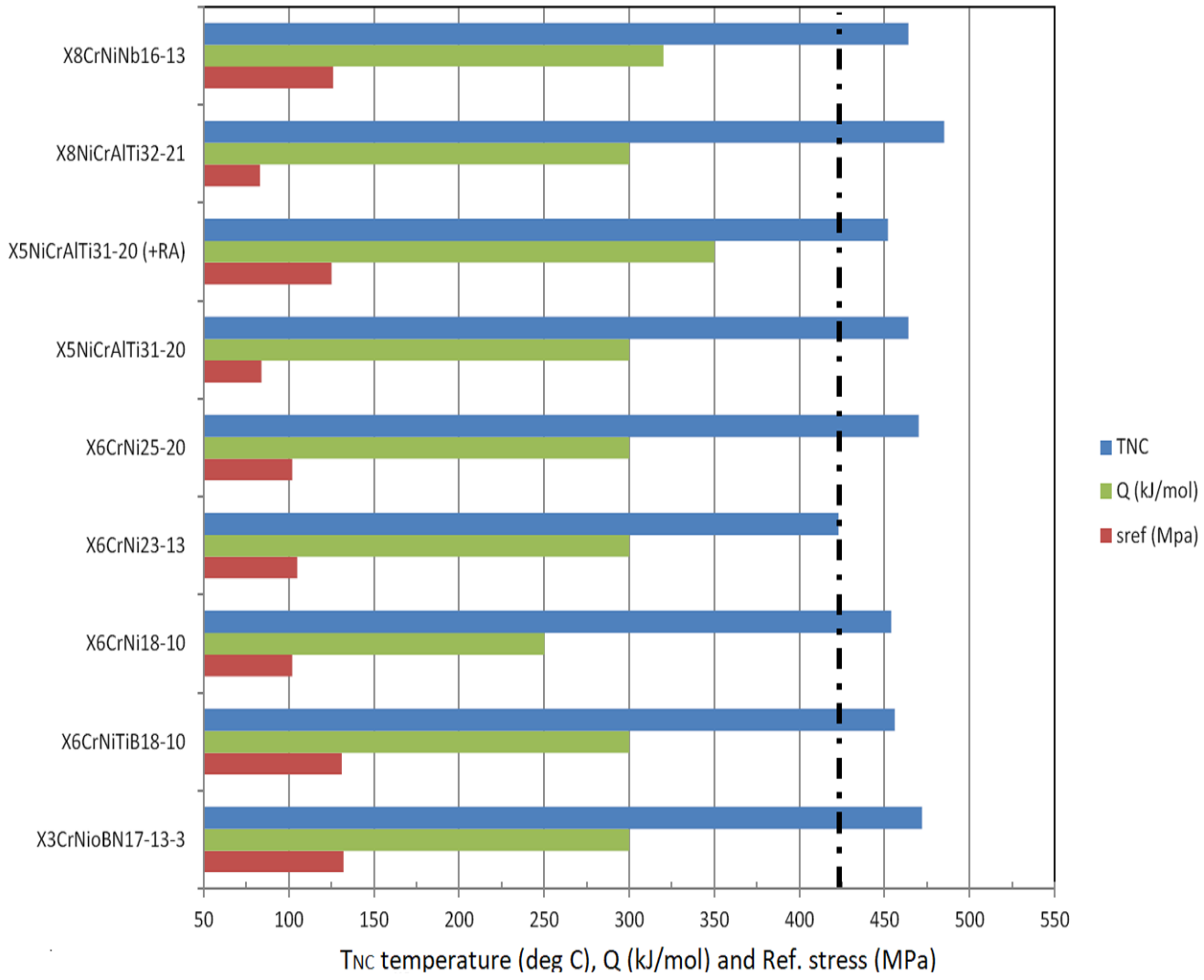

Figure 1.10: $T_{NC}, \sigma ref$ stress and chosen Q for the austenitic steels from EN 10028-7. the classical limit of 425°C is given as a dash-dot line [82].

1.8 Aims and Objectives

It has already been established that the blanket creep zone limits may not be adequate for the many material grades available, though with a relatively simplistic technique. Creep monitoring practitioners in the field will already know that some materials exceed these limits and others do not. Establishing the lifetime monitoring costs associated with design scenarios based on two temperature thresholds appears too simplistic. The range of the creep zone limit appears to be 330 - 400°C for the ferritic/martensitic grades in Figure 1.9 with many potentially creeping below the classical limits which are poorly substantiated by experimental evidence. These materials are either knowingly avoided from creep design,

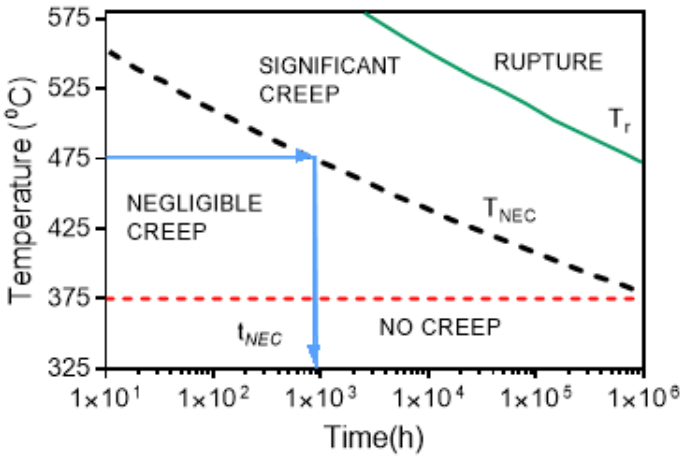

Figure 1.11: Example of an F/M steel negligible creep temperature curve T_{NEC} (black dashed line) defined from the rupture temperature curve T_r (green line). The T_{NC} (red dashed line) limits the T_{NEC} to a minimum value of 375°C at a material-specific time [82].

monitored or at risk in applications. Establishing the real limits for material grades would bring further order and justification for monitoring costs and reduce the risk of creep failure outside the creep range.

The research aim is to further establish the temperature at which creep can be ignored in the design process defined as 0.2% strain in 200k hours in terms of long-term creep data in the literature using analytical/empirical and numerical simulation techniques and experimentally from short-term uniaxial tests. The research objectives are divided into three parts:

- Review the methods and models available to derive the no-creep T_{NC} and negligible creep T_{NEC} temperatures from long-term data available in the literature.
- Review the Wilshire models and equations with a view to their application.
- Using accelerated short-term tests to be developed derive a methodology to experimentally determine the above limits for three materials based on the preliminary findings from data in the literature.

Particular emphasis is placed on practical techniques and recommendations for defining the limits.

1.8.1 The Structure of the Thesis

The thesis consists of seven chapters. Chapter 1 has presented the basic context of the research including the aim and objectives to be accomplished. Chapter 2 describes the extrapolation of the German VDEh creep data set to the temperatures considered the traditional limits using the models available. Chapter 3 reviews and assesses the Wilshire model and equations in view of the proposal to use them to extrapolate existing data and provide temperature limits. Throughout variations and alternatives are considered and compared in terms of providing the limits for design for the NIMS Grade 91 data. Chapter 4 describes the use of an artificial neural network in predicting the limits for the NIMS Grade 91 data for comparison. The next section is the experimental work. Chapter 5 presents the results of 31 short-term creep tests and the methodology to establish the temperature limits for three materials: P265GH, Grade 91 and 316L(N). The methods in the previous Chapters are also considered in view of the results. Chapter 6 focuses on a novel method developed for stress relaxation. Throughout the emphasis is on the practical limitations and recommendations for applying the various techniques in providing the limits. Chapter 7 concludes the general research findings from the work along with recommendations on further work which could further validate the approaches.

Chapter 2

Creep Data Extrapolation to No-Creep Temperatures

2.1 Introduction

Given the costs associated with creep monitoring and/or design avoidance there has been relatively little work in this general area - the area where creep has to be considered. The MATTER Project outcomes in Chapter 1 offered an assessment of the estimated European material creep performances in relation to the 'blanket' design limit. The attention is drawn from potential creep failures outside the creep range and cost savings for design and creep monitoring if individual material limits could be established for some of the higher alloyed and creep-resistant materials suspected to be much higher than the present limit. Lower limits on other materials could avoid potential creep or strain compatibility issues.

From the NIMS [3] data for Grade 91, Holmström developed a simple approach to assess the no-creep temperature of material for the MATTER Project [85] acknowledged as a general approximation. Fitting the Wilshire model to the rupture and specific strain data the relationship was characterised with a factor a time corrected rupture model such that t_f= RTF·t_ε and, for the time to nominal strains of 0.1%, 0.2% and 1% a rupture time factor, RTF of 10,000, 1000, 10 respectively were found to be optimal for Grade 91 [81]. Holmström then used only the data in the European standards to assess the materials no creep temperature. The values are derived from fitting the Wilshire model to the material-specific isochronous creep rupture strength data at 10kh,100kh and 200kh in the EN10028-2 standard applying the RTF with a reference stress of the minimum 0.2% proof strength at calculated temper-

Table 4 — Minimum values for the 0,2 % proof strength at elevated temperatures [a]

Steel grade		Nominal thickness [b] t	Minimum 0,2 % proof strength $R_{p0,2}$ MPa at a temperature in °C of									
Steel name	Steel number	mm	50	100	150	200	250	300	350	400	450	500
P235GH	1.0345	≤ 16	227	214	198	182	167	153	142	133	–	–
		$16 < t \leq 40$	218	205	190	174	160	147	136	128	–	–
		$40 < t \leq 60$	208	196	181	167	153	140	130	122	–	–
		$60 < t \leq 100$	193	182	169	155	142	130	121	114	–	–
		$100 < t \leq 150$	179	168	156	143	131	121	112	105	–	–
		$150 < t \leq 250$	164	155	143	132	121	111	103	97	–	–
P265GH	1.0425	≤ 16	256	241	223	205	188	173	160	150	–	–
		$16 < t \leq 40$	247	232	215	197	181	166	154	145	–	–
		$40 < t \leq 60$	237	223	206	190	174	160	148	139	–	–
		$60 < t \leq 100$	208	196	181	167	153	140	130	122	–	–
		$100 < t \leq 150$	193	182	169	155	142	130	121	114	–	–
		$150 < t \leq 250$	179	168	156	143	131	121	112	105	–	–

Figure 2.1: EN13445-3[67] Example of the Rp0.2,375°C for sample size <16mm for P265GH = 155 MPa.

ature from the standards divided by 1.5. Without specific time to strain data the rupture data fitting parameters are used to derive a 0.2% strain curve at 1/1000 of the rupture time. They are then compared to the blanket classical limit of 375°C for ferritic/martensitic steels acknowledging more work was required for specific material RTF values. Without tensile strength data, the normalisation used a scaling parameter to mimic the tensile strength such that σ/A.Rp $\approx \sigma_{TS}$ or Rm (using the Euro code notation) where Rp is the 0.2% proof stress for ferritic/martensitic materials but 1.0% for austenitic due to the different methods of calculating the maximum allowable design stress in Table 6.1 of EN13445-3 [70]. Figures 2.1 and 2.2 show how the reference stress is calculated from the standards for P265GH which equates to 155/1.5 = 103 MPa.

There are several collations of historical creep data available in the public domain. The detail of available creep test data varies and some contain data for times to specific strain but it is often sparse or incomplete with no time to 0.2% data or little tensile proof strength data at temperatures even approaching as low as 375°C. These are the NIMS data sheets [86], the German Steel Institute VDEh 'Blue Book' [87] compilation and the BSCC 1978 [88] compilation. Most of the creep research modelling work in the public domain uses the NIMS data. The harmonised European standards, however, are largely based on the German DIN standard material properties from the 1960s-1980s which are based on the VDEh data. The data also contains some 0.2% strain data in the 400-450°C range though

Table 6-1 — Maximum allowed values of the nominal design stress for pressure parts other than bolts

Steel designation	Normal operating load cases[a b]	Testing and exceptional load cases[b c]
Steels other than austenitic, as per 6.2 $A < 30\ \%$ [d]	$f_d = \min\left(\frac{R_{p0,2/T}}{1,5}; \frac{R_{m/20}}{2,4}\right)$	$f_{test} = \left(\frac{R_{p0,2/T_{test}}}{1,05}\right)$
Steels other than austenitic, as per 6.3: Alternative route $A < 30\ \%$ [d]	$f_d = \min\left(\frac{R_{p0,2/T}}{1,5}; \frac{R_{m/20}}{1,875}\right)$	$f_{test} = \left(\frac{R_{p0,2/T_{test}}}{1,05}\right)$
Austenitic steels as per 6.4 $30\ \% \le A < 35\ \%$ [d]	$f_d = \left(\frac{R_{p1,0/T}}{1,5}\right)$	$f_{test} = \left(\frac{R_{p1,0/T_{test}}}{1,05}\right)$
Austenitic steels as per 6.5 $A \ge 35\ \%$ [d]	$f_d = \max\left[\left(\frac{R_{p1,0/T}}{1,5}\right); \min\left(\frac{R_{p1,0/T}}{1,2}; \frac{R_{m/T}}{3}\right)\right]$	$f_{test} = \max\left[\left(\frac{R_{p1,0/T_{test}}}{1,05}\right); \left(\frac{R_{m/T\,test}}{2}\right)\right]$
Cast steels as per 6.6	$f_d = \min\left(\frac{R_{p0,2/T}}{1,9}; \frac{R_{m/20}}{3}\right)$	$f_{test} = \left(\frac{R_{p0,2/T_{test}}}{1,33}\right)$

a For testing group 4 the nominal design stress shall be multiplied by 0,9.
b Yield strength R_{eH} may be used in lieu of $R_{p0,2}$ if the latter is not available from the material standard.
c See 5.3.2 and 6.1.2.
d For definition of rupture elongation, see EN 13445-2:2014, Clause 4.

Figure 2.2: EN13445-3 [67] Maximum allowable values of nominal design stress for pressure parts other than bolts.

some associated tensile strength data was not available it is in the public domain in hard copy. Probably only available to those who have been involved with creep for decades, this is an opportunity to analyse the data upon which the European standards for creep design are based. For this chapter, the German Steel Institute VDEh data was digitised and manually cleaned for analysis. A methodology was derived for transposing the data to the classical no-creep temperature, T_{NC} for this group of materials - 375°C. From the general approach, a more detailed investigation of C-Mn (P265GH equivalent) material is carried out with a view to deriving a T_{NC} for the material. The first time this has been carried out. The material is also selected for experimental investigation later.

2.2 Methodology

The challenge is to derive a methodology for estimating the temperature at which a material will achieve a specific creep strain, 0.2% in a fixed period of time 200k hours at a certain stress. Above the method has been to define a reference stress from the elevated temperature

minimum 0.2% proof stress, σref = 2/3.Rp0.2, min, T from the standard for ferritic materials and finding the temperature at which the stress to cause 0.2% creep strain coincides with the reference stress. This approach requires data at the temperature and creep strain and that is not available, at least not in the public domain. However, by accumulating data in a parametric representation (stress v parameter 'collapsed' by temperature) accumulated data could be sufficient to identify materials that have non-conservative no-creep temperatures for further work and confirm or dispel the MATTER Project findings with a more sophisticated methodology [72]. A potential problem is that any activation energy change or 'kink' in the data at lower temperatures is not evident from the transposed data.

Annex R of EN 13445-3 contains a collection of parametric creep models for the extrapolation of creep rupture life to lower stresses based on temperature and stress as introduced in Chapter 1. These models need to represent the physical reality of creep strain accumulation but those presently used can become unstable, they can turn back in time when extrapolated outside the data range and many are asymptotic and do not extrapolate to lower temperatures of interest. Although the Manson-Haferd type models are prone to turn-back at low stress the C-Mn MH4 1974, Eq. 2.1 model can be extrapolated to lower temperatures.

$$\log\left(t_f\right) = f(\sigma)\cdot\left(T_1 - T_0\right)^r + \beta_5 \tag{2.1}$$

where t_f is the time to failure, T1 is the test temperature and

$$\left(f(\sigma) = \beta_0 + \beta_1\cdot\log(\sigma) + \beta_2\cdot\log(\sigma)^2 + \beta_3\cdot\log(\sigma)^3 + \beta_4\cdot\log(\sigma)^4\right) \tag{2.2}$$

with r, T_0 and β_0 – β_5 predefined constants for the specific material from Annex R of BS EN 13445-3. The problem with MH0n models is that T_0 can generally only be fitted by stepping through a range of temperatures in 10°K intervals and the model becomes asymptotic as T approaches T_0. By rearrangement, this can 'transpose' the time to failure t_f at a new target temperature T2 by the following

$$t_{f,new} = 10^{f(\sigma)^*\cdot\left(T_2 - T_0\right)^r + \beta_5} \tag{2.3}$$

Replacing the time to failure with the time to a specific strain and that can be transposed. The parametric parameter can be transposed to either a predetermined temperature of interest 375°C or adjust the temperature until the lower bound of the data points coincides with the

200k hours/stress limits to provide a no-creep temperature. In a similar way, the Wilshire-Scharning model can be transposed using a ratio of stress normalised by the tensile strengths at test and target temperatures such that

$$t_{f,new} = t_f \left[Ln\left(\frac{\sigma/\mathrm{Rm}, T_2}{\sigma/\mathrm{Rm}, T_1}\right)^{1/\mathrm{u}} \cdot \exp\left(\frac{-\mathrm{Qc}^*}{\mathrm{R}} \frac{1}{(T_2 - T_1)}\right)\right] \tag{2.4}$$

If the time to failure is replaced by the time to a specific strain the fitting parameters from the failure data can also be used to transpose the time to 0.2% at the new temperature. This is the method adopted by Holmström above. This leaves a no-creep zone to be defined and using the minimum proof stress Rp0.2% limits from the standards (2/3 of Rp0.2% at 375°C) and the 200k hour time frame provides a standard reference stress. Using the yield stress reverts to the Wilshire-Burt model [89]. This is based on the smallest thickness of material at < 16mm in Table 4 EN10028 standard shown in Figure 2.1 and Figure 2.2. The 0.2% proof stress can reduce with increasing thickness, to be conservative the proof stress of the thinnest section in EN10028 was taken. Any material below this limit up to this time would be creeping in the no-creep zone - below the classical limit of 375°C. The models were fitted to the German historical data set with materials no longer available aligned with their closest modern equivalents and their standard minimum proof stress. These closest modern equivalent materials are listed in brackets and used from here. While they may not have exactly the composition the Euro codes would have been based on this data. Most had mechanical strength properties within modern limits though sulphur and phosphorous levels were generally higher than modern limits.

2.3 Results and Discussion

The models have been fitted to the data using the non-linear optimisation routine in Excel SOLVER. There appears considerable uncertainty in the literature as to the fitting procedure and the data has been fitted allowing the Qc* to vary as a fitting parameter and minimising the error in both terms. The tensile strength data was often not available and the Rp0.2 data is also used, averages were used where individual heat data is not available. The plots in Figure 2.3 and Figure 2.4 are the 0.2% strain data transposed to 375°C using both the Manson-Haferd MH4 (P355) model and the Wilshire model for six materials. The box represents the no-creep zone at 200kh and the reference stress of 2/3 the minimum 0.2% proof strength at

the elevated temperature for each modern equivalent grade as already mentioned above. The plots provide a general view of each material's behaviour in relation to the blanket classical no-creep limit. The MH4 model is more appropriate to the initial plots and the P265GH material in particular and of this model plots, only the C-Mn materials appear to encroach on the no-creep zone. Figure 2.6 shows the tensile data, the median value used and the relation to the modern equivalent limits. In fitting the Wilshire model the values of Qc* were allowed to 'float' in the model fitting, this caused some values very low in comparison to the self-diffusion activation energy of steels 300 kJ/mol. used by Wilshire [76].

Of particular interest is the P265GH plot with the MH4 model used for C-Mn P355GH close to the 17Mo4 and 19Mo4 (P265GH) material from the data set. This shows for both models the lower bounds of the data breach the no-creep zone suggesting the material has a no-creep temperature, T_{NC} well below the classical 375°C. The other materials have some footnotes on the data of particular note is the low value of Qc* reported from the fitting when the WS model appears to place the data further left and with a lower no-creep temperature than the MH4 model. The largest disparity appears for the 10CrMo9-10 material which also has limited tensile data at temperature. The Wilshire model fit provides a low value of Qc* while for the 13CrMo4-5 there is the most similarity between the models when the Qc* is significantly higher and perhaps more as anticipated from the literature. Further analysis of the C-Mn data has been conducted. Figure 2.5 shows the tensile strength data for the material along with the specified lower limits of P265GH from EN10028-2 [90]. If the data were available the normalisation of the test stress would be by the tensile strength at temperature, these are not available. A further complication is the tensile strength of C-Mn steels passes through a local strength maximum - 'hump' -in the range of 250-350°C. A method of including a factored Rp0.2% (x1.25) was adopted to ensure the no data points needed to be excluded as normalised >1. This is just because of the lack of Rp0.2% creep strength data and was suggested as a possible solution for this data set.

Both these plots indicate the no-creep temperature T_{NC} at the reference stress of 2/3Rp0.2min, T at 200kh for P265GH is ∼340°C rather than 375°C and, for this material, the 'blanket' classical limit is non-conservative. This then leads to the question of any evidence for creep related problems with P265GH at or below the limit. Historically there is some indication of creep susceptibility of C-Mn steels at 360°C below 200k hours service [91, 92, 93, 94] though the investigations related to the effect of cold work prestraining increasing the sus-

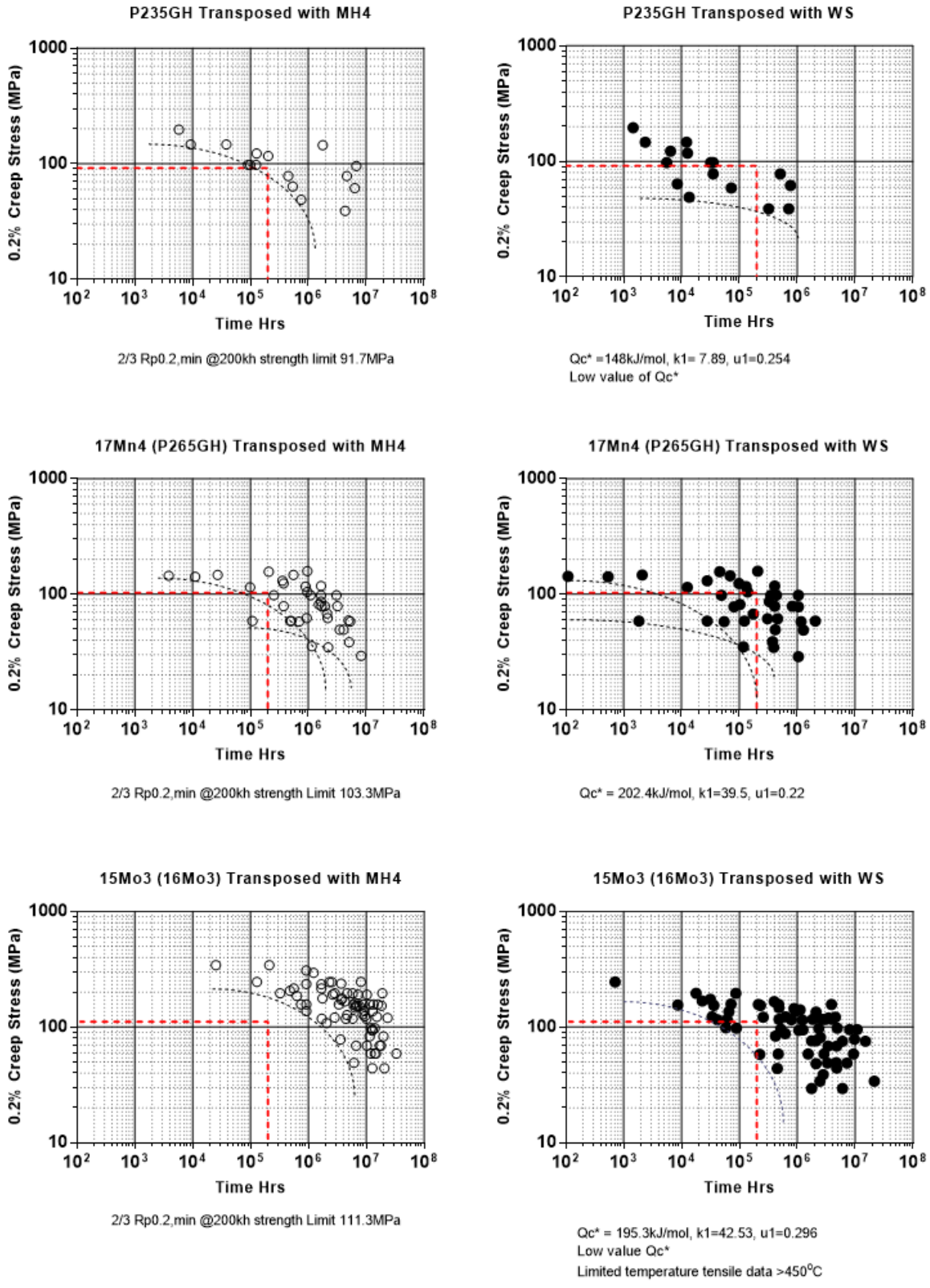

Figure 2.3: Transposition of 0.2% creep strain to 375°C using the factor based on the ratio of tensile strengths at test and target temperature.

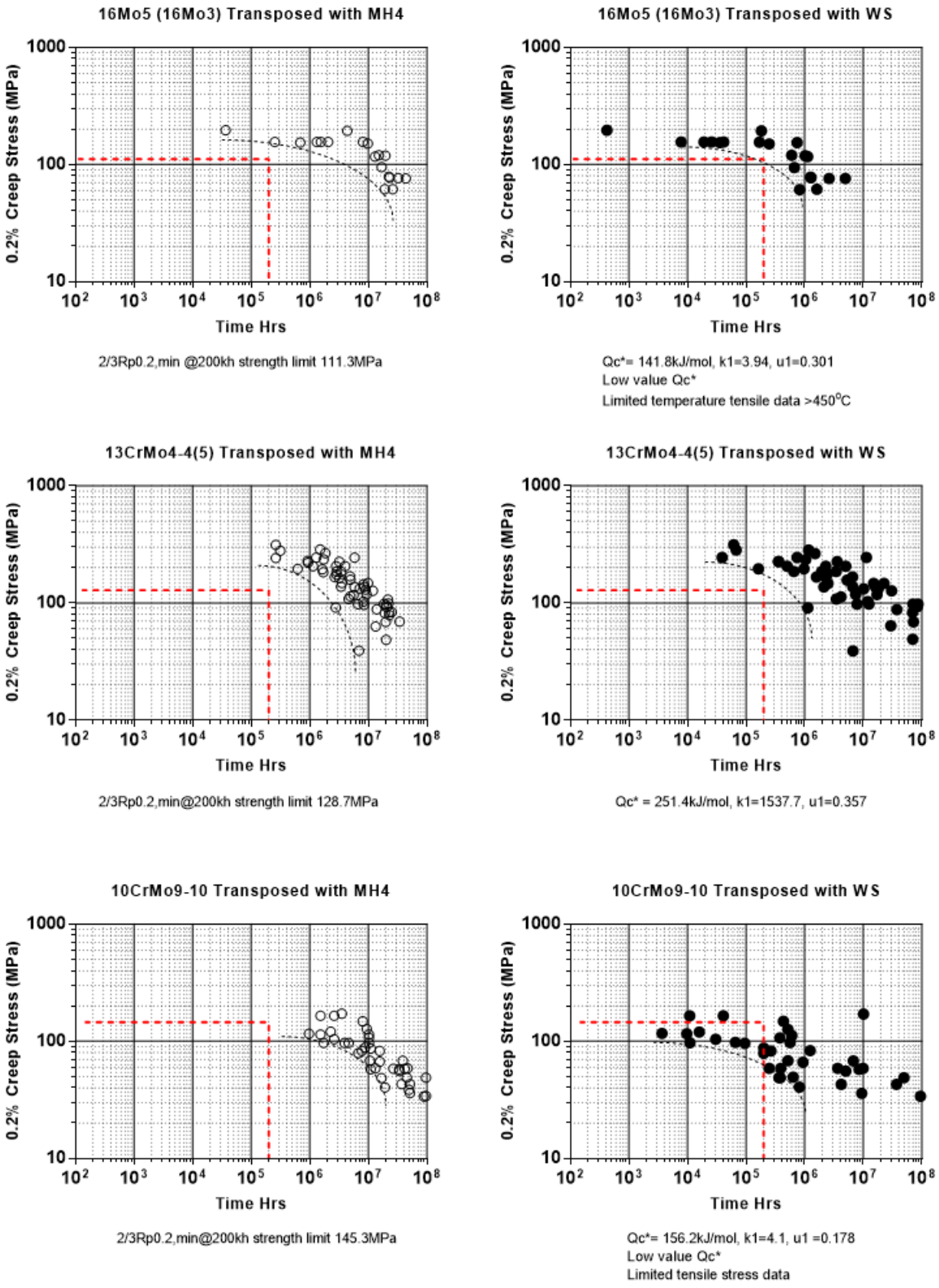

Figure 2.4: Continued. Transposition of 0.2% creep strain data to 375°C using the factor based on ratio of tensile strengths at test and target temperature.

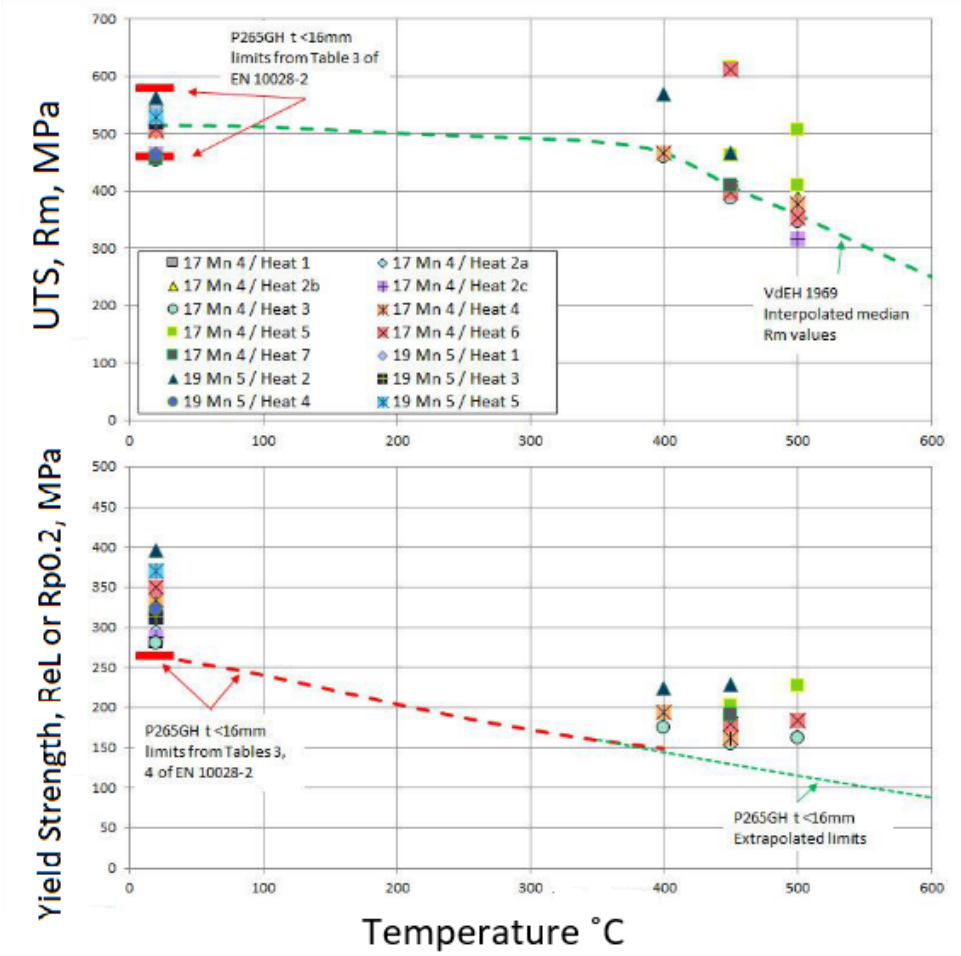

Figure 2.5: VDEh Section BB C-Mn steels, Graphical representation of the tensile data [69].

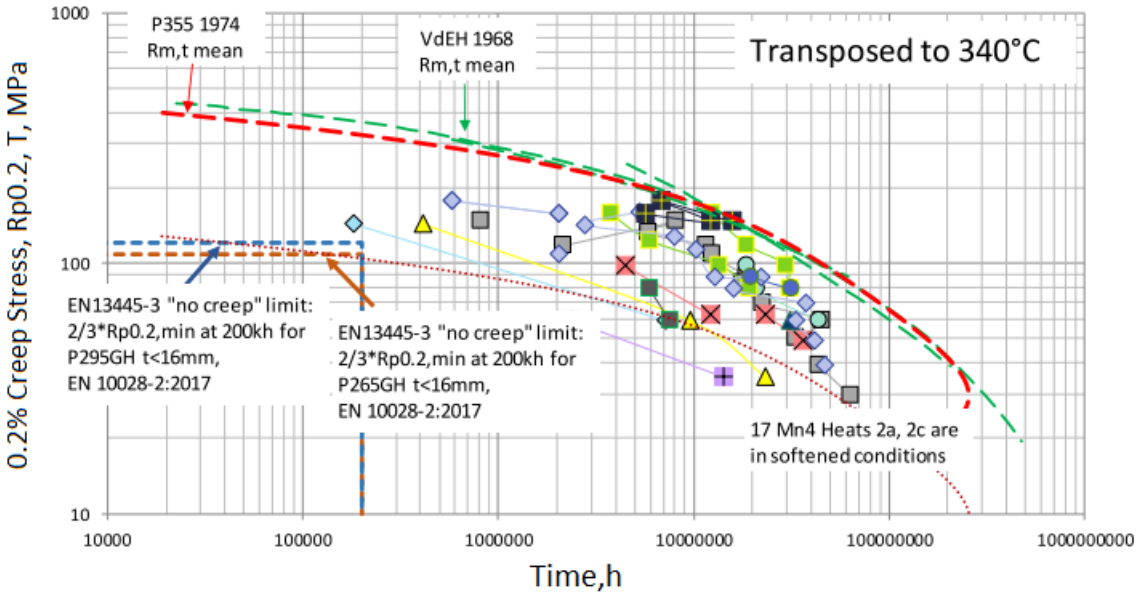

Figure 2.6: 0.2% creep strain data temperature transposition to 340°C via the WS model plotted against the WS parameter and including the rupture mean values.

ceptibility to creep crack growth. This work in the '80s may have led to material avoidance but appears to confirm issues with creep in the proposed no-creep zone around 360°C.

2.4 Concluding Remarks

The historical data set of the German Steel Institute was used to fit Manson-Haferd and Wilshire models; this data is that upon which the Euro code design standards are based. The general plots indicate that a number of C-Mn and low alloyed steels may be creeping below 375°C, in the no-creep zone defined as the temperature to cause 0.2% creep strain in a specified time of 200k hours, in broad agreement with the findings of Holmström [85] using only the data in the European material standards and a rupture time factor. Of particular note is P265GH which both models indicate the lower bounds encroach the no-creep zone in the plots. The higher alloyed materials appear to be well above the limit offering opportunities for cost savings in both design and creep monitoring if they were raised from the classic limit. In fitting the Wilshire model the value of Qc* was allowed to 'float' as a quasi-constant which appeared appropriate given there were a number of materials over a range of temperatures. However, this proved to often provide values considerably lower than what might be expected for an activation energy of self-diffusion and the 300 kJ/mol. value which appears often in the literature. More investigative work is required of the appropriateness of the Wilshire model here which will be covered in the next chapter. The transposition of the P265GH time to 0.2% strain data indicates that the 'no-creep' temperature is $\sim$340°C rather than 375°C which appears to be confirmed by historical evidence. The none trivial challenge is to develop an experimental technique to establish a T_{NC} for a specific material rather than rely on historical data which is often incomplete as well as dated.

Chapter 3

The Wilshire-Scharning model

3.1 Introduction

Having introduced the various methods and models adopted in creep design this chapter will look specifically at the Wilshire-Scharning (WS) model and Wilshire equations (WE). The WS model is a time-temperature parameter (TTP) model as the classical ones described in Chapter 1 developed at the University of Swansea. Over the past dozen or so years the model has gained widespread interest with claims of accurately predicting 100,000-hour stress rupture properties using the data generated from tests of < 5000 hours over a range of materials [95] compared to standard test requirements of 30000 hours (x3) for the extrapolation of the traditional TTP methods. In comparative fitting with some of the classical models in Chapter 1, it has also been claimed as the best for rupture data with a Grade 22 steel [96]. The model has also been criticised as not elaborate enough, based on perceived physical mechanisms, if it is to furnish more reliable extrapolation over a model simply based on data fitting [97]. The ever-increasing library of materials in the public domain which have fitted the model to data, from 1Cr-0.5Mo [54], Grade 91 [98], Grade 92 [99], Grade 122 [99], Grade 22, (2.25Cr-Mo) [48], aluminium alloys [100], Waspaloy [101], 316H [102], 1CrMo0.25V [103][104], titanium [49], nickel-based superalloy 720Li [105] in general report good results for failure prediction. Some have reported issues specifically in the fitting techniques and poor results [106, 107].

As for the validation of the model the WE are not included in the creep design standards. They have been found to be in accordance with International standard [108] rupture extrapolation requirements for European Creep Collaborative Committee Grade 91 data

[109] and have been found comparable with classical models in stress relaxation round-robin tests [110]. Another area where the model has gained attention is as an approach to define the no creep temperature limit, T_{NC} by the European Commission MATTER Project [81, 82, 83, 85, 84] and for inclusion in the European standards [111]. This is a temperature at which a given reference stress achieves a strain of 0.2% in 200k hours; a design limit for a no-creep region where there is no requirement to design for or monitor creep. Itself a challenge to define reliably at temperatures where creep behaviour is traditionally not tested [81]. The attraction is the simplicity of the equations which can be easily rearranged to analytically determine the stress, time or temperature terms. It is this ability to rearrange for the temperature term that is of particular interest here. Though there are many practical examples of fitting the model, extrapolation and prediction of creep rupture data there is little in the way of times to specific strain prediction and the temperature prediction. It is fair to say this model has been developed in the public domain and there have been some significant changes and techniques developed in that time. In this chapter, the development of the model is reviewed and alternatives are offered and considered where it is felt appropriate. The practical example of the model fitting techniques has been carried out using data for a specific material - Grade 91. This has been chosen as the MATTER project work to date utilised the material to establish a no-creep temperature limit, it is an important and widely used creep-resistant steel in pressure vessel and piping systems to 600°C [112] and, more importantly here, there are comprehensive creep test data available in the public domain. Grade 91 material is selected in later chapters for experimental work to establish the temperatures. The original contribution to knowledge in this work includes exploring the practical issues with fitting this model to a specific material with the intention of deriving a temperature for a specific strain in a specific time rather than its usual prediction of time to failure. Alternative models have been explored and proposed to improve the capability of the Wilshire-Scharning model. The Wilshire model is fitted with real data for the MG constant rather than treating it as a fitting parameter for the first time. Also, a new model is presented with a practical fitting procedure for Grade 91. The new model and the real data modified model are compared and contrasted with the existing WS model in basic and modified forms. For the first time, a comparison of the effects of model selection on the no-creep temperature extrapolation is presented.

3.2 Background

Power-law creep as a function of applied stress σ is commonly represented by the Norton creep model

$$\dot{\varepsilon}_{min} = A.\exp\left(-\frac{Q_C}{RT}\right)\left(\frac{\sigma}{G}\right)^n \tag{3.1}$$

where Qc is the activation energy for the process (climb by self-diffusion of vacancies). The problem with this model is that the 'constants' are typically functions of temperature and stress. This is particularly true for the creep exponent, which can vary from n = 2 - 20 for a single material (See Figure 3.1) making the model unreliable for extrapolation and requiring long test duration data. Creep rate is related to time to failure by the Monkman-Grant [80] relation in its basic form

$$\dot{\varepsilon}_{min} t_f = M \tag{3.2}$$

where M is taken as a constant. Wilshire & Burt [89] proposed that a better model, which allows similar data to collapse more readily onto a single curve, is

$$\dot{\varepsilon}_{min} = A^* \exp\left(-\frac{Q_C^*}{RT}\right)\left(\frac{\sigma}{\sigma_Y}\right)^n \tag{3.3}$$

where σ_Y is commonly the 0.2% proof stress, which varies strongly with temperature (unlike the shear modulus it replaces). In later papers [113] this was altered to utilise the tensile strength σ_{TS} instead which became preferred with the rationale it provided a better fit to the data because σ_Y is more difficult to measure precisely [103, 98].

$$\dot{\varepsilon}_{min} = A^* \exp\left(-\frac{Q_C^*}{RT}\right)\left(\frac{\sigma}{\sigma_{TS}}\right)^n \tag{3.4}$$

It also introduces the expectation of the following asymptotic responses

$$\dot{\varepsilon}_{\min} \to 0 \text{ as } \frac{\sigma}{\sigma_{TS}} \to 0 \text{ and } \dot{\varepsilon}_{\min} \to \infty \text{ as } \frac{\sigma}{\sigma_{TS}} \to 1 \tag{3.5}$$

Note that none of the above equations satisfies this relationship. Wilshire also proposed that the stress-dependence could be written as an exponential-dependence (which is another common creep model) rather than a power-law dependence such that

$$\dot{\varepsilon}_{min} = B^* \exp\left(-\frac{Q_C^*}{RT}\right) \exp\left(\frac{V}{RT} \cdot \frac{\sigma}{\sigma_{TS}}\right) \tag{3.6}$$

where B* and V are constants. This still does not obey the asymptotic requirements (Eq. 3.5) but it removes the need for the determination of a highly non-linear creep exponent, which is a major limitation of models (Eq. 3.1 Eq. 3.3 Eq. 3.4) especially when extrapolation to high or low-stress regimes is required. We can re-arrange the above equations of interest such that we can expect to obtain a linear plot. To make interpretation of these easier, we introduce the variables

$$y = \frac{\sigma}{\sigma_{TS}} \quad x = Ln\left[t_f \exp\left(-\frac{Q_c^*}{RT}\right)\right] \tag{3.7}$$

Now using Eq. 3.2 we can write Eq. 3.4 as

$$Ln(y) = -mx + c \tag{3.8}$$

where m= 1/n and c = m*Ln(M/A*) and Eq. 3.6 as

$$y = -m^* x + c^* \tag{3.9}$$

where m* = RT/V and c* = m*Ln(M/B*). The model Eq. 3.4, therefore, predicts that plotting the natural log of y Ln(y) vs x will yield a straight line, if the parameters are constant. Model Eq. 3.6 predicts that plotting y vs x will yield a straight line. These two assumptions have been tested by Wilshire for various materials. The plots in Figure 3.1 [76] are for G92 (9% Cr steel) note the axes use log10 x etc, not the natural log. This does not change the expectation, just the relationship between the slope and the intercept and the definition of the constants in Eq. 3.8 and Eq. 3.9. The key point to note here is that whilst Figure 3.1 b is not linear, as predicted by Eq. 3.6 it is much more linear than Figure 3.1 a where the creep exponent (slope) changes substantially.

As already discussed Wilshire has introduced the expectation that the asymptotics of Eq. 3.5 should be valid if the stress range is to be extended beyond $0.15 < \sigma/\sigma_Y < 0.7$. We can re-write Eq. 3.5 such that the required asymptotics are

$$\begin{aligned} y &\to 0 \quad \text{as} \quad x \to \infty \\ y &\to 1 \quad \text{as} \quad x \to -\infty \end{aligned} \tag{3.10}$$

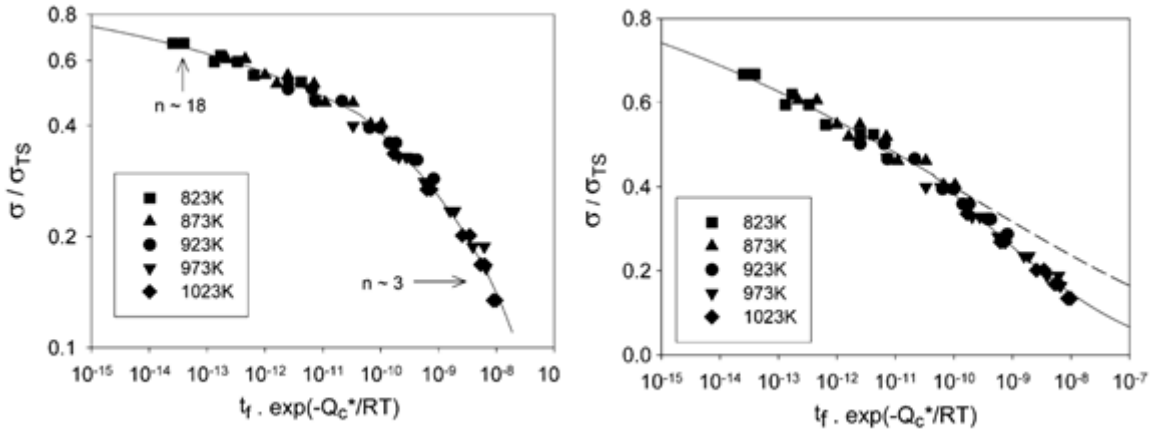

Figure 3.1: The dependence of the temperature-compensated creep life on the normalised stress using (a) Eq. 3.4 and (b) Eq. 3.6 [73].

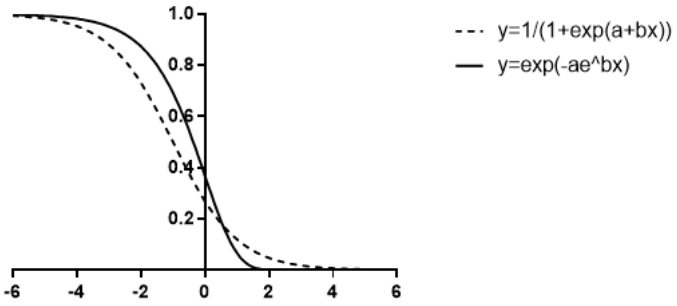

Figure 3.2: Potential sigmoid functions for the representation of the stress function.

Two functions that we might choose that satisfy the expected sigmoidal relationship are

$$y = \frac{1}{1+\exp(a+bx)} \tag{3.11}$$

$$y = \exp\left(-ae^{bx}\right) \tag{3.12}$$

where a and b are fitting constants. These are both plotted in Figure 3.2 if all the constants are unity.

Both have a fairly linear region in the centre that would produce a good fit to the data in Figure 3.1 b and both have the asymptotics required by Eq. 3.10. Wilshire uses Eq. 3.12 without investigating the fit of Eq. 3.11. It is suspected Eq. 3.12 was chosen as it produces a slightly neater result. The fit at the extremes depends on the amount of data at the turning points. Figure 3.1b does not demonstrate there will be much of this, with most being in the linear middle region. Hence the value of these fits should always be questioned. If we

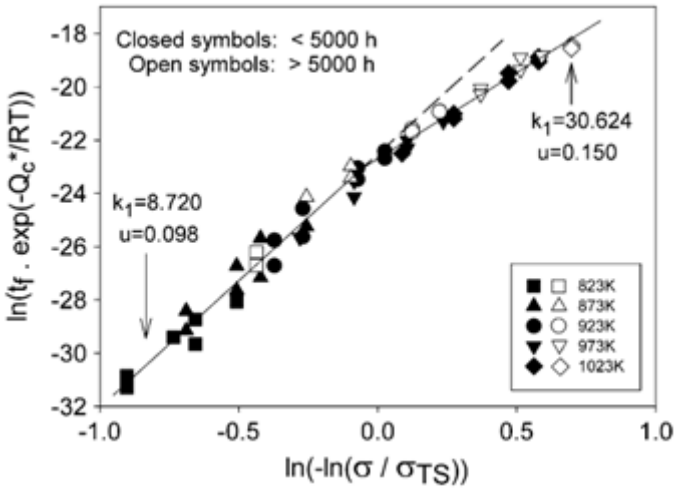

Figure 3.3: Wilshire plot according to Eq. 3.3 [73].

assume the sigmoidal shape is defined by Eq. 3.12 then

$$\frac{\sigma}{\sigma_{TS}} = \exp\left(-ae^{bLn\left[t_f \exp\left(-\frac{Q_c^*}{RT}\right)\right]}\right) \tag{3.13}$$

or

$$\frac{\sigma}{\sigma_{TS}} = \exp\left(-k_1\left[t_f \exp\left(-\frac{Q_c^*}{RT}\right)\right]^u\right) \tag{3.14}$$

which is the form given by Wilshire with a = k1 and b = u allowing the relatively simple re-arrangement for the t_f term to fit the model by minimising the squared error in the dependent t_f to find k1 and u. Equation 11b can also be re-arranged so that

$$Ln(-Ln(y)) = bx + Ln(a) = ux + Ln(k_1) \tag{3.15}$$

gives a straight line. When plotted, as shown in Figure 3.3, this is still not a straight line but is divided into two straight sections, such that different parameters are chosen for the upper and lower parts of the sigmoid.

Possible improvements to the model would aim to make the data a linear fit across the whole range. However, if the mechanisms at high stress and low stress are different there is little reason to assume that they should be able to be described by a single master curve. A generally accepted location of a discontinuity or 'kink' is around the yield stress [114]. Wilshire & Scharning's [103] physical interpretation is that below creep deformation occurs only by the movement of pre-existing dislocations or at grain boundaries and above deform-

ation occurs by the movement of dislocations generated within grains. They are also evident at other stresses and the traditional hypothesis is that there are multiple creep mechanisms in operation over the test conditions and changes to the predominant mechanism alter the slope, these are then treated as different regions for fitting the model [54, 102, 49, 115, 116, 117]. Whether due to a change in mechanism, model inadequacy or lack of good data the region splitting approach should be applied with some caution. Further complimentary evidence should always be gathered before drawing conclusions on the underlying mechanism, but the method can be and is used to improve model creep life predictions [118]. The stress at which kinks are located has been largely by eye or more formally at half or full the yield stress [118] and this lack of a formalised statistical method has been addressed by Evans [119, 116]. More recent work suggests the discontinuities and changes in activation energy are due to changes in the mechanism controlling dislocation movement rather than a complete change of creep mechanism. The values of Qc* $\neq$ Qc, the creep activation energy in Eq. 3.1 and are expected to be slightly lower because they are evaluated at constant normalised stress rather than stress alone [105]. Materials with a high rate of strain hardening undergo a large change in apparent activation energy Qc* either side of the yield and vice versa [114]. This allowed an alternative approach for titanium -with constant Qc* - to regenerate full curves by treating the other two parameters as functions of strain after generating the apparent activation energy, Qc* by the traditional Arrhenius plot of natural log minimum creep rate or Ln t_f vs 1/T (°K) [49]. Wilshire derived the Qc* at a constant σ/σ_{TS} but there is no explanation of the method used. Despite the typical highly variable values of Qc like n in the power-law equations Wilshire *et al.* [95] claim the value of Qc* is equal to the activation energy for lattice diffusion, Q_{SD} or to the activation for vacancy diffusion along lattice dislocations Qpipe. This has more recently been challenged by Evans [120] who recommends a variable activation energy for more accurate prediction and has developed more sophisticated fitting techniques. With some more 'exotic' materials Cedro *et al.* [106, 121, 107] found poor fitting to experimental data attributed to region splitting and regional determination of Qc* (floating value) with a preference for a known Q_{SD} value.

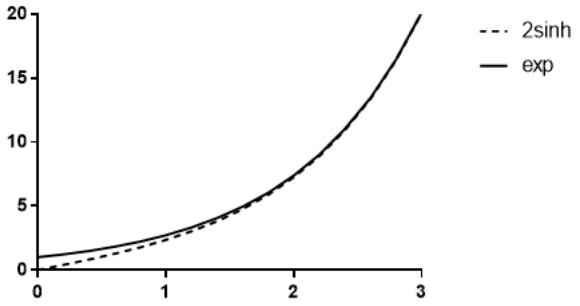

Figure 3.4: 2sinh(x) vs exp(x).

3.3 An alternative model

The derivation of the Wilshire model has never been adequately explained. There are a number of choices that have been made without much justification. Other choices could be explored such as replacing the exponential stress term in Eq. 3.6 with a sinh-dependent stress term. This is used in other creep models and has the advantage of satisfying one of the asymptotic conditions that the minimum creep rate (mcr) = 0 when $\sigma = 0$ whilst keeping the same high-stress response as before. This is because sinh(x) = 1/2(e^x - e^{-x}), so sinh(0) = 0 and 2sinh(x) $\rightarrow$ exp(x) as x gets large.

The following model would improve the fit if the x term < 2 but is much more difficult to rearrange to be of practical use.

$$\dot{\varepsilon}_{min} = \frac{M}{t_f} = B^* \exp\left(-\frac{Q_C^*}{RT}\right) \sinh\left(\frac{V}{RT} \cdot \frac{\sigma}{\sigma_{TS}}\right) \tag{3.16}$$

then

$$\frac{\sigma}{\sigma_{TS}} = \frac{RT}{V} \sinh^{-1}\left(\frac{M}{t_f B^* \exp\left(-\frac{Q_C^*}{RT}\right)}\right) \tag{3.17}$$

The model highlights that the slope is temperature-dependent as in all these models including the Wilshire model e.g. heteroscedasticity can be evident if the error is minimised on the stress term (shown in 3.5).

This can be easily corrected by plotting

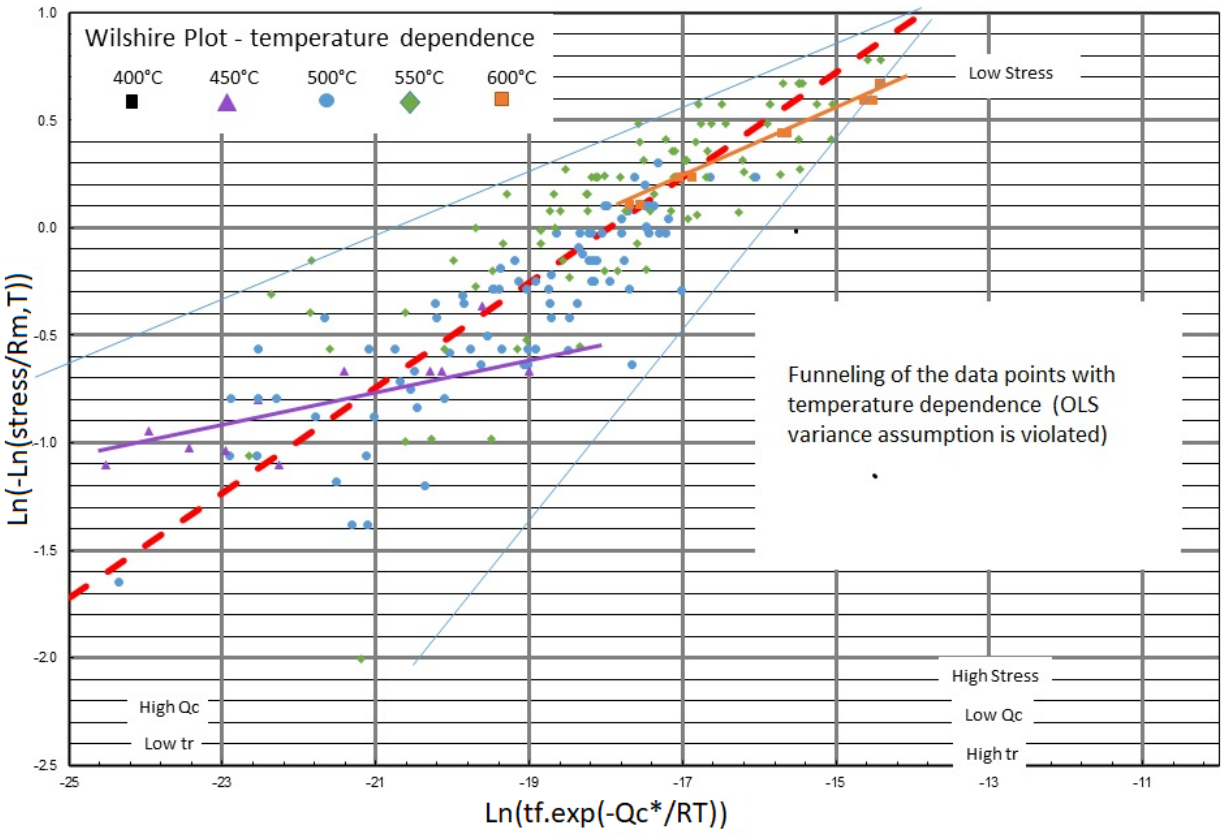

Figure 3.5: Wilshire-Scharning model fitted minimising the error in the stress term.

$$\frac{\sigma}{\sigma_{TS}} \text{ against } RT\sinh^{-1}\left(\frac{M}{B^*t_f\exp\left(-\frac{Qc^*}{RT}\right)}\right) \text{ OR } \frac{1}{RT}\frac{\sigma}{\sigma_{TS}} \text{ against } \sinh^{-1}\left(\frac{M}{B^*t_f\exp\left(-\frac{Qc^*}{RT}\right)}\right) \tag{3.18}$$

Introducing A=M/B* and noting that sinh(x) ≈ ½ exp(x) for x ≥ 2 and

$$\frac{\sigma}{\sigma_{TS}} = \frac{RT}{V}Ln\left(\frac{2M}{B^*t_f\exp\left(-\frac{Qc^*}{RT}\right)}\right) \tag{3.19}$$

will give a very similar fit, unlike the sinh term this can be easily rearranged to

$$\frac{\sigma}{\sigma_{TS}} = -\frac{RT}{V}Ln\left(t_f\exp\left(-\frac{Qc^*}{RT}\right)\right) + \frac{RT}{V}\ln(2A) \tag{3.20}$$

To avoid the temperature dependence of the slope this can be plotted as

$$\frac{1}{RT}\frac{\sigma}{\sigma_{TS}} \text{ against } Ln\left(t_f\exp\left(-\frac{Qc^*}{RT}\right)\right) \tag{3.21}$$

The sinh model has real physical quantities, the underlying assumption of the model is that

$$\dot{\varepsilon}_f t_f = M = \varepsilon_f \tag{3.22}$$

The failure strain is constant. Unfortunately, the strain at failure is often only available in the form of failure elongation percentage which is difficult to measure accurately and thus has considerable variability and scatter.

3.4 The Monkman-Grant relation and the Wilshire Equations

In terms of the Wilshire-Scharning model, the underlying assumption is that the Monkman-Grant (MG) relation in its basic form, Eq. 3.2, allows generalisation to other useful forms Eq. 3.23, Eq. 3.24 and Eq. 3.25 for extrapolation such that u1= -u2 and k1 =k2M^{u1}. The fitting constants change for each i.e. k1 and u1 (or just k and u) relate to the time to failure data, k2 and u2 to the mcr data, k3 and u3 for time to specific strain (or e.g. k0.2, u0.2 for the time to 0.2% strain, $t_{0.2}$). However, only under very special conditions can M be expected to be a constant [122]. Wilshire *et al.* [76] acknowledges that M is a function of stress and temperature and suggests the use of the basic MG relation is based on the 'common practice' of combining it with the power-law equation. Abdallah *et al.* [67] suggests this was based on Davies & Wilshire [123] finding the MG constant independent of stress and temperature above 0.45Tm (dependent below) and finding the exponent was unity for pure nickel and thus ignored. It is acknowledged by Evans [124] that the generalised models for t_f and t_ε (time to a specific strain) may not be appropriate for all materials without a temperature correction to the MG relation. However, this indicates it is the exception rather than the rule and the Wilshire equations are in general appropriate.

$$\left(\frac{\sigma}{\sigma_{TS}}\right) = \exp\left\{-k_2\left[\dot{\varepsilon}_m \exp\left(\frac{-Q_c^*}{RT}\right)\right]^{u_2}\right\} \tag{3.23}$$

$$\left(\frac{\sigma}{\sigma_{\mathrm{TS}}}\right) = \exp\left\{-k_1\left[t_f \exp\left(\frac{-Q_{\mathrm{c}}^*}{RT}\right)\right]^{u_1}\right\} \tag{3.24}$$

$$\left(\frac{\sigma}{\sigma_{\mathrm{TS}}}\right) = \exp\left\{-k_3\left[t_\varepsilon \exp\left(\frac{-Q_{\mathrm{c}}^*}{RT}\right)\right]^{\mathrm{u}_3}\right\} \tag{3.25}$$

Eq. 3.2 is the simplified form of the MG relation with M and ρ material constants when the exponent ρ=1 in Eq. 3.26 which is not always the case, and they may not be constant for Grade 91.

$$t_{\mathrm{f}} = M\dot{\varepsilon}_{min}^{-\rho} \tag{3.26}$$

If the exponent is below unity the Qc* should be the product of the actual value and the exponent as well as being slightly lower than the creep activation energy Qc over the normalised stress. If a known constant value is to be used there is some approximation. A good point to start in the analysis would be the materials MG relation. In order to describe the whole creep curve and stress dependence the relation has further been expanded to include the failure strain by Dobé & Milička [125] who found it more appropriately described by

$$M\varepsilon_{\mathrm{f}} = \dot{\varepsilon}_{min}^{\rho}\mathrm{t}_{\mathrm{f}} \tag{3.27}$$

The variation in M with stress would be expected to be significantly less for this modified form [122]. As for the basis of the relation and this modified form, they have been described as a geometrical relation, a rough approximation of the integral under the strain rate curves with a smoothing out of the scatter from a double logarithmic plot [126]. Thus, its ability to describe an infinite number of full creep curve shapes must be viewed with caution. Despite these problems with the fundamental assumption of the WE, there is an ever-increasing library of work in the public domain on the application of the technique to numerous materials often accompanied by claims of superior predictive capabilities over other models [96].

Evans [124] recommends that a refinement of the original Wilshire equations is required if the material has an MG exponent below unity and a temperature dependent M based on an MG relation of (using Evans's notation)

$$\dot{\varepsilon}_{min}^{\rho}\mathrm{t}_{\mathrm{f}} = Me^{\frac{-b}{RT}} \tag{3.28}$$

$$(\sigma/\sigma_{TS}) = \exp\left\{-k_2 M^{\nu/\rho}\left[t_{\mathrm{f}} \cdot \exp\left([b-\rho]Q_{\mathrm{c}}^*/RT\right)\right]^{-\nu/\rho}\right\} \tag{3.29}$$

such that in Eq. 3.24

$$u = -v/\rho; \quad k_1 = k_2 M^{v/\rho} \tag{3.30}$$

This conveniently allows the stress term to remain on the left-hand side and M within the constant. Framing the new model constants in terms of the original suggests there is no difference in fitting the model just the values derived and a way to reconcile Qc* values that don't appear appropriate. The fitting provides an estimate of (b - ρ)Qc* and it should, depending on the MG relation, be expected to be substantially different than Qc*. The new constants can be derived from a linear fit of Eq. 3.28. In terms of the value of Qc* obtained from the original model, Eq. 3.24 Evans [124] suggests this should then be revised up by the following to correct for a non-constant M and ρ below unity

$$(Qc^* + b)/\rho \tag{3.31}$$

If, however, the appropriate data is available there is no reason to have M wrapped up with the constants in Eq. 3.30 it can be calculated for each data point purposively providing for variation in the MG relation due to temperature and stress.

For the third WE Eq. 3.25, the time to a specific strain, Evans [124] proposes the modified form requires a calculation of the MG relation for each strain such that Mε and pε suggesting significant variation in M. For 1CrMoV Evans shows that Mε varies in a sigmoid over the whole strain range from ∼0-5 but pε only varies substantially at lower strains. These strains are, however, normalised with the strain at failure and of limited use here. The NIMS [86] database provides comprehensive test data for 9Cr-1Mo-V-Nb (Grade91) steel in tube, plate and pipe of various heats or casts. NIMS Data sheet 43A provides information from creep tests to 30-50k hours for several heats (MgA-MgD & MGA-MGG) some of which include full creep curves as well as composition and physical properties. For these heats, the MG relation is clearly both stress and temperature-dependent in Figure 3.7. The ρ exponent is found to be relatively constant at 0.84 (consistent with Maruyama [127] for this material) though there is a sharp deflection at $< 0.15\sigma/\sigma_{TS}$ in Figure 26 which would be consistent with Evans's [124] findings for 1CrMoV. Even if M is constant with ρ = 0.84 there is little justification for using a fixed value of Q_{SD} = 300 kJ/mol. if it is ρQc*. Wilshire & Scharning [98] in fitting the original model to some of the Grade 91 heats (MGA-MGC & MgC in

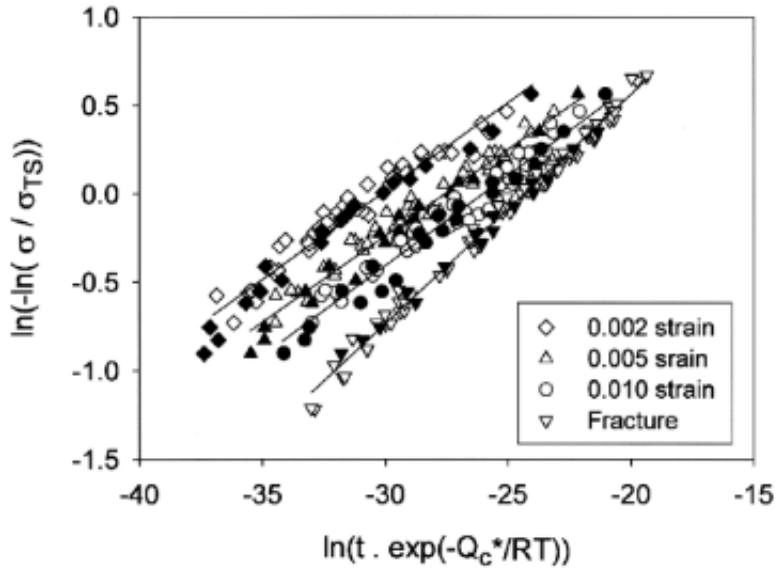

Figure 3.6: Wilshire plot for Grade 91 NIMS 43A heats MGA-MGC & MgC fitted with fixed Qc*=300 kJ/mol. [95].

NIMS Datasheet 43A) used a fixed Qc* = 300 kJ/mol. Using Eq. 3.24 and Eq. 3.25 they compile a family of Wilshire plots, shown in Figure 3.6, of times to specific strains and fracture well represented by straight lines over an extended range of stress and temperature — suggesting an opportunity for long-term extrapolation of incomplete data if their relationship could be characterised. The method was also compared to other classical methods described in Chapter 1 with comparable results for deriving 100,000 hour creep rupture strengths from ECCC Grade 91 data [109] and meeting the requirements of recognised extrapolation standards [108].

3.5 Application of the Wilshire model in its basic form

During the development of the model, there has been some vagueness in the value of the apparent activation energy Qc* to use. Many of the studies have used a fixed value activation energy based on previous literature or an Arrhenius plot. The value often used for steels to derive the fitting parameters is fixed at 300 kJ/mol. but as high as 380 kJ/mol. is quoted for the creep activation energy Qc for many ferritic steels [20], the 'floating' values derived in Chapter 2 were all significantly less than this. Cedro *et al.* [106, 121, 107] suggest using a known Q_{SD} rather than calculating for each data set or region is preferable using the basic model. The present accepted methodology appears to be to fit the model to the data with

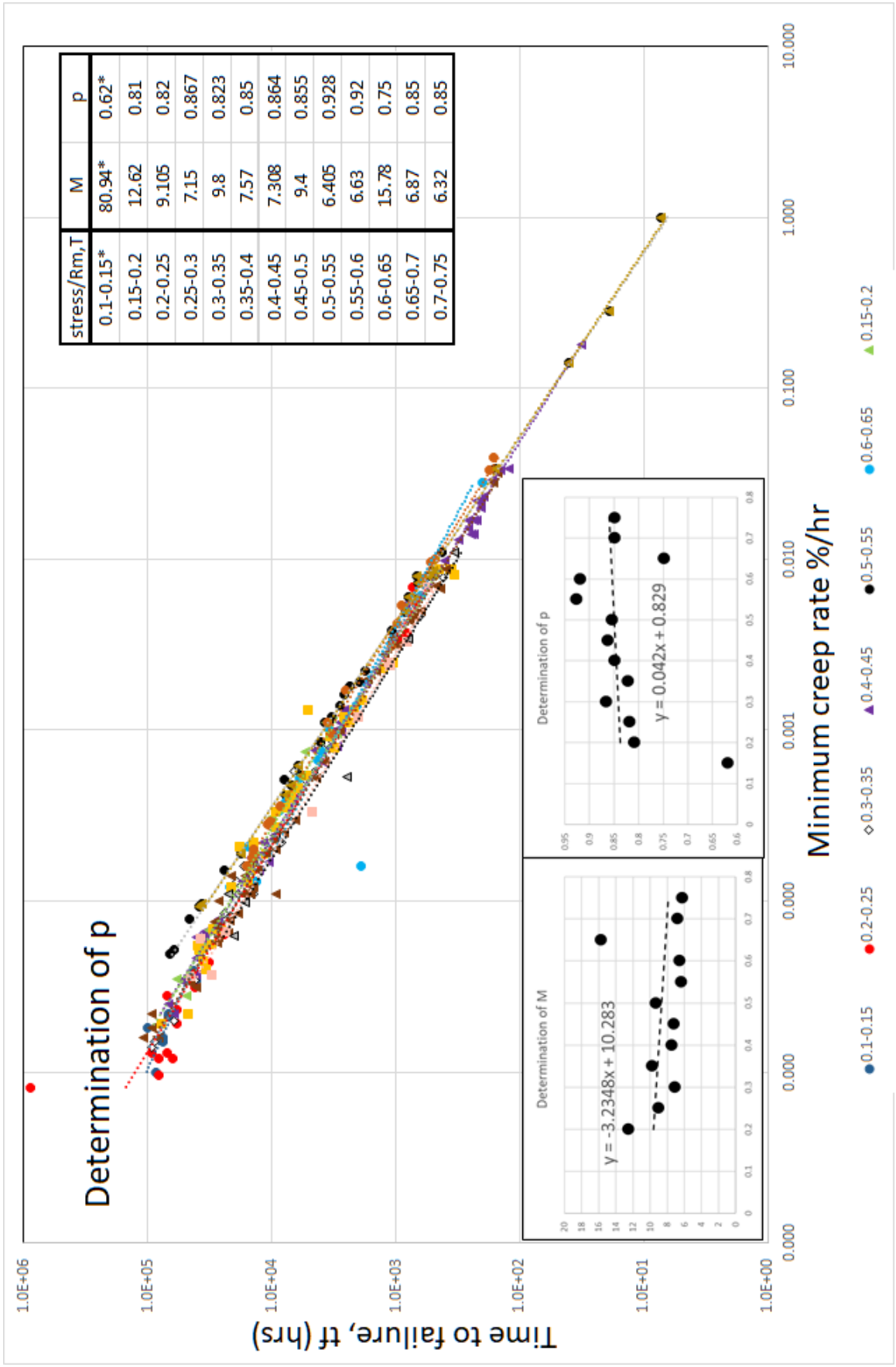

stress/Rm,T	M	p
0.1-0.15*	80.94*	0.62*
0.15-0.2	12.62	0.81
0.2-0.25	9.105	0.82
0.25-0.3	7.15	0.867
0.3-0.35	9.8	0.823
0.35-0.4	7.57	0.85
0.4-0.45	7.308	0.864
0.45-0.5	9.4	0.855
0.5-0.55	6.405	0.928
0.55-0.6	6.63	0.92
0.6-0.65	15.78	0.75
0.65-0.7	6.87	0.85
0.7-0.75	6.32	0.85

Figure 3.7: Relationship between M, ρ and the normalised stress for NIMS 43A heats MgA-MgD and MGA-MGG.

an expected fixed single value of the apparent activation energy Qc* and use this to identify regions where the slope is different. Then treat these regions independently for linear re-fitting treating Qc* as a fitting constant along with the k and u values. These variable Qc* values for each region then provide the basis for improving predictability and/or identifying possible mechanism changes which should always be confirmed microstructurally [115]. It might be prudent to report both methods. A Qc* value of 300 kJ/mol. has been found by optimisation for Grade 91 and used fixed; approximately equal to the value of activation energy for self-diffusion in the lattice [99, 98, 115].

Data set NIMS 43A Grade 91 Heats MgA-MgD (Plates) and MGA — MGG (Tubes) [86] has been used to apply the WE. The raw data are shown in Figure 3.8. This consists of 288 failed data points from 450 - 725°C (723 - 998°K). There is a clear high-stress discontinuity (upper left). Closer inspection of the data reveals that some are collected above the IMechE [43] stress- temperature threshold for 9Cr-1Mo. This is a limit where it is considered that the instantaneous plastic strain on loading will exceed 0.2% and the subsequent creep behaviour may be influenced by the dislocation densities generated. Based on this IMechE criteria all the data above $0.75\sigma/\sigma_{TS}$ is excluded and the apparent discontinuity removed. Of the criticisms in the open literature, there is no prescribed method of optimisation offered and combined with alternating axes there may be some variation in methods used between authors [106]. Here the Wilshire model is fitted using the heat average tensile strength and minimising the error in the y dependent variable, t_f, using the non-linear optimisation routine Excel SOLVER. Some tensile strengths at temperature were not measured and have been interpolated using a polynomial fit to existing data. Figure 3.9 shows the Wilshire plot of all the data with the model parameters for each before and after the cull for 0.2% instant 'plasticity'. Figure 3.10 shows the culled data set with unfailed data removed plotted against normalised stress and Figure 3.11 shows the accompanying Wilshire plot of the culled data set with a fixed Qc* of 300 kJ/mol. The fitting parameters are slightly higher than those derived by Wilshire & Scharning for their subset (MGA-MGC & MgC) of this material at < 70k hours (k1 =23.93, u =0.131). Figure 3.12 is the Wilshire plot fitted with a 'floating' value of Qc* - allowing the software to optimise the value - a quasi-constant.

For the value of Qc* it might be considered appropriate to use a value of 300 or 322 kJ/mol. for this data set. It is not easy to see how well the model fits the data from any of these Wilshire plots so a plot of the model residuals in y against the normalised stress σ/σ_{TS}

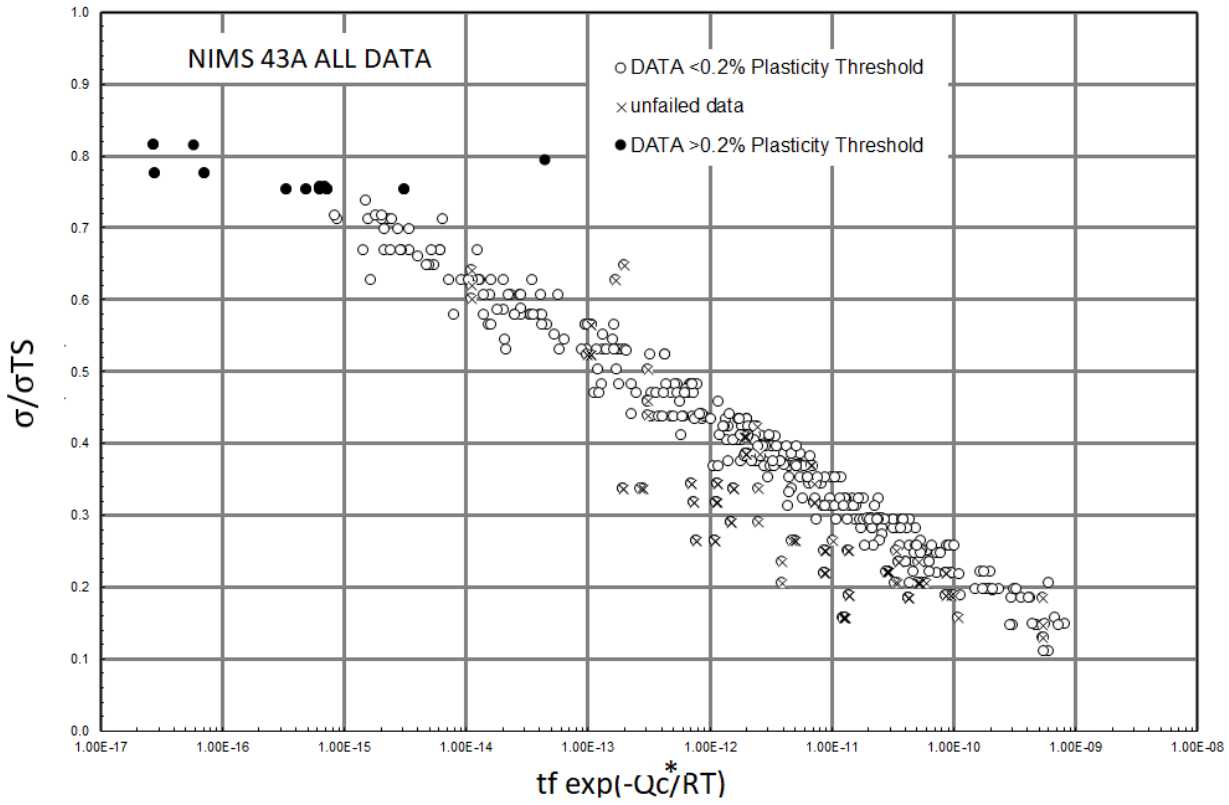

Figure 3.8: NIMS 43A Full data set.

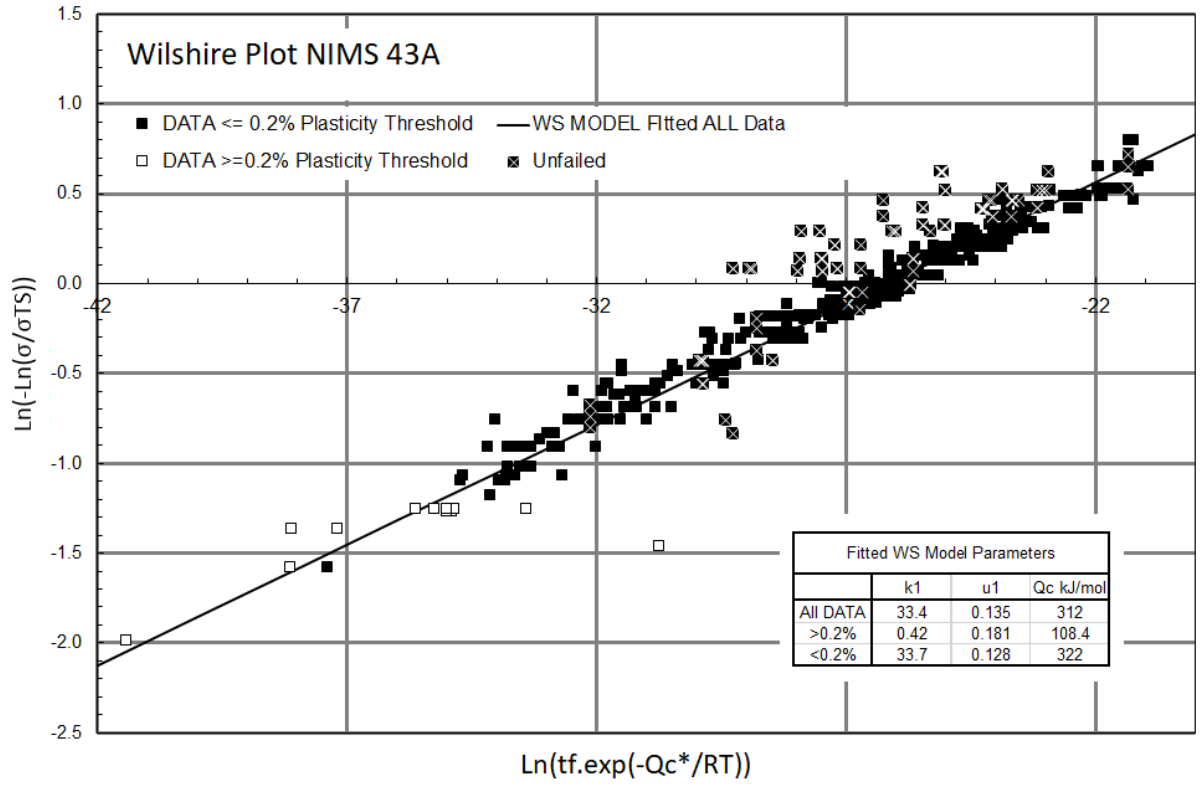

Figure 3.9: Wilshire model applied to the full data set with 'floating' Qc*. Parameters of different fits inset.

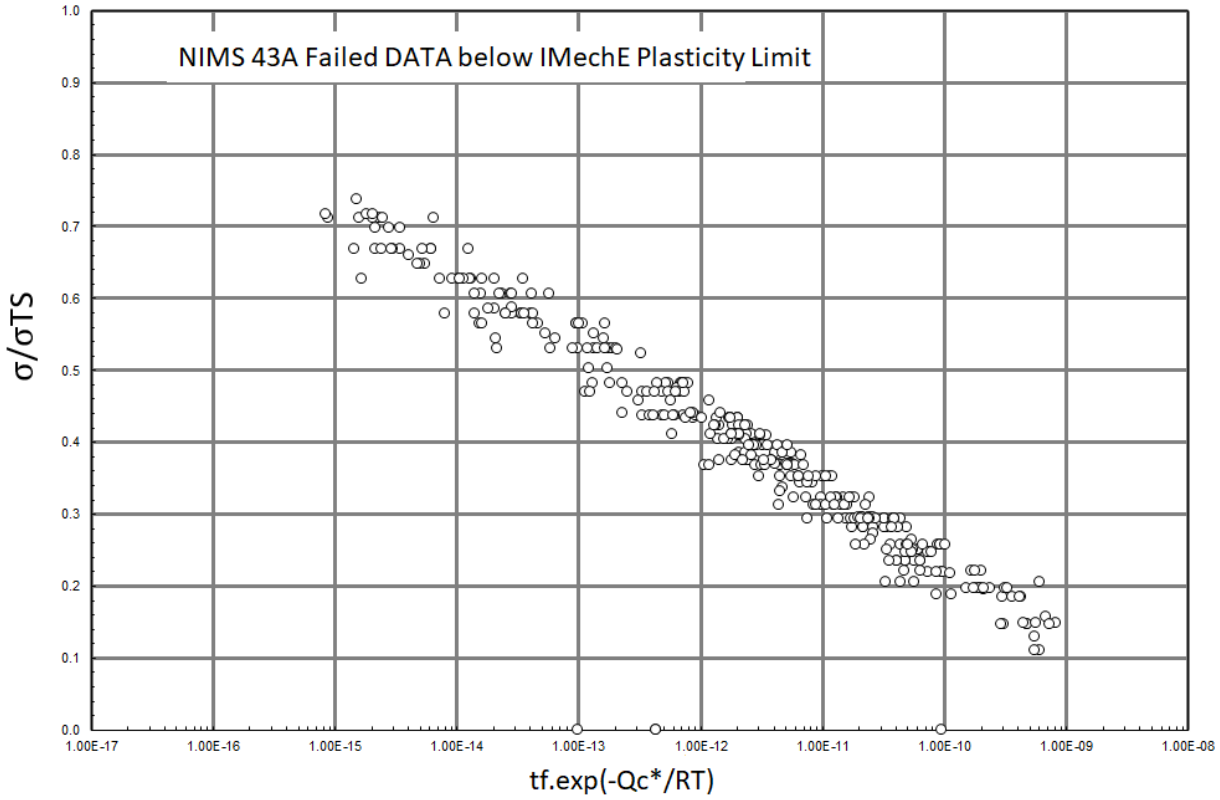

Figure 3.10: NIMS 43A culled data fitted data plotted against normalised stress.

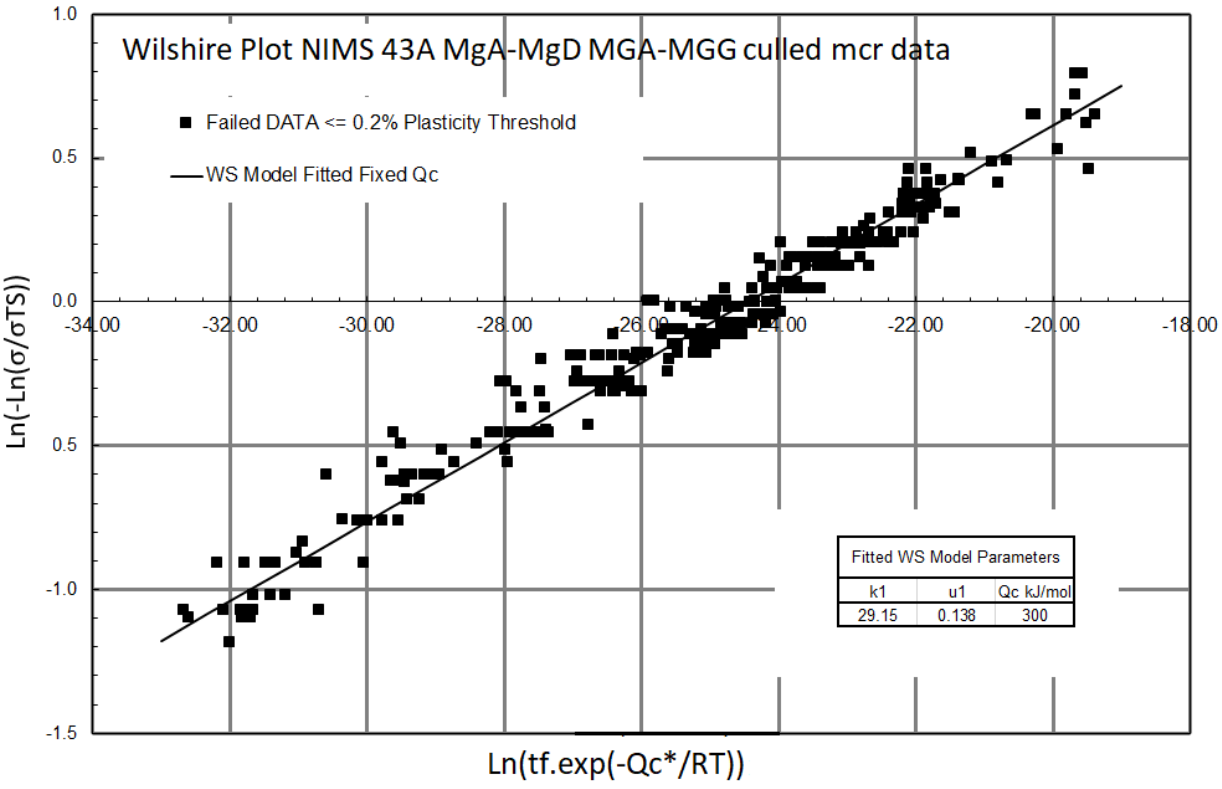

Figure 3.11: Wilshire plot culled NIMS 43A MGA-MGG MgA-MgD fixed Qc*.

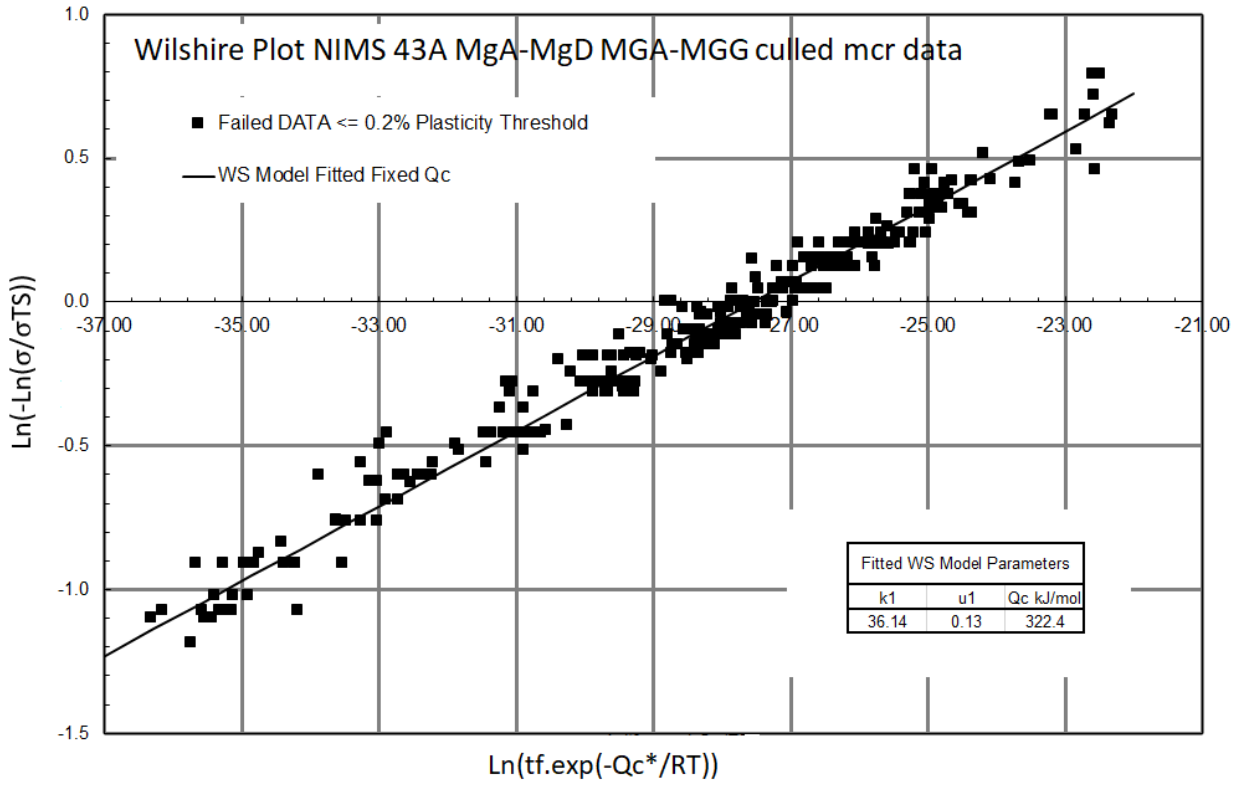

Figure 3.12: Wilshire plot culled NIMS 43A MGA-MGG MgA-MgD floating Qc*.

is shown in Figure 3.13 . The residuals appear slightly skewed $\leq 0.15\sigma/\sigma_{TS}$ and skewed opposite $\geq 0.7\sigma/\sigma_{TS}$. The residuals appear relatively randomly distributed between these limits.

3.6 Application of the Wilshire model in its modified form

Evans [124] acknowledges that the ability of the Wilshire equations to provide a meaningful activation energy is dependent upon the complexity of the MG relation and provides an alternative temperature-dependent relation. Other than the work of Evans there appear no other applications in the open literature. Even in more recent work, the basic model is used without reference to a materials MG relation parameters and thus its applicability. The analysis method appears complex and maybe that is the reason for the limited examples, here we will use the Evans modified model with the NIMS data above. Applying Eq.3.28 to the complete data set with a fixed ρ=0.84 or indeed allowing ρ to vary SOLVER does not provide a solution. Reducing the data set to just the plates (MgA-MgD) and adding tube heats provides the following until breakdown (without reference to the cast composition).

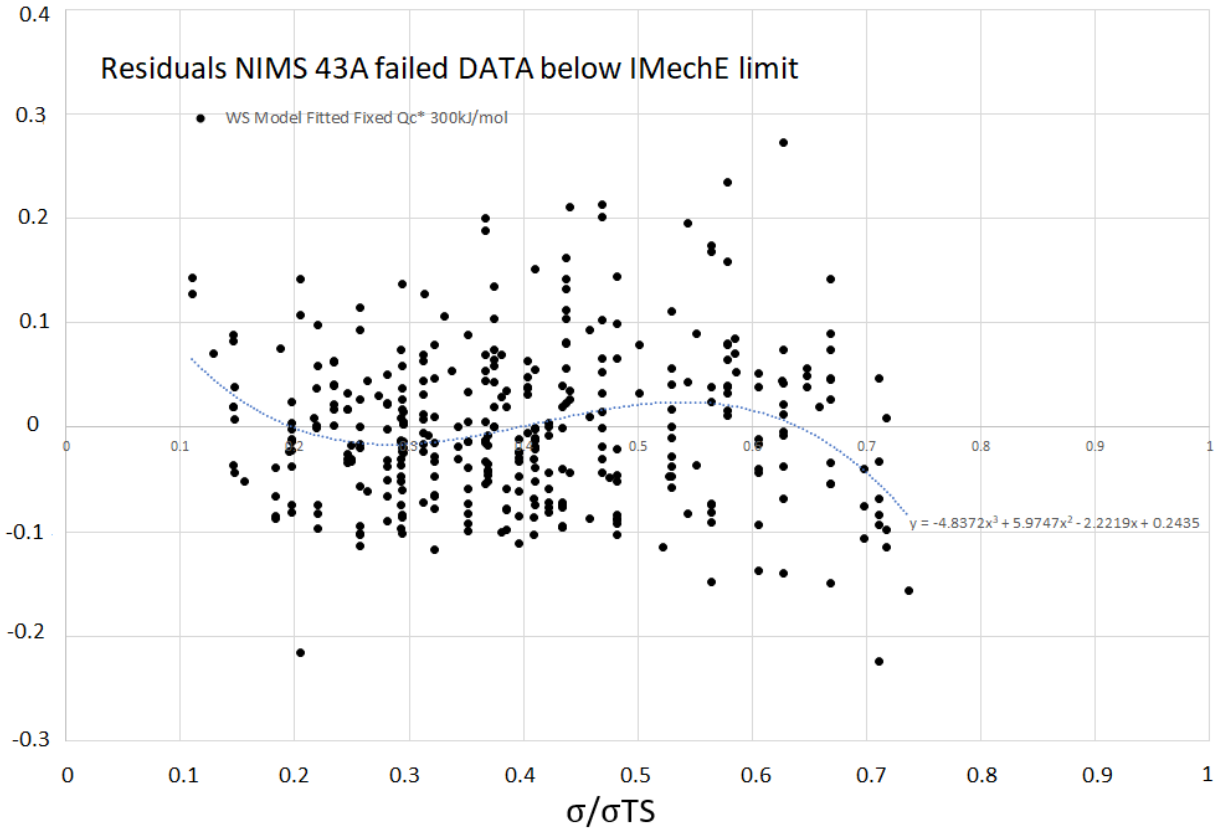

Figure 3.13: Residual of y in the Wilshire plot NIMS 43A culled fixed Qc*.

The point is the fitting of the original model appears satisfactory until the modified model highlights there may be a problem fitting across all casts and the problem appears related to the Monkman-Grant relation. To provide a context of the variation of the data for heats MgA, MgB, MgC and MgD at 600°C and 110 MPa the times to failure varied from 8.4k,10.7k, 35k and 16.7k hours respectively. The different plots for the two subsets MgA-MgD and MGA-MGF are shown in Figure 3.14 and Figure 3.15.

As already stated unfortunately elongation percentage at failure is often the only failure strain data available which is difficult to carry out with any accuracy and highly variable and scattered. Figure 3.16 shows how the available NIMS 43A elongation % at failure varies with stress and temperature. At constant temperature elongation increases approximately constantly with increasing stress. Overall, increasing temperature increases variation and such is the nature of accelerated testing this is at lower stresses. Longer test duration at a higher temperature will lead to higher true stresses during necking and subsequently more complex tertiary regions in terms of damage accumulation.

M is variable with normalised stress even in the simpler form Eq. 3.26. If the failure

Table 3.1: NIMS 43A MgA-MgD modified Wilshire model constants.

Data	ρ fixed	b	M
MgA-MgD	0.84	15139	6.47
MgA-MgD & MGA	0.84	15242	6.94
MgA-MgD, MGA-MGB	0.84	13675	5.85
MgA-MgD, MGA-MGC	0.84	10407	3.45
MgA-MgD, MGA-MGD	0.84	12185	4.14
MgA-MgD, MGA-MGF	0.84	6041	1.60
MGA-MGD	0.84	9972	2.99

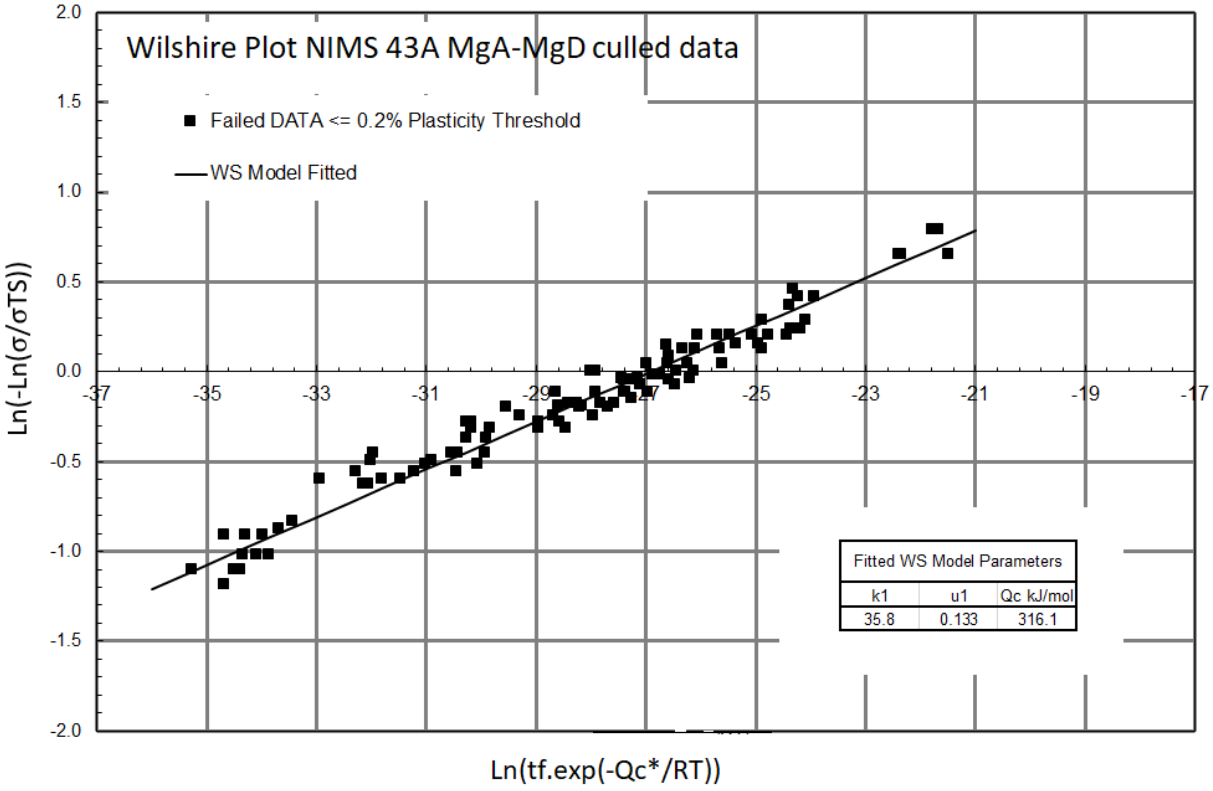

Figure 3.14: Wilshire plot NIMS 43A MgA-MgD.

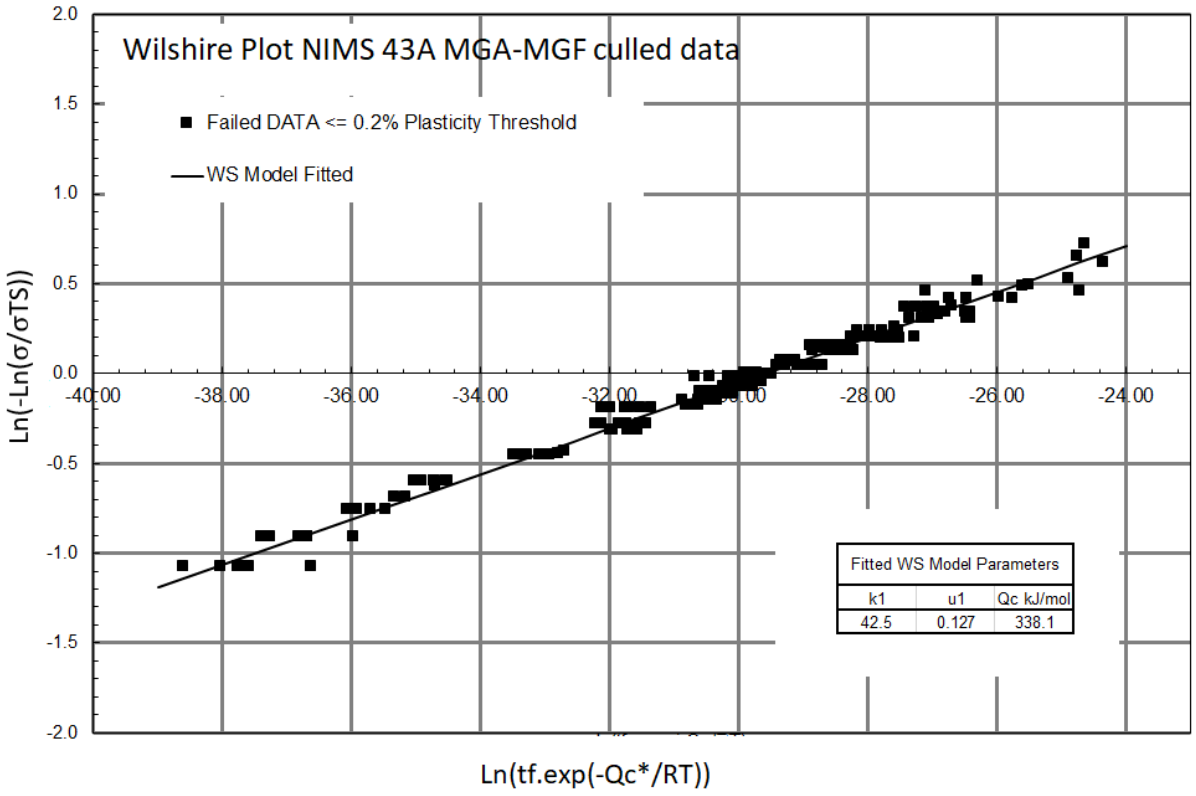

Figure 3.15: Wilshire plot NIMS 43A MGA-MGG.

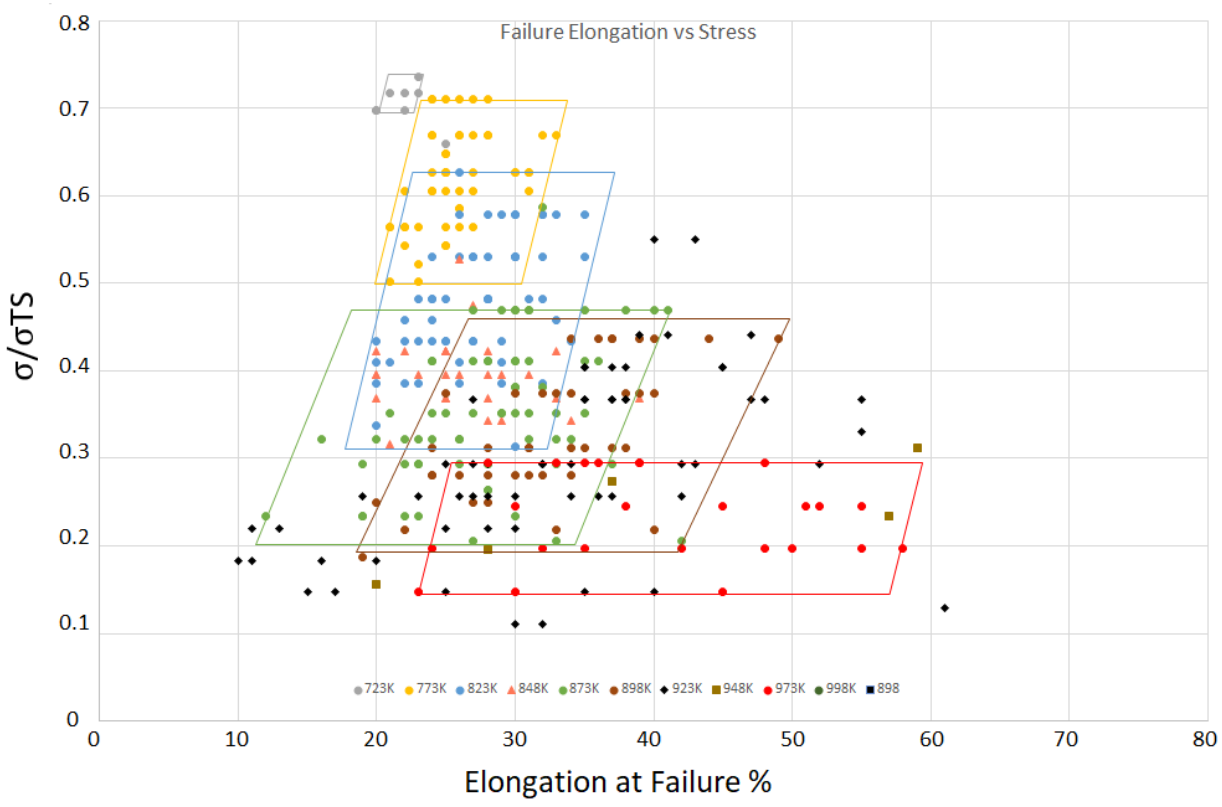

Figure 3.16: NIMS 43A MgA-MgD, MGA-MGG available elongation% at failure.

strain data is available we could utilise Eq. 3.27

$$\left[\mathrm{M}\left(\frac{\varepsilon_f}{t_f}\right)\right]^{1/\rho} = \dot{\varepsilon}_{min} \tag{3.32}$$

Indeed any of the MG relation known values of M for each test data point could be utilised which allows them to be excluded from the constants and Excel SOLVER used to fit the model to establish k and v for a variable M in this rearranged form as (using the Evans modified model notation).

$$\left(\frac{\sigma}{\sigma_{TS}}\right) = exp\left\{-k\left(\frac{M.exp(\rho Qc*/RT)}{t_f}\right)^{v/\rho}\right\} \tag{3.33}$$

With rearranging this allows t_f to be the dependent term for the linear fitting as

$$t_f = exp\left(\frac{\rho Qc*}{RT}\right)\left(-\frac{Ln(\frac{\sigma}{\sigma_{TS}})\cdot M^{\frac{-v}{\rho}}}{k}\right)^{-\rho/v} \tag{3.34}$$

In terms of fitting the model k=k, u=v/p and -p/v=-1/u. Evans claims the original model is perfectly valid for constant M and ρ=1 and the modified model is more appropriate for a temperature-dependent M [124]. NIMS 43A data sheet does provide some further limited strain data for set MgA-MgC plates. A data set culled for the IMechE limit and the available strain data limits it to 69 entries with only one below $0.15\sigma/\sigma_{TS}$. The data temperature range extends from 450-650°C. The individual tensile strengths at temperature for each heat have been used in the calculation of σ/σ_{TS} for this data. Figure 3.17 shows the variation in the Monkman-Grant constant M in both forms Eq.3.26 and Eq.3.27 with these heats for stress. There is a clear difference above and below approximately $0.5\sigma/\sigma_{TS}$. Figure 3.18 and Figure 3.19 illustrate the variation for test duration and temperature. These have implications on the ability to accurately extrapolate the time to failure and to lower temperatures from accelerated tests with this material. There is a marked increase in variation of M with test duration and in the mean value towards longer duration with the failure strain model. This may be considered a reason to limit the model fitting based on test duration at least to ascertain any difference. There is also little to suggest a temperature correction to M will make much difference for this material, however, these may change for lower temperatures and extrapolation must be with caution. The strain at minimum creep rate, ε_m exhibits a

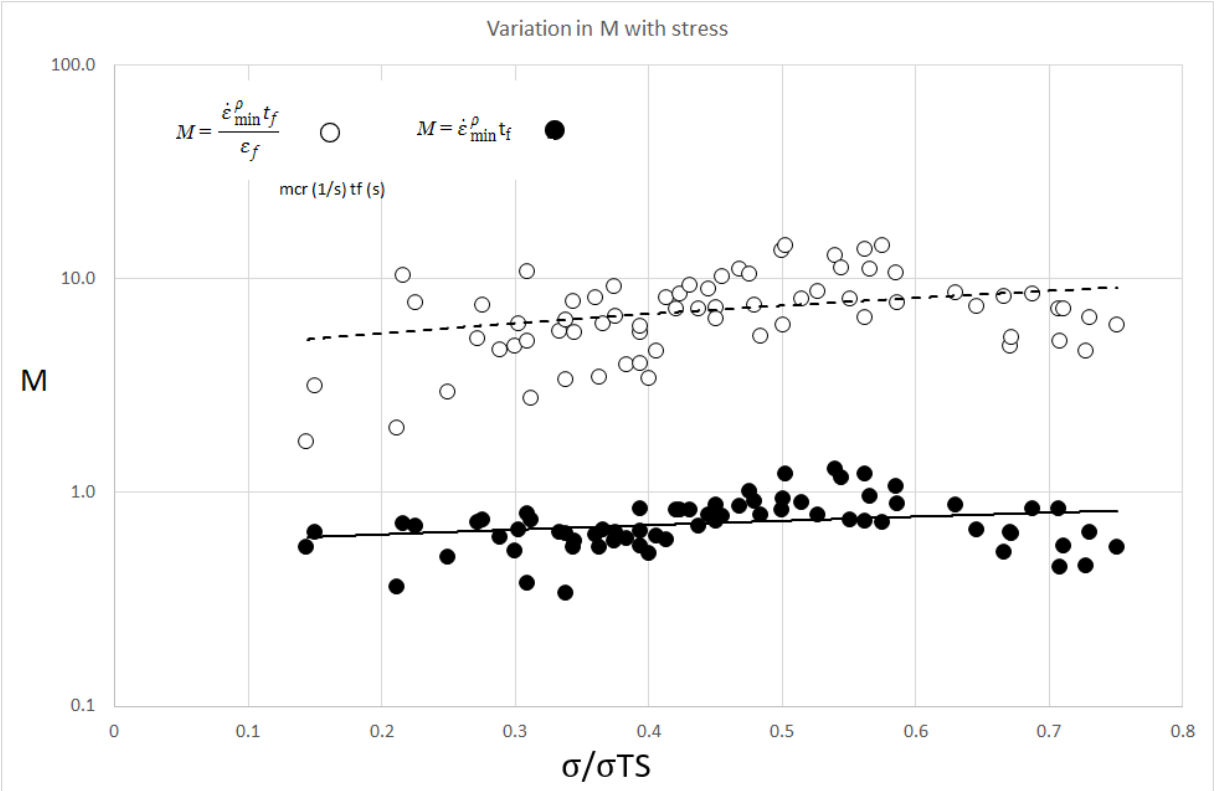

Figure 3.17: NIMS 43A MgA-MgC culled data. Variation in measured M with stress ($\rho = 0.84$).

similar stress dependence to M switching at approximately $0.5\sigma/\sigma_{TS}$ in Figure 3.20. The strain at failure appears relatively constant above $0.4\sigma/\sigma_{TS}$ (the underlying assumption of the sinh model Eq.3.22 was a constant failure strain) but below there is a sharp deflection. Elongation of failure shows a similar pattern to the strain at failure in Figure 3.21.

There is nothing to suggest the Wilshire plot is inappropriate for this data from the plot alone in Figure 3.22 (solid black). The residuals at higher stress (lower left) indicate a possible discontinuity, without a formal method it may be tempting to choose the gap for the kink. Evans [104, 124], has devised a procedure to formally locate the discontinuity by adding a dummy variable and rearranging the WE Eq.3.23, Eq.3.24 and Eq.3.25 for either the natural log of minimum creep rate, t_f or t_ε. For the t_f this is shown in Eq.3.35 where σ^* = Ln(-Ln (σ/σ_{TS}) and σ^*_{kink} is the value at which the kink occurs with a dummy variable, D such that D = 0 when $\sigma^* \geq \sigma^*_{kink}$ and D = 1 otherwise and Δ is a fitting parameter. With all values calculated over the stress range, the location of the smallest residual sum of the squares is the stress at which the kink is located

$$\ln\left(t_f\right) = \frac{-\ln\left(k_1\right)}{u} + \frac{1}{u}\sigma^* + Q^*_c(1/RT) + \Delta\left[\sigma^* - \sigma^*_{\text{kink}}\right]D \tag{3.35}$$

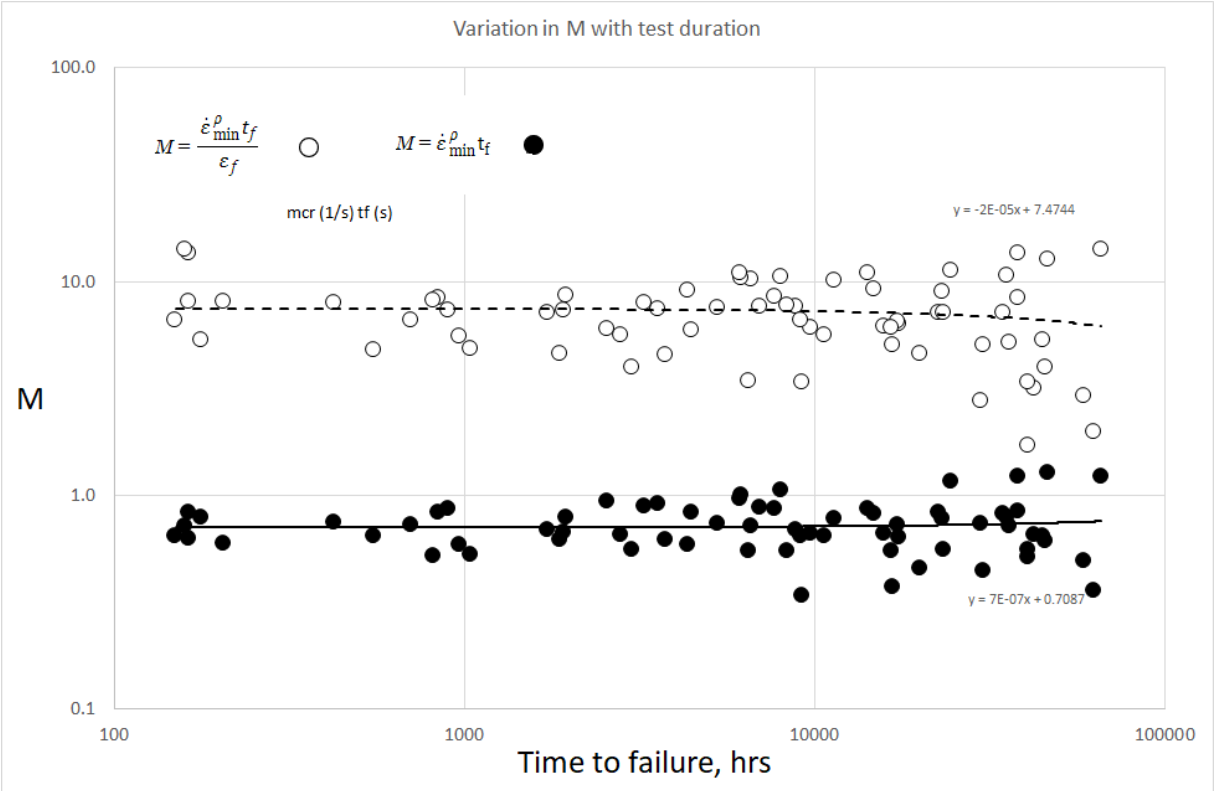

Figure 3.18: NIMS 43A MgA-MgC culled data. Variation in measured M with test duration ($\rho = 0.84$).

Using this procedure provides

$$Ln(t_f) = -30.566 + 8.333\sigma* + 342570(1/RT) - 5.204\,[\sigma* - 0.91]\,D \tag{3.36}$$

Which identifies the location of the discontinuity at $0.67\sigma/\sigma_{TS}$ [Ln(-Ln (-0.91)] and the fitting parameters as Qc* 342.6 kJ/mol. k1 = 39.17 and u = 0.120 which are in good agreement with the fitted parameters shown in Figure 3.22. These are to the original form Eq.3.24 and need adjusting according to the modified model Eq.3.29, Eq.3.30 and Eq.3.31 if the specific values are required. Evans found the kink location remained consistent regardless of whether t_f or minimum creep rate data was used. The location suggests that the IMechE threshold may be too high for this material and the data in this 'region' at > $0.67\sigma/\sigma_{TS}$ is a continuation of that culled.

The full data set provides the parameters for the modified Wilshire model suggested by Evans Equation 27 in Table 8. This would provide an adjusted Qc* according to Equation 30 (Qc* + b)/ϱ = 429.2 kJ/mol.. Refitting with this fixed would then provide the other fitting

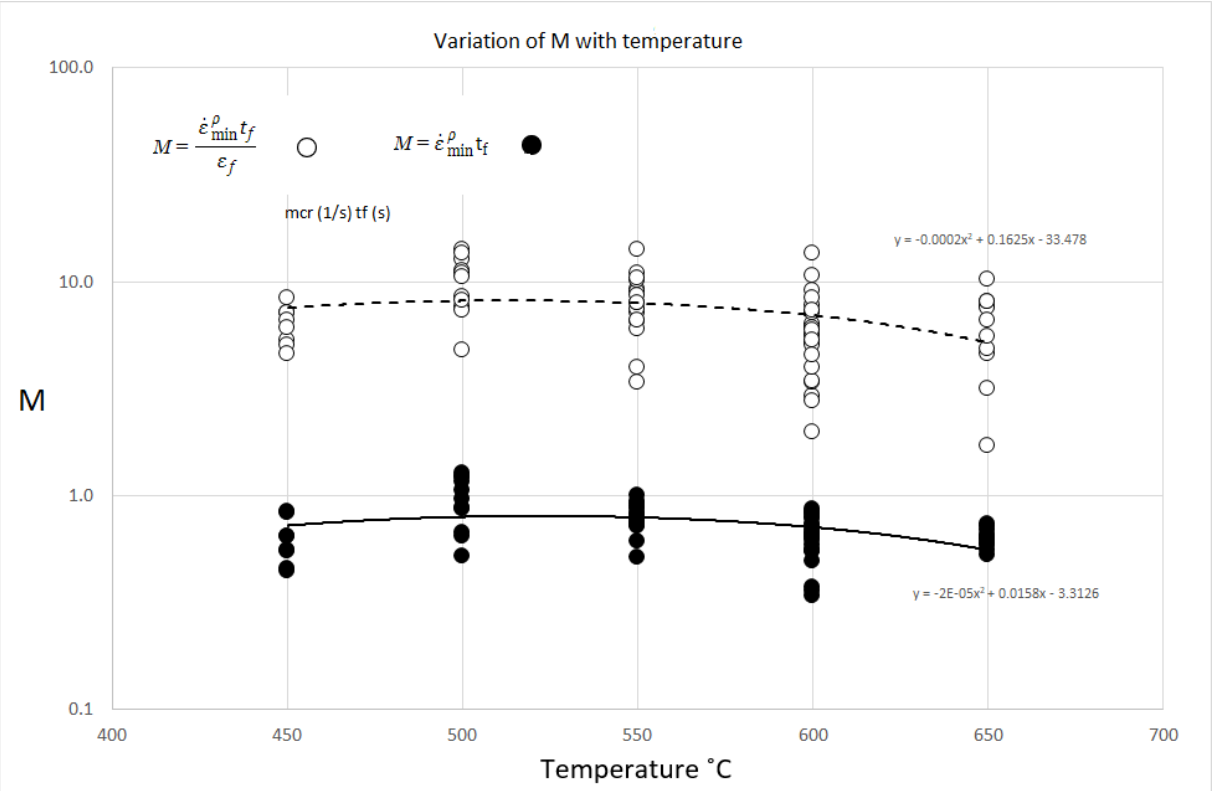

Figure 3.19: NIMS 43A MgA-MgC culled data. Variation in measured M with test temperature ($\rho = 0.84$).

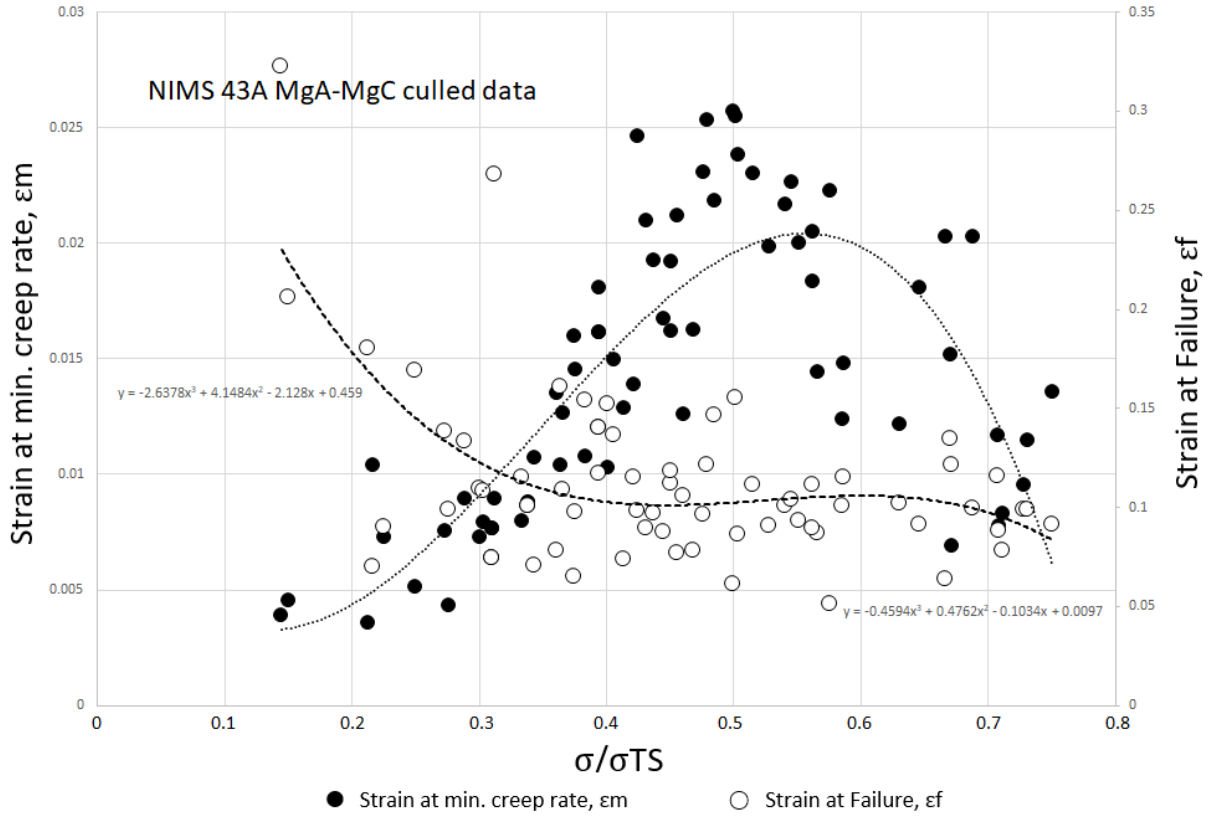

Figure 3.20: NIMS 43A MgA-MgC culled data. Strain at minimum creep rate and failure.

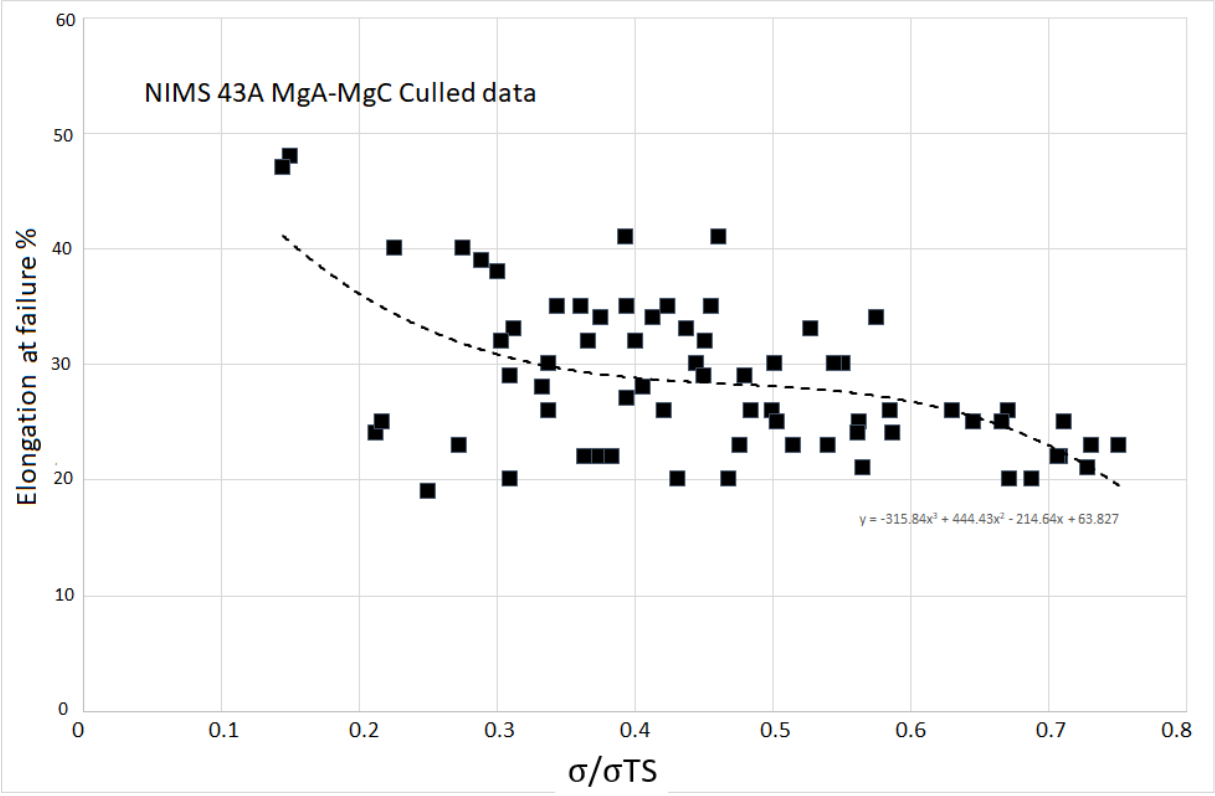

Figure 3.21: NIMS 43A MgA-MgC culled data. Elongation % at failure.

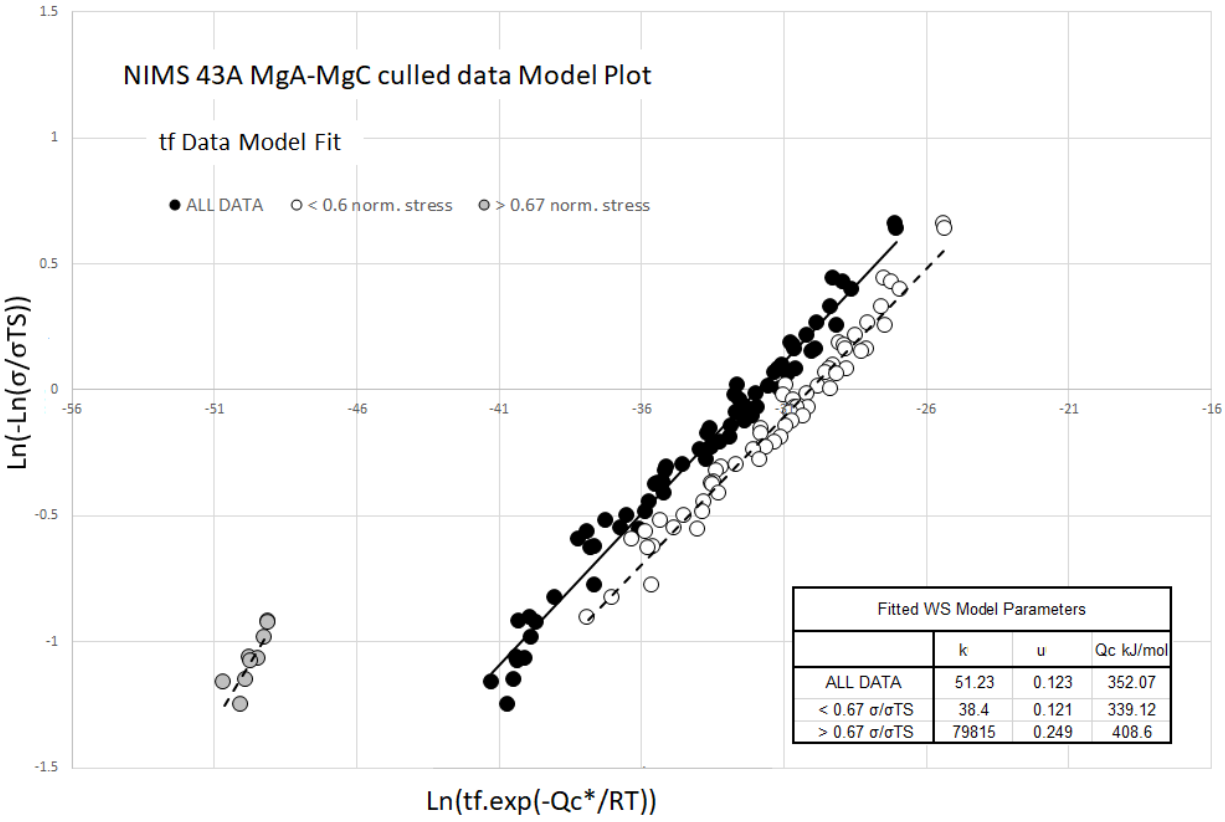

Figure 3.22: NIMS 43A MgA-MgC culled data set Wilshire plot (t_f) and fitting parameters above and below identified kink at $0.67\sigma/\sigma_{TS}$with a floating Qc*.

Table 3.2: NIMS 43A MgA-MgC culled data modified Wilshire Model fitting parameters for failure strain data.

	ρ(fixed)	b	M
MgA-MgC Full Data	0.84	17963	9.06

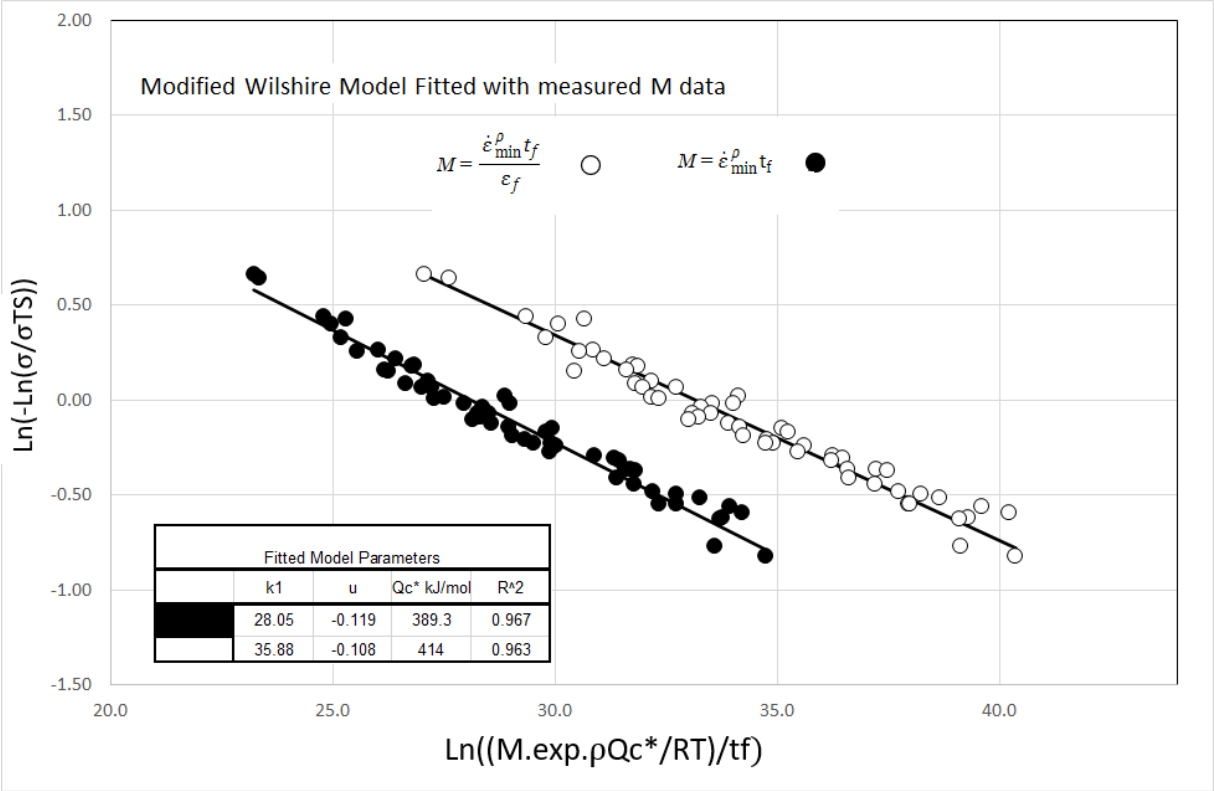

Figure 3.23: Modified Wilshire model to include measured of M using Eq.3.34.

parameters.

The plots so far have fitted the Evans modified model to the data. In Figure 3.23 a modified model with measured values of M using Eq.3.33 and Eq.3.34 has been fitted to the data for the two MG relation constant M Eq,3.26 and Eq.3.27 with a fixed value of ρ= 0.84 and a floating Qc* to the same failure data. Both fit the data well with a significant increase in the apparent activation energy though not as high as that adjusted from the Evans modified model.

These models will be revisited in Section 3.8 to derive a no-creep temperature from the data.

3.7 An alternative to the Wilshire Equations

The fundamental assumption of the Wilshire-Scharning model is that the Monkman-Grant relation is appropriate to describe the relationship between the minimum creep rate and the time to failure. In its basic form, this is a single constant, M and where this is temperature dependent or the exponent ϱ is found not to be unity an additional constant is added to a modified model. The ability of either to describe a full creep curve is limited. At present improvements in the predictive capability may be addressed with the region splitting technique [118] or the modified model approach [124]. If there is enough data in the stress-temperature region of interest, to extrapolate beyond the test temperature caution is required. As discussed in Chapter 1 more recent developments have been toward characterising the whole creep curve shape. For the WE this has been limited to 'regenerating' full curves for a normalised strain when the complete data is available. In the function of relating the time to failure with the minimum creep rate, the measured parameters are limited to minimum creep rate, time to failure and strain at failure. These could include the time and strain to minimum creep rate in characterising the full curve shape. Abe [128] analysed the NIMS 43A data for Grade 91. He concluded that for Grade 91 the variation in the time to failure at the same minimum creep rate is due to variation in the strain and time at which the minimum creep rate occurs as illustrated in Figure 3.24. The findings include empirical relationships which could be used to predict more accurately the time to failure from the minimum creep rate. These are given in Eq.3.37. For the same transient creep region the time to minimum creep rate, t_m and the strain at minimum creep rate ε_m remain unchanged as do the time and strain at failure t_f and ε_f. The time to failuret_f is proportional to t_m with the constant of proportionality g depending on the stress. The mcr is inversely proportional to t_m and proportional to ε_m .

The two empirical relations include parameters of interest - the t_f and the minimum creep rate linked by the time to mcr t_m. By combining and rearranging for $t_m = t_f/g$ the following, Eq.3.38 includes the parameters of interest and offers an alternative to the MG relation.

$$\dot{\varepsilon}_{\min} = 0.54\,(\varepsilon_{\mathrm{m}}/t_{\mathrm{m}}) \quad t_f = g t_{\mathrm{m}} \tag{3.37}$$

$$\frac{B.g.\varepsilon_m}{t_f} = \dot{\varepsilon}_{min} \tag{3.38}$$

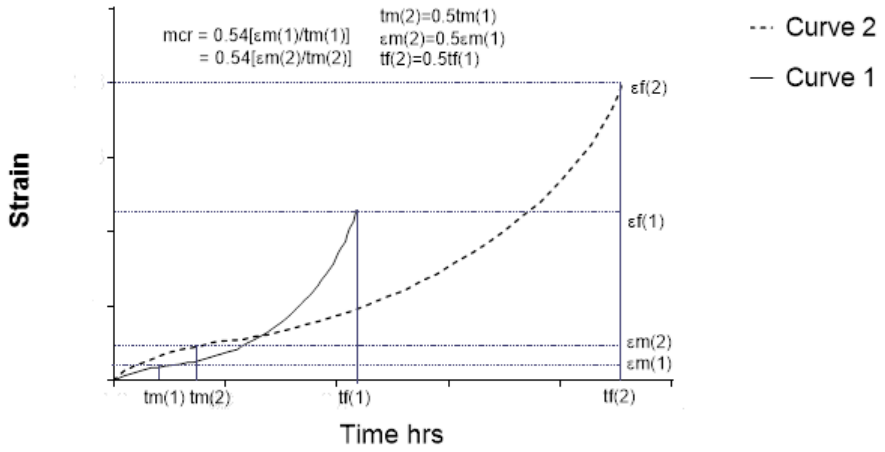

Figure 3.24: Schematic relationship between the time to mcr,t_m and strain at mcr,ε_m with the time to failure,t_f at a constant mcr [5].

For Grade 91 the constant of proportionality B = 0.54. This requires additional measured parameters, the strain at mcr, ε_m and g which is the ratio of t_f/t_m shown in Figure 3.25 for the MgA-MgC data set. With a material-specific constant of g, this offers the opportunity to extrapolate the time to failure from minimum creep rate data.

Combining this with the normalised stress power-law equation in place of the MG relation allows the time to failure to be the dependent variable for linear regression.

$$\frac{B.g.\varepsilon_m}{t_f} = \dot{\varepsilon}_{min} = A^* \exp\left(-\frac{Q_C^*}{RT}\right)\left(\frac{\sigma}{\sigma_{TS}}\right)^n \tag{3.39}$$

Replacing M with $0.54g\varepsilon_m$ provides an alternative relation for Grade 91 which can be re-arranged similar to Eq.3.8 but leaving the minimum creep strain ε_m within x

$$y = \frac{\sigma}{\sigma_{TS}} \quad x = Ln\left[\frac{1}{0.54g\varepsilon_m} t_f \exp\left(-\frac{Q_c^*}{RT}\right)\right] \tag{3.40}$$

$$Ln(y) = -mx + c \tag{3.41}$$

where m = 1/n and c = m*Ln(1/A). This could then be fitted in the same way as the Wilshire model. For the data sets MgA-MgC the required time-strain data is available in the public domain and the model has been applied with time to failure t_f as the dependent variable.

$$\frac{\sigma}{\sigma_{TS}} = \exp\left(-k\left[\frac{1}{0.54g\varepsilon_m} t_f \exp\left(-\frac{Q_c^*}{RT}\right)\right]^u\right) \tag{3.42}$$

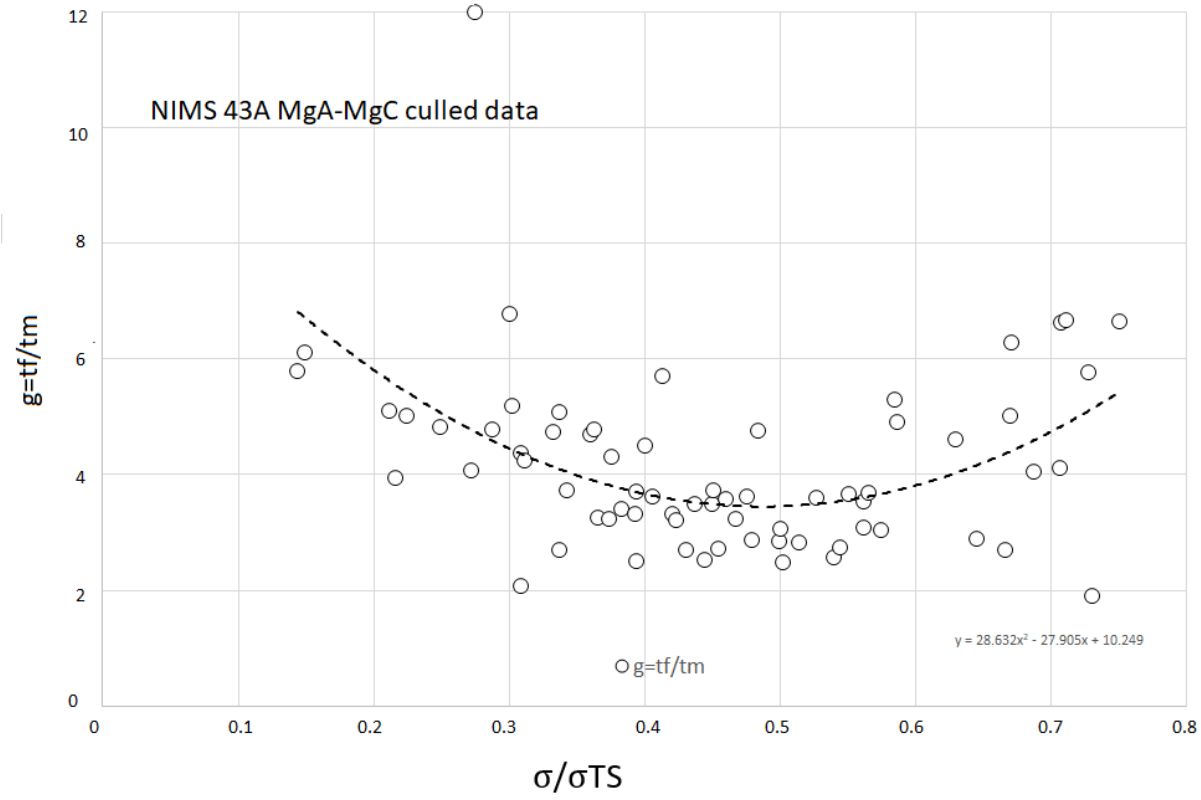

Figure 3.25: g= tf/tm for NIMS 43A MgA-MgC plotted against normalised stress.

$$t_f = \frac{\left[-\frac{1}{k} Ln\left(\frac{\sigma}{\sigma_{TS}}\right)\right]^{\frac{1}{u}}}{\frac{1}{0.54 g \varepsilon_m} \exp\left(\frac{-Qc*}{RT}\right)} \tag{3.43}$$

This provides the plot with a floating Qc* and fitting parameters in Figure 3.26, the value of Qc* is considerably higher.

To address an alternative time to specific strain model Eq.3.25 the relations in Eq.3.37 and Eq.3.38 need to be established for that strain such that for example for $t_{0.2\%}/t_m = g_{0.2}$

$$\frac{0.54\, g_{0.2} \varepsilon_m}{t_{0.2}} = \dot{\varepsilon}_{min} \tag{3.44}$$

and combining this with the normalised power-law equation to give

$$t_{0.2} = \frac{\left[-\frac{1}{k} Ln\left(\frac{\sigma}{\sigma_{TS}}\right)\right]^{\frac{1}{u}}}{\frac{1}{0.54 g_{0.2} \varepsilon_m} \exp\left(\frac{-Qc*}{RT}\right)} \tag{3.45}$$

If this is some protracted length of time, as the no-creep temperature it requires extensive extrapolation for the ε_m and t_m to be of practical use. To calculate a temperature for 200k hr

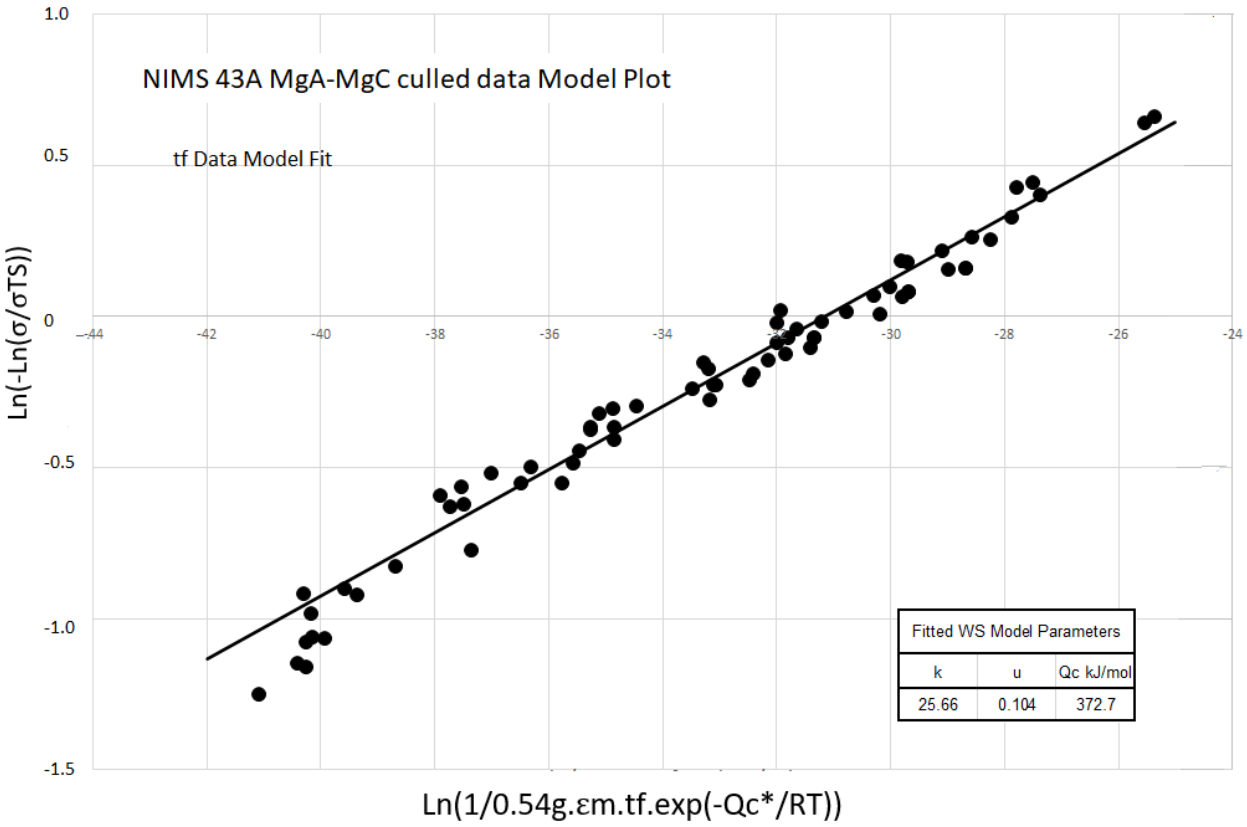

Figure 3.26: NIMS 43A MgA-MgC culled data (<0.67σ/σ_{TS}) model fitting Eq.3.42 with floating Qc*.

time to 0.2% strain would require estimating values for the time to and strain at minimum creep rate that will never be experienced in test or in service and > x300 the data. The model is more appropriate over stress-temperature combinations where the minimum creep rate data can be collected. This may be useful with some historical data. There is a need for comprehensive full curve data so generously provided to date only by the National Institute of Material Science, Japan. Other materials will need to establish the relations in Eq.3.37 and Eq.3.38 from similarly comprehensive test data to show they are equally applicable before the model can be of more practical use.

3.8 The No-Creep Temperature Limit T_{NC}

If, for comparison purposes, the same reference stress of 0.56Rm, T is used as the MATTER Project (the European Standards notation of Rm, T = σ_{TS} the ultimate tensile strength (MPa) at a specified temperature, T). For context, this data set is of test duration up to ∼65k hours failure where the times to 0.2% strain are limited to < ∼2000 hours (only 3 above 1000 hours) in comparison to the time of interest of 200k hours for the no-creep temperature, so are extrapolated at a minimum of ∼x3 failure. The lowest data is collected at 450°C so temperature extrapolation is > 35°C. The other point to note is the material composition; the NIMS data relates specifically to Japanese 9Cr-1Mo-V-Nb ASME SA-387/SA-387M Grade 91(MgA-MgC) and ASME SA213M Grade T91 (MGA-MGG). As has already been mentioned few materials have the extensive test data of Grade 91 in the public domain. For materials of constant M and exponent of unity, the original model should be adequate in providing a no-creep and negligible creep temperature with rearrangement. The original and modified models have the same structure and, as already discussed, it is only the value of the constants that change. The formalised identification of kinks is important to accurately define the region and the appropriate fitting parameters so the Evans method above should be adopted. Plotting a negligible creep curve for the Wilshire Model in its original form can be achieved by rearranging for temperature. With the time to specific strain, $t_{0.2\%}$ set at 200k hours provides the no-creep limit, T_{NC}. It should be noted the temperature is directly proportional to the chosen value of Qc*.

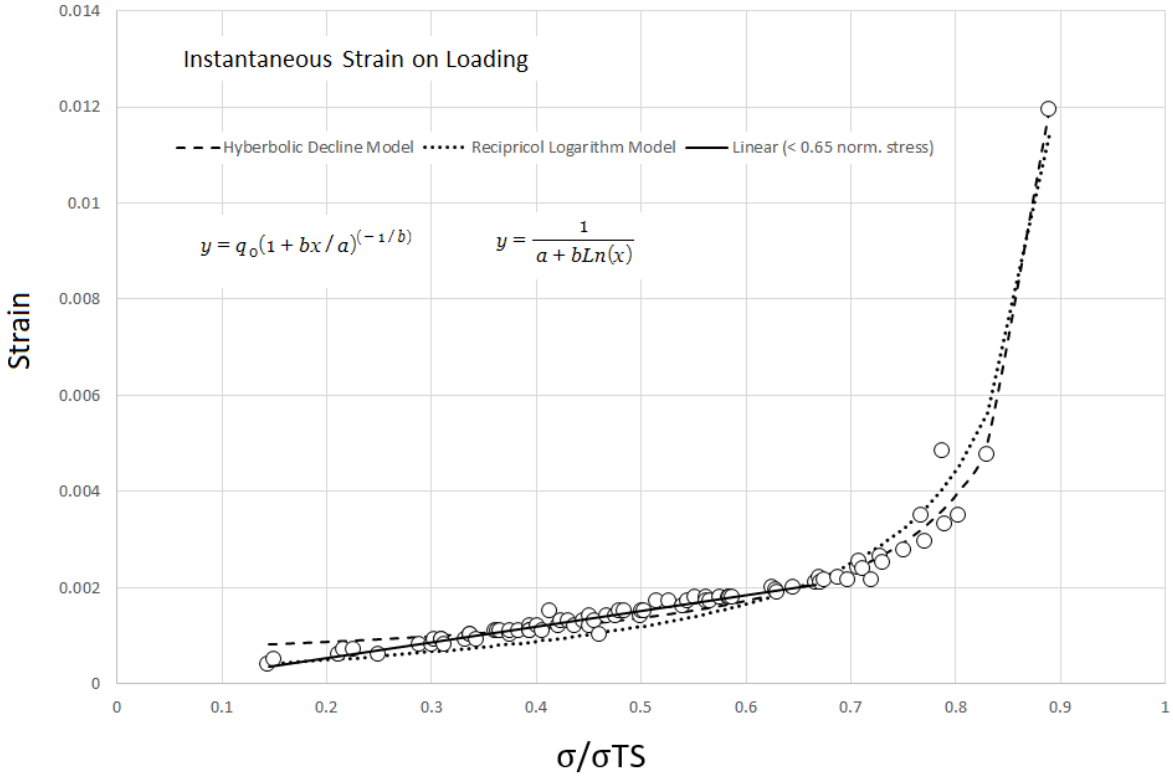

Figure 3.27: NIMS 43A MgA-MgC ALL DATA Instantaneous strain on loading.

$$T = \frac{-Qc*}{R \cdot Ln\left(\frac{\left[-\frac{1}{k0.2}Ln\left(\frac{\sigma}{\sigma_{TS}}\right)\right]^{\frac{1}{u0.2}}}{t_{0.2}}\right)} \tag{3.46}$$

The above models have all been fitted using a data set culled at the IMechE stress-temperature limit for instantaneous 0.2% strain on loading. Figure 3.27 shows the measured instantaneous strain for all the data (MgA-MgC) which has minimum creep rate data. The instant 'plasticity' over the full stress range appears well represented by a hyperbolic decline Eq.3.47 or reciprocal logarithm Eq.3.48 model which indicates the 0.2% threshold is at $0.65\sigma/\sigma_{TS}$. This confirms the kink identified by the Evans method Eq.3.35 at $0.67\sigma/\sigma_{TS}$; the data above exceeds the threshold and should have been culled while the data below is well represented by a linear model. Unfortunately, this eliminates all test data at 450°C which increases the temperature extrapolation to around 100°C which would be considered excessive. These were considerably accelerated with $t_{0.2\%} < 55$ hours. Nonetheless, we will proceed to establish a no-creep temperature with this in mind.

$$y = q_0(1 + bx/a)^{(-1/b)} \tag{3.47}$$

where q0 = 7.0397E-04, a = -1.085 and b = 1.176.

$$y = \frac{1}{a + bLn(x)} \tag{3.48}$$

where a = -6.559E+01 and b = -1.30716E+03.

The original Wilshire model fitted to the $t_{0.2\%}$ data below $0.65\sigma/\sigma_{TS}$ is shown in Figure 3.28 with a floating Qc*. The plot indicates a possible discontinuity with the residuals lower left and the Evans method Eq.3.35 reveals the data may be better represented by two separate regions on either side of a kink at $0.49\sigma/\sigma_{TS}$ and shown individually in Figure 3.29. This limits the region containing the stress of interest to 16 data points. The fitting parameters for the Evans modified model are contained in Eq.3.49. In physical terms, a possible interpretation of the kink in the $t_{0.2\%}$ data is a change in the dominant deformation mechanism above and below the $0.49\sigma/\sigma_{TS}$ stress which is not evident in the model fit of the failure data but was noted for a change in the strain at mcr in Figure 3.20. Figure 3.30 shows a significant change in the relationship of the $t_{0.2\%}$ strain and the time to mcr compared to the t_f in Figure 3.25 from this normalised stress.

$$Ln(t_{0.2}) \;=\; -30.001 + 9.669\sigma* + 294660(1/RT) + 5.257\,[\sigma* - 0.340]\,D \tag{3.49}$$

Various model fitting parameters are shown in Table 3.3 with the corresponding no-creep temperature and there is a 95% probability the T_{NC} is within the prediction intervals according to the models. Included are models fitted with a fixed Qc* as used by Wilshire & Scharning and from the time to failure data above for comparison. The fixed Qc* values are broadly in agreement with Holmström using a fixed Qc* of 300 kJ/mol. on European Grade 91 Tube (X10CrMoVNb9-1) and the classical limit of 375°C. However, fitting to a statistically derived region with a floating Qc* provides the lowest value and the 95% PI indicates it is lower than the classical limit. This material belongs to a group of creep-resistant materials and would be expected to easily exceed the classic limit which also covers the C-Mn and low alloy materials. This highlights the problem of allowing Qc* to be a quasi-constant fitting parameter.

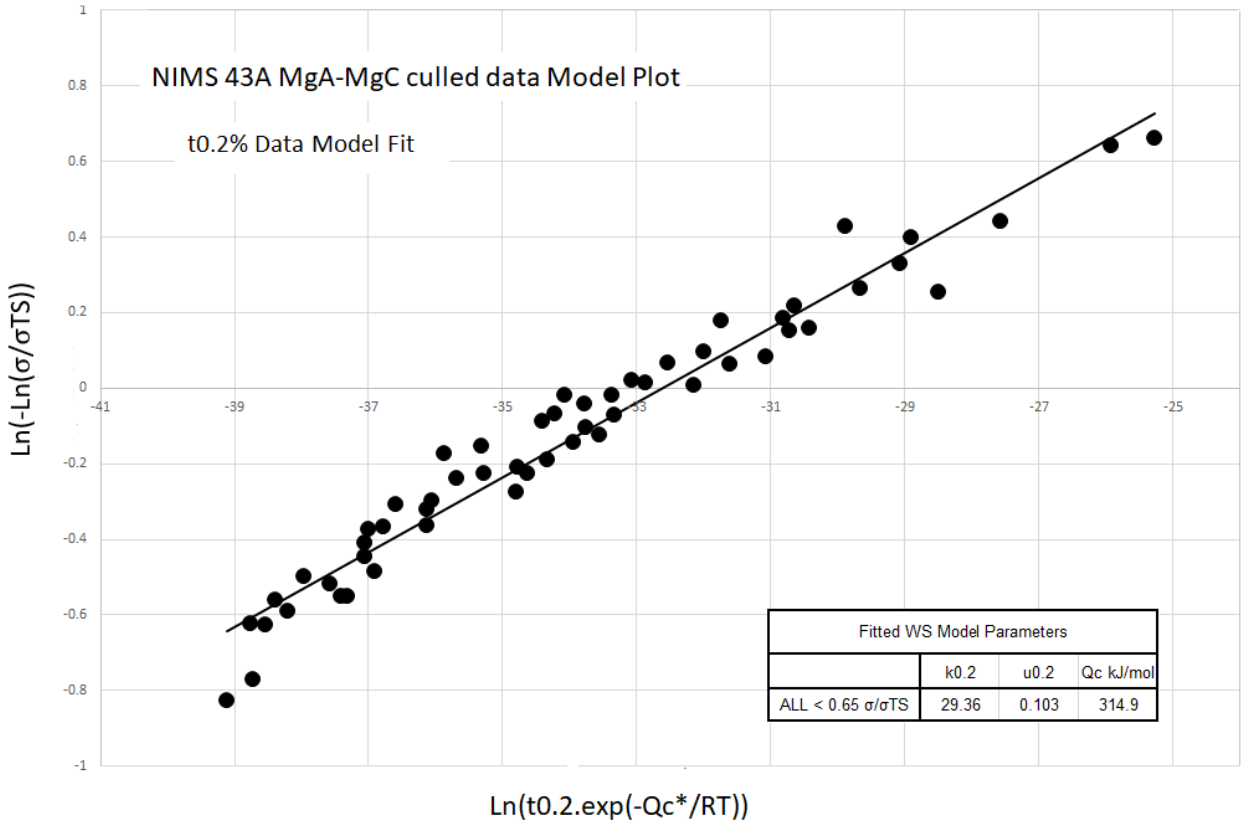

Figure 3.28: NIMS 43A MgA-MgC original Wilshire model fitted to the t0.2% ALL DATA $< 0.65\sigma/\sigma_{TS}$.

Table 3.3: Original Wilshire model fitting parameters for t0.2% data, regions and T_{NC} for $0.56\sigma/\sigma_{TS}$.

Data	Qc*kJ/mol.	k0.2	u0.2	T_{NC}(°C)	95%PI	R^2
ALL $<0.65\sigma/\sigma_{TS}$	300(Fixed)	26.2	0.107	370.1	(353.5,387.5)	0.94
ALL $<0.65\sigma/\sigma_{TS}$	322(Fixed)	30.94	0.102	378.9	(363.1,395.5)	0.94
ALL $<0.65\sigma/\sigma_{TS}$	314.9	29.37	0.103	376.2	(360.2,393)	0.96
0.49-$0.65\sigma/\sigma_{TS}$	281.2	400.5	0.200	364.9	(355.6,374.5)	0.80
0.49-$0.65\sigma/\sigma_{TS}$	300(Fixed)	401.68	0.184	373	(363.7,382.5)	0.80

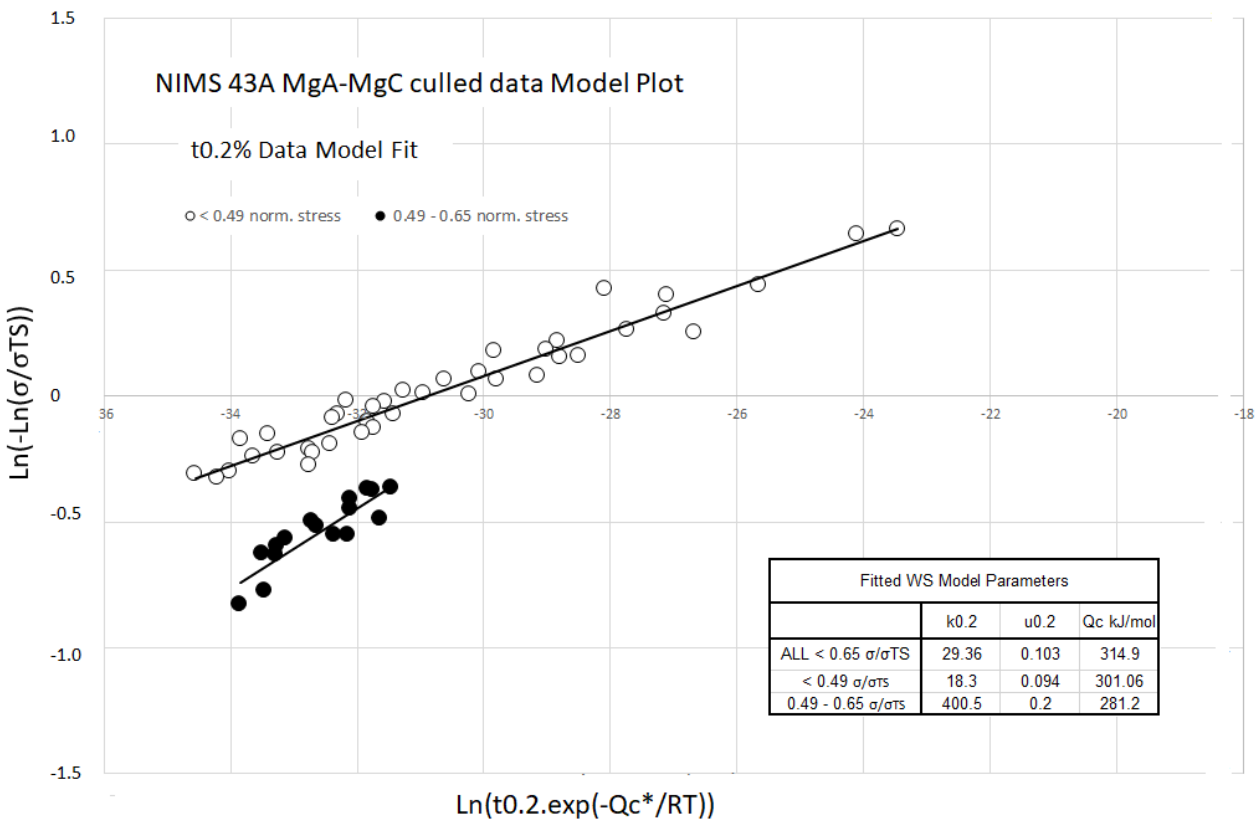

Figure 3.29: NIMS 43A MgA-MgC original Wilshire model fitted to the t0.2% data either side of 'kink' (<0.49σ/σ_{TS} and 0.49-0.65σ/σ_{TS}).

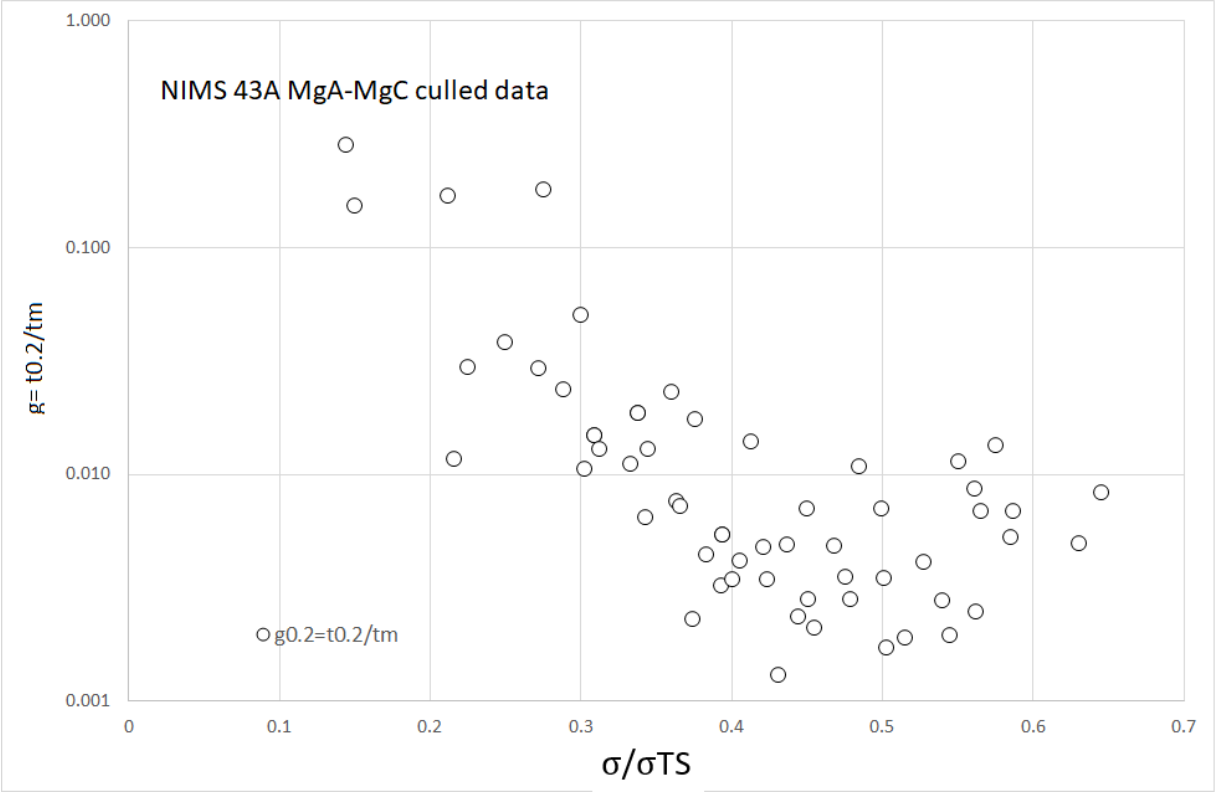

Figure 3.30: g0.2= t0.2/tm for NIMS 43A MgA-MgC plotted against normalised stress.

Table 3.4: NIMS 43A MgA-MgC culled data modified Wilshire mode fitting parameters for 0.2% strain data.

Data	ρfixed	b0.2	M0.2
MgA-MgC 0.2% <0.65σ/σ_{TS}	0.84	82441.7	186.6

It has already been shown the material does not have a constant M and exponent of unity and thus a modified model should be more appropriate. For the modified model Evans [124] suggests ρ like M may be strain-dependent and a different version of the MG relation is appropriate

$$\dot{\varepsilon}_{\min}^{\rho_{0.2}} t_{0.2} = M_{0.2} e^{\frac{-b}{RT}} \tag{3.50}$$

$$(\sigma/\sigma_{TS}) = \exp\left\{-k_2 M_{0.2}^{v/\rho_{0.2}} \left[t_{0.2} \cdot \exp\left(\left[b-\rho_{0.2}\right] Q_c^*/RT\right)\right]^{-v/\rho_{0.2}}\right\} \tag{3.51}$$

In terms of the original model instead of Qc* the estimate is of (b - ρ0.2)Qc*, and

$$u = -v/\rho_{0.2}; k_1 = k_2 M_{0.2}^{v/\rho_{0.2}} \tag{3.52}$$

Rearranging for Temperature, T

$$T = \frac{b_{0.2} - \rho_{0.2} Qc*}{R \cdot Ln\left(\frac{\left[-\frac{1}{k1} Ln\left(\frac{\sigma}{\sigma_{TS}}\right)\right]^{\frac{1}{u}}}{t_{0.2}}\right)} \tag{3.53}$$

For the Evans modified form, Eq.3.51, SOLVER provides the fitting parameters for the full data < 0.65σ/σ_{TS} in Table 3.4. For simplicity, ρ has been left at 0.84. According to Evans the derived Qc* in Eq. 3.49 (294.7 kJ/mol.) should be replaced by Qc* adjusted for the strain derived values of b0.2 and ρ0.2 with Eq.3.31 ; Qc* = (294.7 + 82.44)/0.84 = 449 kJ/mol. This is slightly different to the adjusted value from the failure data in Section 2.6, 429.2 kJ/mol.. Table 3.5 provides the parameters on refitting with a constant Qc* and the temperature T_{NC} for the modified model adjusted Qc* all data < 0.65σ/σ_{TS} and 0.49 - 0.65σ/σ_{TS}. For comparison, the failure data fitting parameters are included. Figure 3.31 shows the modified model plot.

The values of T_{NC} are significantly different fitting the Evans modified model compared to the original Wilshire Equation. A T_{NC} of **416°C** is in general agreement with Holmström

Table 3.5: Refitting with the adjusted Qc* fitting parameters.

Data	Qc* kJ/mol.	k0.2	u0.2	T_{NC}(°C)	95%PI	R^2
ALL<0.65σ/σ_{TS}	449.0	64.03	0.081	415.5	(398.6, 433.4)	0.95
0.49<0.65σ/σ_{TS}	449.0	423.8	0.114	416.0	(398.4, 434.6)	0.83
0.49<0.65σ/σ_{TS}	429.2	80.45*	0.090*	412.0	(394.0, 431.0)	0.86

* fitting parameters k1 and u1

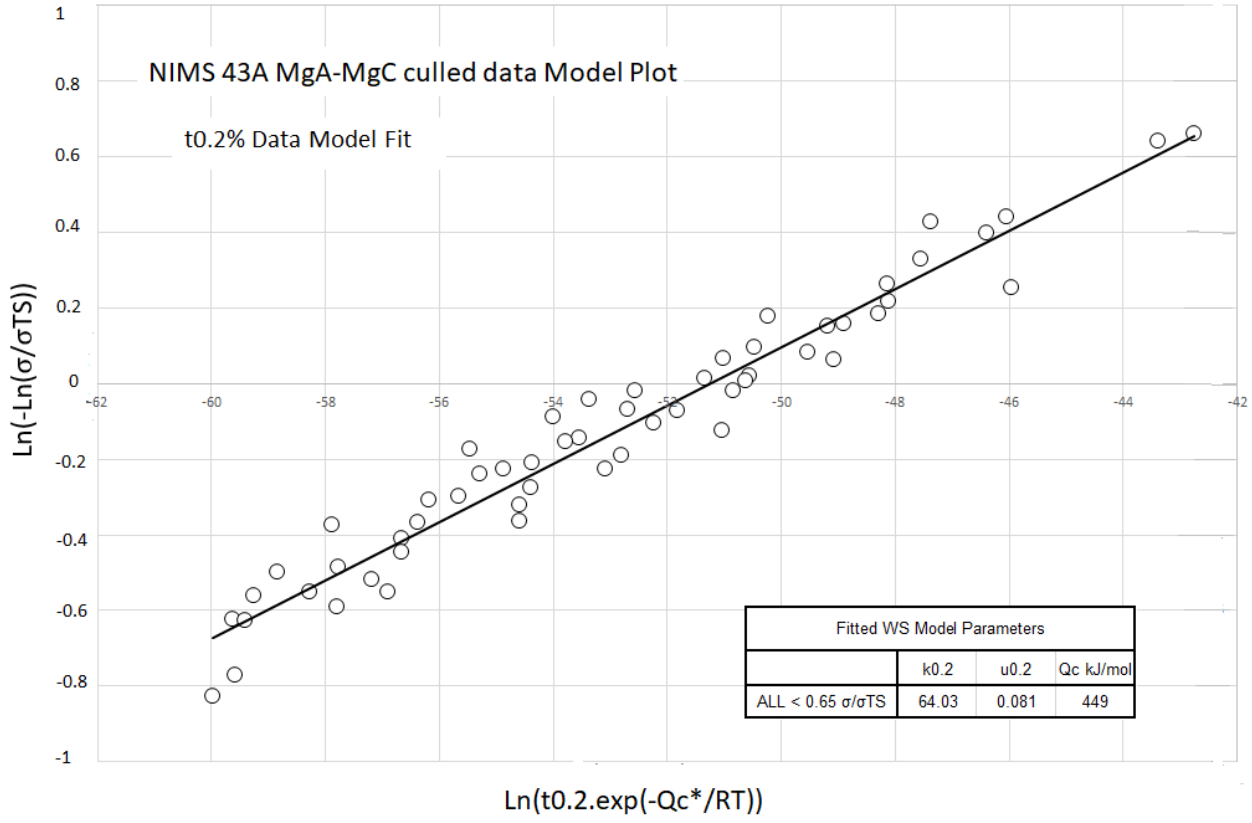

Figure 3.31: Modified model fitting to all data <0.65σ/σ_{TS}.

et al. [129] for X10CrMoVNb9-1 Grade P91 steel using a factored proof stress for normalisation and an 'optimised' Qc*. Incidentally, that analysis included a kink in the plot at $0.35\sigma/\sigma_{TS}$ stress.

For the MgC data set at a normalised reference stress 2/3Rp0.2% of 297 MPa and an Rm, T of 564 MPa which is a slightly lower normalised stress of $0.53\sigma/\sigma_{TS}$ provides a T_{NC} of 407°C at an 'optimised' fixed Qc* of 348 kJ/mol. The modified model parameters give a T_{NC} of **425°C** at $0.53\sigma/\sigma_{TS}$.

At approximately 40-50°C higher than the original model fit it also suggests the classical limit is too conservative for this Grade 91 in agreement with Holmström [85]. Using the original model with either a historical fixed or floating value for Qc*; provides a conservative estimate of the T_{NC} in comparison as does the Evans modified model fitted to the failure data and within the PI of the 0.2% data. There appears potential to use failure data to estimate the no-creep temperature which would be significant for historical data sets which often only include failure data. In fitting the modified model the kink is evident at $0.49\sigma/\sigma_{TS}$ and the separate regions do not appear to significantly affect the result in this case. The original model showed little difference in the $T_{NC}$when historical or even floating values from full failure data are used with the exception of the regionalised floating value of Qc*. However, fitting the modified model underlines the need for appropriate model selection when the material has a non-constant M and ρ less than unity. Failure predictions may be equally different between the two models. For the modified model Evans has shown that Mε can vary significantly from M at failure. An additional value of M is required from a minimum creep rate at the stress and the temperature of interest if the real values of M are included.

$$M_{0.2} = \dot{\varepsilon}_{\min}^{\rho} t_{0.2} \tag{3.54}$$

$$T = \frac{\rho Qc*}{R \cdot Ln\left(\frac{t_{0.2}\left[-\frac{1}{k}Ln\left(\frac{\sigma}{\sigma_{TS}}\right)\right]^{\frac{\rho}{v}}}{M}\right)} \tag{3.55}$$

The fitting parameters for the model to include measured M with a floating Qc* are contained in Table 3.6. The value of Qc* is similar to that derived from the failure data. To use this model requires a measured value of M and therefore a mcr at the stress and temperature of interest which makes the model impractical.

Table 3.6: Modified model to include measured m fitting parameters.

Qc* kJ/mol.	k0.2	u0.2	R^2
418.34	38.85	-0.143	0.97

It is possible to return to the first WE Eq.3.23 and fit it to the mcr data to derive the mcr for a range of temperatures at the stress of interest, again keeping in mind the extrapolation taking place. This then returns to the issue of what value of Qc* to use in the fitting and thus leads back to fitting Evans's modified model to derive it.

3.9 Recommendations for fitting the Wilshire model

- The appropriate model should be selected based on the MG reation established for the material from literature, databases etc. Historical fitting and results of the original WE should be viewed in the context that their MG relations have not been explored to establish its suitability.

- The appropriate model should be used based on this information whether its the original Wilshire-Scharning or the Evans-Wilshire-Scharning model when the M and ρ are not constant or unity. These can easily be fitted with Excel and SOLVER.

- A better fit of data to the original model can apparently be achieved using a optimised Qc* variable with stress term as the dependent term. This might indicate the model is inappropriate. The method used should be explicitly described, time as the dependent term has been used here throughout.

- Data should be culled at the 0.2% IPS IMechE recommendation. This can be identified from a kink in the Wilshire plot using Evans's statistical method which is preferrable to any 'by eye' method or indeed the approximate stress/temperature limits published by the IMechE. Inaccurate establishing of the kink will have an effect on the resulting parameters and value obtained.

- Evans's statistical method should be adopted as the standard method to identify discontinuities regardless of the appropriate Wilshire model.

- In using the Evans-Wilshire-Scharning model the (b-ρ)Qc* should be established by

the linear fitting of

$$\dot{\varepsilon}_{\min}^{\rho_{0.2}} t_{0.2} = M_{0.2} e^{\frac{-b}{RT}}$$

using Excel and the SOLVER add-in or some other optimisation tool and

$$(\sigma/\sigma_{TS}) = \exp\left\{-k_2 M_{0.2}^{v/\rho_{0.2}} \left[t_{0.2} \cdot \exp\left(\left[b-\rho_{0.2}\right] Q_c^*/RT\right)\right]^{-v/\rho_{0.2}}\right\}$$

where

$$u = -v/\rho_{0.2}; k_1 = k_2 M_{0.2}^{v/\rho_{0.2}}$$

- Adjusting the value for (b0.2 - ρ0.2)Qc* fixing it and refitting allows the other terms to be established and putting all those values into the rearranged equation for temperature below, with the time, $t_{0.2}$ at 200k hours provides the no creep tempertaure, T=T_{NC}.

$$T_{NC} = \frac{b_{0.2} - \rho_{0.2} Qc*}{R \cdot Ln\left(\frac{\left[-\frac{1}{k1} Ln\left(\frac{\sigma}{\sigma_{TS}}\right)\right]^{\frac{1}{u}}}{t_{0.2}}\right)}$$

- The total strain is preferable to the creep strain where it is known for the reasons discussed in later chapters.

- The original Wilshire model appears to provide overly conservative values of T_{NC} if the Qc* is allowed to 'float' as others have found. It also appears to provide conservative lower values when used instead of the appropriate Evans-Wilshire-Scharning model as shown here with the NIMS Grade 91 data.

3.10 Alternative Sigmoidal Fit

As previously discussed above the reasoning for the choice of sigmoidal fit Eq.3.11 is not offered. Replacing the axes by

$$Ln\left(\frac{1-y}{y}\right) = a + bx \tag{3.56}$$

provides an alternative sigmoid. This model has been applied to the full NIMS 43A MgA-MgD, MGA-MGG data set with a floating Qc* value and Figure 3.32 shows the lack of fit at the extremes.

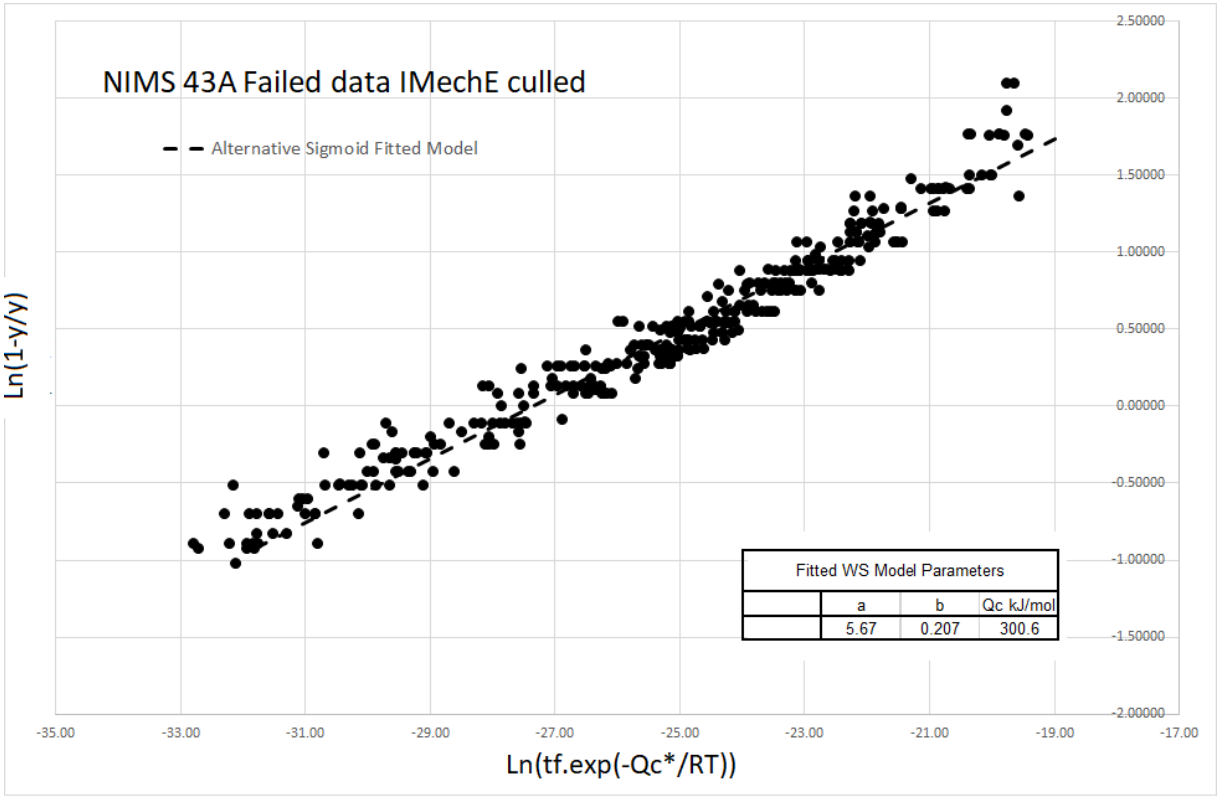

Figure 3.32: NIMS 43A MgA-MgD MGA-MGG Alternative Sigmoid fit.

3.11 Concluding Remarks

The Wilshire-Scharning model in its original form has been modified for models with a non-constant M and ρ below unity which would include Grade 91. This modified form is not widely applied in publications in the public domain and author communications suggest it is not well-known. The Wilshire-Scharning model has been reviewed in its general applicability and more specifically to Grade 91 data. The fundamental assumption of the model is the Monkman-Grant relation and the ability of this relation to characterise full creep curve shapes is limited even for the modified form. Various alternatives have been presented here and applied using the most comprehensive NIMS test data set available in the public domain and an alternative to the Wilshire-Scharning model proposed. None of the NIMS data is below what would be its maximum allowable design stress, or without the effects of instant plasticity strain, below 500°C. In fitting the Wilshire models to NIMS Grade 91 data a number of practical issues have been highlighted which are not clear from the open literature. The modified model method proposed by Evans is required to accurately locate kinks in the data for region splitting. The location of the IMechE threshold for instant 'plasticity' may

be too high for this material and the statistical method to identify discontinuities is preferable. The use of floating or historical apparent activation energies Qc* from the fitting of the original model cannot be relied upon to provide accurate estimates of specific temperatures if the material has a non-constant M or ρ of less than unity. The modified model is required to establish an appropriate value to use in the fitting process. For the first time, the measured MG constant has been included in the fitting of the modified model for comparison. This is the first time empirical test data for stress-temperature-time-strain accumulation has also been applied to replace the Monkman-Grant relation in the Wilshire-Scharning model format. This new model allows fitting to materials with a non-constant MG relation which is temperature and stress-dependent and has an exponent below unity. The requirements for fitting the model have been provided and plotted for Grade 91 for the time to failure and time to a specific strain. Further fitting of the model to other materials requires calibration of the creep curve characteristics from comprehensive test data. Fitting the Evans modified Wilshire-Scharning model to the NIMS Grade 91 data shows the T_{NC} for 0.2% creep strain in 200k hours is 416°C, some 40°C higher than the 375°C values provided by the original WS model with various values of Qc*. This is the first comparison of the effects of the WS model selection on the calculated no-creep temperature and the derived value for the modified model. There also appears to be potential in the method for estimating the no-creep temperature from failure data or other strain data which would be useful for historical data sets.

Chapter 4

Artificial Neural Network

4.1 Introduction

Artificial neural networks (ANN) are extremely useful in recognising patterns in complex data [130] and examples of their ever-expanding use in engineering are evident in the open literature. The ANN is a computing technique where interconnected artificial neurons or nodes simulate the human brain's method of problem solving through training. Visually this can be represented by a series of inputs followed by a series of 'hidden' layers of nodes and the outputs for multi-layer networks. Each node has inputs and outputs which are connected to multiple other nodes via weighted links which specify the importance of the input on the output. At each node, a non-linear activation function processes the weighted sum of all the inputs combined with a bias to produce the output. The goal of the neural network is to estimate a function f that gives an estimate for the set outputs for a given set of inputs treating measured raw data variables as either initial inputs or target outputs. These known outputs allow the inputs to be 'training' data for supervised learning where an error function calculates the difference between the neural network output and the target with the error reduced by adjusting the weights. The error is commonly the mean square error. To minimise the calculated error a back-propagation algorithm is commonly used which efficiently derives the error function minima using the chain rule. The derived weights and bias values represent the information within the network. Popular activation functions have developed from sigmoid, tanh to rectified linear unit ReLU and the leaky LReLU function to deal with vanishing gradient and 'dead' neuron issues [131].

The attraction is neural networks enable the study of diverse phenomena which are not

accessible to physical modelling, however, they can only learn from the empirical data used and thus unconstrained extrapolation will include large uncertainties [130]. There is limited information in the open literature on the application of ANN's to creep other than the time to rupture but could include extrapolating time series data to full creep curves as well as providing a no creep temperature T_{NC} for a given reference stress and limits. Srinivasan *et al.* [132] extrapolated the creep rupture strength data of 1-60k hours, 500-600°C for NIMS mod. 9Cr-1Mo up to 525k hours using Larson-Miller [60], Orr-Sherby-Dorn [21], Wilshire [76] and an ANN. An optimised Qc* corresponding to the highest R^2, a similar method to Holmström *et al.* [129], for the 9Cr-1Mo a Qc* of 375 kJ/mol. was used for the original Wilshire model and comparable strength values were obtained from all approaches. Evans [133] compared some of the parametric models, Larson-Miller [60], Manson-Haferd [63], Minimum Commitment [69] and Soviet [68] to an artificial neural network for the extrapolation of rupture lives with significantly improved predictions. Liang *et al.* [134] also showed an improvement over TTP methods for extrapolation of rupture times from up to 17k hours to 41k hours of NIMS 43A data for 9Cr-1Mo-V-Nb. Hybrid models can be created by training neural networks on data generated by physical models [130] and an interesting approach has been a hybrid model guided neural network when there is limited data. A combination of a neural network with a physics-based model, the Feltham equation [135] (a common model [110]), has been used to extrapolate secondary creep behaviour based only on primary creep data; this found the LReLU activation function performed best with reduced error in extrapolation [131]. Expanding the data to include alloy composition as well as mechanical properties has been used for creep prediction of reactor components [136].

This chapter demonstrates the application of an artificial neural network (ANN) using MATLAB for the prediction of the no creep temperature T_{NC}, the temperature at which 0.2% creep strain is attained in 200k hours at a reference stress, for comparison with the methods in previous chapters. The NIMS heats MgA and MgC used in the previous chapter have individually been used to train networks. Given they represent the upper and lower bounds of the tensile strength data for the plate heats this will provide some insight to the hypothesis of higher tensile strength providing higher creep resistance and therefore a higher no creep temperature, as well as reduce the digitising required. The trained networks were then used to predict the creep strain at a constant time of 200k hours with varying normalised stress

and temperature in the region of 400-450°C to locate the T_{NC} for varying reference stress. No data has been culled in this case, all the creep curves for each heat as presented in the D2 Atlas [4] were digitised to allow the network to learn from the patterns and trends. This is the first time the method has been used on the NIMS data set to provide a no creep temperature, at least in the public domain.

4.2 Methodology

Of the methods used in the public domain, Ghatak & Robi [137] provides a relatively simple technique using MATLAB based on $\varepsilon = f(\sigma, T, t)$. While the technique appears useful for the purpose required here considerable extrapolation outside the data set is required by approximately x3 the time to 200k hours and up to -50°C.

The network consists of stress, temperature and time input parameters and creep strain as the target output parameter. The network details are shown in Figure 4.3 using a three-layer feed-forward back-propagation network having a 15 neuron hidden layer using the Levenberg-Marquardt optimisation algorithm and trainlm. The tansig and purelin processing functions were adopted in the 2 layers respectively. These are the network functions and the number of neurons found optimum for creep curves by Ghatak & Robi. It is acknowledged that further predictive improvement to the network may be possible using the rectified linear functions in place of the hyberbolic tangent-sigmoid (tansig); for simplicity, their approach has been adopted.

The quantitative comparison of multi-heat grades is complicated by the variation in allowable maximum design stress. This is based on the 0.2% proof strength and room temperature tensile strength in Table 6.1 EN13445-3 shown in Chapter 2 Figure 2.2. In defining a limit for a grade the criteria would be dependent on a combination of maximum design stress and tensile properties. By applying the ANN to individual heats this can be further expounded. For this section, the full creep curves of two of the heats used in Chapter 3, MgA and MgC, which represent the upper and lower bounds of the tensile strength data for the plate heats within the grade are used. A summary of the tensile properties and instantaneous strain is provided in Figure 4.1 and Figure 4.2. Of note is the plateauing and apparent shift in the relationship between the ultimate tensile strength and 0.2% proof stress around 400 - 450°C for the MgA data which is also the case for subset MgB - all subset UTS val-

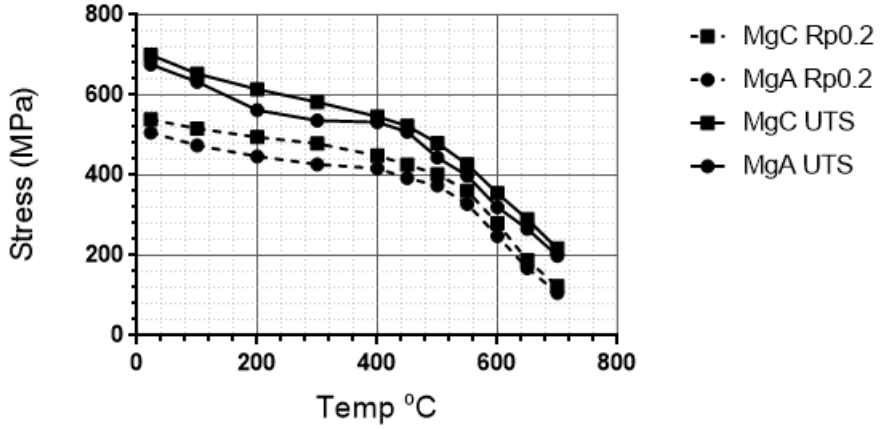

Figure 4.1: Tensile properties of the two data sets MgA and MgC.

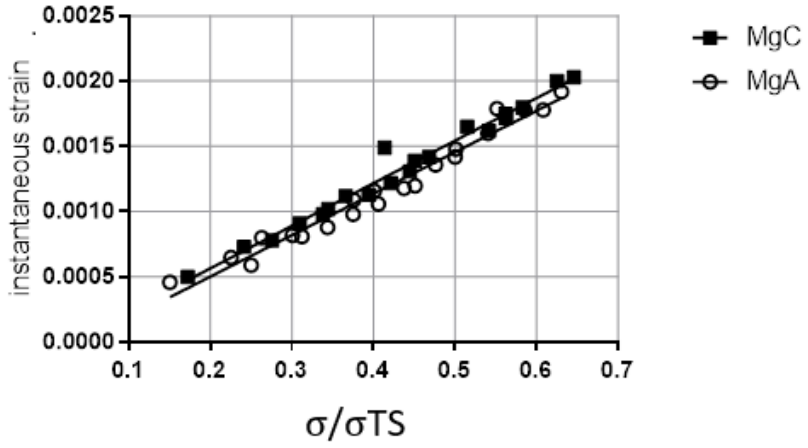

Figure 4.2: Instantaneous strain on loading for heats MgA and MgC.

ues lie within 3% (15 MPa) at 400 and 450°C. The instantaneous strain on loading appears consistently higher for the MgC heat at ∼+4% at $0.56\sigma/\sigma_{TS}$ from the linear model in Figure 4.2.

A summary of the data sets is shown in Table 4.1. For the data pre-processing the log10 data values were used for creep strain and time scaled from 0.1 - 0.9 along with the temperature data scaled from 0.2 - 0.9 to allow for extrapolation and the already normalised stress, σ/σ_{TS}. A number of input-output sets of $\varepsilon = f(\sigma, T, t)$ were obtained from the NIMS digitised plots and the networks trained separately for each heat. The data input-output sets were randomly assigned for training, testing and validation as 70%,15% and 15%. The error goal was set at 0.0001 but the network was protected against overfitting, when the test and validation errors become divergent, with the default.

Table 4.1: Data set summary.

	MgA	MgC
Duration hours	<59209	<61673
Temperatures °C	450-650	450-650
Normalised stress σ/σ_{TS}	0.15-0.787	0.172-0.803
Number curves	26	24
Number input-output sets (data points)	1873	1503

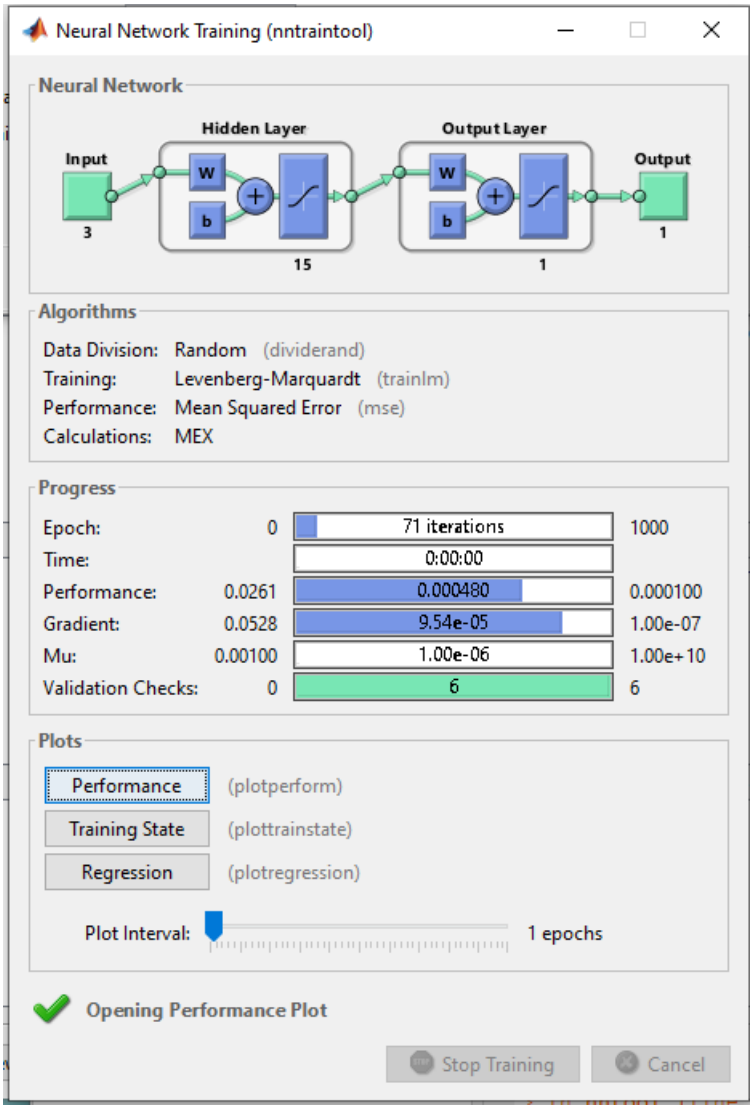

Figure 4.3: MgC neural network training details.

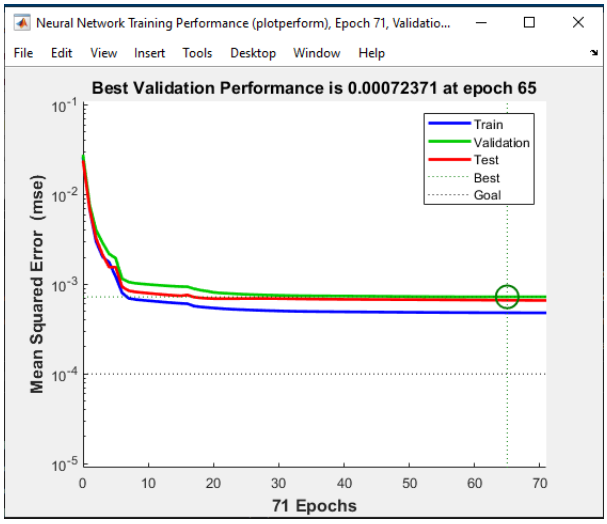

Figure 4.4: MgC ANN training performance summary.

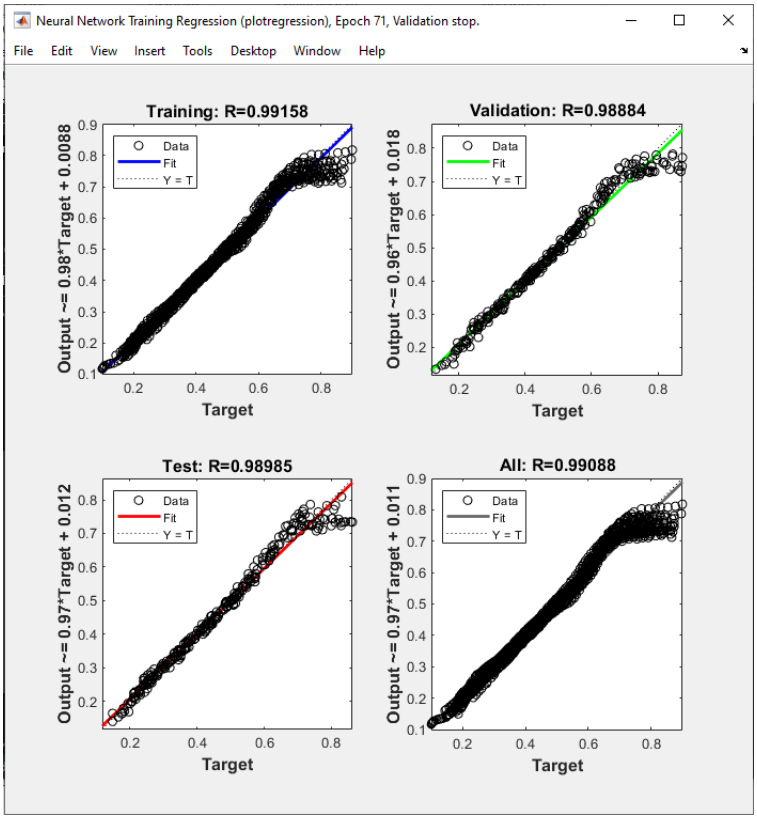

Figure 4.5: MgC ANN regression plots.

4.3 Results and Discussion

As with the previous chapter the results must be viewed in the context of considerable extrapolation of temperature and normalised stress with the neural network, in addition, the plots indicate the networks lack of fit at the extreme. Figure 4.3, Figure 4.4 and Figure 4.5 show the details of the MATLAB ANN, the performance plot and regression plots for the MgC data set, similar values were obtained for the MgA set with a performance of 0.000546. The predictions for both heats from the Artificial Neural Network in MATLAB are shown in Figure 4.6. These are based on the prediction of creep strain from an array of fixed time (200k hours) at varying reference stresses and temperatures in the region of interest, the plots have been limited over the range of 0.15-0.25% strain and 400-450°C. The isochronous plots indicate both the heats have a similar T_{NC} of $\sim$**440°C** at $0.56\sigma/\sigma_{TS}$ reference stress which is 23°C higher than those obtained for the modified Wilshire model on the complete set in the previous chapter and again significantly higher than the classical limit of 375°C.

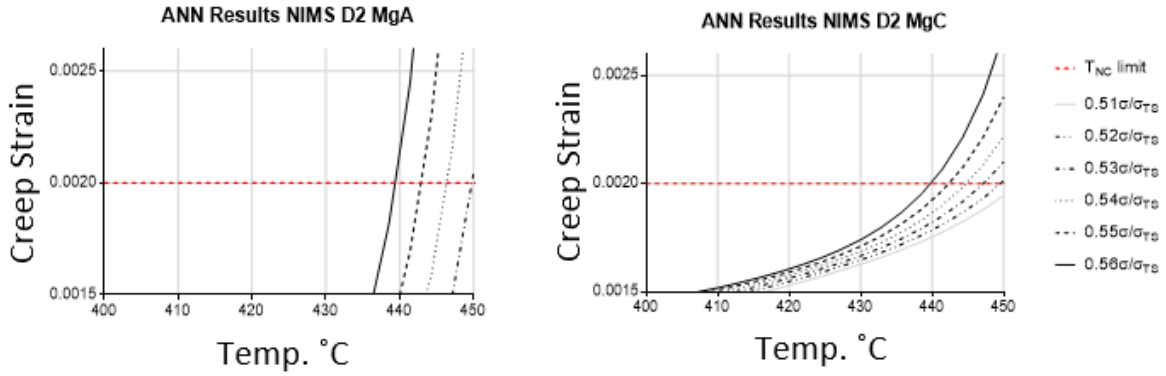

Figure 4.6: Network prediction of creep strain v temperature at 200kh for heats MgA and MgC.

The hypothesis that higher tensile strength equates to higher creep resistance and therefore a higher T_{NC} overall is not supported in this case, although over the temperature range of interest the ultimate tensile strengths are much closer than elsewhere as shown in Figure 4.1. The 0.2% proof strengths, however, are consistently lower in the MgA heat ($\sim$7% from 400-450°C). The T_{NC} values are consistent with the small heat-to-heat variation in time to rupture for 9Cr-1Mo, attributed to the narrow range of nitrogen and aluminium concentrations as well as the tensile strengths [138]. The shape of the isochrones indicates a family of constant stress creep curves, at various temperatures, would be considerably closer for

the MgC heat than the MgA in terms of creep strain at 200k hours. This may be interpreted as MgA heat further progressed in tertiary creep. The isochrones are well represented by a hyperbolic decline model Equation 3.47. With the comprehensive tensile data in Figure 4.1 and Table 6.1, EN13445-3 design criteria in Chapter 2 the maximum allowed nominal design stress for these two heats can be calculated to provide a σref reference stress. Using this design stress has been proposed as an approach to defining the T_{NC} for the particular heat [129]. Interpolating, with a simple linear model, the strengths in Figure 4.1 between 400 — 450°C, the lower 0.2% proof stress for MgA equates to a 0.52Rm, T (using the EN notation = σ/σ_{TS}) reference stress with 0.55Rm,T for MgC. The adjusted T_{NC} is then ∼453°C for MgA and ∼442°C for MgC. In this case, due to the reference stress criteria, the lower proof stress heat would not provide a lower T_{NC} by which to limit the grade overall. In order to provide this the reference stress at the temperature of interest needs to be the maximum allowable normalised stress, σ/σ_{TS}, under the design criteria which depends on the relationship between the proof and tensile strengths at temperature; the closer the relation the lower the T_{NC} because a higher normalised design stress is allowed. The tensile strength at temperature is not required to calculate the design stress for steels other than austenitics in Table 6.1, EN13445-3 but the tensile strength at room temperature provides a limit on the design stress. This indicates a heat with the lowest value of tensile strength around the temperature of interest combined with a relatively high proof stress could provide the worst case scenario for a grade. The tensile and proof strengths may be the minimum recorded in tests. In general, a lower tensile strength at elevated temperature might be expected from a lower room temperature tensile strength [129].

There are a couple of issues with this simple approach to the problem - firstly there is some IPS with this data, as has already been discussed the 450°C curves and some 500°C high stress curves would exceed the IMechE limit with an expected effect on the creep curve shape and secondly there is some substantial strain developed with these tests which would marginalise the 0.2% estimate. The network training is repeated on the individual data sets culled of any curve data exceeding the 0.2% IPS limit (the 450°C and some 500°C curves). The total strain is adopted in view of the accelerated tests and the slightly higher IPS for the MgC heat and any total strain > 0.5% data omitted. This highlights the limitations of the NIMS data - the longest duration at 0.5% total strain is 8709hrs for MgA and 4100 for MgC with data > 500°C and results must be viewed in this context. The standardisation of the log

time data is extended to 250kh to allow extrapolation. The results are shown in Figure 4.7. The predictions are $\sim$ 30°C lower at $\sim$410°C than the creep strain prediction highlighting the need to include IPS with accelerated data. The MgC heat has the lowest T_{NC} for the $0.56\sigma/\sigma_{TS}$ stress but has much wider isochrones and heat MgA would be lower as the stress lowers. Given the extrapolation involved a T_{NC} of 407 - 425°C for 0.55 - $0.56\sigma/_{TS}$ between the two data sets are in good agreement with the values in the previous chapter with modified Wilshire model of 416°C though that used the $t_{0.2\%}$, creep strain data.

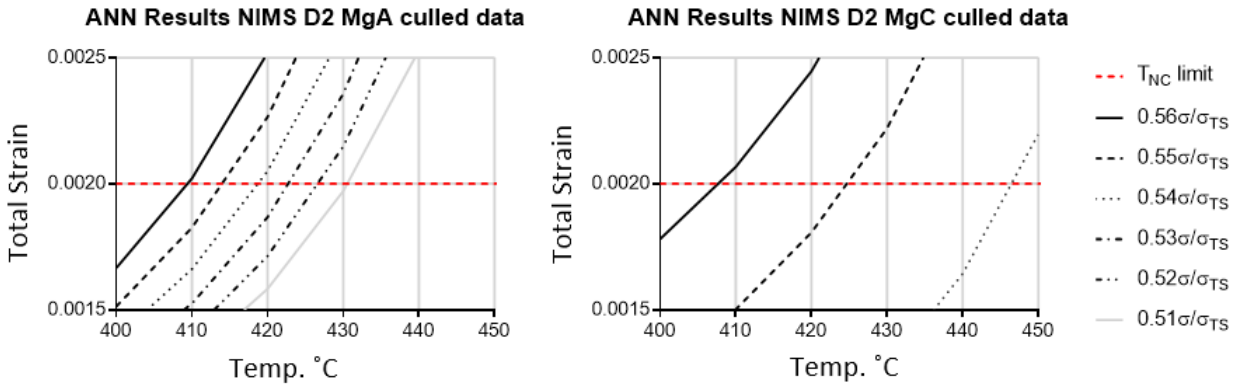

Figure 4.7: Network prediction of total strain v temperature at 200kh for heats MgA and MgC using culled data.

Individual cast trained ANN

The other NIMS cast data curves were digitised and used to train the ANN individually as above. The data summary is included in Table 4.2 with the results in Table 4.3.

Table 4.2: NIMS Individual cast data information.

Cast	Number data points	Temperature °C	Number of Curves	Comment
MgB (Plate)	721	500,550,600,650	25	
MGA (Tube)	361	550,600	10	
MGB (Tube)	721	550,600	11	
MGC (Tube)	496	550,600,625,650	16	Data culled at 650°C

Table 4.4: NIMS [3, 4][3, 4] Grade 91 cast composition data.

	Ni % mass	N :Al ratio	Grain size	Hardness HRC
MgA*	0.09	5.9	9.0	13
MgB*	0.09	5.9	9.0	14
MgC	0.04	4.2	8.7	17
MGA	0.12	5	9.2	16
MGB	0.2	2.1	8.8	16
MGC	0.28	44	9.2	18

Table 4.3: ANN Predictions of no-creep temperature for individual casts.

Stress/Cast	0.56σ/σTS	0.55σ/σTS	0.54σ/σTS	0.53σ/σTS	0.52σ/σTS	0.51σ/σTS
MgB (Plate)	470°C	473°C	476°C	477°C	481°C	485°C
MGA (Tube)	380°C	400°C	410°C	420°C	425°C	435°C
MGB (Tube)	445°C	460°C	475°C	490°C	>500°C	>500°C
MGC (Tube)	428°C	440°C	443°C	450°C	451°C	456°C

The values derived show considerable differences in the spread of the no-creep temperature prediction with normalised stress, as was evident for the MgA and MgC casts. A point of note is the no-creep temperature for the MgB cast is significantly higher than either MgA or MgC plate casts predicted earlier at ~410°C at 0.56 σ/σTS, accompanied by a reduced spread with total strain indicates relatively creep brittle behaviour compared to the other casts.

There is little to indicate there should be any significant difference between the plate casts - both MgA and MgB have the same composition and grain size with MgB a slightly higher hardness and different processing history but relative creep brittle behaviour is predicted for cast MgB. The yield strength of MgB also lies between that of MgA and MgC and, in general, the tensile strengths of all the plate casts have a limited spread (14/15 MPa at 400/450°C). How the significant difference in strain rate with normalised stress relates to a propensity for creep cracking also needs further investigation. Has cast MgA overall better creep resistance properties (including ductility, creep cracking and weld integrity) than cast MgC? A significant spread of predicted T_{NC} with normalised stress might be considered an

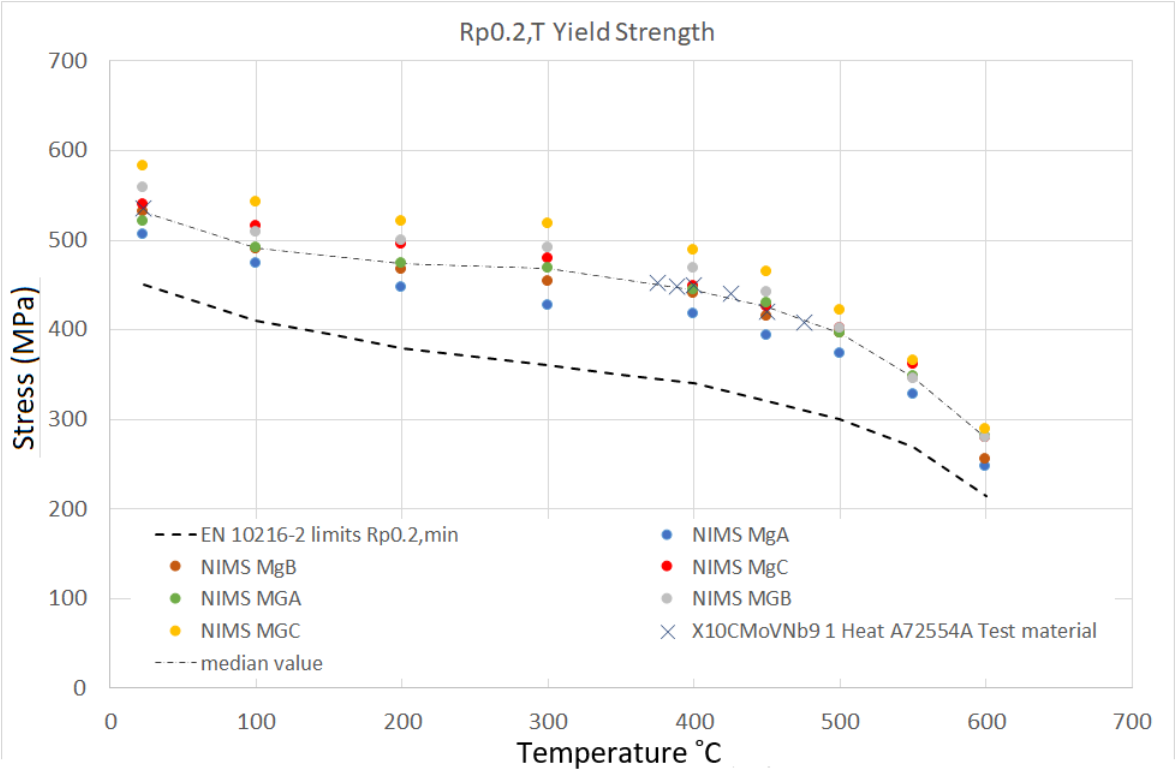

Figure 4.8: NIMS Individual cast Yield Strength data

indicator of strain compatibility problems prior to the 0.2% 200k hour threshold for components and welds in service for the MgC material. The single no-creep temperature concept is limited in ascertaining these.

ANN trained with multicast data

Figure 4.8 shows the individual cast yield strengths. Both EN10216 and EN10028 provide minimum allowable yield strengths at temperature for X10CrMOVNb9-1 material with EN10216 slightly lower - that is also plotted in Figure 4.8.

The MGC tube cast has the higher yield strengths with the highest hardness, highest Ni% and a significantly higher N: Al ratio than other casts, MgC plate has the lower overall as shown in Table 4.4. The values indicate a more complex relation than simply a higher yield strength equates to a higher creep resistance and lower no-creep temperature. Cast MGA has 0.12% Ni and a N: Al ratio of 5 but less time to rupture than the other tube casts at the lowest available temperature of 550°C. The MGA and MGB cast data is also limited to two temperatures with a difference of 50°C when the extrapolation is > 150°C.

Using the same settings for a single cast curve plot the ANN function has been expanded to include a number of additional yield strength parameters. To predict the T_{NC} for the lowest allowable yield strength an extrapolation in time, temperature and yield strength is required

using the multicast data. The ANN was trained using the same methodology with strain as a function of stress, temperature, time and Rp0.2, T using the values in Figure 4.8. Where the values are not explicitly available they have been interpolated from a polynomial fit of the available data. The Rp0.2, T values used are RT, 100, 200, 300, 400, 450, 500 and 600˚C. The predictions fall outside the prediction range at < 350 ˚C.

The NIMS data also included composition information, grain size and hardness variables which can also be used to expand the strain function such that strain is a function of stress, temperature, time, apparent grain size, hardness, Ni%, N%, Al%, C%, Si%, Mn%, P%, S%, Cr%, V% and Nb% (no Boron data) to train a multicast ANN. The additional variables were also standardised to lie between 0.1 and 0.9 from the minimum and maximum data values.

The multicast data consists of 100 curves of the 6 casts. Again the curve plots were terminated at 0.5% strain and any with an IPS > 0.2% removed. The apparent grain size is limited to 4 levels from 8.7 – 9.2 and the hardness to 4 levels from 13 - 18 in the NIMS data. The no creep temperatures were predicted for a single normalised stress value of $0.56\sigma/\sigma_{TS}$ again using an array of temperature (400-450˚C) and strain (0.15-0.25%) of interest. The composition variables C, Si, Mn, P, S, Cr, V, Nb variables were set to the median of measured values. The non-uniform 3D data of individual predictions were then interpolated to a surface using the INTERPXYZ function in Excel. Predictions for the no-creep temperature, T_{NC} are shown in Figures 4.9and 4.10 for two grain size levels and two hardness levels. The temperature extrapolation was again limited to 350˚C. The first point to note is that the multicast ANN does not replicate the T_{NC} values from the individual cast ANN's, e.g. the MgC cast with a grain size of 8,7, HRC of 17, N: Al ratio ~4 and a Ni content of 0.04% produces a T_{NC} of < 350˚C compared to the 410˚C provided by the individual cast ANN. The trends in the data may, however, provide some insight into the relationships. Recommendations for N: Al >4 and Ni content <0.2% mass [139] (towards the front corner of the plots) appear to increase strain rate and ductility. In general, the predictions are for a higher T_{NC} (with an associated lower strain rate) with an increasing nickel content and a lower N: Al ratio. This appears less pronounced for Ni content for the higher grain size and lower hardness (9.2, HRC 12). The smaller grain size provides a lower T_{NC}, in general, which indicates a higher strain rate. A change in hardness from HRC 12 to HRC 18 indicates a lower T_{NC} for the smaller grain size but for the larger grain size the relation is more complex - the higher hardness indicates a greater range of T_{NC}. At the higher hardness, Figure 4.9(a) there appears a

significant difference in the predicted strain developed with grain size compared to the lower hardness, Figure 4.10(a), the difference is > 80 ˚C in T_{NC} at the higher nickel content.

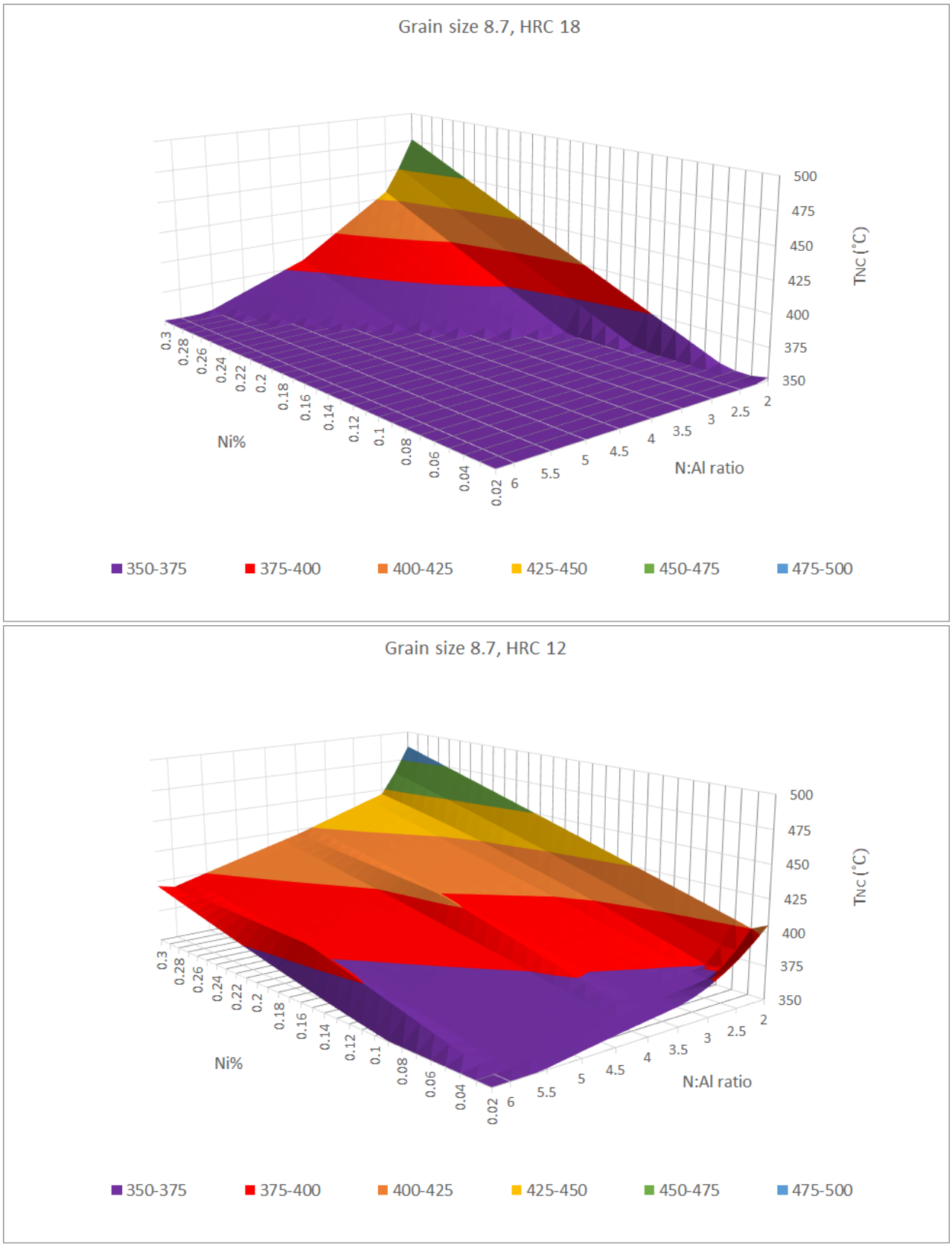

Figure 4.9: ANN No-creep temperature predictions from multicast data, Grain size 8.7 (a) 18 HRC hardness (b) 12 HRC hardness.

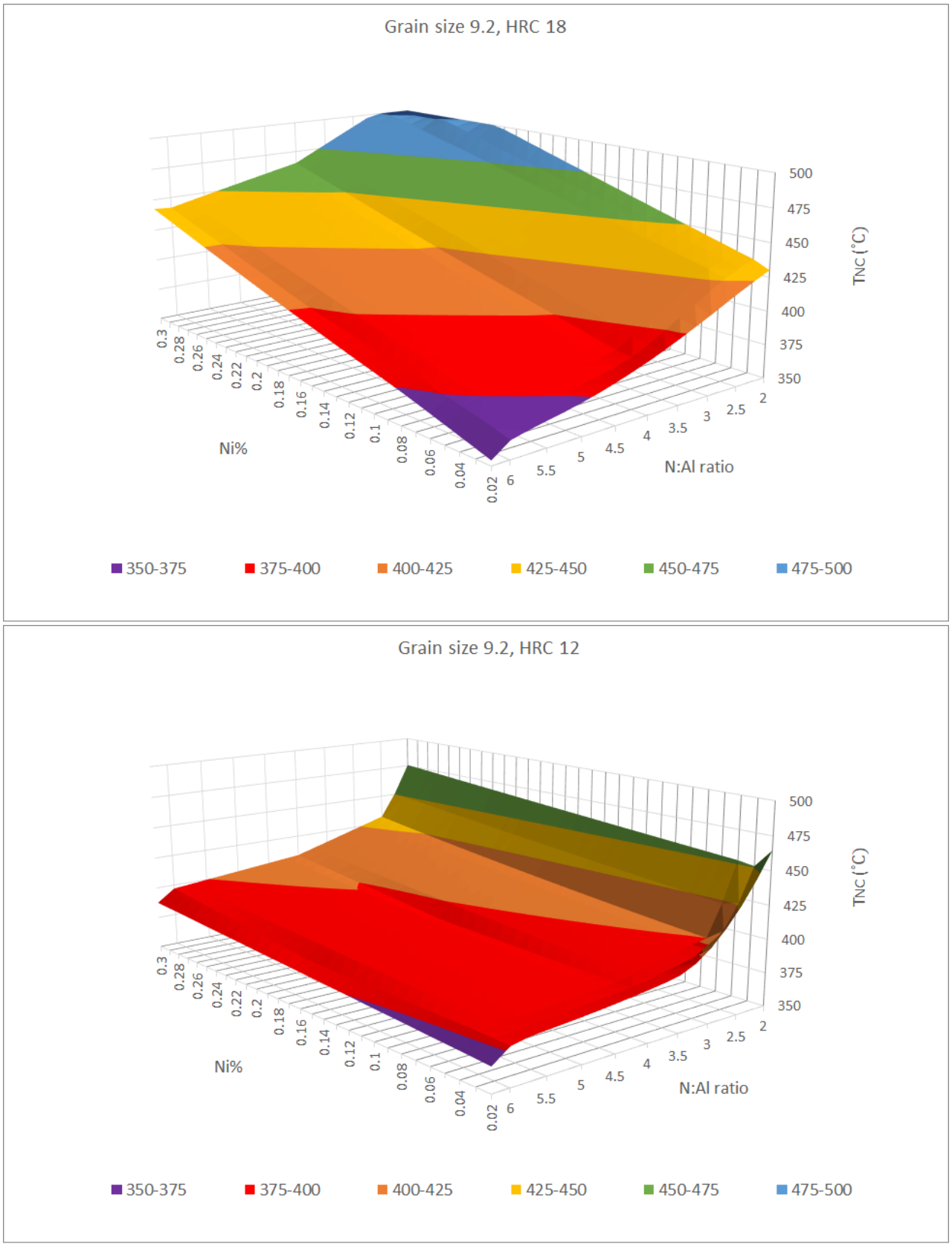

Figure 4.10: ANN no-creep temperature predictions from multicast data, Grain size 9.2 (a) 18 HRC hardness (b) 12 HRC hardness.

4.4 Concluding Remarks

The ANN has predicted a T_{NC} for the NIMS D2 Grade 91 material significantly higher than the models in the previous chapters using the creep strain alone. Using the total strain and data culled at 0.5% total strain and eliminating all curves with an IPS >0.2% appears to provide a reasonable value given the extrapolation involved. The difference between the two heats MgA and MgC in this section also indicates that they may have different curve shapes and the same T_{NC} and data need to be gathered upon which to assess the heat-to-heat variation within the grade. The results need to be considered in terms of the network training where the collected data at stress levels at or below a typical maximum allowable design stress for Grade 91 is not available below 500°C. Using $t_{0.2\%}$creep strain with historical accelerated data will provide a non-conservative estimate of the T_{NC} with an ANN based on this result and the previous Chapter. The use of total strain rather than creep strain with accelerated data saves leaving any IPS from the estimates though it may be negligible at the temperature of interest. The use of total strain rather than creep strain in the calculation of T_{NC} is the recommendation [129] though with historical data the latter may be all that is available or require considerable recalculation of tabulated data with introduced error in the case of the NIMS data.

As already discussed there are practical limitations using the models available to extrapolate to lower temperature and stress. Many are simply unable to adequately model the relationship between stress and strain and there is little data in the design stress/temperature regime upon which to validate these models for extrapolation. This complicates a hybrid model ANN with the possibility of potentially introducing incorrect constraints from models.

The additional individual predictions indicate that no-creep temperature estimation may be subject to significant variation as other creep data between casts. The predicted T_{NC} values also indicate cast MgB has creep brittle behaviour relative to casts MgA and MgC with a high $T_{NC}$and limited spread and little variation in the properties provided. A lower bound of 410˚C appears appropriate for the data set given the limited temperature range and extent of the extrapolation of casts MGA and MGB with some note that the spread is significant and for MGA 410˚C is the predicted T_{NC} for $0.54\sigma/\sigma_{TS}$.

In terms of the yield strength a multicast ANN predicts the standard limits allowed in the standards will produce a no-creep temperature below 350˚C. There is a complex interrela-

tionship between hardness, grain size, composition and no-creep temperature. The multicast ANN predicts a general increased total strain rate and an associated lower no-creep temperature for an increasing N: Al ratio and lowering of Ni content (towards the front corner of the plots). The plots indicate the recommendation for N: Al ratio >4 and a Ni content of <0.2% [139] will increase ductility with a lower no-creep temperature to 0.2% total strain and also reduce the difference in strain rate and no-creep temperature between the grain sizes. Why cast MgB has a significantly different predicted T_{NC} and spread than cast MgA and MgC is not answered from the property data available.

Further work is required to establish how the spread of no-creep temperatures and the differences in creep and total strain rate with normalised stress is an indicator of creep cracking susceptibility and brittle creep behaviour.

Chapter 5

Experimental Work

5.1 Introduction

Previous chapters have provided several values for the T_{NC} of both P265GH and a Grade 91 material which concur with the broad conclusions of the MATTER project and Ren *et al.* [140] for the Grade 91. They could be significantly different from the blanket values adopted. The models used to establish a no creep temperature can provide erroneous values if the material relationships are not fully considered. The modelling approaches do, however, appear to provide conservative estimates of the T_{NC} which is preferable until more data is collected. There could be safety issues with creep using C-Mn materials in the traditional no creep zone which can be managed with a lower temperature. There could be significant financial savings made with unnecessary creep monitoring of Grade 91. The approaches adopted so far have relied on both extrapolation and accelerated stress and temperature test conditions with assumptions on the relative time-dependent development of the microstructure and properties. No data are available in the stress-temperature regime where the creep strain approaches 0.2% in around 200k hours in the public domain. As seen with the NIMS data the extrapolation may be further extended if the effects of initial plastic strain are to be eliminated. The effects are material dependent and can either increase or reduce the time to a specific strain. An experimental technique to establish the T_{NC} from accelerated testing is not a trivial task. Isostress testing is a common methodology for the assessment of the remaining life of a component from post-service material samples [141]. The deformation mechanism and rupture strength remain unchanged in constant load tests at the service stress of interest over a range of accelerated temperatures in contrast to variable load isothermal tests which

do not have a linear relation [20]. It became common to include isostress tests conducted at a common stress at several temperatures to extrapolate rupture lives to estimate behaviour at the design stage [142]. It was notable that plotting temperature against the logarithm of rupture time generally gave a straight line rather than the theoretical physically-based reciprocal temperature model [143, 56] as Eq.5.1.

$$t_f = A\exp(-KT) \quad vs. \quad t_f = B\exp\left(\frac{Q}{RT}\right) \tag{5.1}$$

It has been shown there is little difference between the two over a limited temperature range and the linear model will generate conservative predictions if the reciprocal is more appropriate [144][143]. The method has been shown to provide reasonable agreement with data extrapolated x100 in time [56] and used on time to specific strain data [143]. Timmins & Smith [143] found constant slope plots can be achieved if the data is collected in primary or tertiary regions but not both as shown in Figure 5.1. The method appears to lend itself to the prediction of low strains over a limited temperature range providing the data is collected below the minimum creep rates.

In terms of the TTP models, it was shown in Chapter 1 that e.g. the Larson-Miller and Manson-Haferd parameters have a similar form to Manson's generalised parameter and for EN13445-3 similar to the Mendelson-Roberts-Manson Figure 1.7. In terms of the EN13445-3 time to rupture models listed in Figure 1.7, $\sim 75\%$ have a temperature exponent, r of +1 indicating $\propto$T this includes Grade 91 (MH4 model). For P265 the Larson-Miller model is used with a $\propto$ 1/T relation but for C-Mn P335 a Manson-Haferd (MH4) with $\propto$T.

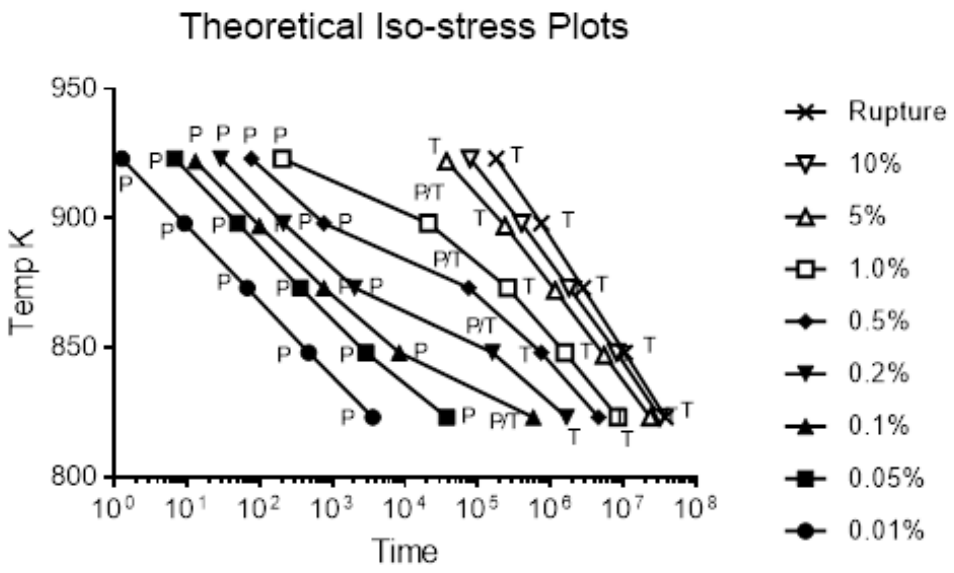

Figure 5.1: Theoretical isostress plots over the primary P, tertiary T, and transition P/T creep regions [141].

In terms of the data available in the public domain and the times to specific strain, the NIMS D1 [3] and D2 [4] data for Grade 91 has few tests carried out at the same stress and only provides two points connected at a 50°C interval. NIMS 9B [86] data sheet does provide enough information to add to the convincing case for the approach in Figure 5.2 [142].

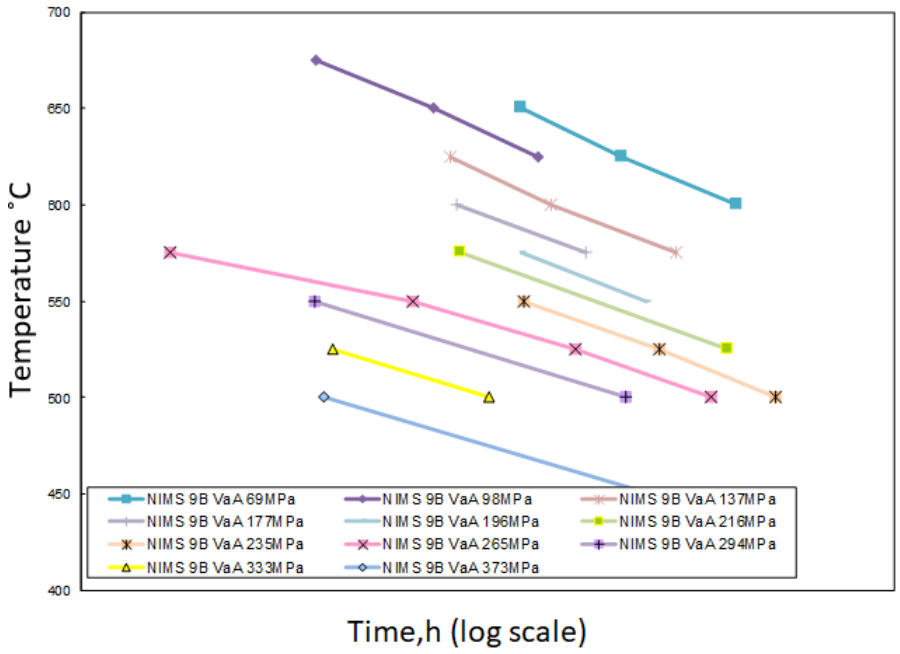

Figure 5.2: Example isostress data from NIMS 9B. times to 1% creep strain for ASTM A470 D Class 8 rotor steel [140]..

Requiring only relatively straightforward tensile and creep tests the approach appears to offer an experimental technique in the stress-temperature regime of interest without accelerated conditions, relying only on extrapolation of data. The extent of the extrapolation required is limited by the time frame and budget but, with the facilities, it is possible to provide interim values with tests still in progress to provide additional data later. A test matrix of creep tests at constant load at the traditional T_{NC} and at increasing intervals of 25°C could be used to gather the required times to specific strains and provide the Isostress plots to extrapolate the 0.2% strain line to 200k hours and the T_{NC}. If these could be terminated above a 0.2% strain the data could also be used to provide an extrapolation based on the original Wilshire equations.

5.2 Materials

From previous chapters, a number of materials are of particular interest for the experimental section. Firstly, a C-Mn material, P265GH. The data extrapolation from both the Manson-Haferd and Wilshire models indicated it was creeping in the no-creep zone with a very low T_{NC} in relation to the blanket limit quantified at around 340°C. This is supported by evidence of creep damage at 360°C in the literature. Secondly, since 1990 Grade 91 has been the 'work horse' material for the fossil power industry and as European X10CrMoVNNb9 1 or Japanese 9Cr-1Mo-V-Nb, there is considerable interest and data available in the public domain for this creep-resistant steel. Previous chapters have used the NIMS data to ascertain the T_{NC} using various methods and models. It would be appropriate to ascertain the T_{NC} for the European material to compare given there is little data available. An additional material was also made available 316L(N), an austenitic considered for nuclear power generation.

5.3 Determination of no-creep temperature,T_{NC} using isostress testing

5.4 Methodology

Using a reference stress of the maximum allowable design stress at the traditional no creep limit temperature for the material is the basis for the test matrix. An additional stress level

of 0.8σref is included to provide two series. A series of tests at 25°C intervals from that base either higher if e.g. the material is creep-resistant or including lower intervals if the material is suspected of creeping below the traditional limit e.g. the C-Mn steels. These test curves then provide the times to specific plastic strains which have been shown to produce a linear relation The particular requirement is to provide a consistent method of extracting the time to a specific strain within the noise in the data. DIN 50118 [55] provides a geometric mean interpolation and averaging method that was adopted. There is a need for tensile strength data at elevated temperatures for the materials to establish their reference stresses, σref = 2/3.Rp0.2, T. Testing was performed at room temperature, at the current no-creep temperature, and at 25°C intervals to about 100°C above.

5.5 Determination of tensile properties at elevated temperature

Tensile tests on the materials were conducted on test pieces taken in the longitudinal direction according to BS EN ISO 6892 [145], at room temperature and elevated temperature. The rolling direction, of the P265GH stock piece, was assessed by grain orientation, it was clearly identified on the other materials. Tensile strength cylindrical samples in accordance with BS EN ISO 6892-2 Table A3 of 6mm diameter at the parallel length, 30mm gauge length and M10 thread were used to establish the elevated temperature tensile properties. Samples were measured using a Keyence IM-6125 image dimension measuring system and scored for elongation measurements. Two R type thermocouples were attached to the sample surface above and below the extensometer rods with heat-resistant string. The samples were tested using an Instron 1342 test frame with high-temperature grips and an air-cooled MTS sensor arm extensometer of 25mm gauge length mounted on a 3 zone split furnace. The high-temperature extensometer was fitted with V-groove chisel edge ceramic rods which extend into the furnace and held in contact via a proprietary spring-loaded jig and heat shield. With a minimum of 10 minutes soaking at the required temperatures tests were conducted at a strain rate of 0.04%/min up to 4% and then at a rate of 5mm/min to failure. The subsequent stress-strain data was analysed to calculate the modulus and determine several offset strains from 0.01% to 1%, including the 0.2% proof stress, Rp0.2, T. There are several phenomena related to these materials and test results that merits further explanation and exploration.

These are included with the results for each material.

5.6 P265GH (1.4025)

5.6.1 Identification/Composition

Tables 5.1 and 5.2 contain the supplied information.

Table 5.1: Dillinger Hutte P265GH 1.4025 heat 423302 Rolled plate Composition.

%	C	Si	Mn	P	S	N	Al	Cr
Cast	0.111	0.329	1.18	0.009	0.0007	0.0071	0.037	0.065
Product	0.113	0.326	1.17	0.009	0.0005	0.0064	0.035	0.065
%	Cu	Mo	Nb	Ni	Ti	V	Other	
Cast	0.026	0.013	0.000	0.035	0.001	0.001		
Product	0.029	0.015	0.001	0.041	0.001	0.001	0.15	

Table 5.2: Mechanical Tests Cert. No. 407558-02.

P265GH 1.4025	Thickness	Tensile Strength Rm	Yield Strength ReH	A5 Long	kv trans -20°C
	mm	MPa	MPa	%	J
Cast	50	458	338	40	309Av

5.6.2 Tensile Properties

The tensile plots at temperature are shown in Figure 5.3. The first point of note is the yield point phenomena with the P265GH. The yield plateau is evident to around 425°C which might be a higher temperature than expected from the open literature [146]. The phenomenon is still not fully understood, commonly found in low carbon steels and associated with small amounts of solute interstitial atoms, typically carbon or nitrogen which hinder the movement of dislocations. During tensile tests, the applied stress drops abruptly from the upper yield to a lower yield point and plastic flow begins. The phenomenon is attributed to interstitial solute elements (typically carbon or nitrogen) migrating to the space provided by dislocation segregation in Cottrell atmospheres and strongly pinning the dislocations [147]. The

application of the upper yield threshold unlocks them which, combined with new dislocation generation, allows glide and slip to occur at the lower yield stress forming a plateau with localised Luders band formation. When these are completed the curve continues on the strain-hardening curve to necking and failure which can also be accompanied by strain ageing with serrated flow [148] from the Portevin-LeChatelier effect [149]. The yield-point can be temporarily removed by applying a small plastic strain — static strain ageing — commonly used in manufacturing to remove unsightly bands. Unloading within the plateau range and reloading without ageing can result in a smaller upper yield to overcome band propagation, the same lower yield and very little non-elastic deformation [150].

Nitrogen content and the N: Al ratio are important for ductility, weld integrity and susceptibility to creep damage. Strengthening and non-linearity of isostress rupture plots after 153kh service at 627°C have been attributed to solid solution strengthening with extra nitrogen collected in service [151]. Han & Kwon [152] suggests it is the free nitrogen content that influences the creep properties in the C-Mn steels. A local maxima 'hump' in the UTS at 250°C is eliminated in a low free nitrogen material and accompanied by larger primary and secondary regions and a higher minimum creep rate. This suggests a heat with a low free nitrogen content might produce a lower T_{NC} but with lower yield and tensile strengths allow a lower reference stress. Moreover, it highlights compositional variables in the ANN training, even if the creep-composition relation is not fully understood, could improve prediction in multi heat data. Hardness is another property that might improve ANN prediction for the C-Mn steels [94]. The Rp0.01-2.0% strengths are shown in Figure 5.3 and the properties relative to the standard's limits and the test reference stresses are shown in Figure 5.4. Based on the minimum specified tensile properties the heat might be considered a marginal material for the purpose of establishing a T_{NC} for the grade.

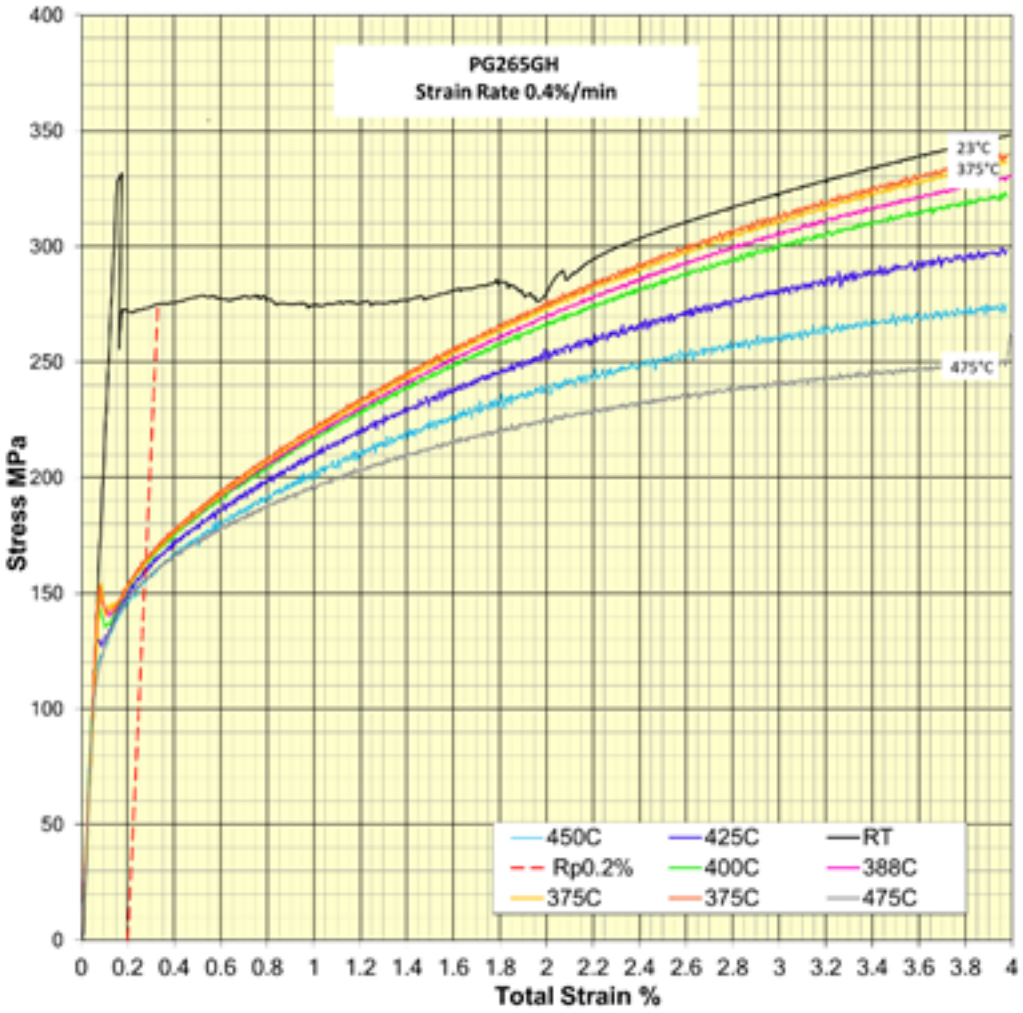

Figure 5.3: P265GH Tensile strength plots BS EN ISO 6892-2:2018 [143].

Table 5.3: Tensile properties at temperature P265GH

TEST ID	Target Temp. °C	Average Top/Bot. °C	Cold Modulus GPa	Hot Modulus GPa	Rp0.01 MPa	Rp0.02 MPa	Rp0.05 MPa	Rp0.1 MPa	Rp0.2 MPa	Rp0.5 MPa	Rp1.0 MPa	Rp2.0 MPa	Rm MPa	Elong. A %	Reduc. Z %
W7379	23	-	212.3		330.2	322.1	272.8	271.9	274.9	276.9	275.7	289.6	446	31.6	91.7
W7375	375	374.7	228	202.6	150.5	146.5	142.5	147.9	164.9	194	228.8	281.5	419	42.6	91.8
W7376	375	375	194.7	178.2	148.7	143	145.1	148.2	165.5	192.5	227.6	280.5	415	39.8	91.7
W7377	388	388	208.7	196.5	146	146.9	140.7	148.4	164.3	191.4	224.9	275.6	407	42.7	91.5
W7378	400	400.1	227	207.6	144.5	139.6	137.1	146.6	163.2	190.5	222.6	271.5	398	37.8	91.6
W7380	425	425.3	215.8	204.5	129.6	128.7	131	144.2	160.3	185.1	214.2	258	370	45.4	91.8
W7381	450	450	184.1	186.6	119.8	122.9	131.5	142.6	156.7	180.2	204.7	242.6	343	46.5	91.6
W7382	475	475	218	187.6	114.4	121.4	132.9	144.3	156.2	176.7	199.4	227.3	316	40.3	90.9

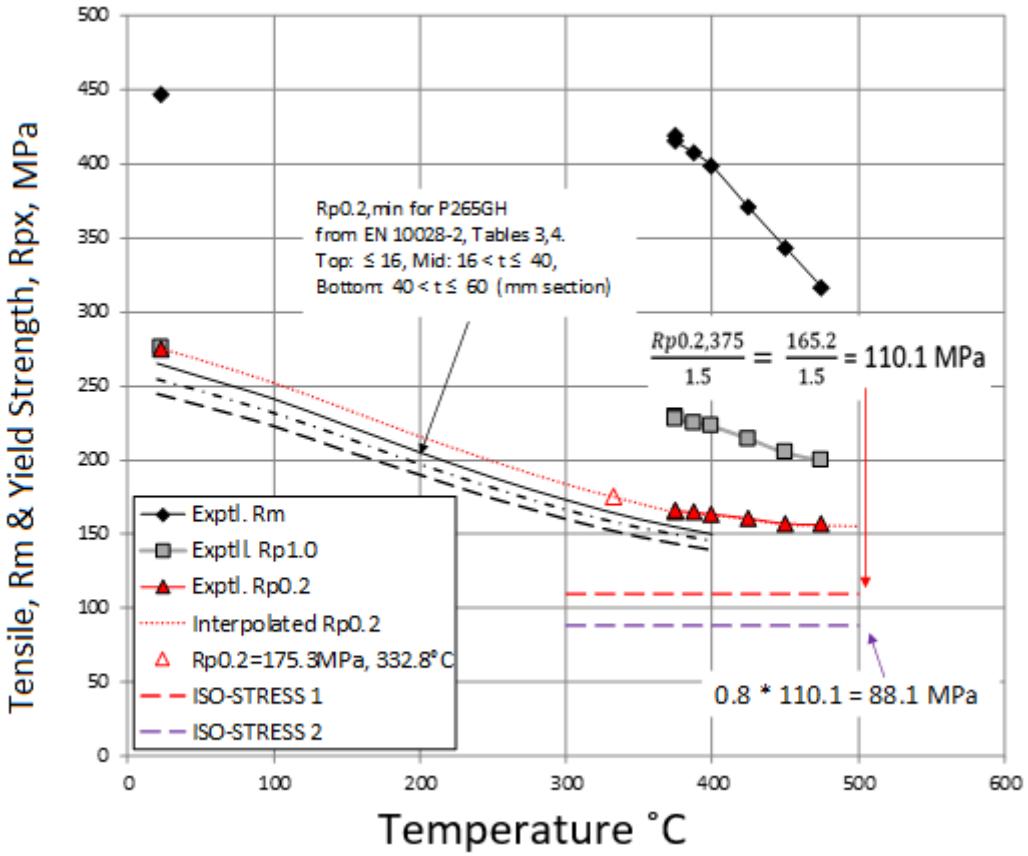

Figure 5.4: Tensile test results P265GH heat 423302.

5.7 X10CrMoVNb9 1 Grade 91 (1.4903)

CSEF steels gain their creep strength in part due to precipitates and dislocation arrangement and distribution and both composition and heat treatment are important in establishing the creep properties [153]. The creep resistance of the broad group of 9-12%Cr tempered ferritic-martensitic steels can be drastically reduced by low cycle fatigue [154]. Dynamic Strain Ageing (DSA) has also been observed in some grades below 500°C [154].

5.7.1 Identification/Composition

Corus GE Specification: STV M23016A (STV M13113) Bar.

Heat Treatment

Harden at 1050°C; for 02:00; time to 05:58; total time 07:58; Oil Quenched from 42°C

Temper at 730°C; for 04:00; time to 06:24; total time 10:24; Air-cooled

Stress Relieve at 710°C; for 02:00; time to 06:11; total time 08:11; Air-cooled

Tables 5.4 and 5.5 contain the supplied information.

Table 5.4: Corus GE STV M23016A Grade 91 Bar Cast No. A7255A Composition.

%	C	Si	Mn	P	Cu	Cr	Mo	Ni
	0.095	0.44	0.47	0.01	0.11	8.44	0.92	0.17
%	Sn	Al	Co	N	Nb	V	S	
	0.007	0.015	0.011	0.042	0.067	0.2	0.0025	

Table 5.5: Mechanical tests. Grade 91. Tested to EN10002-1Cert No. 00208686/1.

Test No.	Ingot ID	Ingot Pos.	Orient	Temp.	0.2%PS	U.T.S.	Elong.	Hardness	Hardness
				°C	N/mm^2	N/mm^2	%	HBW 10/3000	HBW 10/3000
975025	28	M	M	23	545	709	25	212	212

5.7.2 Tensile Properties

The tensile plot at temperature is shown in Figure 5.5 with the derived Rp0.01-2% strengths in Table 5.6. The properties relative to the standard's limits and the test reference stresses shown in Figure 5.6. There are a number of issues to consider with Grade 91. Creep cracking of 9%Cr Grade P91 steel welds have led to a review of the material in the U.S. [155] with microstructural variation from tempered martensite of parent material to ferritic. Poor heat treatment practices and variation in composition with accompanying performance reductions had not been accounted for in weld strength factors and allowable design stress [139]. The aberrant material also appears to have a different Monkman-Grant relation [156]. The U.S. criteria might lead to the view that a marginal heat would have a maximum limit of Ni (0.30% [90]), the lowest N: Al ratio and maximum limits of trace elements as well as a low tensile strength to provide a lower bound for the grade. These are, however, based on reduced creep ductility, strength, void nucleation and weld cracking rather than the creep rate to 0.2% strain. From this and the minimum specified test data in Figure 5.4 the test material could not be considered marginal. The NIMS grades MgA, MgB and MgC (plates), considered in the previous chapters, have lower levels of Ni (<0.09%). MGC (tube) has the highest Ni (exceeding the new ASME Type II criteria) but a significantly higher N: Al ratio, and generally the highest tensile and proof stress. The API [157] suggest 9Cr-1Mo-V Grade

91is likely to have a localised maxima 'hump' in the 0.2% proof stress accompanied by a plateauing of the UTS in the region of 300-400°C which also appears to be the case for this material. It also recommends significantly lower allowable design stresses than the European material.

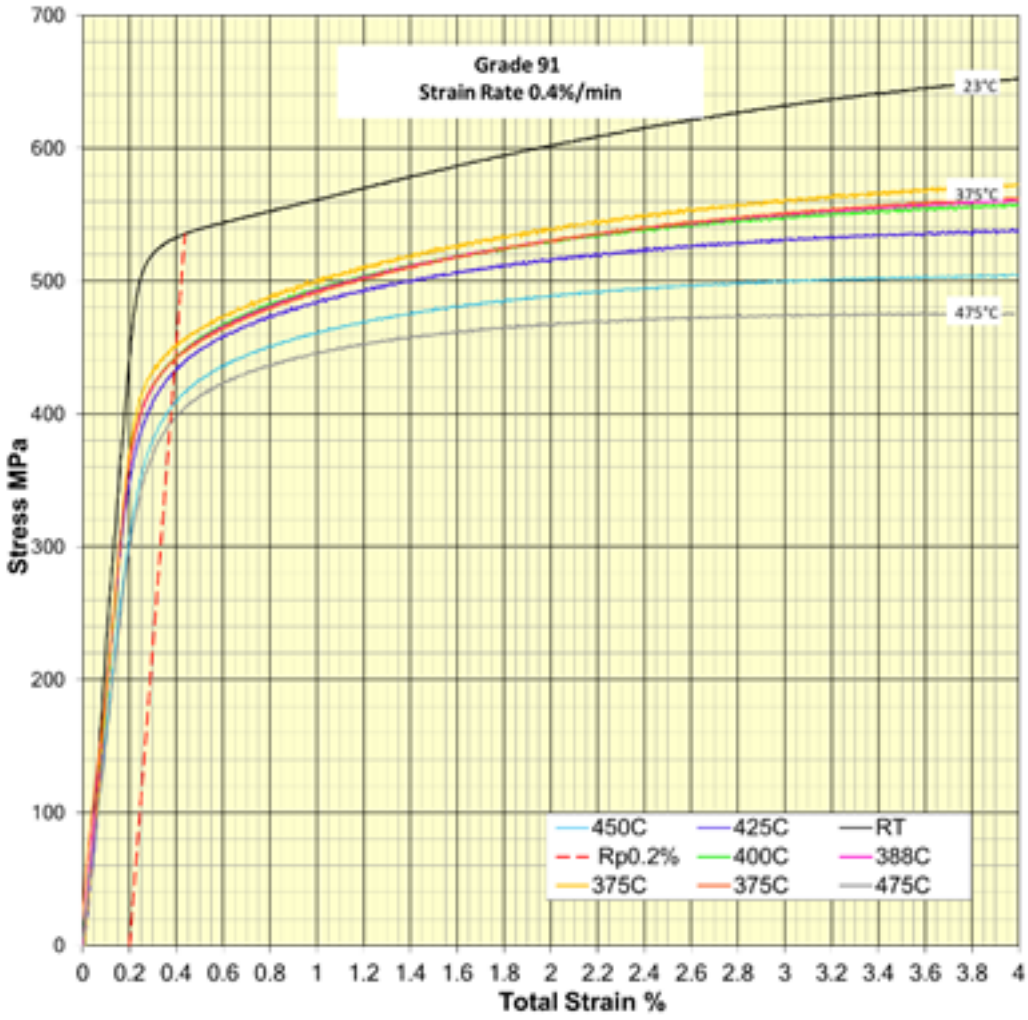

Figure 5.5: Grade 91Tensile strength plots BS EN ISO 6892-2:2018.

Table 5.6: Tensile properties Grade 91.

TEST ID	Target Temp. °C	Average Top/Bot. °C	Cold Modulus GPa	Hot Modulus GPa	Rp0.01 MPa	Rp0.02 MPa	Rp0.05 MPa	Rp0.1 MPa	Rp0.2 MPa	Rp0.5 MPa	Rp1.0 MPa	Rp2.0 MPa	Rm MPa	Elong. A %	Reduc. Z%
W7307	23		218		480.3	497.1	515.2	525.9	535.6	549.8	572.9	611	695	24.7	72
W7308	375	375.2	216	190	386.9	401.5	424.7	440.8	457	485.6	512.7	546.8	573	18.1	73.1
W7314	375	374.8	207	189	372.7	387.6	410.7	428.1	447.3	476.5	504.2	538.8	563	16.9	72.6
W7311	388	387.8	215	188.5	367.5	384	409	427.3	448	478.1	506.1	537.3	561	16.9	72.7
W7309	400	401	206	186	377.9	390.8	410.8	428.5	449.3	479.5	505.9	535.9	561	17	73
W7310	425	425.3	202	184.4	347	365.7	393.5	417.1	440.6	470.2	494.8	521.6	551	17.3	73.1
W7312	450	449.7	204	160.3	312.1	338.2	372.2	396.3	419.7	449.4	472.6	493.3	524	18.8	73.8
W7313	475	475.1	212	154.3	309.4	329.7	363.6	386.4	408.6	435.1	434.7	470.1	500	19.9	75.6

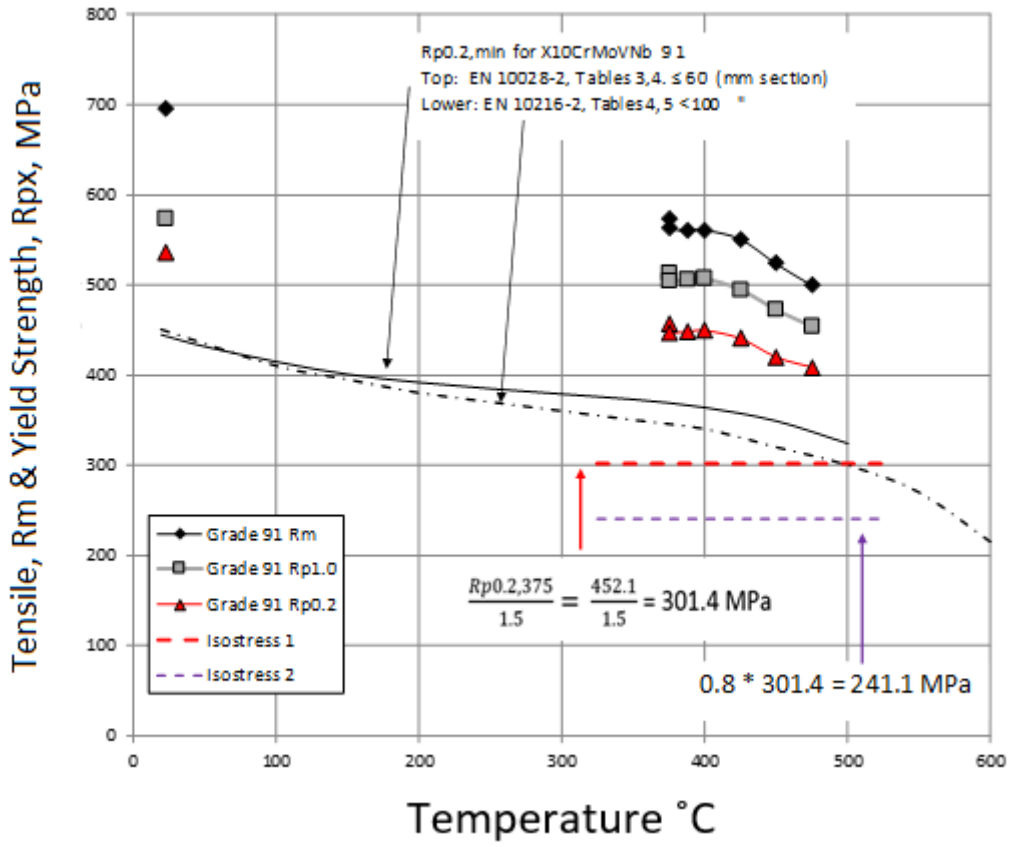

Figure 5.6: Tensile test results Grade 91 heat A72554A.

5.8 316L(N)

5.8.1 Identification/Composition

The Arcelor Mittal 316L(N) material arrived as a 350mm x 250mm x 50 mm thickness plate, Product 42906.011 Heat AO366. Tables 5.7 and 5.8 contain the supplied information.

Table 5.7: Arcelor Mittal 316L(N) Product 42906.011 Cast AO366 Composition.

%	C	Mn%	Si%	P%	S%	Cr%
	0.023	1.72	0.21	0.021	0.000	17.3
%	Ni	Mo	Co	N	B	Cu
	12.21	2.39	0.04	0.066	0.0005	0.15

Table 5.8: Mechanical Tests EN10204:2004 cert No 2012-309012.

No. Lot	Temp.	Rp0.2	Rp1.0	Rm	Z	ALo=5d	Toughness
	°C	%	%	MPa	%	%	J
42906,011-T.1/4 Top	20	325	365	564	82	54	130,134,128,131
42906,011-P.1/4 Bottom	20	313	354	560	83	55	152,164,156,157
42906,011-T.1/4	550°C	172		404		36	

5.8.2 Tensile Properties

The tensile plots are shown in Figure 5.7, the Rp0.01-2% strengths in Table 5.9 and the properties in relation to the standard limits shown in Figure 5.8. There were some issues with the tensile testing of the 316L(N) material above 450°C. 316L(N) is known to be susceptible to dynamic strain ageing (DSA) and serrated flow at elevated temperatures [158, 159]. The imposed strain rate of the tensile machine cross-head is exceeded by the plastic strain rate of the sample with a drop in load. This may also occur in creep tests [148] but there appears no evidence in the public domain for this in 316L(N) [1, 160]. Above 450°C it appears the material experienced serrated flow at the testing strain rate. At 525°C the plot became so erratic testing was terminated believed to be a machine problem rather than due to the serrated flow.

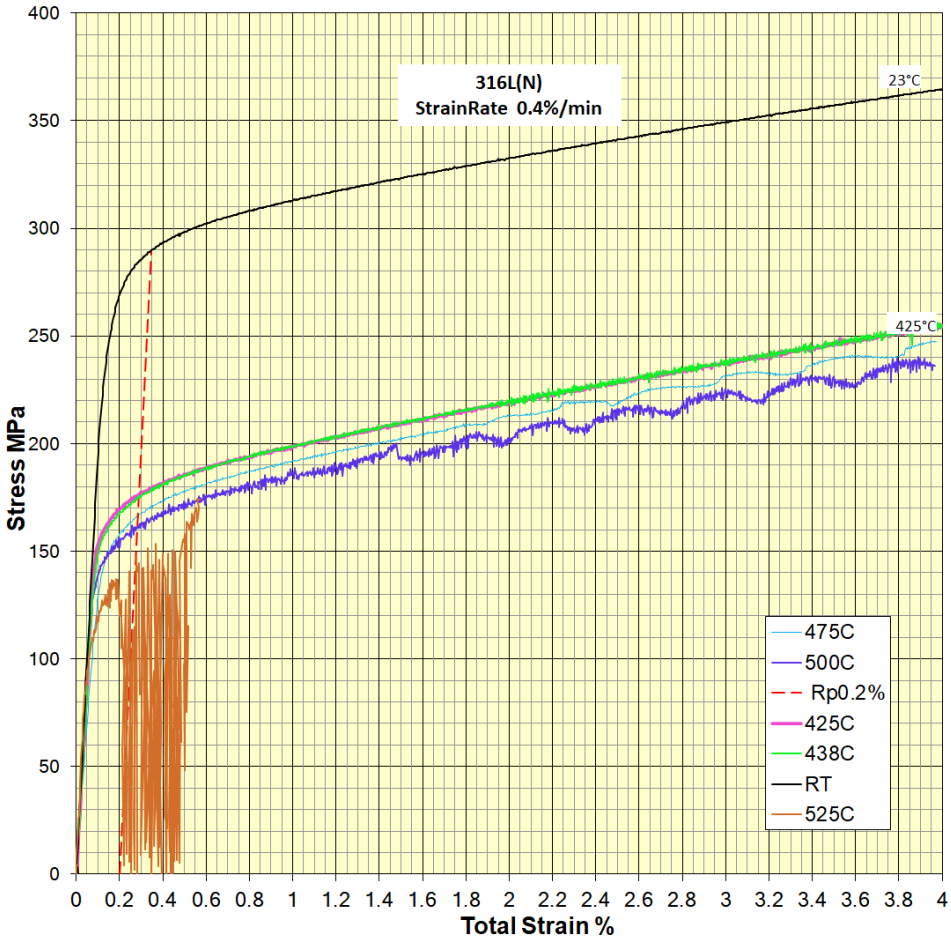

Figure 5.7: 316L(N) Tensile strength plots BS EN ISO 6892-2:2018.

Table 5.9: Tensile properties 316L(N)

TEST ID	Target Temp. °C	Average Top/Bot. °C	Cold Modulus GPa	Hot Modulus GPa	Rp0.01 MPa	Rp0.02 MPa	Rp0.05 MPa	Rp0.1 MPa	Rp0.2 MPa	Rp0.5 MPa	Rp1.0 MPa	Rp2.0 MPa	Rm MPa	Elong. A %	Reduce. Z %	
W7289	23		196.1		226.8	242	264	278.3	289.7	304.0	316.5	335.5	367	58.1	85.6	
W7290	425	425.7		178	150.8	155.6	162.4	169.1	177.4	188.7	200.6	221.3	441	42.2	85.2	
W7291	438	438.3	208.6	174.4	143.7	150.4	159.5	167.5	175.8	189.1	201.6	222.9	442	42.7	84.3	
W7292	450	450	208.9	137.3				143.6	155.0	169.7	182.9	205.1	434	44.2	84.5	Missing data
W7296	475	474.9	190	139.8	131.1	140.7	151.4	159.8	169.1	182.3	194.6	214.5	432	43.2	84.2	
W7297	500	500.1	203.3	188.9	151.5	134.3	143.2	151.5	161.3	174.5	185.6	205.3	422	43.8	91.7	
W7295	525	525	208	203.9	96.2	107.6	120.9	134.2	141.5				388	408	84.7	Missing data

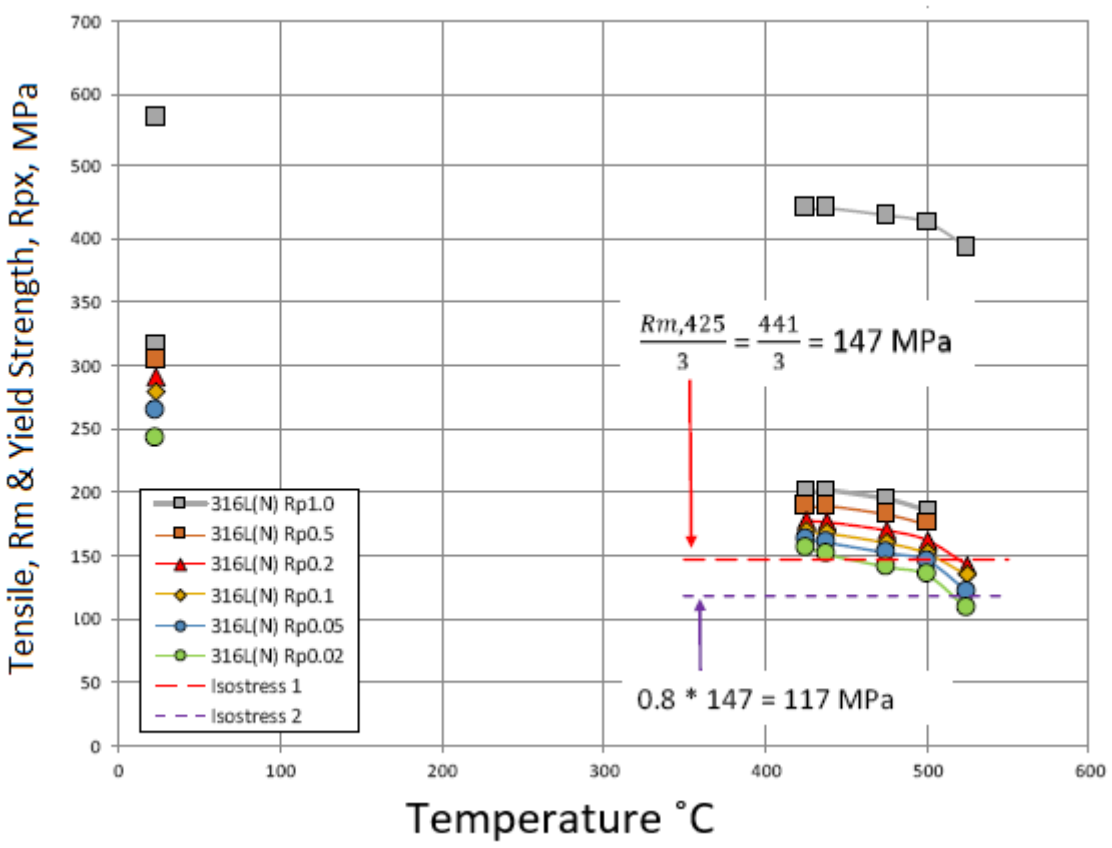

Figure 5.8: Tensile Properties for 316L(N) heat AO366.

5.9 Reference Stresses

The reference stresses for each material were calculated in accordance with the EN13445-3 Table 6.1 criteria for the maximum allowable design stress based on the tensile properties at the traditional T_{NC}, 375°C for the P265GH/Grade 91 and 425°C for 316L(N), shown in Table 5.10. As is typical with creep tests these are based on single tests at temperature, they do have uncertainty. Wilshire-Scharning's basis for using the tensile strength over the proof strength. The uncertainty of the tensile strength from single tests does warrant further investigation.

Table 5.10: Calculated reference stresses at traditional no-creep temperatures from tensile test data.

Material	σref	σ/σ_{TS}	0.8σref	σ/σ_{TS}
P265GH	110.1	0.26	88.1	0.21
Grade 91	301.1	0.53	240.8	0.42
316L(N)	147.4	0.33	117.4	0.27

5.10 High Sensitivity Creep Testing

The samples used for the creep testing had a gauge length of 100mm and 9mm diameter shown in Figures 5.9 and 5.10.

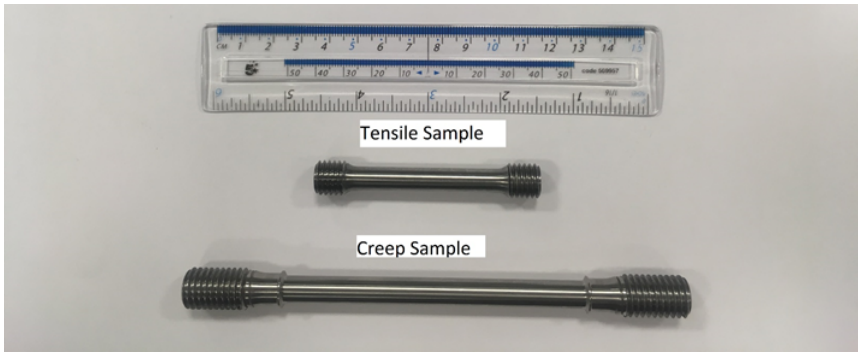

Figure 5.9: Test samples for the experimental programme.

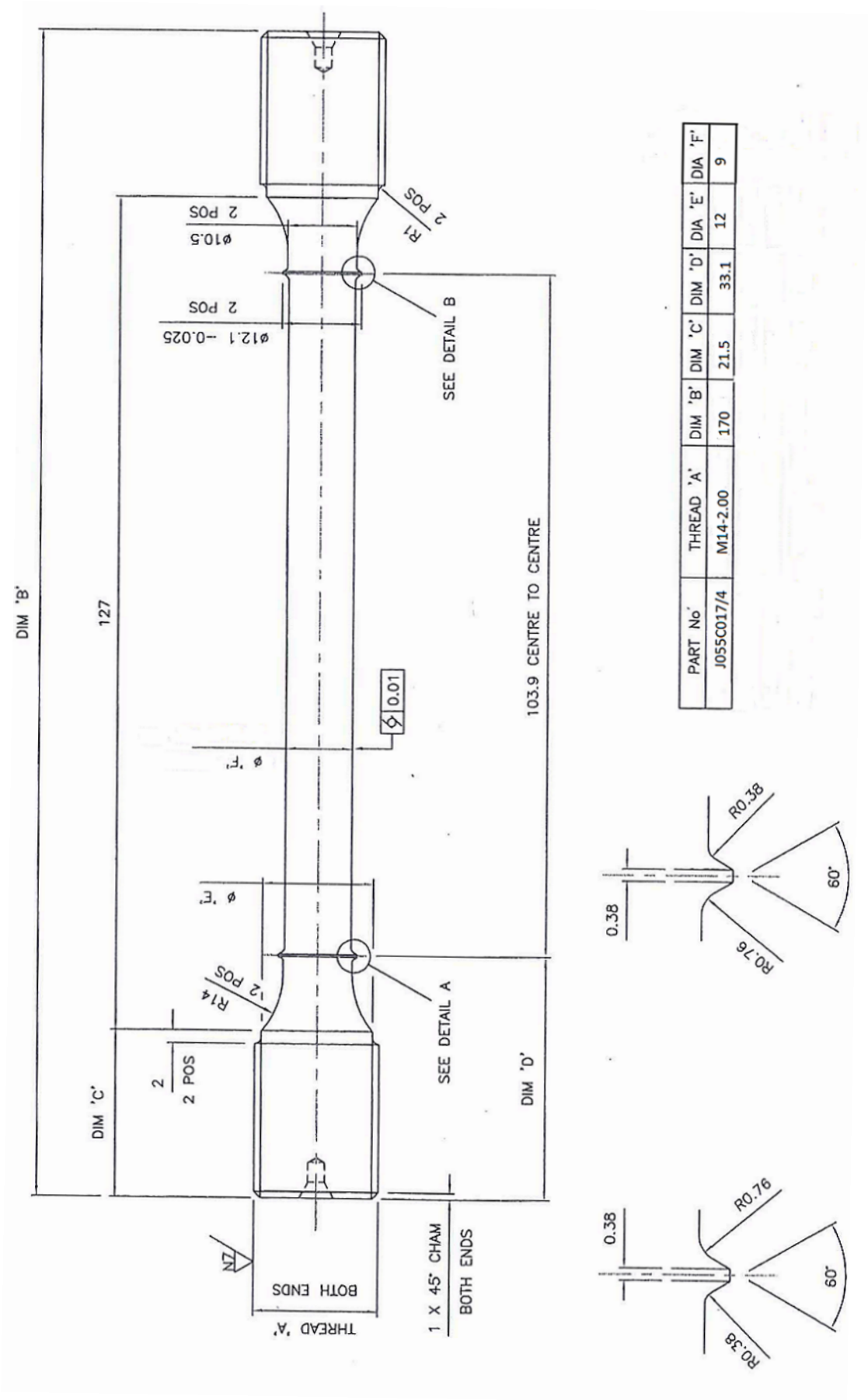

PART No'	THREAD 'A'	DIM 'B'	DIM 'C'	DIM 'D'	DIA 'E'	DIA 'F'
J055C017/4	M14-2.00	170	21.5	33.1	12	9

Figure 5.10: Details of 100mm gauge length, 9mm diameter, M14 High-sensitivity creep samples.

5.10.1 Experimental procedure

All testing was completed in an established creep laboratory with recognised quality and management systems and suitably calibrated frames, transducers, extensometers, thermocouples and measuring and control systems. All constant load tests were carried out in accordance with BS EN ISO 204:2018 [161] on single test piece machines fitted with triple-zone cylinder furnaces. A total of six different test frame configurations (Denison T45 & T48, BNF, NPL, Crowther, and MSP) were used randomly allocated on availability. Each frame type had different configurations and arm ratios and thus loads and loading rates. Loading was manually placing dead weights on the lever pan, except for the T45 which used a jockey-weight arm. The samples were measured using a Keyence IM-6125 image dimension measuring system with loads calculated based on the minimum cross-sectional area for the specified stress. Calibrated stainless steel spring-on extensometers mounted on the sample collars were used with ASL or RDP transducers to measure the extension. The maximum uncertainty in the calibration of the extensometer and transducers was $\pm$ 4μm. A typical extensometer layout is shown in Figure 5.11 with three R type thermocouples in intimate contact with the sample surface via heat-resistant string, in the middle of the gauge length and at upper and lower ends. Throughout the sample placing and set-up checks and adjustments were made to ensure load axiality and the two transducers attached to the extensometer had synchronised displacement. A cold modulus measure was made with half the test load as a final check. A small nominal load was applied to align the load train during heating with the furnaces controlled to achieve the target temperature within 2°C within 24 hours. When this was achieved for a minimum of 1 hour loading commenced. With typically a minimum of 8 increments, the test load was applied to provide a hot modulus with a stable balance on completion. An automated system logged the elastic and instant plastic strain, hot modulus and continuously the extension measurement averaged and the sample temperatures. The tests were terminated typically when a creep strain of 0.2% was achieved or the facility was no longer available. There were no extraordinary incidents to report.

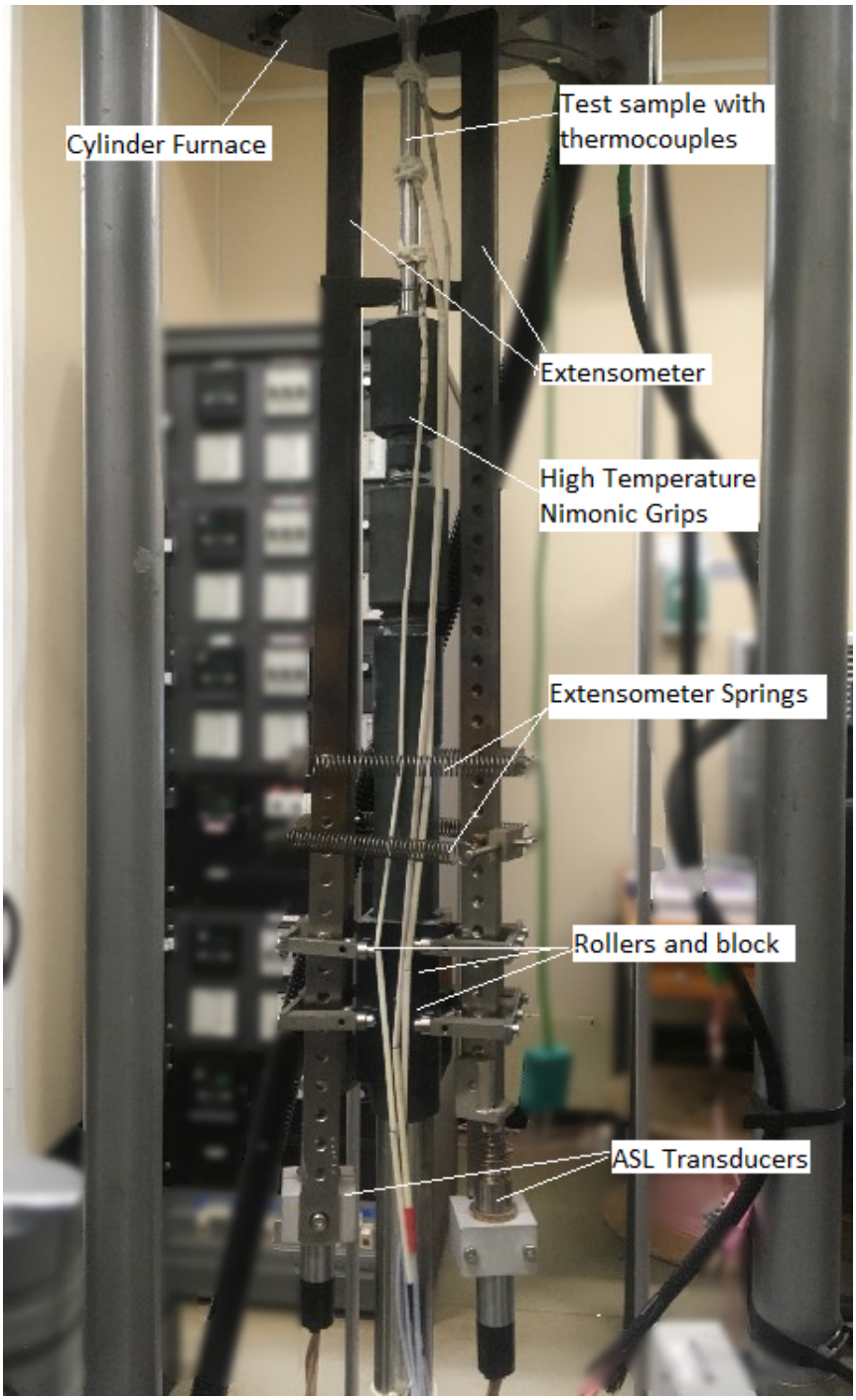

Figure 5.11: Typical extensometer rig with the cylinder furnace to be lowered to just above the springs (to align the sample and furnace centres).

The initial planned test matrix is outlined in Table 5.11, the rationale being the array should adequately capture the strain developed in the region of the material T_{NC} with some accelerated data. However, this proved to be an over simplistic approach for all three materials with the final temperatures shown in the results. Firstly the 316L(N) proved to provide little strain in the initial tests up to 500°C and the tests were adjusted to significantly higher

Table 5.11: Planned test matrix to approx. 10k hrs.

Material/Test/Temperature	1	2	3	4	5	6
P265GH &Grade 91	375°C	388°C	400°C	425°C	450°C	475°C
316L(N)	425°C	438°C	450°C	475°C	500°C	525°C

temperatures to collect any data within the limited time frame. In contrast, it became evident early in the 375°C test for P265GH that creep was significant and a lower temperature would be needed to provide more relevant information. The time available for test duration was also significantly less than the planned 10k hours to suitably progress the lower temperature curves. The approach for future testing should be to start with a single test at 25°C above the speculative T_{NC} which might be 375°C for most of the low alloy materials and 425°C for the CSEF materials. Austenitics might require a substantially higher initial temperature of +100°C based on the 316L(N). With a progressed curve the matrix can then be developed depending on the results and time frame available.

5.10.2 Results and Discussion

The details of experimental loading and unloading are rarely reported and could have a profound effect on the measured results [162].

The instantaneous plastic strain (IPS) for each of the materials is plotted in Figure 5.12. Both the P265GH and Grade 91 materials appear well represented by an exponential growth model. The 316L(N) material lower stress is of the same order as the other materials, however, for the higher level the IPS is both significantly higher and erratic. The 575°C and 600°C specimens were both loaded on the same frame configuration with the difference attributed to the time required to obtain a stable balanced loading. As the proof stress is reached the recording of IPS and creep strain can be highly subjective. It is important to point out each sample set used at least two different frame types with different loading rates. These are singular tests but there appears no significant correlation between the loading rates (frame type) and the IPS — where an individual test was repeated on a different frame the IPS was 5% higher.

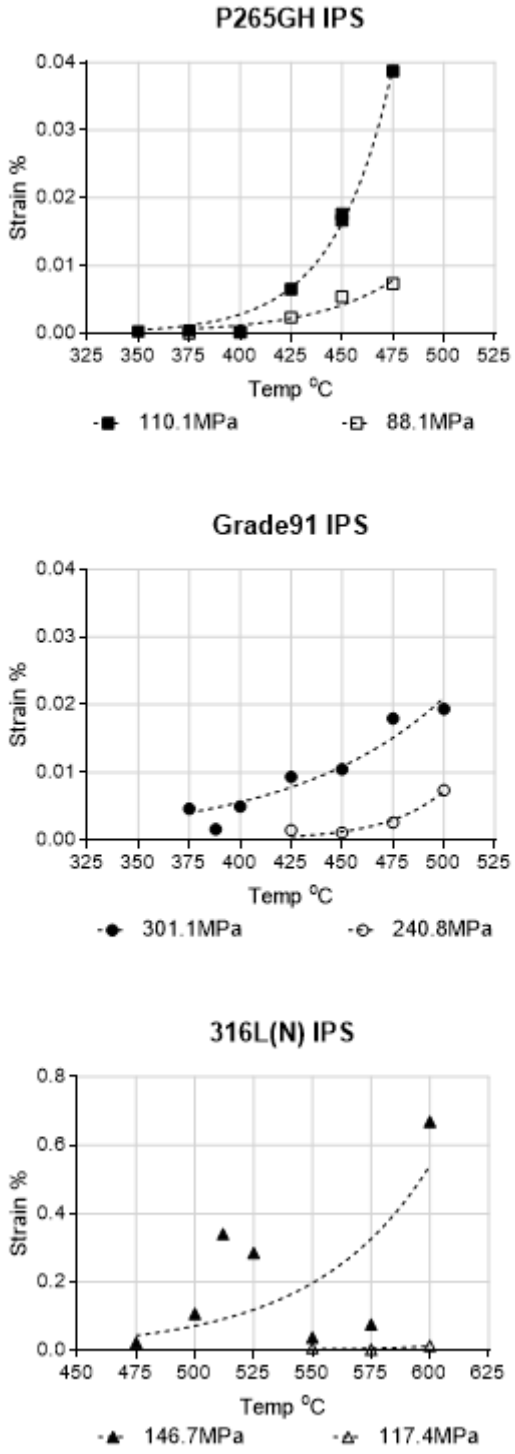

Figure 5.12: Instantaneous 'plastic' strain IPS on loading creep tests.

The plots indicate a clear temperature relationship with instantaneous plasticity for the P265GH and Grade 91 materials. For the 316L(N) the relationship appears more complex and variable. The exponential growth fitted model predictions of the temperature to 0.2% IPS

Table 5.12: Exponential growth model predictions of 0.2% IPS limit temperatures.

Grade 91		P265GH	
301.1 MPa	241.1 MPa	110.1 MPa	88.1 MPa
631°C	657°C	510°C	526°C

are contained in Table 5.12 — the limits on the accelerated tests for these materials. These indicate some margin to prevent IPS effects. The Grade 91 plot indicates the IPS is significant, up to 0.01% over the temperature range of interest 400-450°C for the T_{NC}calculation, although for the P265GH it would have much less of an effect on the calculation. The recommendation is that the total strain be used in the calculation rather than creep strain [129]. The Elastic Modulus measurements during the tests are shown in Figure 5.13.

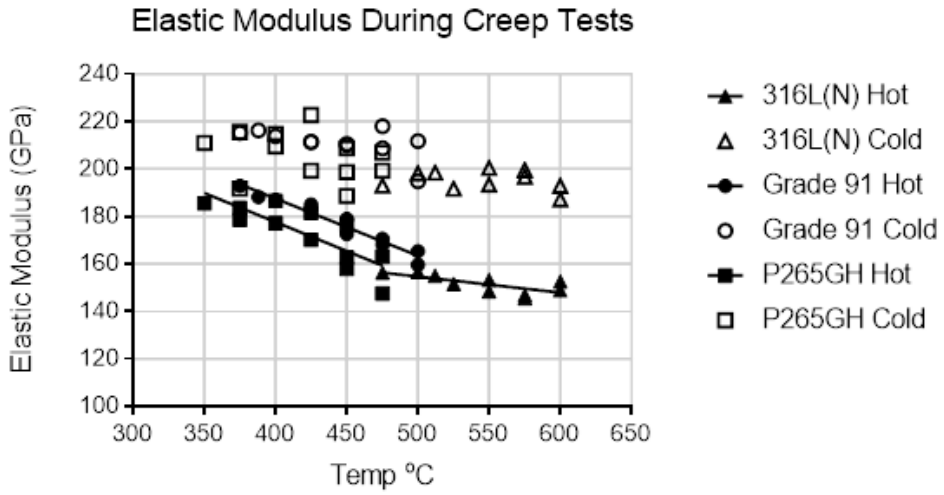

Figure 5.13: Elastic modulus measured during creep tests.

5.10.3 P265GH (1.4025)

The total plastic strain v time data from the tests are shown in Figure 5.14 and Figure 5.15. The times to a specific strain, determined by the DIN 50118 linear interpolation method are indicated by red circles. For each data point, the log strain value is linearly interpolated between successive experimentally measured data points. For multiple time values, the Excel GEOMEAN function is then used which is the nth root of the product of all values. The experimental times to a specific strain have been fitted to an exponential plastic strain-time model and extrapolated as green squares. Extrapolation is shown extended but limited to <10% of the measured data for the purpose of fitting the isostress lines. A simple plastic

strain-time model relating the log(time) to log(strain)1/n (see Appendix A) for the P265GH model appears to fit the data well accommodating the low levels of initial plastic strain evident in the higher temperature tests. The model fit to P265GH at 110.1 MPa 375°C parameters is shown in Eq. 5.2.

$$\log(t,h) = -1.3930.\log(\varepsilon,\%)^{2.10} + 4.9050 \quad (t >\sim 5h) \tag{5.2}$$

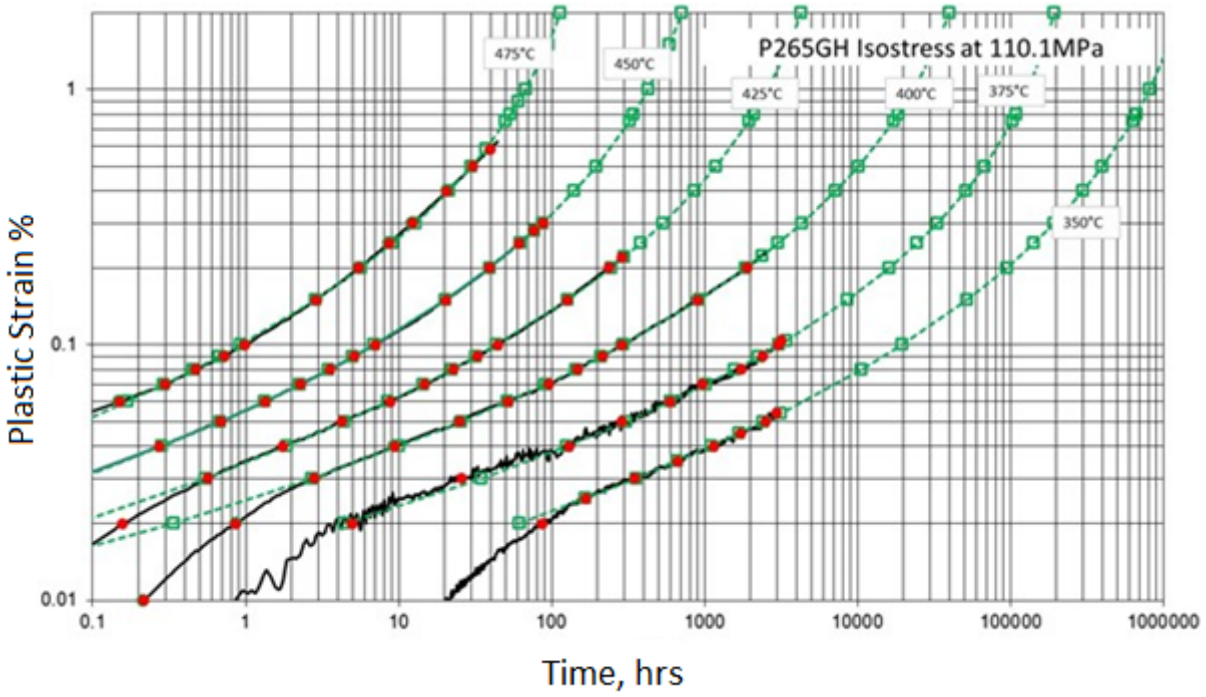

Figure 5.14: Creep test results at 110.1 MPa on P265GH. Test data are black lines with red dots at specified strains. Fitted points from the strain-time model are shown with extrapolation beyond test data in green

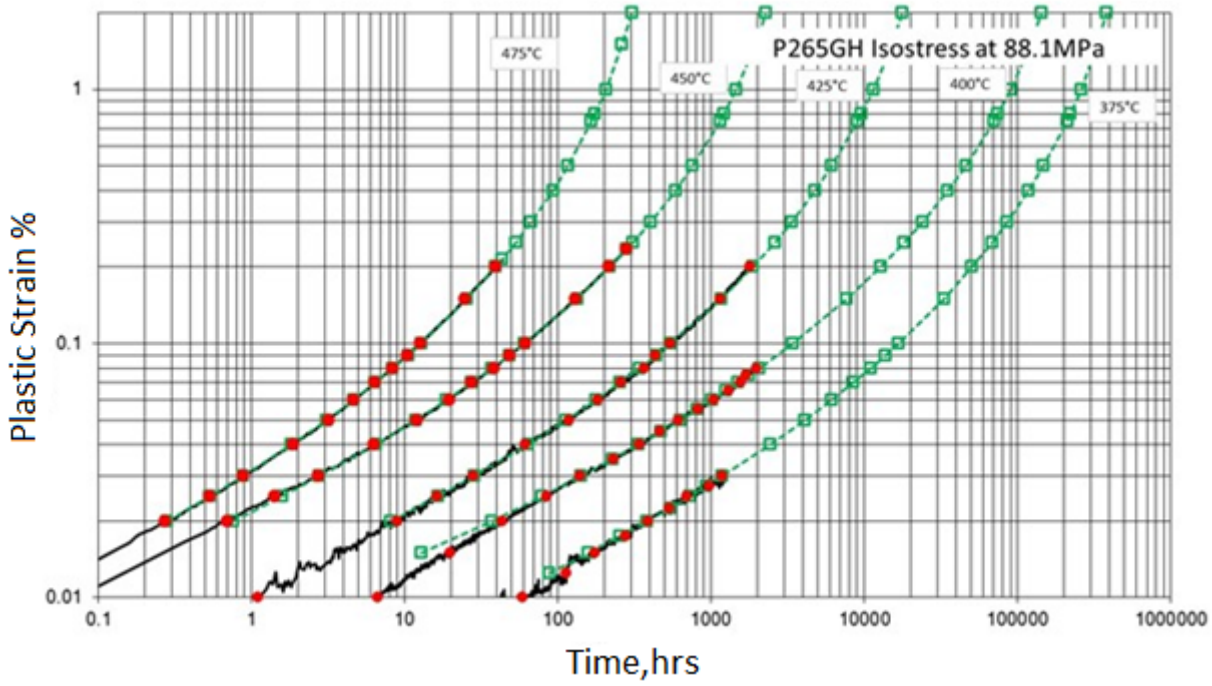

Figure 5.15: Creep tests at 88.1 MPa on P265GH. test data are black lines with red dots at specified strains. Fitted points from the strain-time model are shown with extrapolation beyond test data in green

The isostress plots are shown in Figure 5.16 and Figure 5.17. The plots appear to be reasonably parallel > 0.02% strain and there is no reason to doubt the suitability of linear extrapolation of the 0.2% strain isostress lines to the 200kh datum according to the findings of Timmins and Smith above.

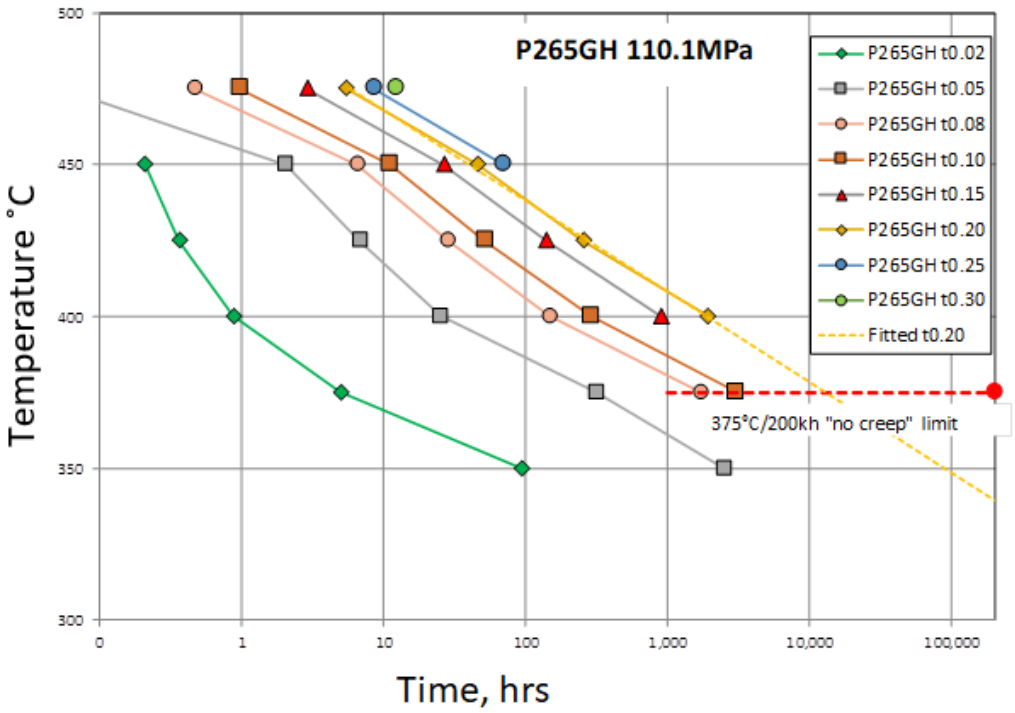

Figure 5.16: Times to specific total plastic strain at 110.1 MPa (upper) on P265GH. The extrapolated 0.2% line in yellow.

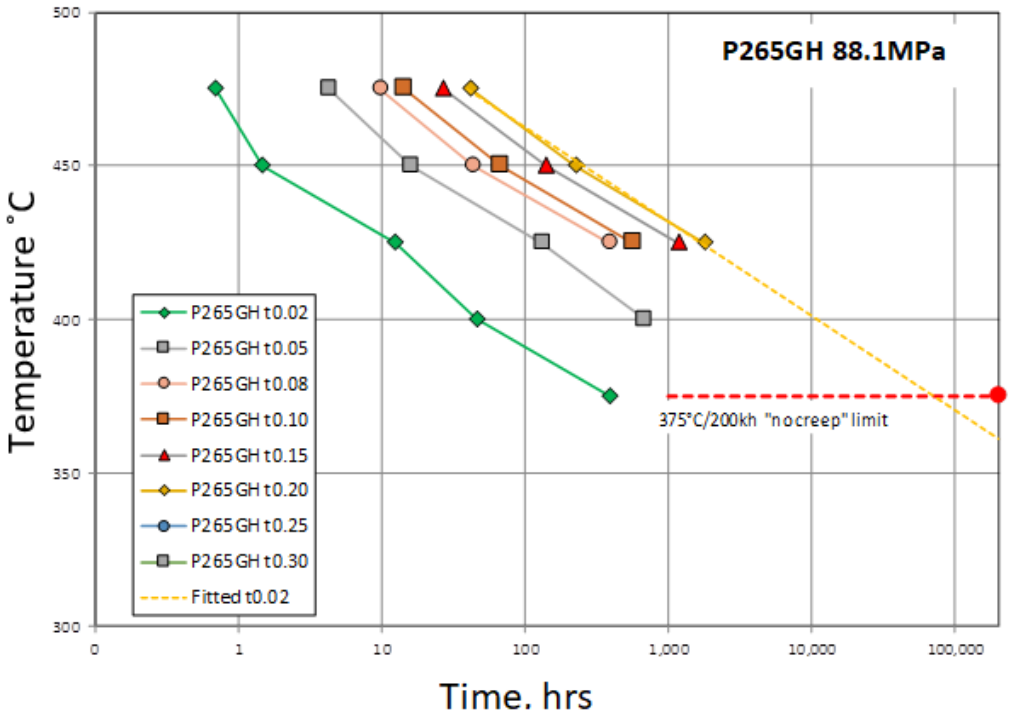

Figure 5.17: Times to specific total plastic strain at 88.1 MPa (lower) on P265GH. The extrapolated 0.2% line in yellow.

The T_{NC} has been assumed as 375°C for the reference stress and this needs to be cor-

rected for the experimentally derived value. A simple linear relation between the no-creep temperatures and the reference stress is assumed to converge the values by iteration. The extrapolation in Figure 5.18 includes the corrected isostress plot. The 200kh T_{NC} for both the experimental data and for the recalculated reference stress of 116.8 MPa, from iteration - a T_{NC} of 331.8°C.

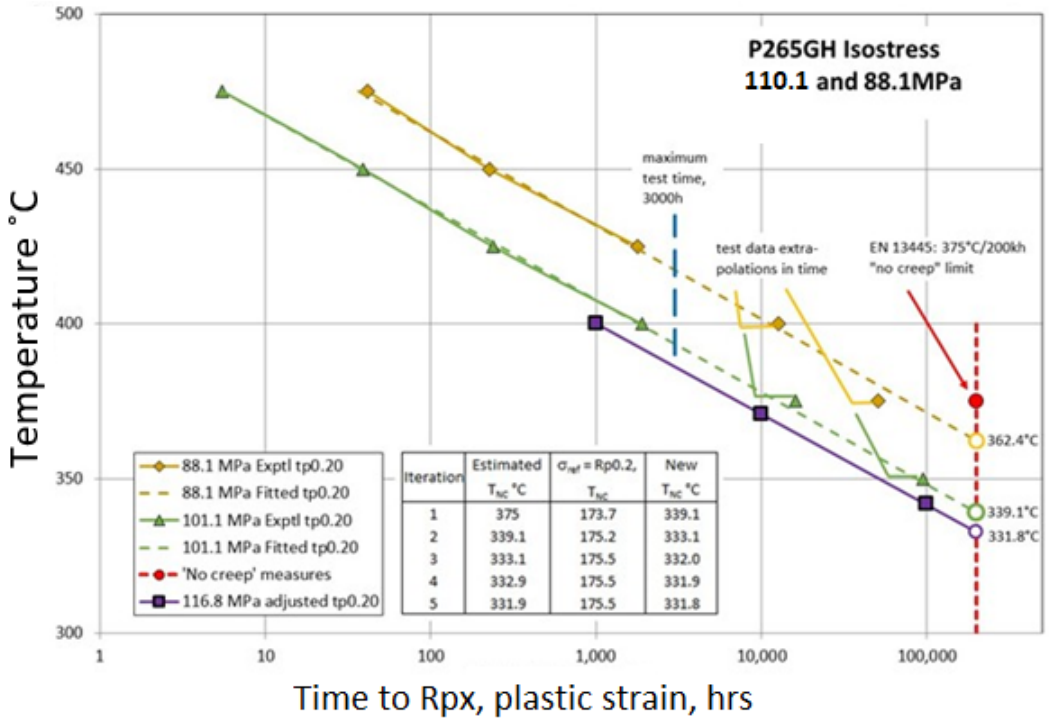

Figure 5.18: Isostress lines for both upper and lower reference stress levels for the heat at 375°C. Points beyond 3000h are extrapolated from the strain-time experimental data.

These values are in line with those estimated from the original Wilshire and the Manson-Haferd MH4 models of the VDEh data for the historical equivalent of P265GH in Chapter 2. The estimate of 0.2% strain at 375°C, the T_{NEC} negligible creep region limit is ∼7kh and for 360°C ∼23kh to put this material in context with the historical failures.

5.10.4 X10CrMoVNb9-1 Grade 91 (1.4903)

The more complex behaviour of the Grade 91 heat is not as well represented by the simple plastic strain-time model over the full test curve. An exponent n = 3.2 which appears more appropriate to the later stages higher temperature tests has been used for limited extrapolation. It has been assumed the lower temperature tests regime is also appropriately described by the same model as the upper. The values extrapolated in Figures 5.21 and 5.22 show some

reasonable values compared to the isostress plots.

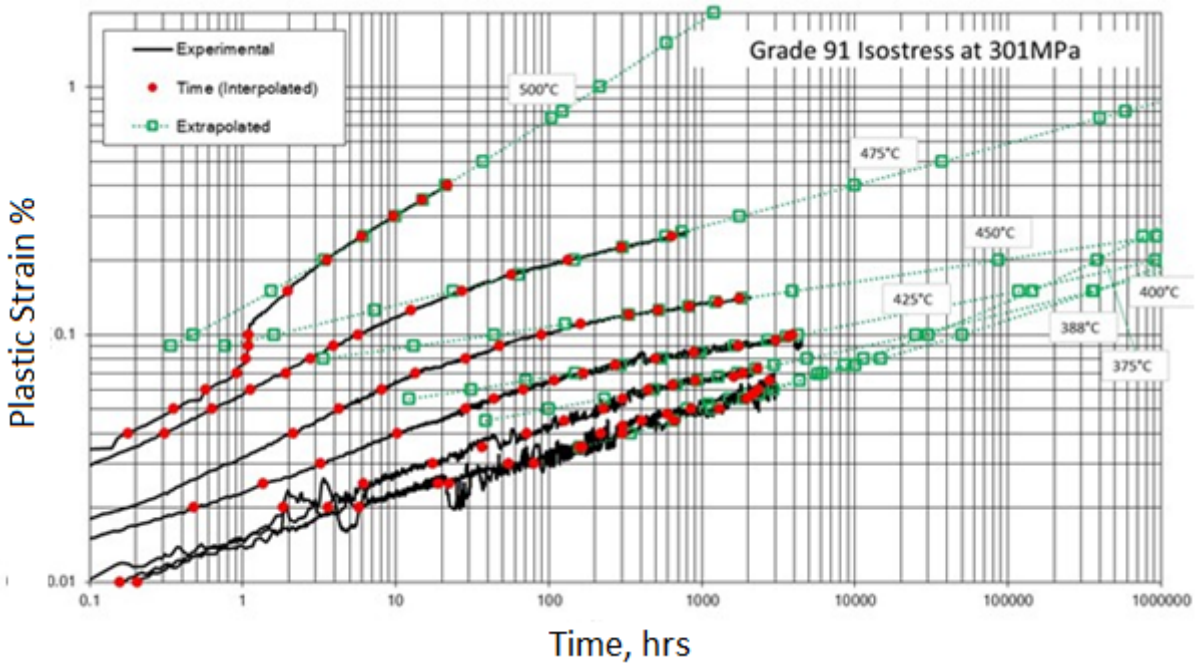

Figure 5.19: Creep test results at 301.1 MPa (upper) on X10CrMoVNb9-1 Grade 91. Test data as black lines with red dots at specified strains. Fitted points from the strain-time model are shown with extrapolation beyond test data in green.

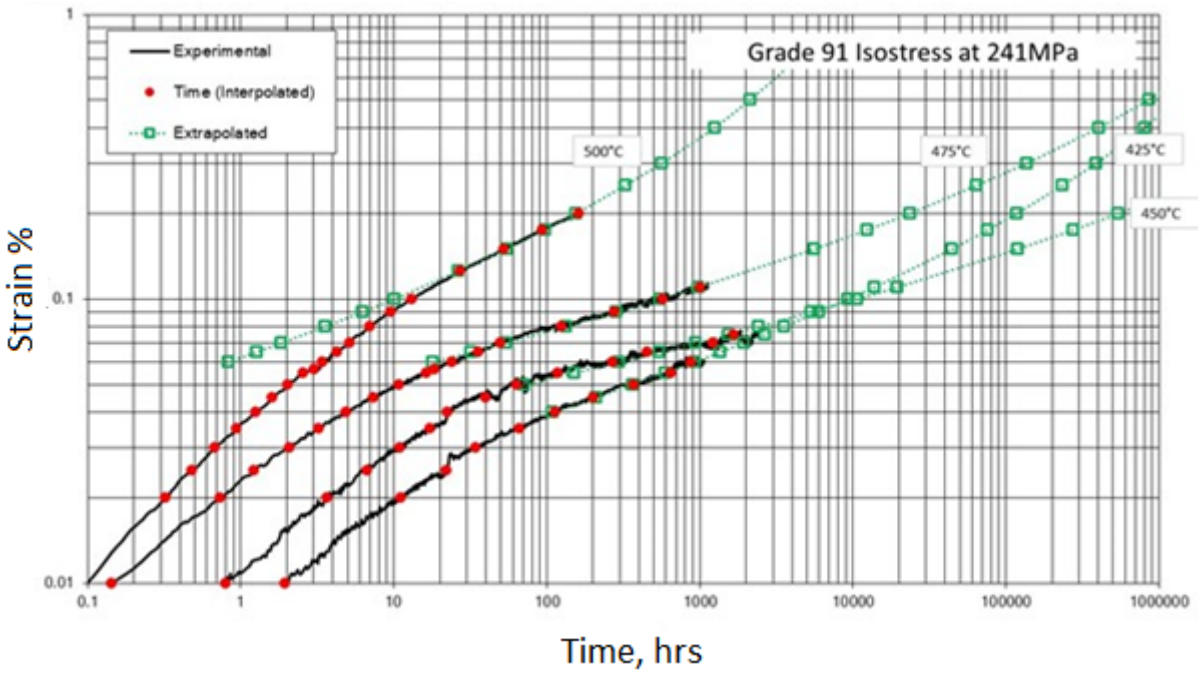

Figure 5.20: Creep test data at 242.1 MPa (lower) on x10CRMoVNb9-1 Grade 91. Test data as black lines with red dots at specified strains. fitted points from the strain-time model are shown with extrapolation beyond test data in green.

The isostress plots for the Grade 91 material appear to be reasonably parallel for the 0.02 and 0.05% strain levels at 301 MPa but the remaining lines are of a non-constant slope. This would be consistent with the data collected within both the primary and secondary regimes in the findings of Timmins & Smith [143].

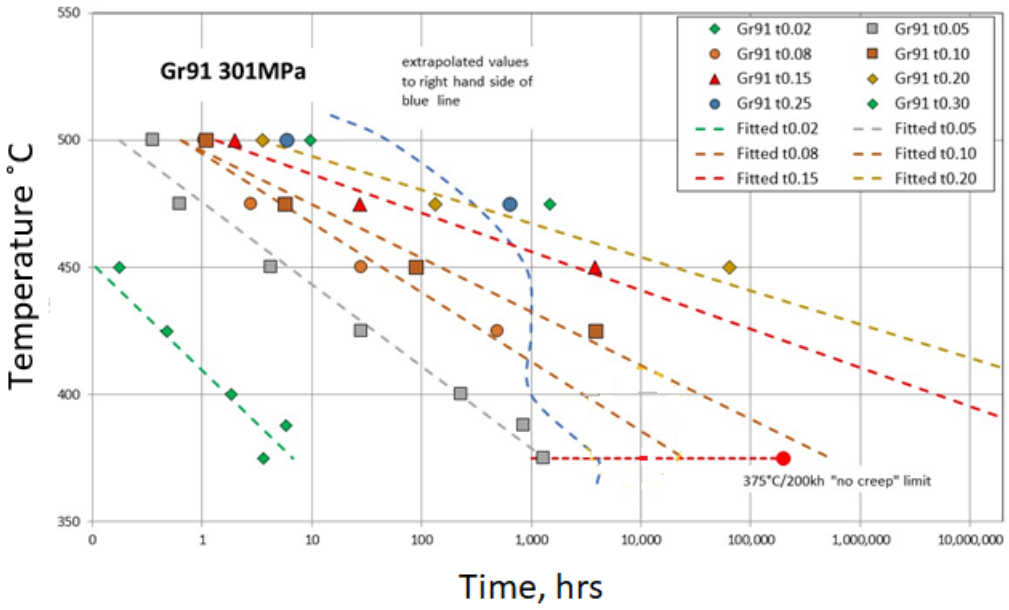

Figure 5.21: Times to specific total plastic strain at 301.4 MPa (upper) on Grade 91. The blue line indicates the limit of test data.

Times to specific total plastic strain at 301.4 MPa (upper) and 241.1 MPa (lower) on Grade 91 heat A72554A. Several strain levels are plotted on each figure, and the fitted lines include extrapolations to up to x10 the longest experimental point. The blue dashed line divides the measured test data from the extrapolated to the right.

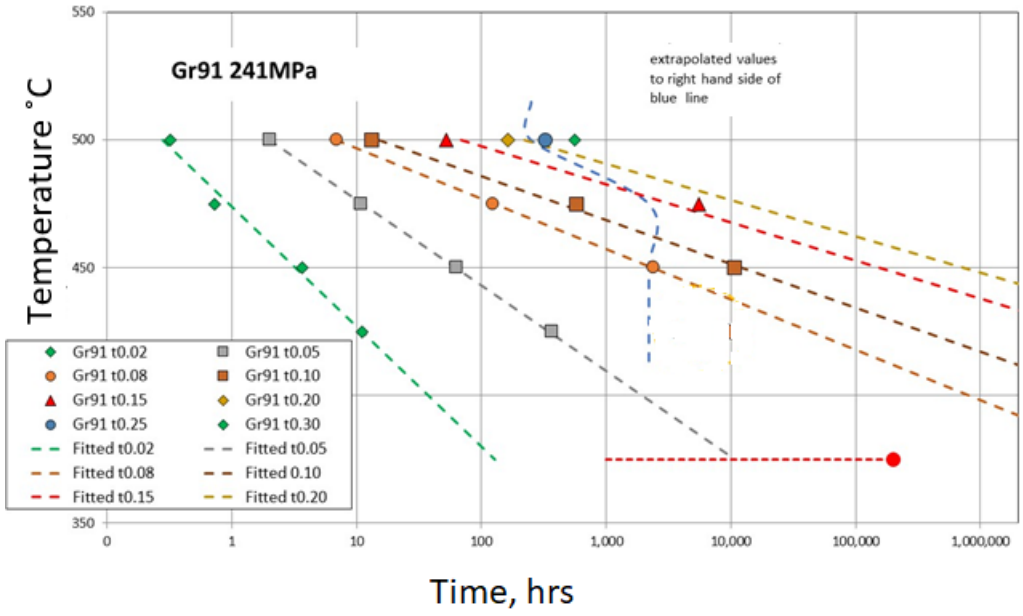

Figure 5.22: Times to specific total plastic strain at 241.1 MPa (lower) on Grade 91.

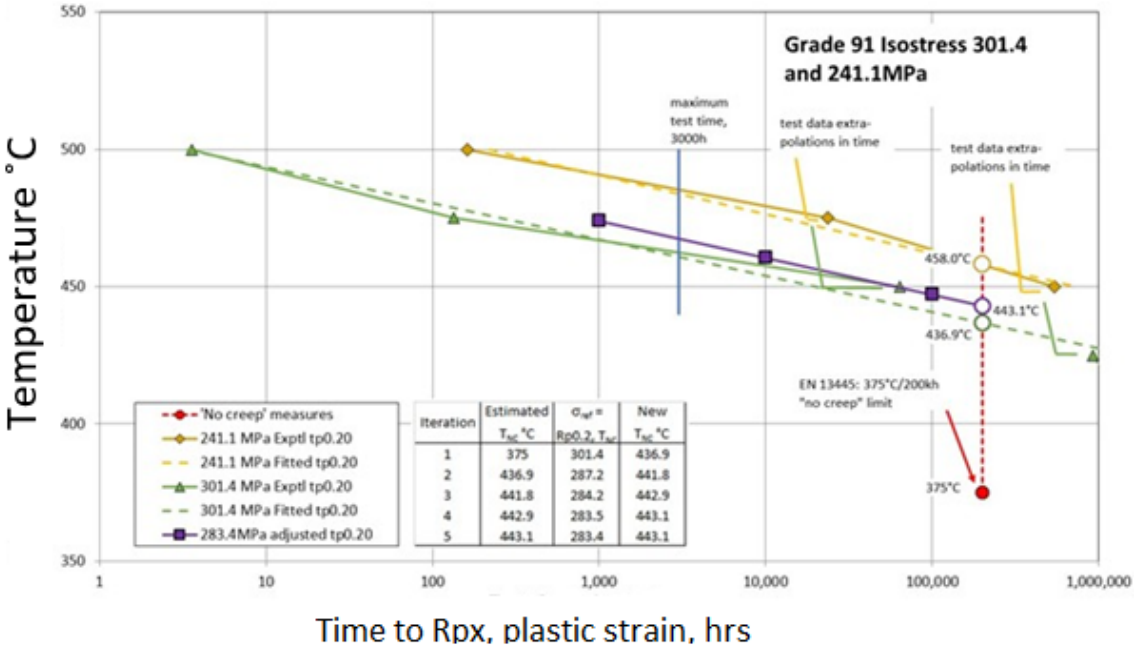

Figure 5.23: isostress lines for both upper and lower reference stress levels for the heat. The 200kh T_{NC} for both the experimental data and for the recalculated reference stress of 283.4 MPa, from iteration - a T_{NC} of 443.1 MPa.

Creep test results on Grade 91 heat A72554A. The isostress lines at 0.2% plastic strain from experiments are shown at 301.4 and 241.1 MPa, corresponding to σref and 0.8σref for the heat at 375°C. Points beyond 3,000h are extrapolated from the strain-time experimental data, as shown in Figure 5.21 and Figure 5.22 (the fitted lines are based on data within x10

of the test end). In Figure 5.23 the 0.2% strain isostress lines are shown extrapolated to the 200kh no-creep temperatures for both sets of experimental data, and for the reference stress of 283.4 MPa at 443.1°C, obtained by iteration, which is $0.54\sigma/\sigma_{TS}$. This is ∼27°C higher than might be expected from the previous Chapters on the NIMS 9Cr-1Mo-V-Nb Grade 91 and for x10CrMoVNNb9 1 [129]. There are a number of issues with the Grade 91 results and extrapolation

- uncertainty in the extrapolation given the limited test duration and 0.2% strain data. In this case, an interim result might provide a non-conservative estimate of the T_{NC}- if the method is to be adopted sufficient test duration to gather 0.2% total strain data must be allowed - the curve trajectories indicate >10kh would be required for this material with a slightly lower reference stress. In the meantime, the lower value estimated from the models (410°C rounded down) would appear appropriate.

- unlike the P265GH data and isostress plots the isostress lines appear 'flared' with non-constant slope ≥0.08% strain which would indicate the data is collected over the transition region. If this is the case the lines may not follow the linear extrapolation and turn downwards as they enter the tertiary region. The 200kh datum will be achieved at a lower temperature as shown in Figure 5.1 as they return to be parallel with the lower strains. This adds further uncertainty to the result and the possibility that a non-conservative T_{NC} is provided by inappropriate linear extrapolation. Of course, this would suggest that 0.2% total strain is going to be in the tertiary region which is contrary to the basic assumption that 0.2% is a fraction of the mcr which typically occurs around 1% [129].

5.10.5 316L(N)

The plots for 316L(N) are of limited data and without multiple times to 0.2% strain the isostress plot trajectory would have to rely on extrapolated data. This appears to indicate the material T_{NC} is above 525°C at the upper reference stress. At 500°C the reference stress would reduce to 140.7 MPa and at 525°C 129.3 MPa.

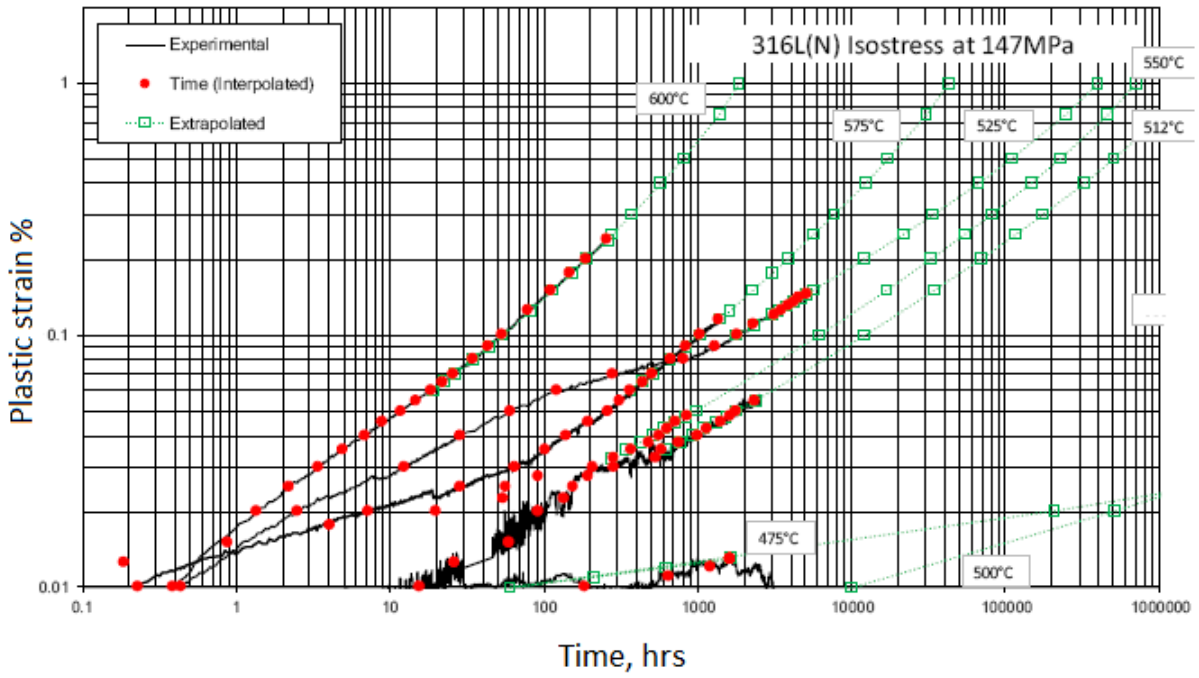

Figure 5.24: Creep test results at 147.4 MPa (upper) on 316L(N).

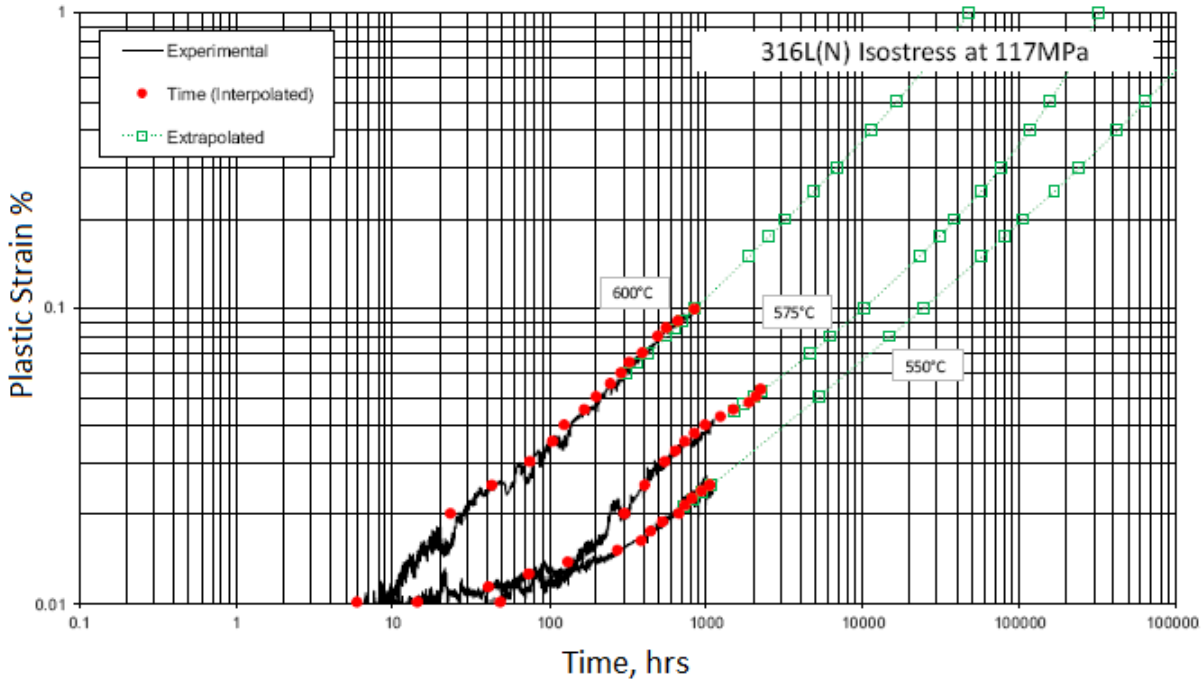

Figure 5.25: creep test results at 117 MPa (lower) on 316L(N).

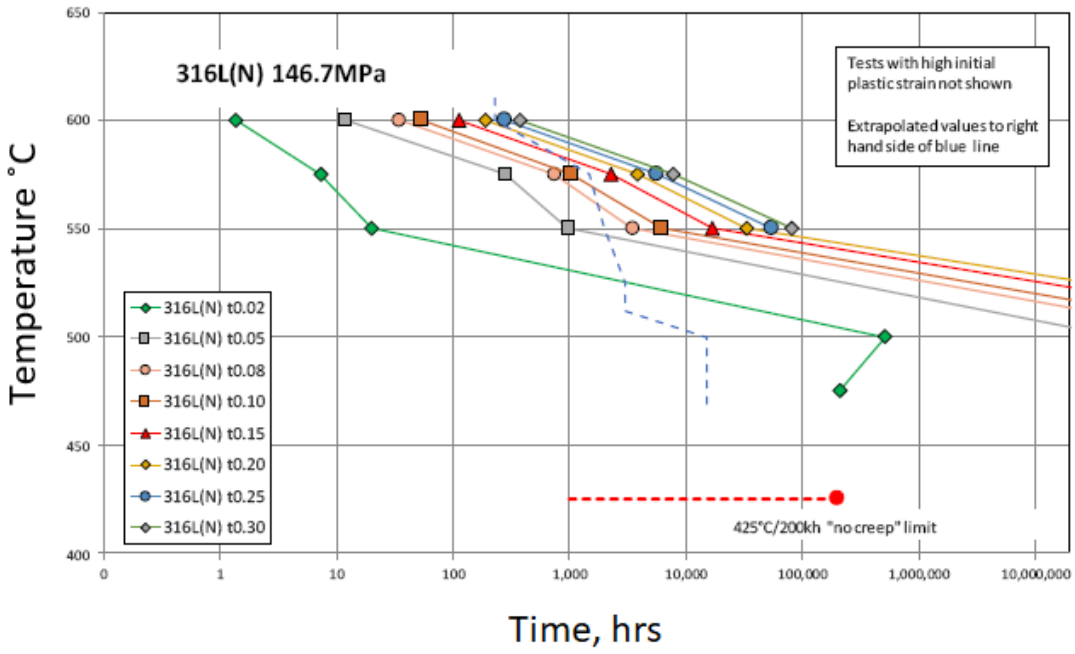

Figure 5.26: 316L(N) Isostress plot 146.7 MPa (upper).

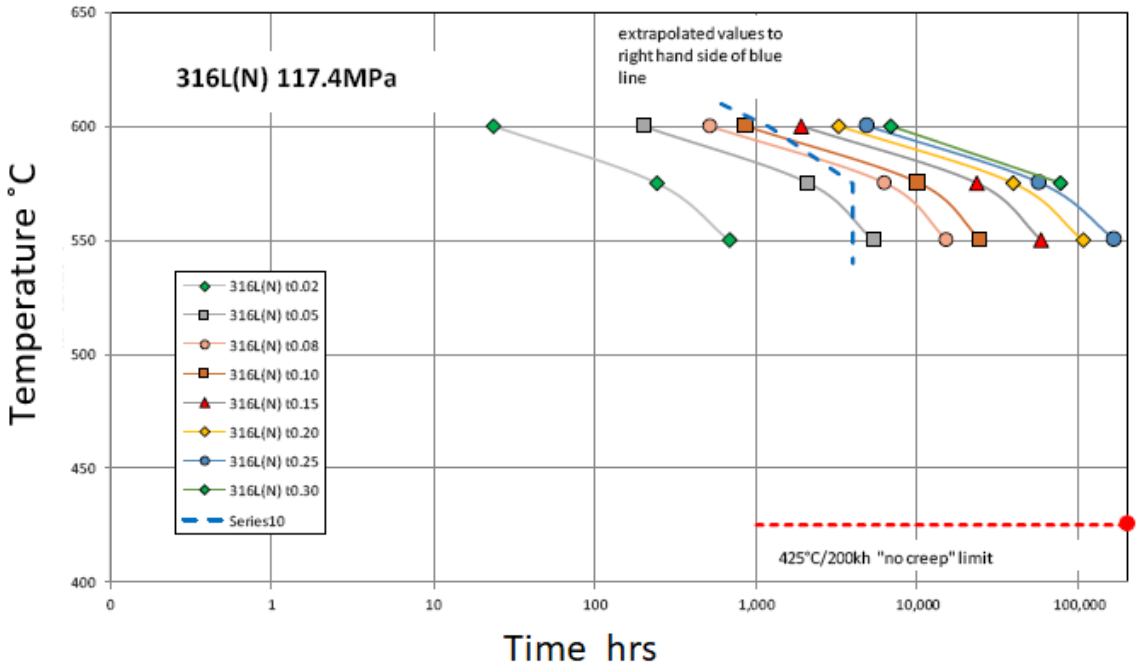

Figure 5.27: 316L(N) Isostress plot 117.4 MPa (lower).

The 316L(N) material appears to have a T_{NC} considerably higher than the classic value and thus the reference stress used in hindsight could have been considerably lower. The reference stress method for austenitics requires careful selection of the reference stress as it approaches the proof stress. In the 316L(N) experiment the value was just too high for the accelerated temperatures with high IPS but for the lower temperatures did not provide

enough creep strain within the time frame. A longer test time should be planned for these materials. In this case, it turned out a reference stress midway between the two chosen would perhaps be more appropriate. If the T_{NC} is suspected of easily exceeding the classic value, as with this material, a reference stress of the maximum allowable design stress in EN13445 Table 6.1 and 100°C higher may be a better starting point.

5.10.6 Model fitting P265GH

There are a limited number of measured times to 0.2% strain data for P265GH, seven data points from 400 - 475°C at the two stress levels all at < 1909 hours. Fitting the original Wilshire-Scharning model Equation 3.25 to the data to obtain the fitting parameters for extrapolation to 200k hours would be considered excessive at x100 the measured time. The values in Table 5.13 show the T_{NC} extrapolated (using Eq. 3.46) for a reference stresses of $0.264\sigma/\sigma_{TS}$ and $0.21\sigma/\sigma_{TS}$ (110.1 MPa & 88.1 MPa respectively) and the parameters with either a fixed Qc* or floating to compare with the isostress method above. Iteration will adjust these as the values above in Figure 5.18. The floating value of Qc* appears to represent a conservative estimate compared to the isostress method which would be consistent with the findings of Chapter 3. The fixed value of 300 kJ/mol for Qc would appear appropriate from a traditional plot of natural log minimum/steady-state creep rate achieved against the 1/T (°K) is shown in Figure 5.29. It provides a non-conservative estimate compared to the isostress extrapolation. The plots below 400°C do not appear to be progressed sufficiently to approach a steady-state/minimum creep rate.

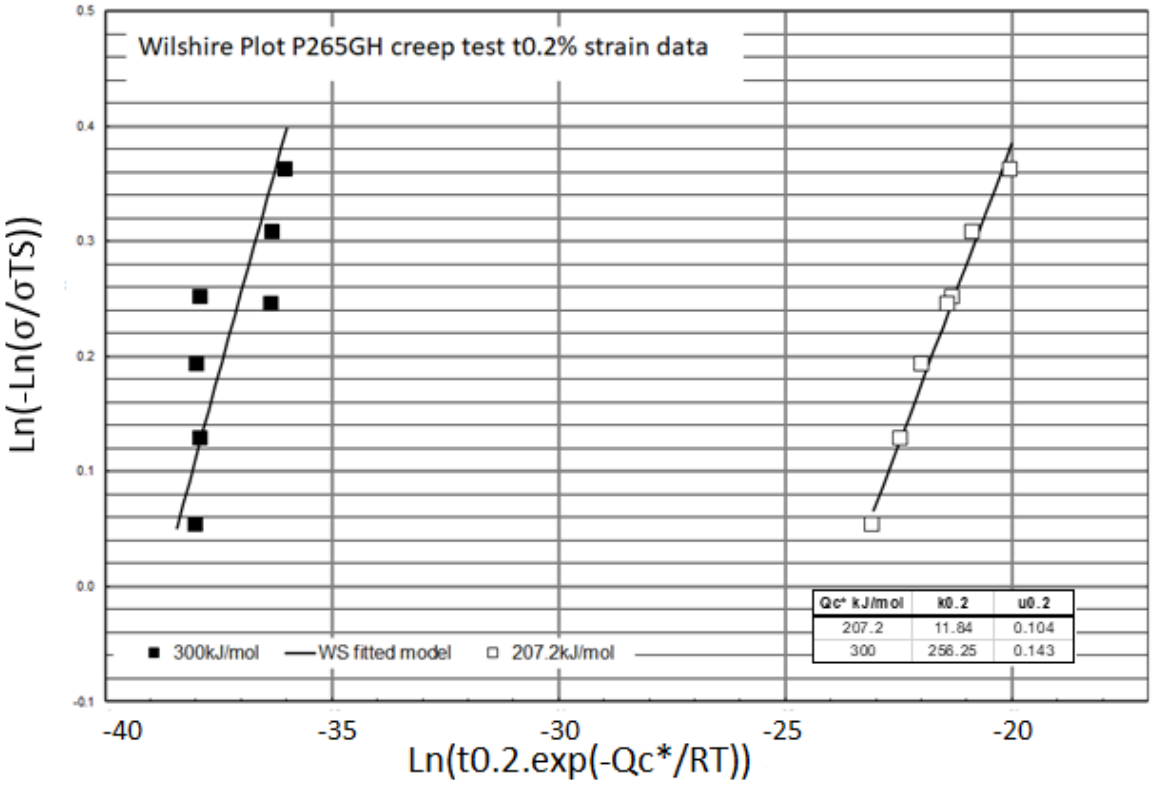

Figure 5.28: Original Wilshire model fitted to time to 0.2% total strain data from creep tests.

Table 5.13: Fitting parameters of the original Wilshire-Scharning model to the measured test data to 0.2% total strain. For 110.1 MPa and 88.1 MPa (0.264 and $0.21\sigma/\sigma_{TS}$).

Norm. Stress	Qc*	k0.2	u0.2	T_{NC}	95%PI	R^2
110.1 MPa / $0.264\sigma/\sigma_{TS}$	300 kJ/mol Fixed	256.25	0.143	**359.3°C**	(340.1,378.6)	0.631
	207.2 kJ/mol	11.84	0.104	**330.0°C**	(324.5,335.6)	0.985
88.1 MPa / $0.21\sigma/\sigma_{TS}$	300 kJ/mol Fixed	256.25	0.143	**372.2°C**	(347.0,397.4)	0.631
	207.2 kJ/mol	11.84	0.104	**353.1°C**	(345.6,360.6)	0.985

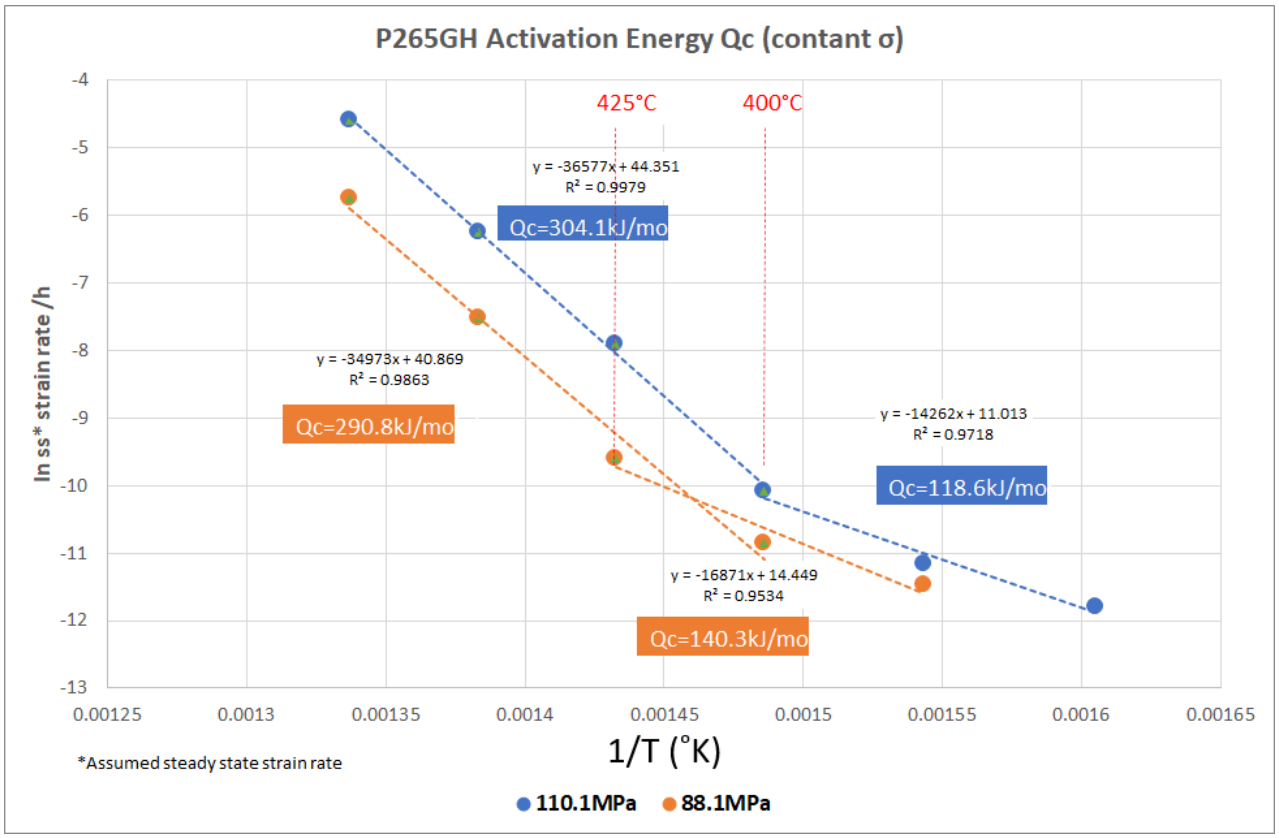

Figure 5.29: Plot of natural log assumed steady state creep rate/h vs 1/T(°K).

Of the models introduced the Gray & Whittaker model (Eq. 5.3 and 5.4) offers the potential to provide full creep curves from empirical data. This means the model is flexible to include any tertiary upturn in the data. It is, however, clear a good overall fit of the model can be lacking a good fit in the early stages and vice versa and extrapolation is not the intended us. Other models also require tertiary or rupture data to work well (Theta, LCSP 1.5) and/or extensive pre-processing. This does offer the opportunity to provide a value as tests progress or for historical data sets with times to higher specific strains.

$$\mathrm{t}(\varepsilon)\exp\left(-Q_c^*/_{RT}\right) = M(\varepsilon)\left(1-\frac{\sigma}{\sigma_{TS}}\right)^{P(\varepsilon)} \tag{5.3}$$

where,

$$\begin{aligned} M(\varepsilon) &= A_1\exp\left(-\left(\frac{\varepsilon}{A_2}\right)^{-A_3}\right) \\ P(\varepsilon) &= \frac{A_4}{\varepsilon A_5\sqrt{2\pi}}\exp\left(-\frac{[\ln(A_6\varepsilon)]^2}{2A_5^2}\right)+A_7 \end{aligned} \tag{5.4}$$

The T_{NC} can be found by rearranging such that

$$T = \frac{-Qc^*}{R \cdot Ln(A/t(\varepsilon))} \; where \; A = M(\varepsilon)\left(1 - \frac{\sigma}{\sigma_{TS}}\right)^{P(\varepsilon)} \tag{5.5}$$

The Qc* at a constant normalised stress, as the Wilshire equations, is explicitly specified for the model, but without detail on the method to derive it. Having derived a value of 207.2 kJ/mol with a floating Qc* in the Wilshire model fit this has been compared to the traditional approach value of 300 kJ/mol to obtain a T_{NC} for comparison with the other methods here. Chapter 3 indicated the floating Qc* approach provided overly conservative estimates for the Grade 91 material. From the raw creep data for both stress levels, the time to specific strains of 0.02, 0.05, 0.08, 0.10, 0.13, 0.15 and 0.2 % were extracted using the DIN 50118 geometric mean method described earlier. The data used is all $\leq$ 0.2% and $\leq$ 0.1% at < 400°C. For each strain t(ε)exp (-Qc*/RT) v. 1-σ/σ_{TS} is plotted (the divisor could be UTS, yield or proof stress again) and a power-based trend line of the form y = MxP fitted in Figure 5.30. The values of M(ε) and P(ε) were then used to derive the constants A1 — A7 using the non-linear SOLVER routine in Excel. Adding the fitting constants and the required values of 0.2% creep strain, normalised stress and 200kh back into Eq. 5.5 provides the T_{NC}values. A requirement for tensile strength at the 350°C temperature (Rm,350 or σ_{TS}) was not envisioned for the planned test matrix and required extrapolated with a 2nd order polynomial from the other temperature tests at 436 MPa for the limited data. This also provided a local maxima around 200°C in the plot typical of P265GH.

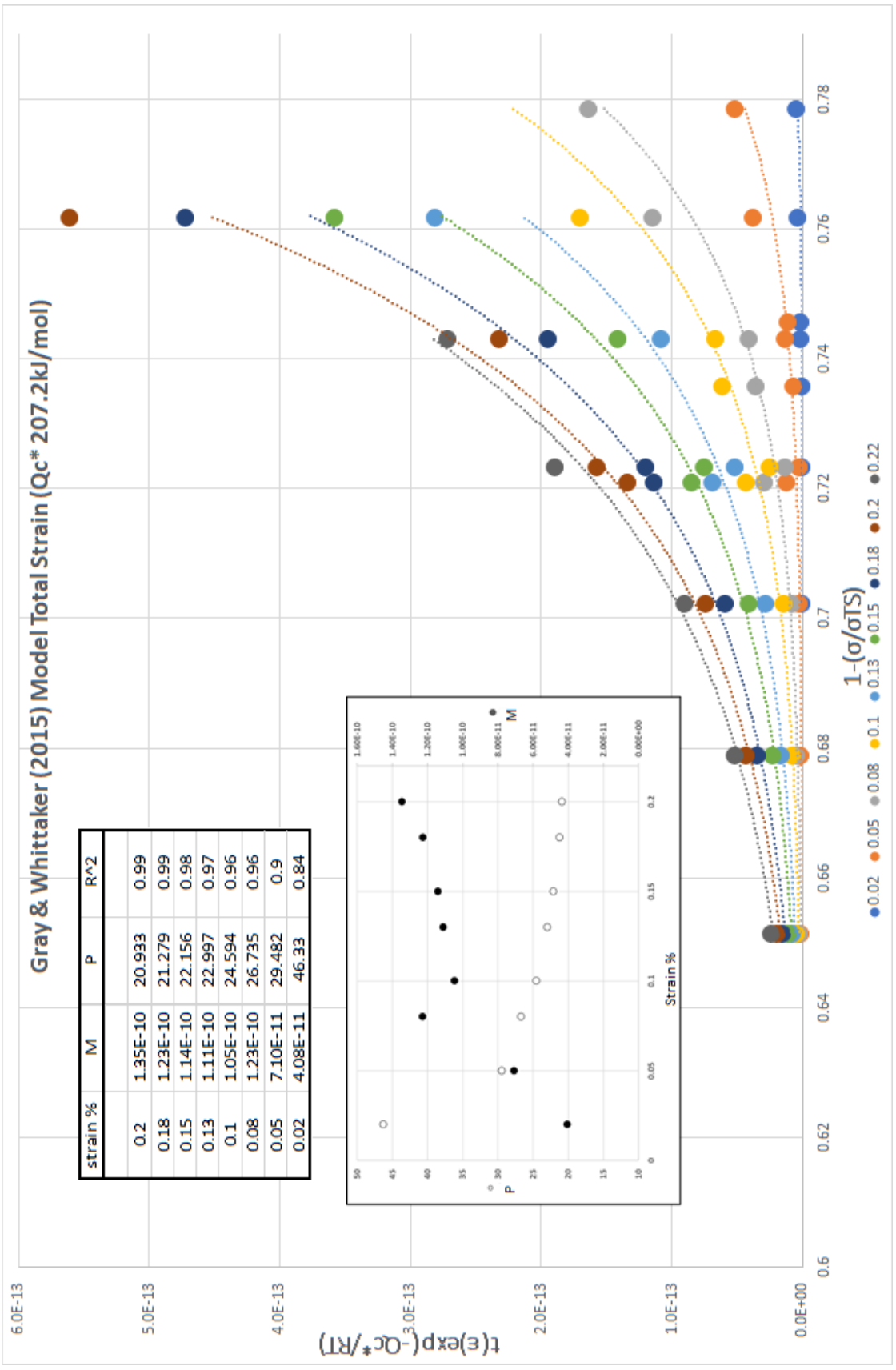

Figure 5.30: Gray & Whittaker model fitting constants.

The fitting constants derived using SOLVER for the apparent activation energy Qc* de-

rived from the Wilshire model is compared to the average activation energy in Figure 5.29 and shown in Table 5.14. The model indicates a T_{NC} of ~330°C for 110 MPa which is ~10°C lower than the isostress method and similar to the Wilshire model, using the same Qc*. Similar iteration corrections would be required to establish it more precisely. A variation in the temperature of ± 3°C in the model equates to a difference of ± ~5 years to achieve 0.2% strain (18.6 - 28.1 years). It should be noted Gray & Whittaker do clearly indicate the model is to provide a full curve not a minimum creep rate point on a curve and it was developed using more full curve data at higher strains starting at 0.2%.

Table 5.14: The fitting constants derived for the Gray & Whittaker model for time to 0.02-0.2% specific strains from P265GH creep test data at 110.1 and 88.1 MPa.

Qc*	207.2 kJ/mol	300 kJ/mol
A1	1.55698E-10	1.6432E-17
A2	2.9370189E-02	1.5085E+01
A3	8.429841E-01	4.2027E-01
A4	2.7514709E+01	2.13254E+02
A5	9.6060880	2.1457
A6	6.53983691E-04	8.3217E-02
A7	1.7434915E+01	-2.8566E+01
T_{NC}**(110.1 MPa)**	**328°C**	**348.3°C**

The model does not appear to be a good fit for the strain data above 400°C in Figure 5.31 with the model underestimating the strain but below, the model appears a good fit to the test data. Note the inset log-log plot indicates the model is only a good fit to the >10h 375°C data.

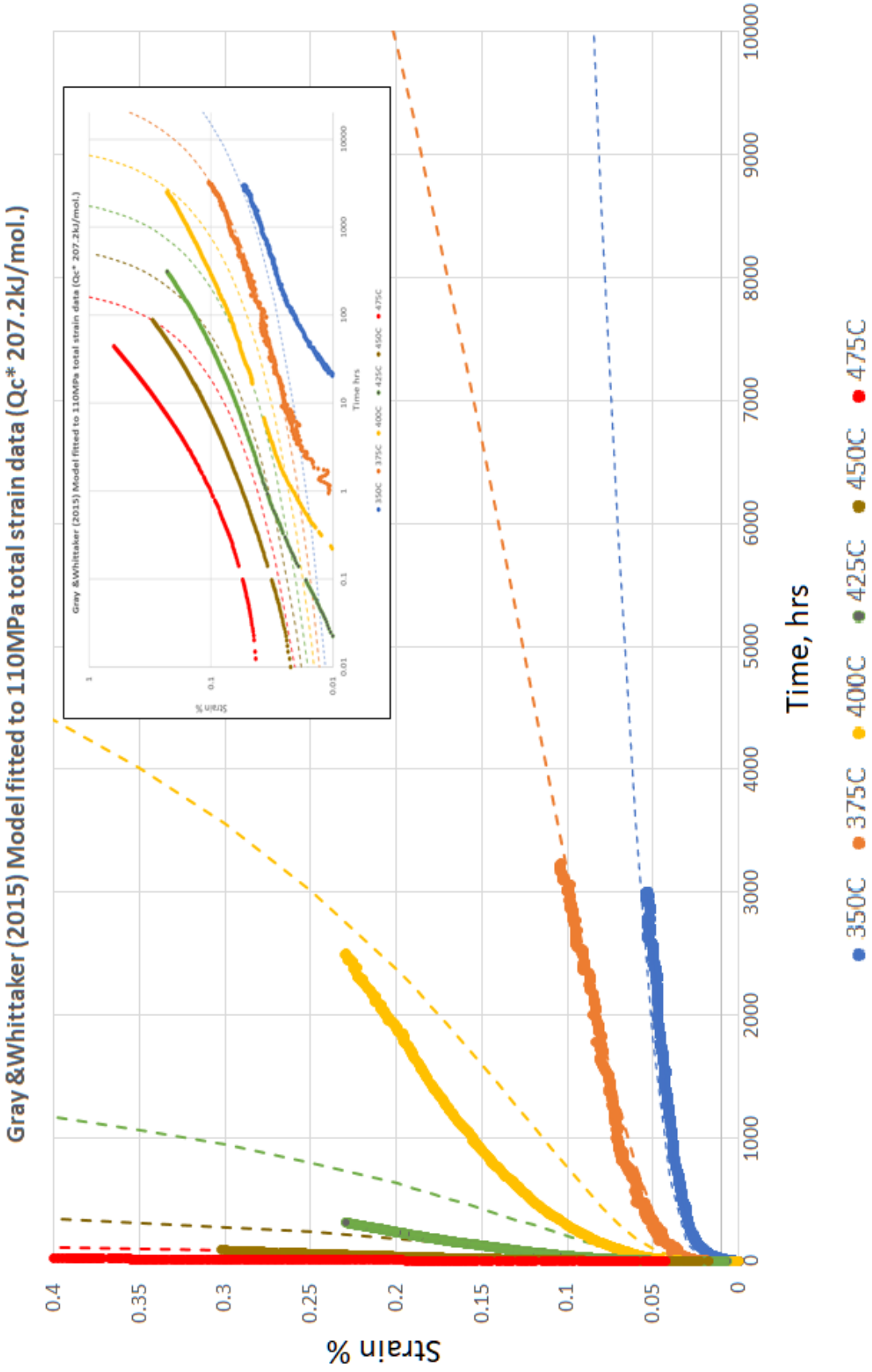

Figure 5.31: Gray & Whittaker model fitted to total strain data P265GH at 110.1 MPa (Qc& 207.2 kJ/mol).

The data used was limited to 0.2% strain and there can be considerable uncertainty extrapolating this model. Of particular note the model predicts the P265GH at the 375°C limit would enter tertiary creep around 0.2% and < 30kh at 360°C (60kh at 350°C), based on a simple visual deviation from linearity rather than a specified offset shown in Figure 5.32. 360°C is the temperature of the historical creep cracking failures in C-Mn steels at service lives of 8-100kh mentioned earlier. The parallel isostress lines in Figure 5.16, however, do not indicate the plots are in the primary/tertiary transition region up to 0.2% strain and this extrapolation must be viewed with caution. The model is based on a full curve shape and the upturn may be an artefact of the limited data used. The basis for the choice of the 0.2% strain limit for no creep and negligible creep limits is the assumption it is significantly lower than the minimum creep rate. There is no European requirement to limit the allowable stress to, for example, 80% of the stress to cause initiation of tertiary creep as for ASME [163]. The level of strain deemed negligible at a reference stress requires engineering judgement and sufficient test data [140]. If, for example, the negligible creep diagram is to be used with plant excursions at higher temperatures. The creep void development and associated susceptibility to cracking would require further investigation. Testing to higher strains and cross-weld creep testing would provide the designer with the required information for operating above the T_{NC}. The NIMS data for the MgA and MgC heats referred to in previous Chapters indicate the minimum creep rate is achieved with a couple of hundred hours at 500°C at around the reference stress compared to single digit values of time to 0.2% strain. This compares to a T_{NC} calculated of around 420-440°C. Whether the limited negligible creep region and the uncertainty with its upper limit at higher temperature and short durations is worth establishing is for individual materials and scenarios.

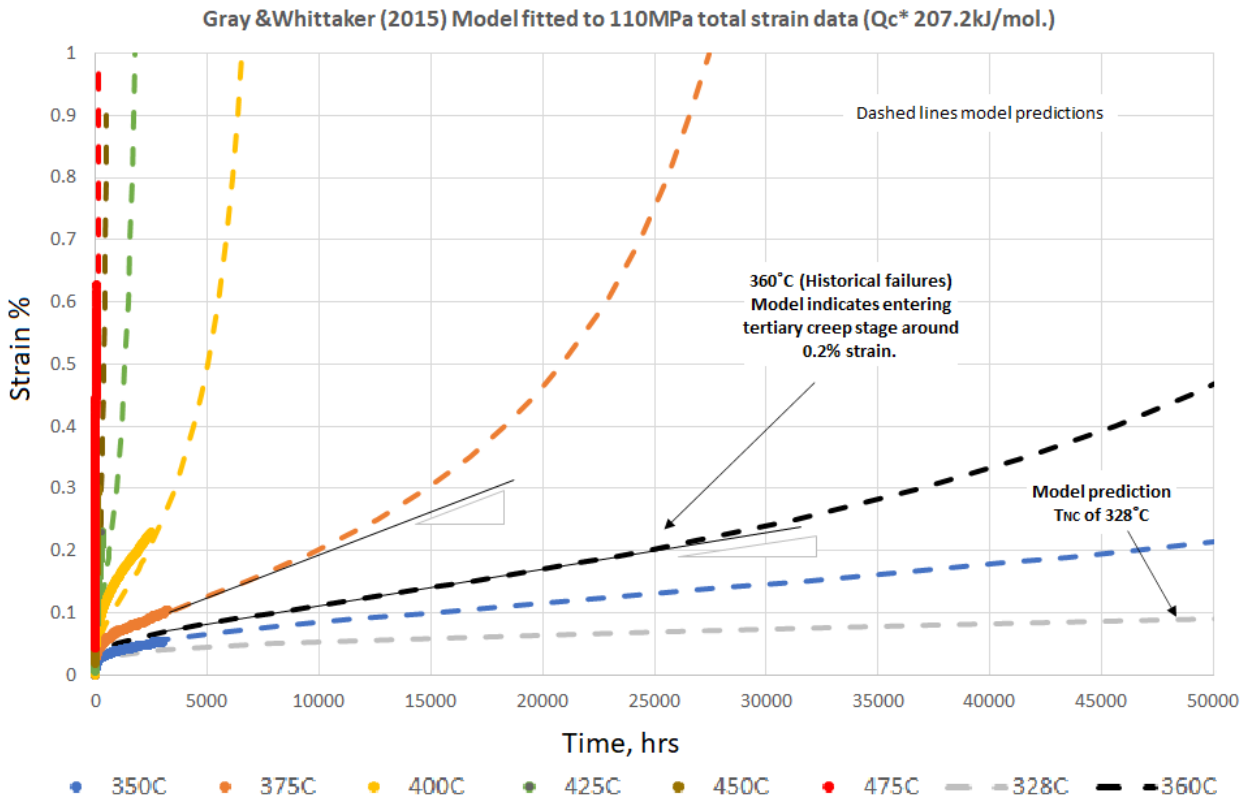

Figure 5.32: G&W model predictions of T_{NC} and the shape of curves.

Both the original Wilshire-Scharning model and the Gray & Whittaker model (Eq. 5.3) appear to bound the isostress value depending on the Qc* used - without correction ∼340 ± 10°C. With a correction for a higher allowable stress of ∼+7 MPa at ∼330°C. Both provide similar values for the lower value at 110 MPa, the problem with both models is deriving the Qc*, but for this material, they appear to provide a conservative estimate of the experimental isostress method only when the Qc* is allowed to float. If an arbitrary Qc* value is used it appears non-conservative compared to the isostress result and therefore, given the uncertainty the experimental isostress method value is preferred.

With the test data limited to ∼3k, a network as in Chapter 4 was trained using the same methodology and both sets of test data for the P265GH for a limited extrapolation to the times to 0.2% strain for comparison with the exponential model and the Grey & Whittaker (G&W) models used. The ANN provided reasonably shaped curves from the limited training data compared to the other models in Figure 5.33. For comparison to the isostress linear extrapolation used in Figure 77 the extrapolated times to specific strain using each model are shown in Figure 5.34 The extrapolated points are ∼15x, 21x and 32x the data for the 350°C curve at 46kh, 63kh and 95kh for the G&W, ANN and exponential models respectively.

The exponential model is closely aligned with the linear isostress extrapolation as are the ANN extrapolated points, neither indicating any significant change to the T_{NC}. The G&W extrapolated points indicate a shorter time to 0.2% strain, a downturn in the plot indicating a transition to tertiary which might be expected after a flared primary/tertiary region rather than the parallel isostress lines in the primary region in Figure 5.1 and a lower T_{NC}. Extrapolation in log terms is highly dependent on the accurate recording of the upper-temperature data points. The difference of 32kh between the ANN and Exponential model 0.2%, 350°C data points only represents a couple of degrees difference in the linear extrapolation of the T_{NC}. However, a kink with the G&W points would indicate a ~12°C lower T_{NC}.

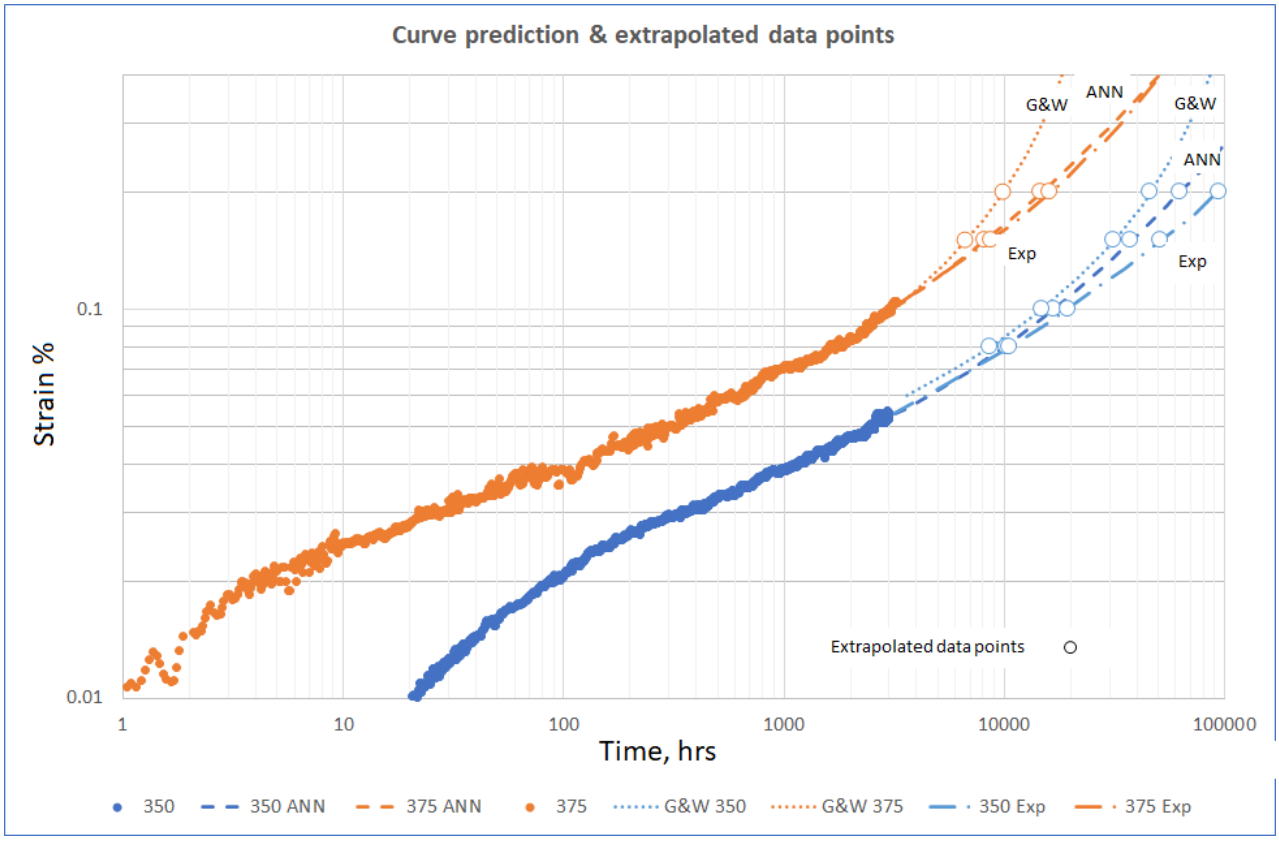

Figure 5.33: Extrapolated data points using the ANN, exponential plastic strain model and the G&W model.

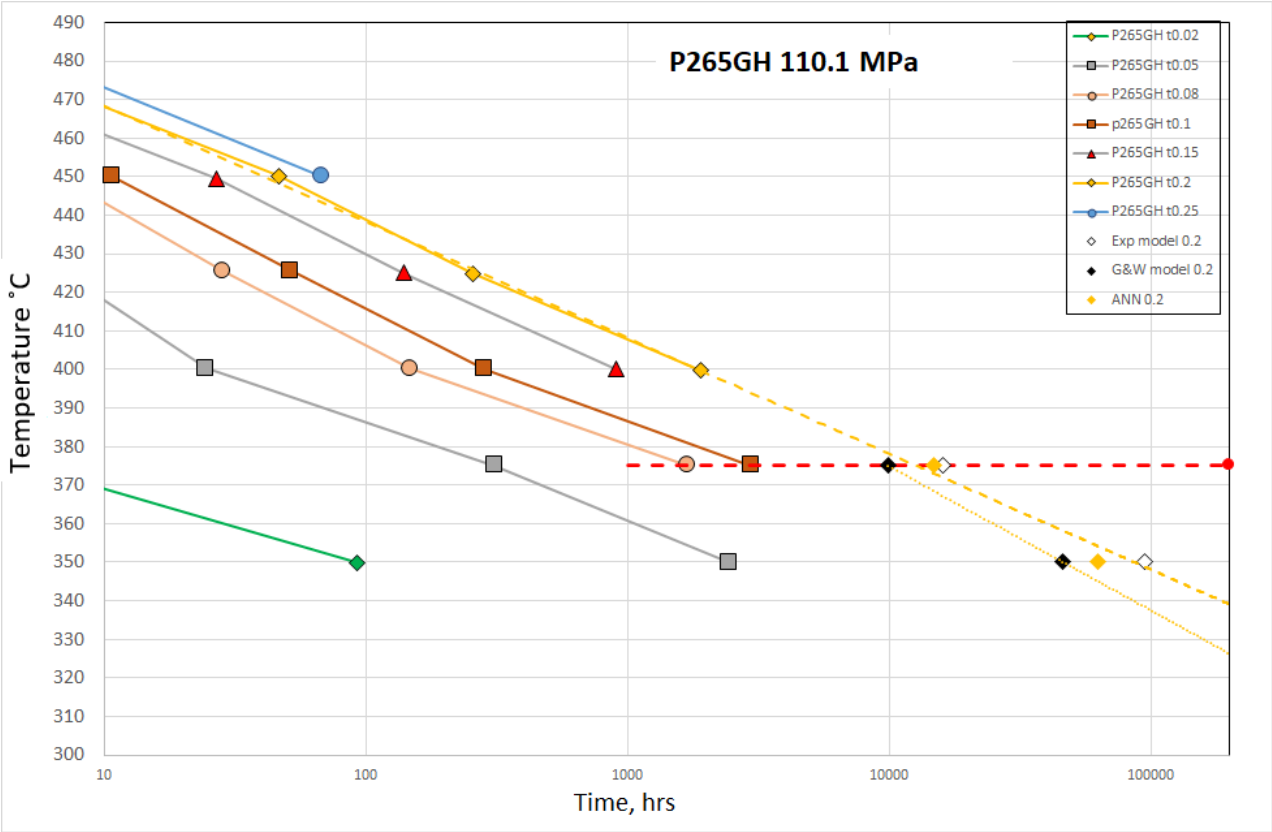

Figure 5.34: Extrapolated data points on an isostress plot.

5.10.7 Model fitting 316L(N)

Around the temperatures indicated from the isostress results, there is some creep data for 316L(N) in the public domain at 550 and 600°C and around design stresses [1]. The creep curves, tensile properties and IPS plots are shown in Figure 5.35. The tensile data for the CRM 11477 heat is contained in an older reference [2] which is not easy to read. The tensile properties appear slightly lower than those of the material used in the tests. There is no indication serrated flow was experienced during testing. Of the 7 curves at 550°C (100 MPa-250 MPa) and 6 at 600°C (60-170 MPa) (807 data points), 8 plots have considerable test duration to 85kh with 200mm gauge length samples used for the low-stress regime. The IPS plot indicates that 0.2% strain is achieved instantaneously at around 125 MPa as the proof stress is reached. The high IPS in the tests at the upper reference stress would be consistent with these findings, the variability consistent with the change in slope and the subjectivity of strain apportioned to IPS or creep as the deadweight load is applied manually. Incidentally, the Monkman-Grant exponent for three heats of this material was found to be 0.94-1.01 (0.96 CRM heat) [2] which is different from 316LN at 0.9 - 0.94 [164].

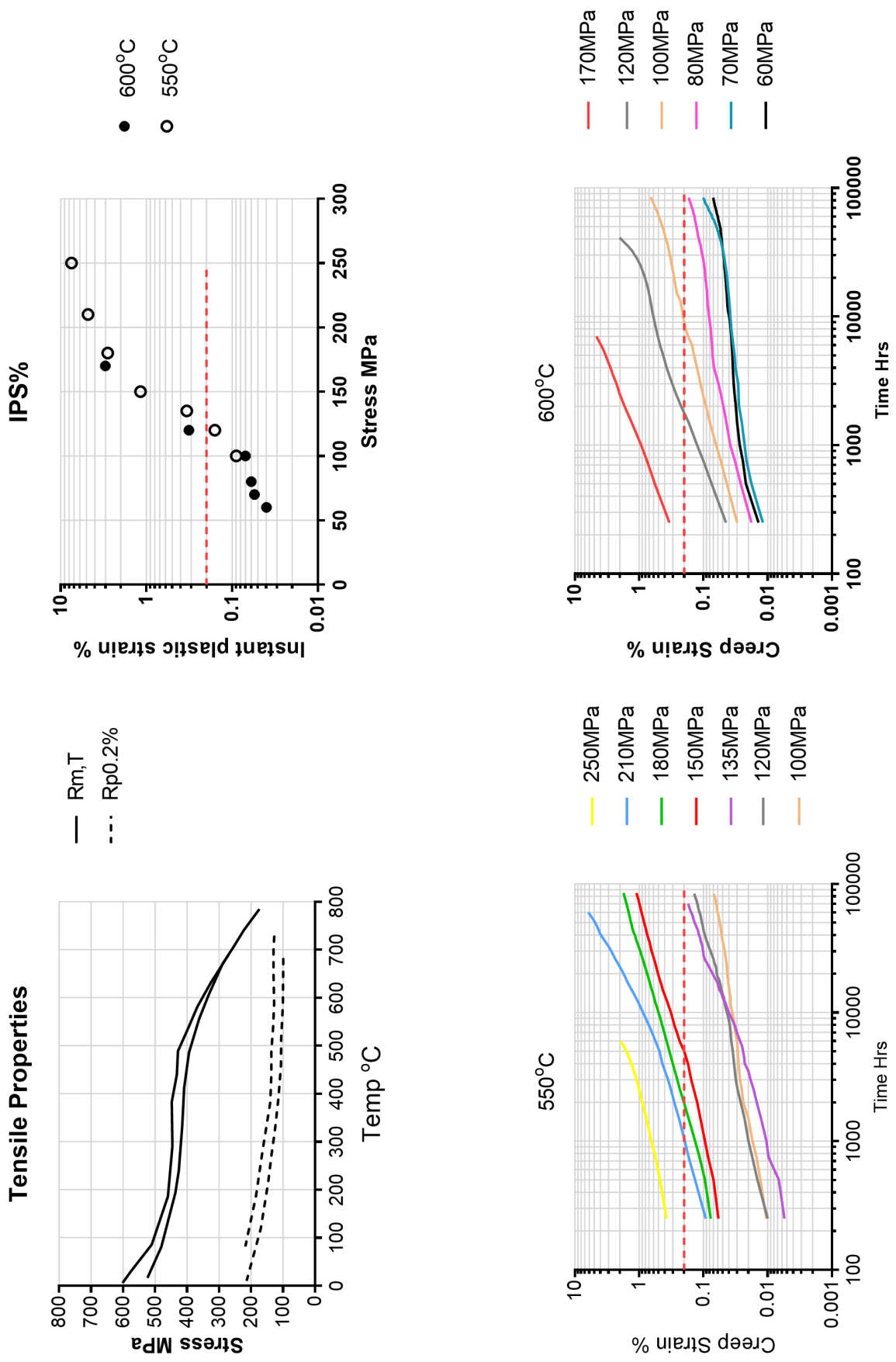

Figure 5.35: Low stress creep strain data 316L(N) [1, 2].

Using an average value of 370 MPa for Rm,550 (σ_{TS}) and 342 MPa for Rm,600 the original Wilshire equation can be used for time to 0.2% creep strain (t0.2%) with linear interpolation of data points. The data provides only 3 data points for total strain (no measurements are available at <250h) but 5 for creep strain from 1 - 9kh at a normalised stress of 0.29 - 0.57σ/σ_{TS}. Such is the data much of the long term information is not utilised. A number of curves are progressed beyond 0.14% and 84kh which would provide the data with extrapolation. The value of apparent activation energy appears expected to be similar to ferritic/martensitic grades 250-300 kJ/mol. [129], Holmstrom used a Qc* of 300 kJ/mol for 316L. Fitting the original Wilshire model and putting the parameters back into Eq.3.46 provides the T_{NC} values in Table 5.15. There is a significant difference in the values. The normalised stress equates to around 115 — 125 MPa at 1/3 of Rm, T between 500 — 550°C which appears to be the reference stress from the EN13445-3 criteria and the approximate tensile data in Figure 5.35. The 120 MPa, 550°C curve has achieved ∼0.14% creep strain at 83kh so the T_{NC} based on creep strain is well below this. For this austenitic material, there can be significant IPS as the reference stress approaches the proof stress. The effect of prestrain on 316L(N) has been shown to significantly reduce the primary strain and the minimum creep rate but reduce creep ductility [165, 158]. The increased creep resistance at particularly longer durations [165] and reduced creep damage are attributed to the nitrogen and hardening [166].

Table 5.15: T_{NC} values for 0.33σ/σ_{TS} stress (∼125 MPa) from the fitted WE (Based on creep strain alone) Rieth *et al.* [159] 316L(N) data.

Qc*	k0.2	u0.2	T_{NC}	95%PI
300 kJ/mol Fixed	154.03	0.193	**512.1°C**	(485.5,540.8)
165.5 kJ/mol	7.60	0.283	**460°C**	(444.5,476)

The WE figures indicate considerable extrapolation would be required in temperature (perhaps >100°C) to use an ANN from data collected at just two levels separated by 50°C. The data also contains large strains (> 6%) which would marginalise a 0.2% strain extrapolation. A number of curves, however, are progressed beyond 0.14% to 84kh which could be extrapolated in time to provide additional time to 0.2% data and enable fitting the WE to the total strain data. The ANN used in Chapter 4 was applied to the Rieth *et al.* [1] data curves culled at 0.5% strain to provide additional times to 0.2% (t0.2%) for total and creep strain.

The curve data used to train the ANN and the ANN extrapolated curves to the t0.2%are shown in Figure 5.36. These extrapolated points were then used with the measured values to fit the WE for total and creep strain with the results in Table 5.16.

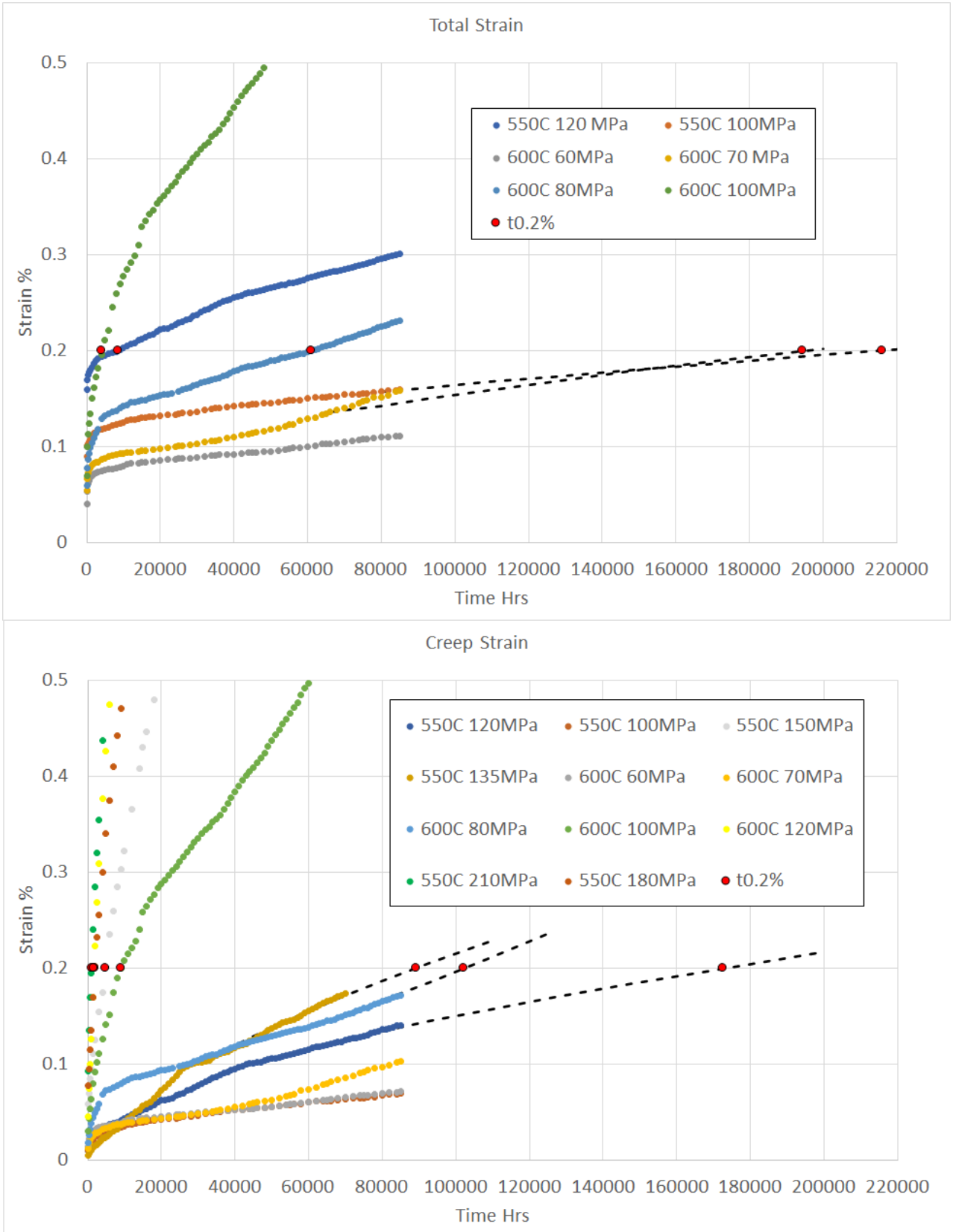

Figure 5.36: Rieth *et al.* [159] 316L(N) creep data used to train the ANN and the extrapolated results for time to 0.2% strain (a) total and (b) creep.

Table 5.16: WE parameters and $T_{NC}$for Rieth *et al.* [159] 316L(N) data.

	Qc*	k0.2	u0.2	T_{NC}	95% P.I.
Total Strain %	300 kJ/mol Fixed	5.69	0.062	**494.3°C**	(469.7, 518.9)
	324.6 kJ/mol	6.69	0.060	**498.5°C**	(476.4, 520.6)
Creep Strain %	300 kJ/mol Fixed	26.69	0.131	**535.5°C**	(492.9, 578.1)
	374.1 kJ/mol	71.66	0.120	**542.7°C**	(509.3, 576.0)

The extrapolated data has a significant effect on the creep strain result. The fixed Qc* T_{NC} increases and the floating Qc* value now exceeds the fixed value with a corresponding increase in the T_{NC}. The shorter term data appears to provide a conservative estimate compared to the longer term data - with the potential for interim estimates as tests progress. The floating value of Qc* is also higher for the total strain but the values would provide the same rounded down to the nearest decade. The Qc* is often significantly lower when the parameter is allowed to float. A value of 490°C for the total strain is significantly lower than the isostress estimate with limited data — this material appears to have similar tensile but lower proof stress properties.

5.11 Concluding Remarks

The results of the isostress extrapolation indicate significant differences to the T_{NC} for these materials over the classical 375°C. For the Grade 91 around 410°C and the P265GH around 330°C which has been further validated with extrapolation using the Wilshire-Scarning model and the Gray-Whittaker model. Extrapolation into the negligible creep region with a predicted creep curve shape appears to confirm the expectation of historically unstable creep cracking failures within a limited in-service life for P265GH. The G&W model indicates a component of this material would have significant tertiary creep strain operating at the classical T_{NC} of 375°C at the maximum allowable design stress (upper reference stress). The 'negligible creep zone' is based on strain assuming the minimum creep rate is in the significant creep region. The isostress lines being parallel do not indicate a transition from primary to tertiary, if it occurred during the extrapolation the plot would be expected to 'flare out' and achieve the time of 200kh at a higher temperature according to Figure 5.1 thus the value provided would be conservative. The experimental data also allows a direct comparison with the Wilshire applied to the 0.2% total strain data collected during the isostress method. This

indicates that an arbitrary 300 kJ/mol value of Qc* produces a non-conservative estimate of the T_{NC} compared to the isostress extrapolation for both reference stresses and the floating Qc* provides a value much closer to the extrapolated value. This indicates the Wilshire equations should be used with caution. The isostress method suitably progressed would be preferred in that both methods can be used on the same data.

For the X10CrMoVNb9-1 Grade 91 the isostress extrapolation of a T_{NC} of 443°C at $0.54\sigma/\sigma_{TS}$ would be higher than the modified Wilshire model in Chapter 3 for the NIMS 9Cr-1Mo-V-Nb material and higher than Holmstrom *et al.* [129] for X10CrMoVNBb9 1. If the non-constant slope is indicative of the transition from primary to tertiary then the plot would be expected to turn downwards as it moves into tertiary according to Figure 5.1 and the provided T_{NC}would be non-conservative. The basic assumption is that total strain 0.2% is much lower than the mcr at $\sim$1% [129] and therefore linear extrapolation is appropriate. When flaring of the isostress lines occurs linear extrapolation must be done with caution and the reliability of the derived T_{NC} viewed as such. Sufficient test duration to provide enough data to establish accurate isostress plots is essential for the Grade 91 material. The lower model predictions of $\sim$410°C (rounded down) would be appropriate.

It should also be noted that the uncertainties in the operating conditions can affect the results of such tests, and attention to detail is paramount in conducting the tests successfully [142].

- Within the tensile test, the elastic modulus at elevated temperature must be measured accurately, requiring sufficient stress-strain-time points to be recorded so that the modulus can be fitted over a sufficient range whilst avoiding any curvature due to the influence of creep at higher stresses. The determination of the proof stresses below 0.2% strain are particularly susceptible to uncertainties in the measured modulus.

- Normal creep temperature limits of $\pm$3°C would potentially lead to systematic uncertainties in times to specific strain. Noting that a 30°C reduction in temperature corresponds to an order of magnitude increase in times to a specific strain, even a 3°C deviation from the required temperature can lead to a difference in measured time of 26%. Similarly, random fluctuations in temperature of a specific test, within the specified limits, could conceivably lead to inconsistent intervals between the measured times to specific strain. In this work, laboratory practice insured that limits of better than $\pm$2°C were achieved.

- Creep specimens typically have a gauge length of 25-50mm for general use, and laboratory transducers normally have a resolution of 0.5μm. In sample creeping at 0.2% strain longer specimens will be preferable — for a 100mm gauge length used in this study 0.2% corresponds to 200μm with an uncertainty of ± 4μm (2%) measured in accordance with BS EN 9513:2012 [167].

- Inevitably, some noise may be present in the recorded creep strain time, hence it is advisable to use the DIN50118 interpolation and geometric averaging method of determining the time to specific strain. This is particularly true for the higher strength materials in which the strain-time curve is initially very flat; small amounts of noise require careful evaluation rather than taking the first point at which the curve meets or passes the required strain level.

- It must be pointed out that some creep strengthening mechanisms (especially large grain size, development of beneficial phases over the long term) are not necessarily beneficial for tensile properties, or do not occur in a sufficiently short time frame. However, such mechanisms are generally more important at the higher temperatures of the materials creep-resistant range [129].

- Equally, long-term detrimental effects, spherodisation in low alloy steels (not evident in higher Cr steels [168]), formation of Z-phase [169, 170], and necking with increased stress are reduced or eliminated in relatively short duration tests.

- Variations in the composition that could result in significant changes to the T_{NC} have been noted for any future assessment of heat-to-heat variation within grades.

- The derived values of the time-independent zone represent significant changes to the classical limits for these materials. Operation above these limits will require testing to establish the minimum creep rate and the negligible creep zone.

- The 316L(N) material does highlight the difference in creep and total strain for the austenitics in particular and the greater care required in the test matrix formulation to avoid approaching the proof stress at accelerated temperature.

- The no-creep temperatures identified have an associated reference stress as the maximum allowable design stress at that temperature. Designing below the no-creep temperature allows that design stress to increase in relation to the material-specific tensile

properties as Table 6.1 EN13445-3. The 316L(N) test data illustrates a significant strain can be achieved on loading with an excursion to a higher temperature. The strain would become evident within in-service loading cycles. The Grade 91 IPS data also suggest any increase in the stress allowed could produce a significant portion of a 0.2% strain. Moreover from a design at lower temperature, any excursion or in-service adjustment up to the no-creep temperature would enter the negligible or substantial creep region by virtue of the higher stress level. This would also be the case for any introduction in the standards of a higher no-creep temperature over the classical limits. The indication that creep does not need to be considered below a no-creep temperature is somewhat misleading in these terms with more emphasis required on the combined temperature-stress limit.

Holdsworth *et al*. [38] found a number of other models (modified Graham-Walles, Bolton, modified Sandstrőm) best describe the times to lower specified creep strains (0.2-0.5%) and further work with these may provide useful comparisons.

Chapter 6

Stress Relaxation with a modified model bolt

6.1 Stress Relaxation and Creep

Stress relaxation (SR) is the time-dependent reduction of stress at a constant strain while creep is the increase in strain at constant stress or, more commonly, load. The net effect is similar in that both lead to the eventual exhaustion of the ductility [171]. Of course, microstructural evolution is limited to the test duration and as such, the applicability to creep rate requires consideration, e.g. relatively high dislocation density reduces during long-term creep exposure in e.g. Grade 91 [172] and as such SR provides a creep rate with a high level of dislocation density [173]. Bose *et al.* [174], however, note microstructural changes in SR tests similar to long term creep.

The relationship is based on a constant total strain during stress relaxation which has both elastic and plastic components. the plastic components can be further broken down to a time-independent plastic strain ε_p, and a time-dependent creep strain, $\varepsilon_c$combined such that the total strain after loading is

$$\varepsilon_t = \varepsilon_e + \varepsilon_{pl} + \varepsilon_c \tag{6.1}$$

Given that this is constant and the plastic strain on loading is not time-dependent this is simplified as

$$C = \varepsilon_e + \varepsilon_c \tag{6.2}$$

Differentiating

$$0 = \dot{\varepsilon}_e + \dot{\varepsilon}_c \tag{6.3}$$

and the elastic stress relaxes and substituting for Hooke's law $\sigma = E\sigma_e$

$$\dot{\varepsilon_c} = -\dot{\sigma}/\mathrm{E} \tag{6.4}$$

Thus the creep rate can be calculated at any time during relaxation from the stress rate knowing the Elastic modulus at temperature. An acceptable approach is a polynomial curve fit of a plot of stress v Ln time, when the stress level reaches that of the creep test the stress relaxation rate is equivalent to the minimum creep rate [175]. Beddoes [176] argues that the creep strain rate and stress relaxation derived rate cannot be assumed at all stress and temperatures because of the differences in the deformation processes. The creep strain rate balances concurrent hardening from the constant load with softening caused by the elevated temperature whilst during stress relaxation hardening occurs during the initial loading but subsequently, no further hardening takes place and only recovery processes take over. Hardening occurs during the initial loading but no further hardening occurs and recovery takes over with softening. The hardening and softening rates are both temperature and stress dependent.

The creep strain could further be considered to have a recoverable (anelastic creep) as well as a non-recoverable plastic component. Lubahn & Felgar [41] proposed a threshold below which all creep is anelastic while above it is partly anelastic and partly plastic until at higher stresses recovery effects are negligible. Woodford [175]suggests the recoverable anelastic component is less than 10% and ignored for the SR tests.

Traditional BS EN 10319-1:2003 [177] stress relaxation testing is both demanding and difficult to perform consistently [178, 179], with specific problems regarding the initial loading and rate which may indicate issues with IPS. Indeed many of the stress relaxation tests in the public domain are carried out at temperatures well into the creep range and often at significant prestrain. Bose *et al.* 0.2%-1% [180], 0.7% and 1.25% [174], Guguloth *et al.* 0.8% and 1.8% [173], Kim *et al.* 0.6% [181] while others have limited the prestrain, Holmstrőm

et al. 0.25%, 0.35% [182] and De Bruycker *et al.* 0.5% and 0.3% [183]. Woodford and Bose acknowledge that that higher strain levels would affect the resulting stress relaxation. Bose *et al.* [174] show high strains better correlate with long term creep rupture life with the similar microstructural degradation in terms of coarsening and lath grains with Grade 91 while Guguloth *et al.* [173][184] found the SR did not give a direct estimation of creep strain rate.

De Bruyker [183] indicates a prestrain at the start of the secondary region or 0.5% for steels so that the relaxation curve passes the primary region Woodford [185] recommends just above yield stress to reduce anelastic effects and typically 0.4% total prestrain.

The methodology appears to be relatively limited in terms of the available data in the public domain which may also be indicative of the costs or complexity of the testing in relation to standard creep tests.

There are two principal methods available for stress relaxation testing (SRT) in the standard [177, 186] the first can be carried out on creep test frames and involves a step-down reduction in the load to maintain the strain level which is repeated to maintain it. This generally involves constant monitoring and adjustment in the first few days to maintain the strain within limits until a daily adjustment is reached. The second method involves a model bolt assembly (a series of them) where a bolt is measured and prestrained between a casing and nuts. After soaking for the required time the overall length is measured or a strain gauge attached to the inner bolt surface. The reverse extension is used to establish the residual strain from using the Elastic modulus at temperature. The nuts are removed destructively so as not to affect the measurement and the reverse extension measured from either the overall length change or the strain gauge. Each bolt assembly provides a single data point on the stress relaxation curve. A series of individual experimental data points requires models for relaxation.

A review of models predictive ability to 3000h hold time of relaxed stress was recently carried out by a team from the ECCC [110] and summarized in 6.1. The data was collected at 450-550°C at strains of 0.1, 0.15 and 0.2% and an additional 0.25% strain at 500°C. The Wilshire and TTP models performed best in extrapolation outside the range of data (>10kh). Some of the models were applied to creep data with a modified Graham-Walles model providing particularly impressive results. The Garafalo and Graham-Walles models have been found to generally underestimate the decrease in stress within the first 30 hours

Table 6.1: Round Robin models used by ECCC. Long term stress relaxation [107].

Model	Equation
Modified Kohlrausch	$\sigma = \sigma_0 \cdot \exp\left(-\alpha \cdot t^{\beta}\right)$ $\alpha = x_1 + x_2 T\varepsilon + x_3 T^3 + x_4 T + x_5 \varepsilon$ $\beta = c_1 + c_2 T\varepsilon + c_3 T^3 + c_4 \cdot T^2 + c_5 \varepsilon$
Feltham	$\sigma(t) = \sigma_0 \cdot (1 - B'' \ln(bt+1))$
TTP (Larson-Miller)	$\sigma/\sigma_0 = 26.26 + 4.727 \cdot \varepsilon + 0.3664 \cdot \mathrm{LMP}^2 - 5.38 \cdot \mathrm{LMP} - 0.3315 \cdot \varepsilon \cdot \mathrm{LMP} - 0.008303 \cdot \mathrm{LMP}^3$ $LMP = (\log_{10}(\mathrm{t}_\varepsilon) + \mathrm{C})\,(\mathrm{T})$
Wilshire relaxation WE-R	$\frac{\sigma}{\sigma_0} = \exp\left(-k\left(t_{rel} \cdot \exp\left(\frac{-Q}{R \cdot T}\right)\right)^{u}\right) \cdot PCF(\varepsilon)$
Modified Garafalo	$\varepsilon_{pr}(\sigma, T) = A_{pr} \exp(-Q_{pr}/RT)\,\sigma^m (1 - \exp(-a + b\sigma)t)$ $\dot{\varepsilon}_{ss}(\sigma, T) = A \exp(-Q/RT)(\sinh(B\sigma))^n$
Modified Graham-Walles	$\dot{\varepsilon}_{\mathrm{f}} = 10^{\mathrm{Al}} \cdot \left[\frac{\sigma}{1-\mathrm{D}}\right]^{\mathrm{n1}} \cdot \varepsilon_{\mathrm{f}}^{\mathrm{ml}} + 10^{\mathrm{A2}} \cdot \left[\frac{\sigma}{1-\mathrm{D}}\right]^{\mathrm{n}^2} \cdot \varepsilon_{\mathrm{f}}^{\mathrm{m2}}$
Norton	$\dot{\sigma} = -E\dot{\varepsilon}_c$

[187]. Another model of note is the Peleg model [188] highlighted by Kim *et al.* [181] as a potentially useful model for Grade 91 stress relaxation.

$$\sigma(t) = \sigma_o \left(1 - \frac{t^n}{k_1 + k_2 t^n}\right) \tag{6.5}$$

where $\sigma_0$is the initials stress, t is the time and n its exponent, k1 and k2 are fitting parameters. The notation is broadly the same for the models in Table 6.1 or as previously described.

The EN 10319 [186] Model Bolt methodology requires less specialist equipment and skills than the traditional step-down SRT but is expensive; a complete model bolt assembly is required per data point, hence there is little experimental research data available in the public domain. This chapter describes a modified model bolt methodology that provides a complete relaxation curve per model bolt assembly. The motivation is the obvious cost savings and accessibility with only a simple tensile test machine, furnaces and measuring equipment required.

6.2 Principle of the New Methodology

The standard model bolt methodology described above relies on a single measure of the reverse extension per sample for a single data point on the SR curve whilst the traditional step-down load method requires continual monitoring and adjustment to provide the SR curve. The first method is expensive and the second demanding in terms of the equipment and skills requires to obtain a curve. A modified model bolt (MMB) method has been in development at GE, Rugby. The method takes the traditional model bolt methodology and with some modifications to the assembly seeks to provide a series of stress relaxation data points from a single assembly and thus a useful SR curve at a far lower cost with simply a tensile test frame, precision measuring equipment and furnaces.

The MMB components are shown in Figure 6.1 for comparison to the other test sample pieces and the details available in Figures 6.2, 6.3 and 6.4. There are a number of modifications to the normal bolted joint for this modified method.

- The strain gauge slots in the standard model B bolt [186] are replaced by two holes in the casing to allow extensometer ceramic legs to be spring-loaded in contact with the bolt surface inside the casing during the tensile test.

- A series of slots have been made in the threaded section of the bolt to prevent rotation of the bolt in a jig device if the sample is to be prestrained by rotation of the nuts only.

- Circumferential v grooves have been machined in the casing to allow accurate and repeated measurement of the casing length even with oxidation scaling. With accurate measuring equipment, this allows monitoring of the relaxation by casing length extension (from a 9:1 ratio of cross-sectional area)

- A series of 'flats' have been machined in the casing (shown in Figure 6.3) to ensure the casing is measured at fixed locations equally spaced around the circumference.

- The gauge length of the sample was established using a strain gauge.

The modified method relies on the same techniques to prestrain the bolt without bending or torsion either in a jig or other device. The difference between the methods is in the measurement of the retained stress. The principle of the MMB methodology is that the bolt within the assembly can be loaded in tension as a tensile test reducing the prestrain until

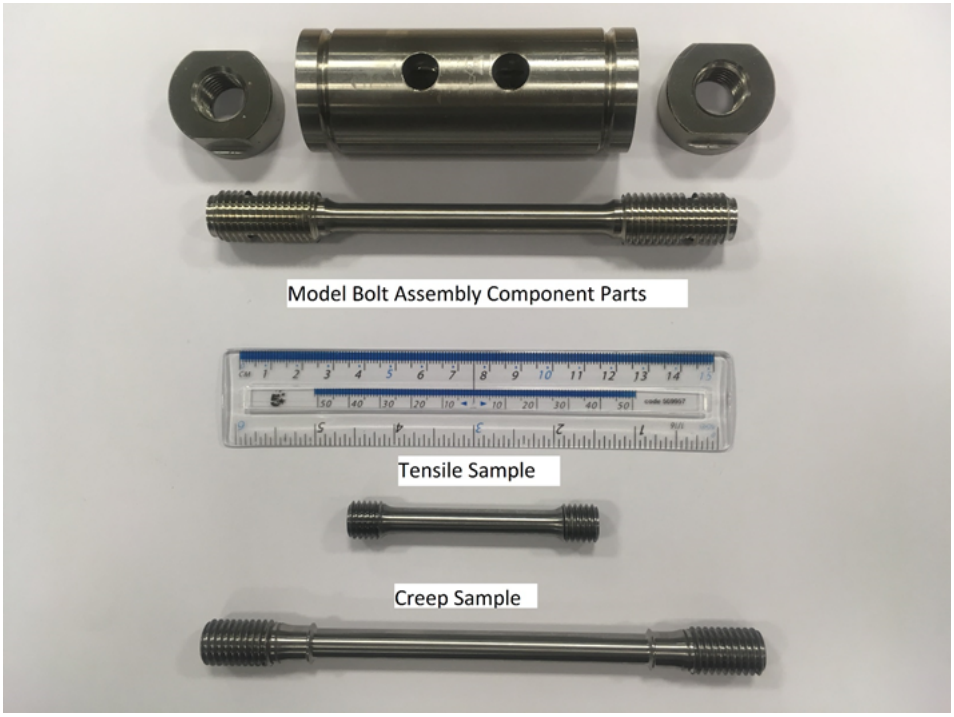

Figure 6.1: MMB assembly components compared to the other sample test pieces.

the bolt becomes free of the casing and the subsequent plot is of the free bolt modulus. Remaining within the linear elastic range of the material the bolt is unloaded at the same rate, 're-assembled' and the displacement plot retraced back to the start at zero strain as shown in Figure 6.5. Provided the free bolt modulus remains within a linear elastic range of the material this portion can be retraced to the origin of zero strain which will provide the retained stress. The principle relies on the assumption that the bolt assembly can be separated and reassembled without altering the prestrain. Repeated soaking cycles and testing provides a measure of the retained stress relaxation in the bolt at the temperature of interest as shown in Figure 6.6. The displacement plot is ascending through the assembly modulus until complete separation within the elastic range to the free bolt modulus and then descending load, at the same rate to complete reassembly and the same prestrain. All the testing is carried out at room temperature on a simple tensile test machine, albeit with a specific extensometer rig, with the hours of soaking requiring only furnaces and thermocouple monitoring equipment as the standard model bolt method. Figure 6.7 shows the extensometer ceramic legs in contact with the model bolt inside the assembly during a tensile test.

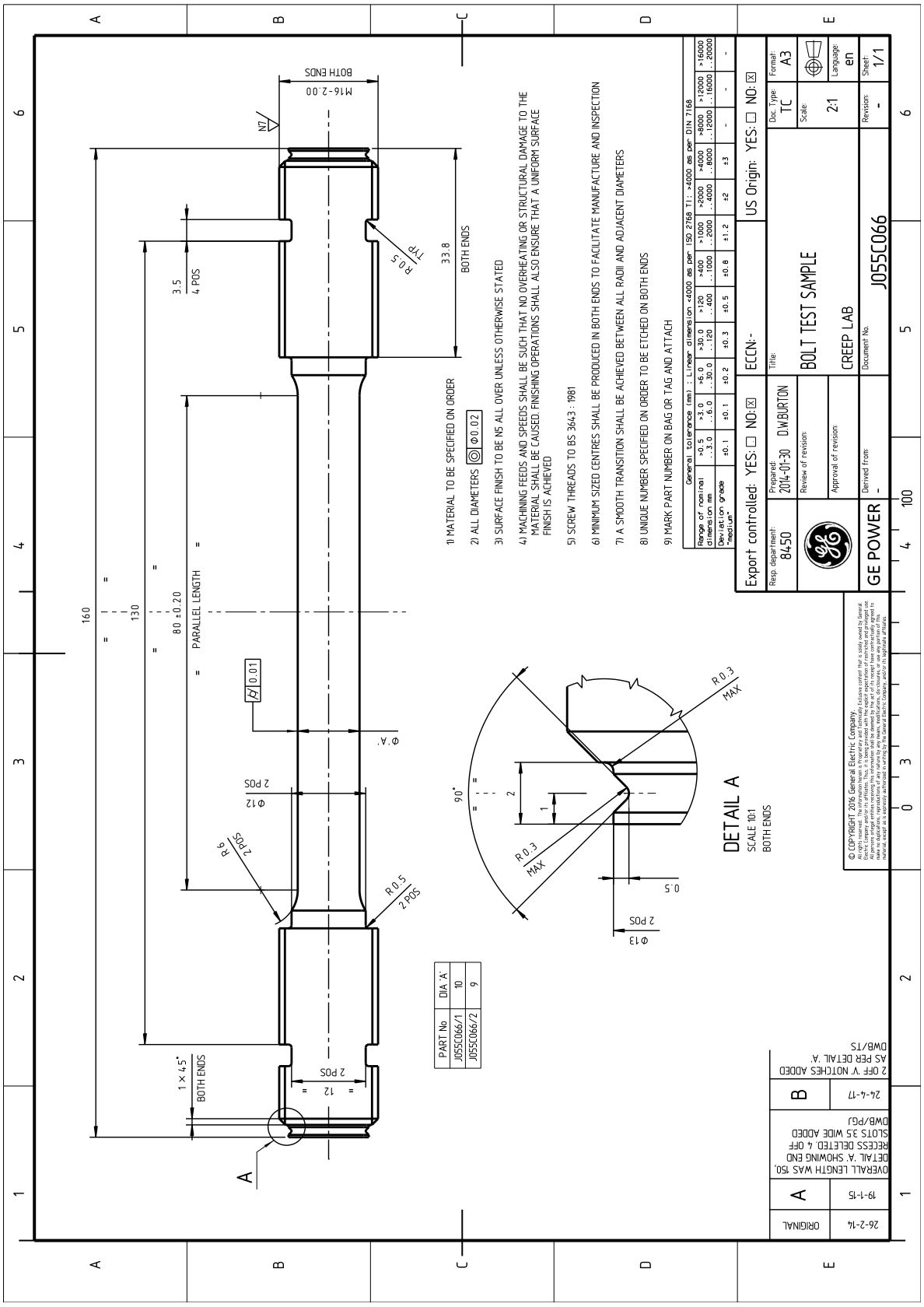

Figure 6.2: MMB Bolt Details.

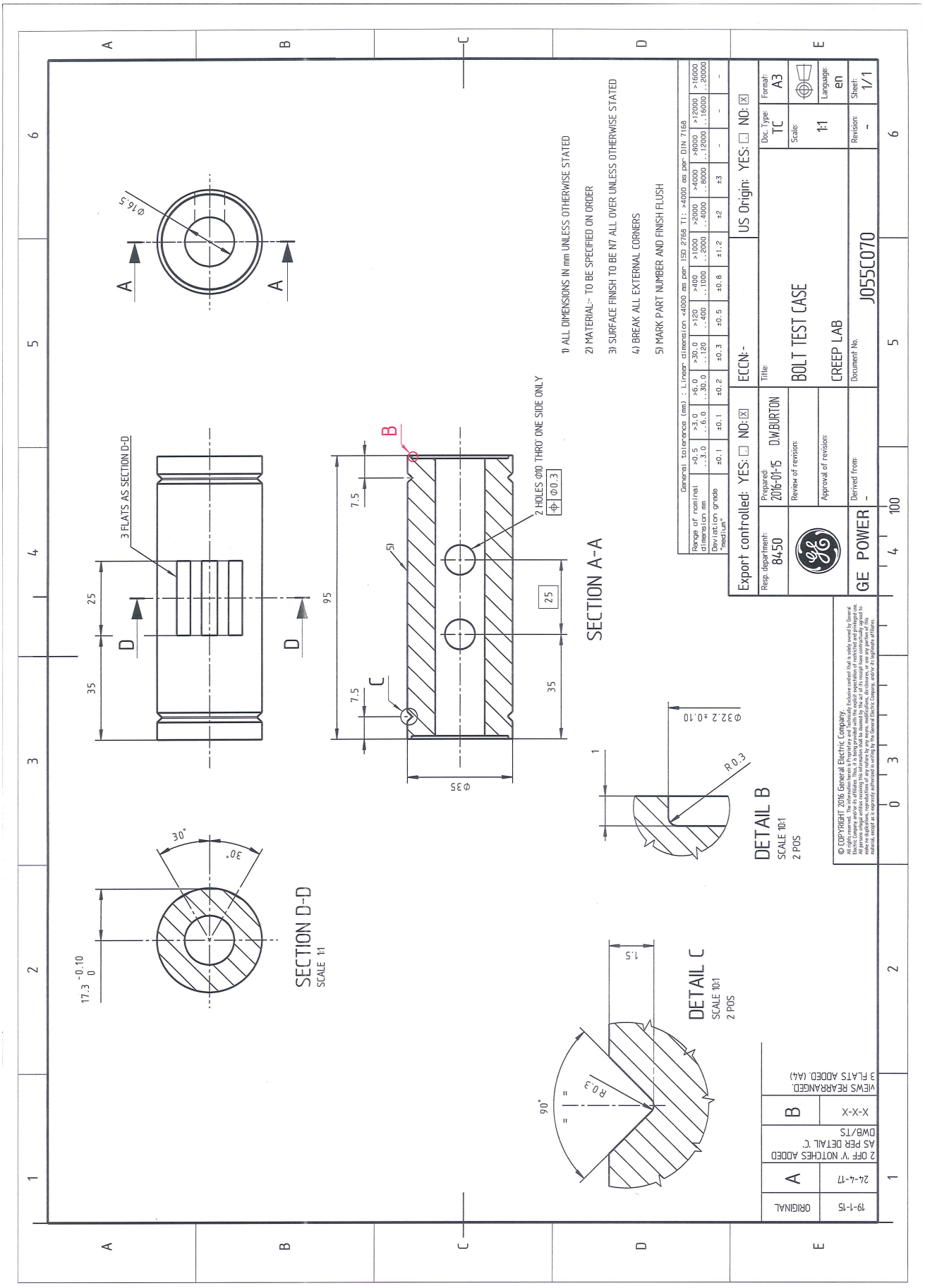

Figure 6.3: MMB Casing Details.

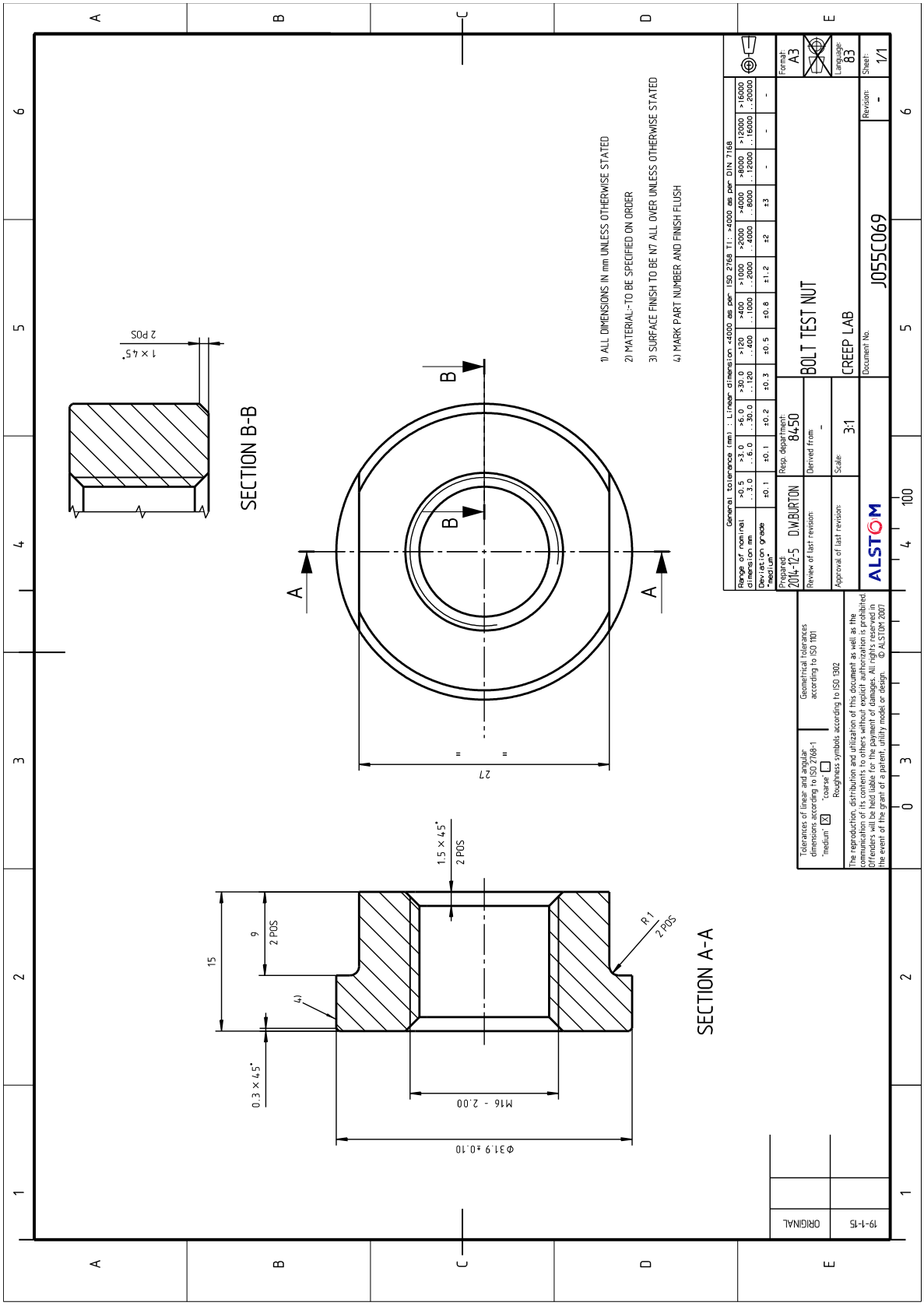

Figure 6.4: MMB Nut Details.

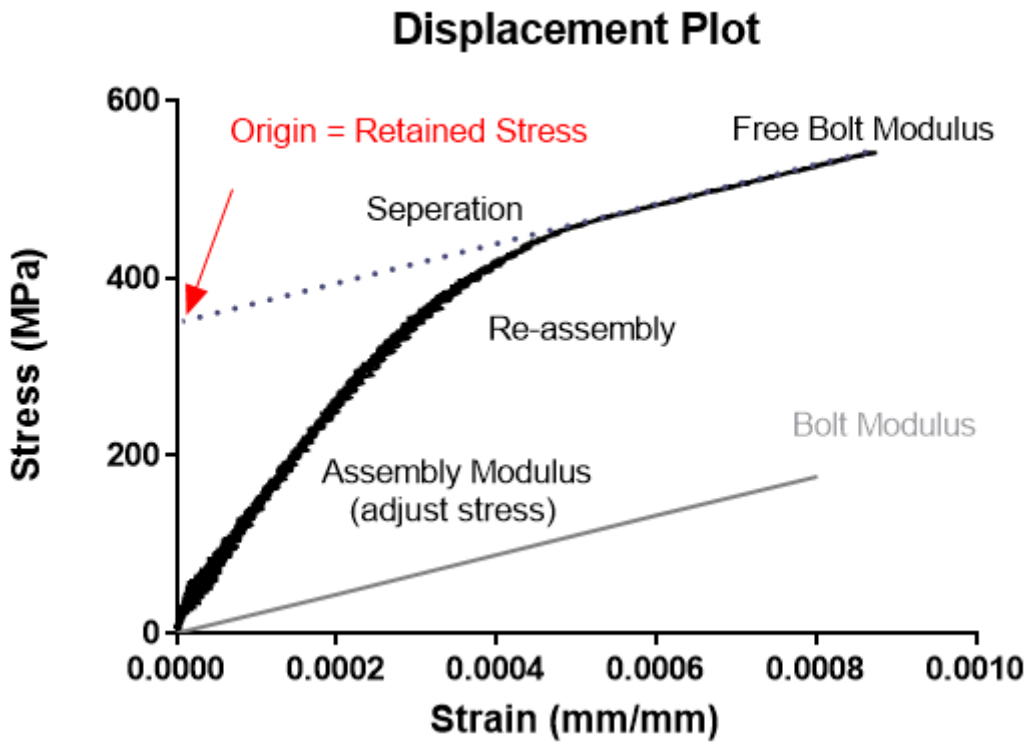

Figure 6.5: MMB Tensile test plot.

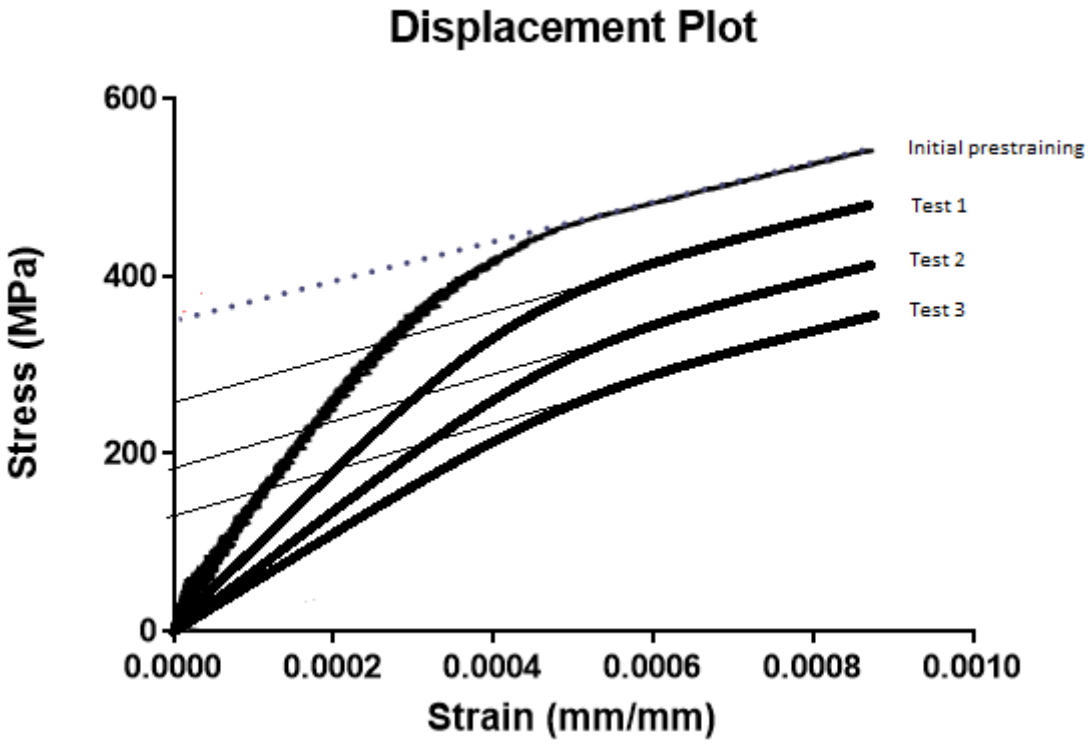

Figure 6.6: MMB Series of tensile tests after soaking cycles.

Figure 6.7: MMB Assembly Test.

The plots shown above does not show the jolts and disruption by the breaking of oxidation scales often experienced in the first test after a soaking and the adopted protocol is to ignore the initial plot and take the average of the subsequent two plots. The particular challenge with the method is the limited window available to provide a linear portion of free bolt modulus without inducing yielding, plasticity and ratcheting while prestraining sufficiently to provide the creep information. There are a number of issues considered with the modified model bolt development, only the same material for all components has been considered.

- Elastic follow-up is the reaction of the casing, which is still in an elastic state, on the bolt to reduce the relaxation force. Provided the ratio of cross-sectional areas of the bolt and flange is > 9 then elastic follow-up is negligible [189].

- The torsional and bending effects must be minimised in prestraining the bolt. the standard allows for a jig device to hold the bolt thread while the bolt is prestrained by applying torque to one of the nuts.

- The standard requires that the bolt should be strained about three times up to the ini-

tial strain. This is to eliminate setting effects between the threads and the casing nut interface. This was also adopted in the initial prestraining of the modified model bolt. Since no further adjustment of the nut is carried out the method assumes the setting effects are negligible after subsequent soaking/test cycles.

- The effects of oxidation on the bearing surfaces and the possibility of oxide 'jacking' effect to increase the stress.

- The schematic does not show disruption by the breaking of oxidation scale on the stress-strain plot. The first plot is usually disrupted by oxide scale cracking and the initial plot discarded with the average of subsequent two plots used to provide the retained stress.

- A limitation of the methodology is the window required within the elastic regime of the material for a linear portion of the stress-strain plot to calculate the retained stress. Predefined material load limits based on the tensile properties need to be applied to prevent introducing plasticity.

- Another challenge of the methodology is the variability of the initial prestrain.

The requirement for the creep-stress relaxation relation is that the stress relaxation curve passes through the stress of interest - to relate the results to the creep tests carried out would require the plot to pass through the reference stress. A sufficient portion of linear free bolt modulus without introducing yielding, plasticity and ratcheting into the bolt during the tests requires a retained stress in the elastic range. Clearly, the prestrains listed above in the literature would not provide a linear portion. To use the methodology requires either a different method for the initial prestraining, relying on bolt length extension is possible with associated error and uncertainty - that is the standard method. This also requires some 'art' in guessing that the first cycle soak will reduce the retained stress so that subsequent tests provide a linear portion. Alternatively, the prestrains associated with the creep tests could be used with the hope of 'catching' the curve as it passes through the lower reference stress and thus provide some relation to those creep plots.

The alternative higher initial strain measured by bolt extension would probably have provided better data and relations to calculate the stress rate at the reference stresses.

6.3 Experimental Procedure

This procedure was carried out on the P265GH and Grade 91 materials.The materials were prestrained to 0.065% and 0.05% P265GH and 0.12% and 0.1% Grade 91. Loading limits were set rounded Rp0.01%, RT at 250 MPa P265GH and 400 MPa Grade 91 from the tensile data in the previous chapter. These prestrains allowed a sufficient portion of linear plot to calculate the initial retained stress. Though the stress levels were insufficient to find a stress rate of interest for Grade 91 and the P265GH had low prestrains to apply the methodology was applied with a view of developing the methodology rather than providing a stress rate to compare with the creep rate data. The method does require validation with standard step-down stress relaxation methods.

Prior to assembling the bolt only was loaded to typically 2/3 of the load limit to establish the free bolt modulus. The samples were assembled with magnesium hydroxide solution on the threads and casing/nut interfaces and loaded into the tensile test machine. The assembly was then placed in an Instron 1342 servo-electric test frame with suitable grips. The position of the cross-head was noted and the sample preloaded to 0.5kN in load control. The sample was then prestrained to the required value using the change in overall length (based on the reference length of 100mm) using a set of spanners on the upper and lower nuts. The sample was then unstrained noting the position; this process of straining and un-straining was repeated three times and on the third iteration the bolt was left in the prestrained condition. This was the requirement of the standard model bolt method to eliminate the effects of thread, nut and interface setting. The load was then reduced to 0.2kN and the MTS 25mm ceramic v-shaped rods of the extensometer were mounted on the sample surface and zeroed. Load limits were set at 250 MPa and 400 MPa for the P265GH and Grade 91 respectively to ensure they remained within the elastic range. The sample was then loaded in tension using a profile sequence at a rate of 125N/s, a pause at the material limit for 10 seconds and a return unloading at the same rate. The displacement curve was plotted on return to 0.2kN preload and the sequence repeated three times. This sequence for the initial prestraining was repeated for the subsequent tests after soaking. Soaking was carried out in Carbolite furnaces with considerable thermal mass to stabilise temperatures, N-type thermocouples were placed in intimate contact with the model bolt surface throughout with thermal string. After soaking samples were left to stabilise at room temperature for >1 hour prior to testing.

Each test cycle would typically be a series of three tensile tests either to the load limit cal-

Table 6.2: Initial prestrains for P265GH.

Temp	350°C	375°C	400°C	425°C	450°C
0.065%	128.56 MPa	124.74 MPa	143.04 MPa	115.97 MPa	
0.05%		101.1 MPa	111.65 MPa	96.97 MPa	101.8 MPa

culated or, as the retained stress decreased until a sufficient linear plot is achieved. The initial plot after soaking is often subject to extensometer jolts and displacement due to oxidation cracking and the retained stress was recorded as the average of the two later retracements. A nominal 20% of the free bolt upper plot was generally used to calculate the modulus and retrace to the origin once the retained stress is low enough. Because of the small window available for these materials this was limited to 10% for the 0hrs calculations. The initial plot would be adjusted for any disruption to check the return plot has zeroed as expected. The extensometer was not zeroed unless there was a significant disturbance on loading. Modulus checks were conducted on the ascending and descending plots.

6.4 Results and Discussion

6.4.1 P265GH

The initial prestrains are provided in Table 6.2 and the results are shown in Figure 6.8. In both cases, there was a significant drop in the retained stress over the initial 24hours. Three from four of the 0.065% data also showed an apparent increase in the retained stress at the 168 hour test. The plots are broadly as expected with a higher reduction in retained stress with higher temperature. The difficulty in obtaining a consistent initial prestrain is evident with the 0.065% data and an overlap in the normalised retained stress plot at 400 and 425°C. The initial drop is significant and the variation in data makes it difficult to draw conclusions at these stress levels. The modulus checks during loading and unloading are shown in Figure 6.9, beyond 1200 hours the bolt surfaces are polished to remove oxide scale prior to tensile testing which appears to have an effect on the modulus values recorded and more of an effect on the unloading modulus (dashed lines).

The model parameters shown in Table 6.3 were obtained using GRAPHPAD's non-linear least-squares routine. The Peleg model does appear to represent the initial stress relaxation better than the Feltham or Kohlrausch models for the P265GH material at these levels.

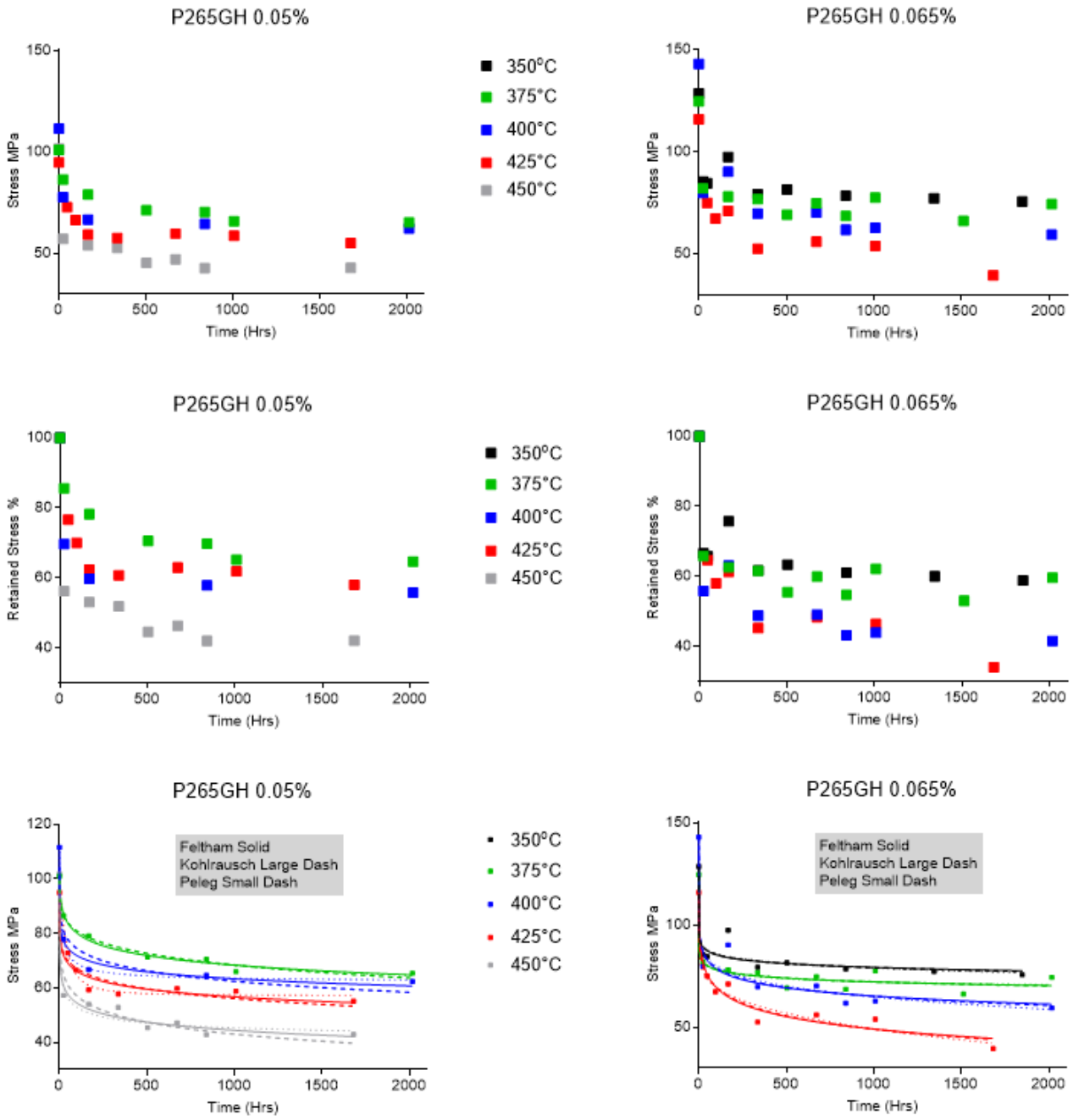

Figure 6.8: P265GH MMB Stress Relaxation Results.

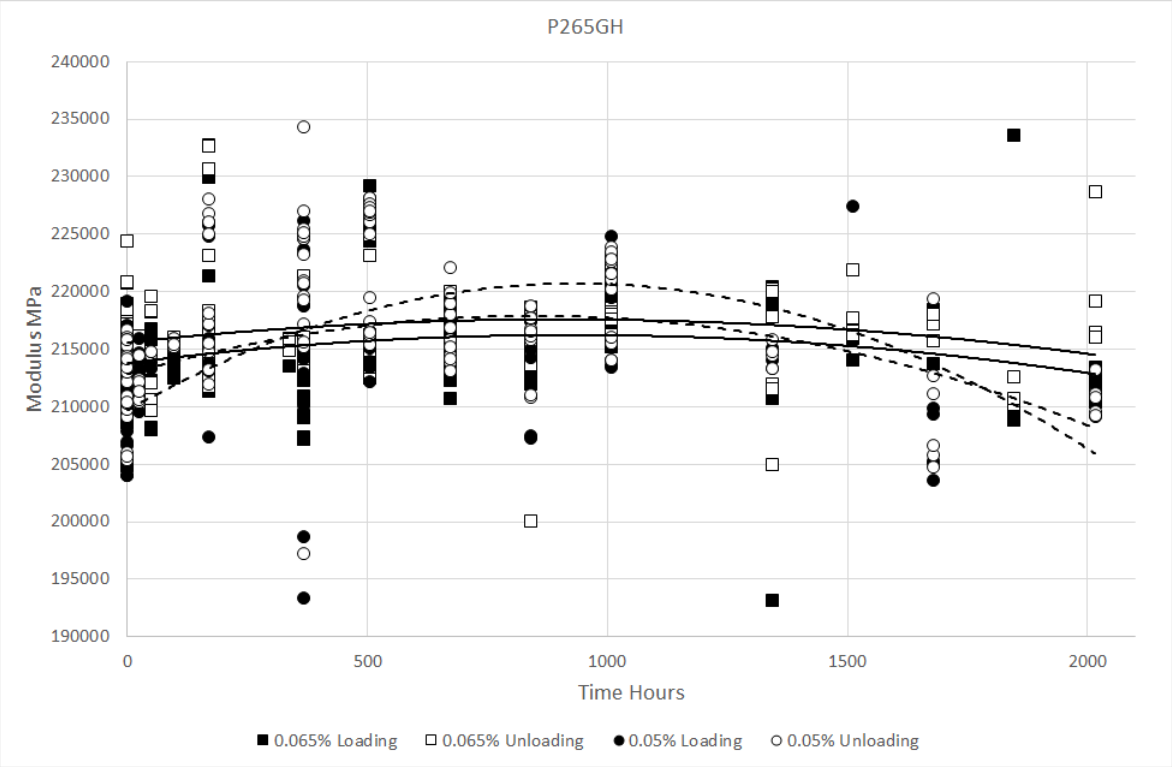

Figure 6.9: Variation in Modulus during testing P265GH.(Solid loading, dashed unloading)(2nd order Poly).

Table 6.3: P265GH Model fitting parameters using GRAPHPAD's non-linear least-squares routine.

		0.065%				0.05%			
Model		350°C	375°C	400°C	425°C	375°C	400°C	425°C	450°C
Peleg	n		0.2363		0.021	0.3722	0.7348	1.501	
	$k1$		2.082		17.62	17.76	10.73	622.1	
	$k2$		1.968		-13.48	1.722	2.254	2.509	
Feltham	B''	0.0208	0.021	0.0403	0.07626	0.0509	0.030	0.0431	0.0371
	b	102717	496020	714	1.919	0.5803	1618	11.65	33425
Kohlrausch	α	0.285	0.3381	0.3352	0.179	0.0726	0.2819	0.1838	0.385
	β	0.0771	0.0695	0.1236	0.2274	0.2378	0.099	0.1488	0.1094

Figure 6.10: MMB surfaces after removal of the nuts by drilling.

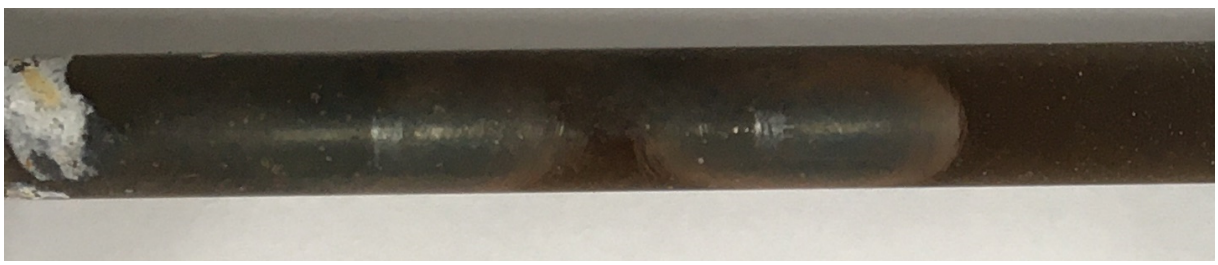

Figure 6.11: P265GH typical bolt surface after 2kh and multiple tests.

There was no indication in any of the plots that yielding plasticity had been incurred during the loading process. This would be shown by divergence of the unloading from the loading in the upper free-bolt region. For the P265GH the initial displacement plots showed a gap evident at the reassembly stage with unloading lower than loading. Subsequent plots showed the gap narrowed in plot 2 until the loading/ unloading plots were indistinguishable on test 3. This occurred again after a 15 minute wait indicating a time phenomenon rather than a setting issue with threads or interface. This was evident with P265GH only. The possible effects of a varying anelastic contribution as the stress is relaxed need further investigation.

The sample photographs after dismantling by drilling the nuts from the bolts are shown in Figure 6.10 there is considerable oxidation on the bolt surface which was removed prior to the later tests through the holes with a rotary brush. The bolt surface in Figure 6.11 does appear to be scored by the successive mounting of the extensometer ceramic rods repeatedly at the same location and their influence on the results cannot be ruled out. The nut/casing interface surfaces appear relatively free of oxide scaling.

6.4.2 Grade 91

The initial prestrains are provided in Table 6.4 and the results are shown in Figure 6.12. The Grade 91 results again show a significant drop in the retained stress over the initial 24 hours. The temperature plots are broadly as expected with a higher relaxation at higher temperatures except the 500°C 0.1% plot. The data includes multiple increases in the recorded values for the retained stress in the 0.1% prestrain data. There is no indication this is a real increase in the retained stress induced from the tests evident which would be evident from a cross-over of the descending plot over the ascending from a reassembly to a shorter length. This may be an indication that the relaxation rate is low and the variability in the measurements is greater than the reduction. The difference in the return plots was typically within $3\mu m$ for both materials. The 0.12% prestrain data does indicate there is some further relaxation at the higher temperatures. The modulus checks in Figure 6.13 show less variation in the modulus measures with less oxidation effects.

The Peleg model does not show any superiority over the other models with this material.

There is much less evidence of oxide scaling on the Grade 91 samples and less evidence of scoring on the bolt surface in Figures 6.14 and6.15.

Table 6.4: Initial prestrains for Grade 91.

Temp	400°C	425°C	450°C	475°C	500°C
0.12%	256.47 MPa	253.6 MPa	255.7 MPa	246.75 MPa	
0.1%	-	202.38 MPa	218.95 MPa	201.84 MPa	222.09 MPa

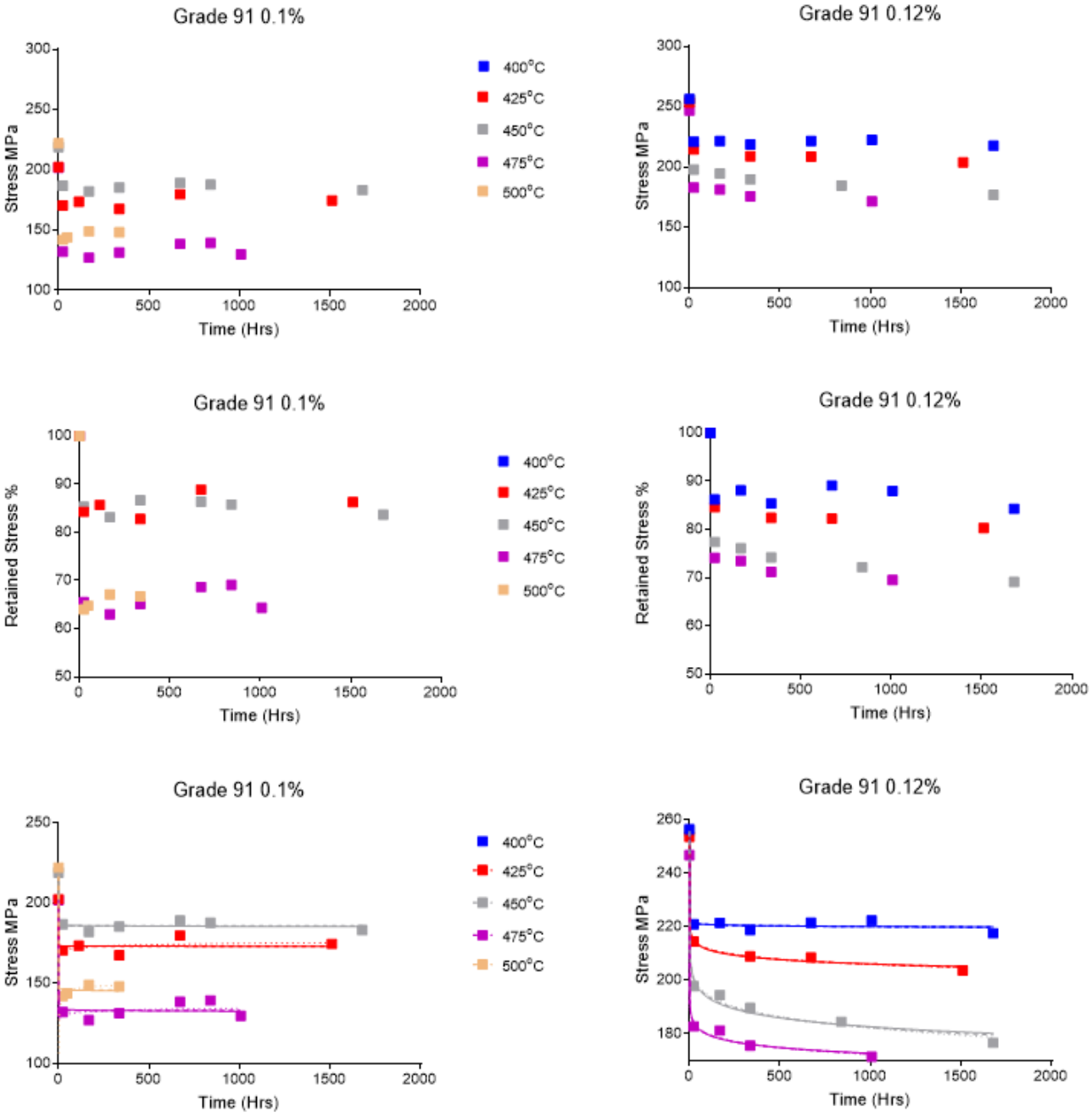

Figure 6.12: Grade 91 Stress Relaxation Results.

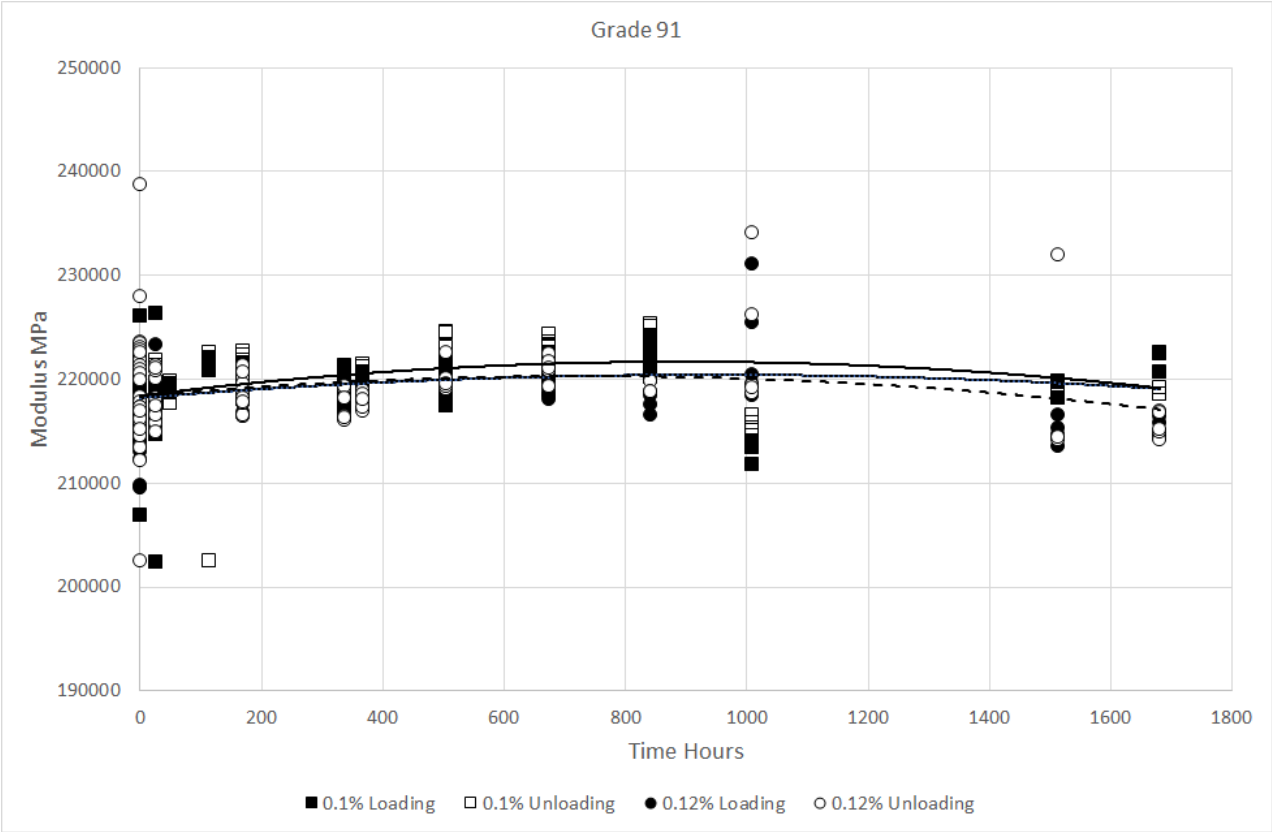

Figure 6.13: Variation in Modulus during testing Grade 91.(Solid loading, dashed unloading)(2nd order Poly).

Table 6.5: Grade 91 model fitting parameters using GRAPHPAD's non-linear routine.

		0.12%				0.1%			
Model		400°C	425°C	450°C	475°C	425°C	450°C	475°C	500°C
Peleg	n								0.4424
	$k1$								-1.577
	$k2$								3.153
Feltham	B''	0.0013	0.0093	0.0187	0.0124				
	b	5.1E+43	538062	4328	3.5E+5				
Kohlrausch	α	0.1427	0.1363	0.1837	0.2467	0.1557	0.1634	0.4163	0.4201
	β	0.0100	0.0608	0.0880	0.0537	3.0E-5	0.0009	4.2E-5	7.1E-5

Figure 6.14: Model bolt surfaces at temperature extremes.

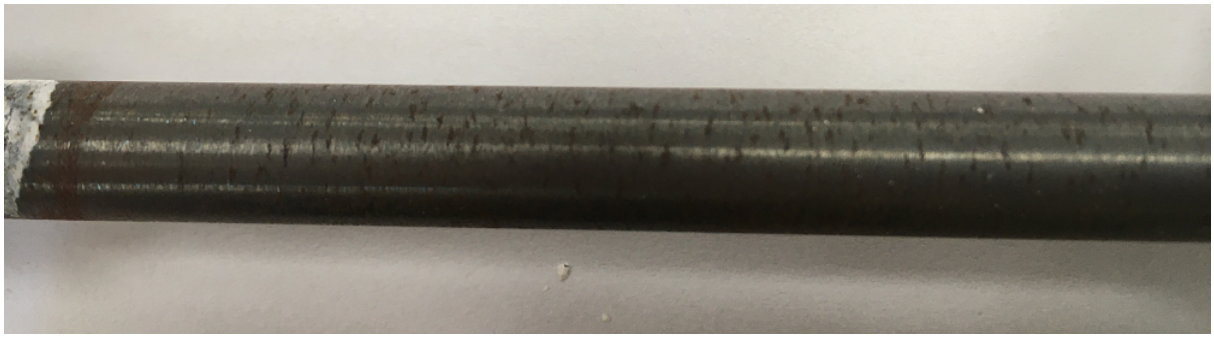

Figure 6.15: Grade 91 typical bolt surface after $\sim$ 1700h and multiple tests.

6.5 Finite Element Analysis

The creep test data is collected at only two stress levels and a limited temperature range which would normally be considered inadequate to estimate the Norton constants. The constants have been derived as shown in Figures 6.16 and 6.17 and Table 6.6 simultaneously using Solver in Excel assuming

$$\dot{\varepsilon} = A_0 \exp\left(\frac{Q}{RT}\right) \sigma^{n_0+n_1 T} \tag{6.6}$$

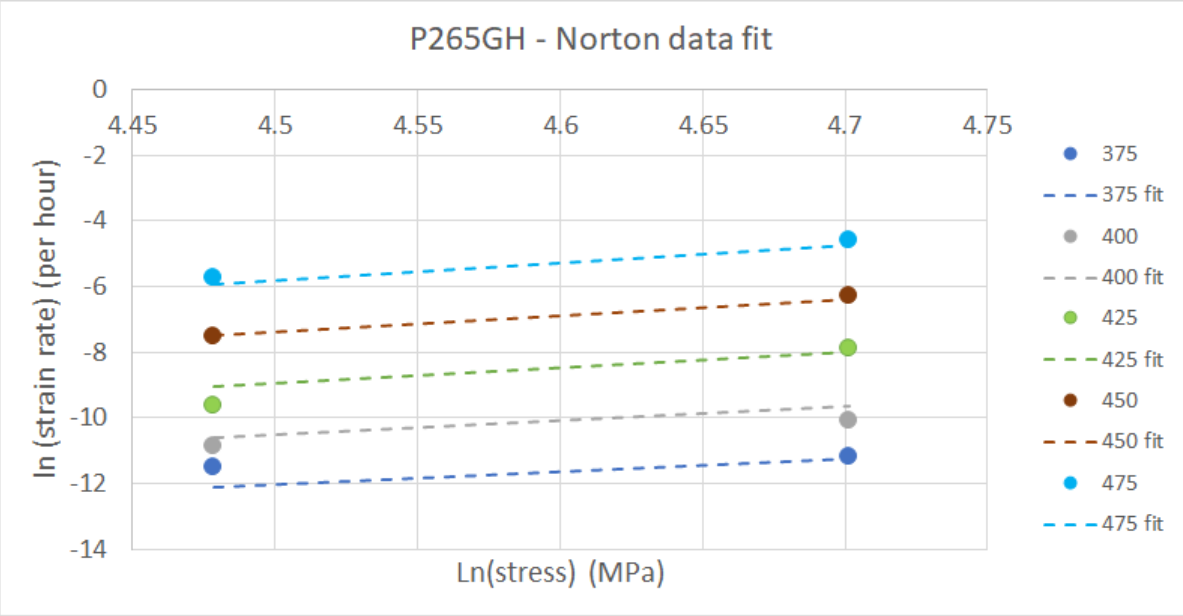

Figure 6.16: P265GH Norton data fit.

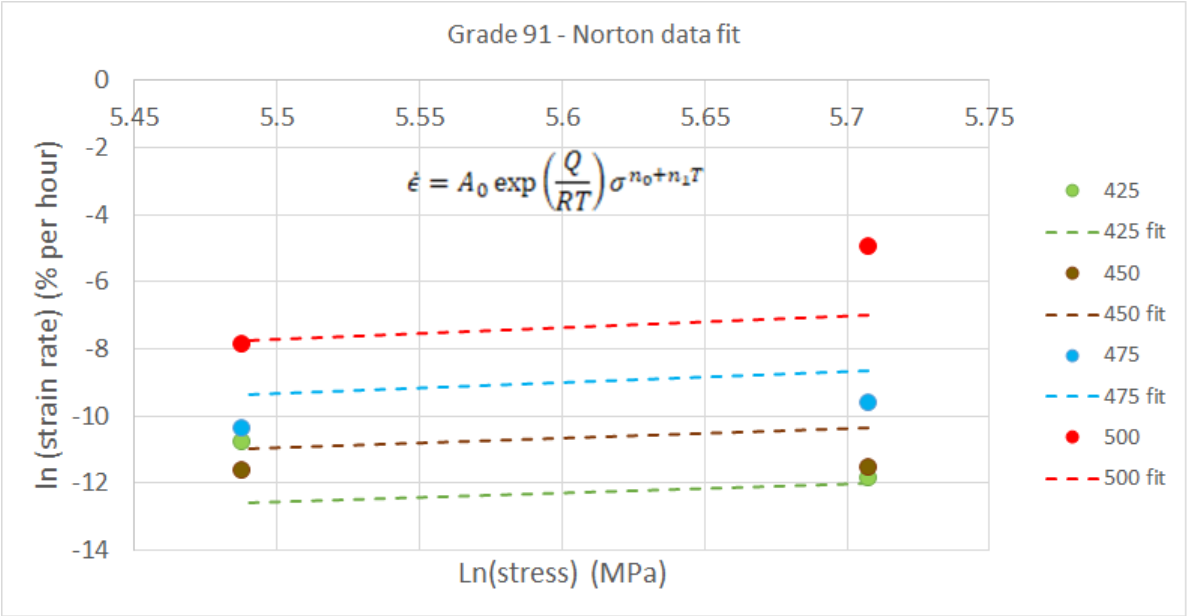

Figure 6.17: Grade 91 Norton data fit.

Table 6.6: Norton fitting parameters.

	P265GH	Grade 91
n_0	-1.19638	-2.42124
n_1	0.013785	0.011737
LnA_0	-29.9176	-26.6513
Q	-0.00519	-99.9008

The stress relaxation model for a representative bolt model was implemented in COMSOL Multiphysics v5.6. The three-dimensional bolt geometry was pre-loaded using an elastic analysis by applying an appropriate displacement to one end of the sample, with the other end constrained. The elastic modulus was defined as a linear function of temperature (as Figure 5.13). The resulting stress state is shown in Tables 6.2 and 6.4. This was used as the initial input condition for a time-dependent creep analysis. The constant end displacement was retained and the material was allowed to relax over time. The temperature-dependent parameters for the creep model are shown in Table 6.6. An example of the final creep strain in the bar for a P265GH specimen for a T = 450°C and nominal stress = 88 MPa is shown in Figure 6.18, where it is shown that the creep strain in the thicker end sections is much lower than in the rest of the specimen, as required. The stress in the centre of the bar, away from the ends, is plotted as a function of time in Figures 6.19 and 6.20 for the range of temperature and actual test stresses considered in the experimental bolt tests.

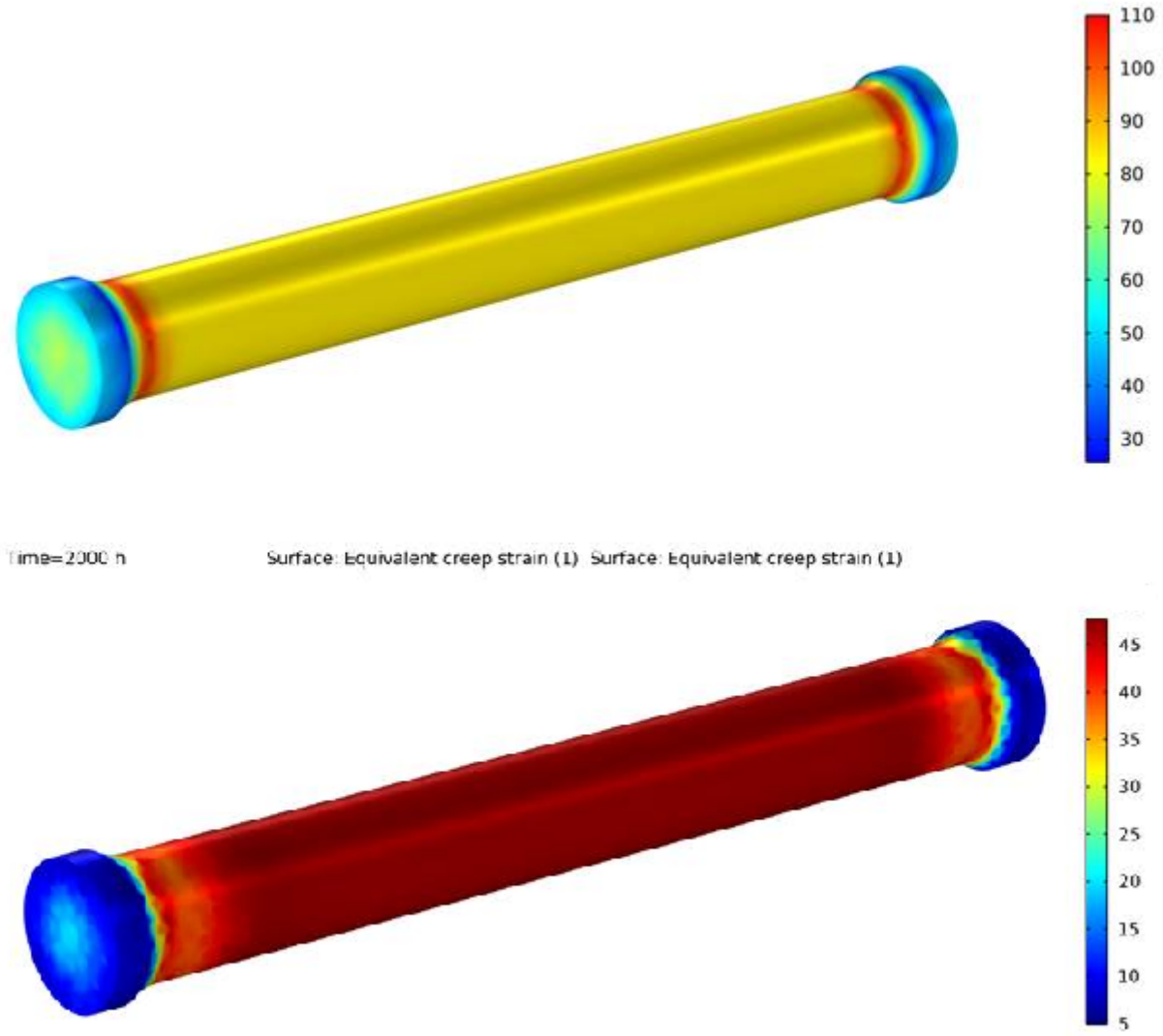

Figure 6.18: COMSOL FEA Example of P265GH 450°C relaxation from 88 MPa (a) 0 hours to (b) 2000 hours.

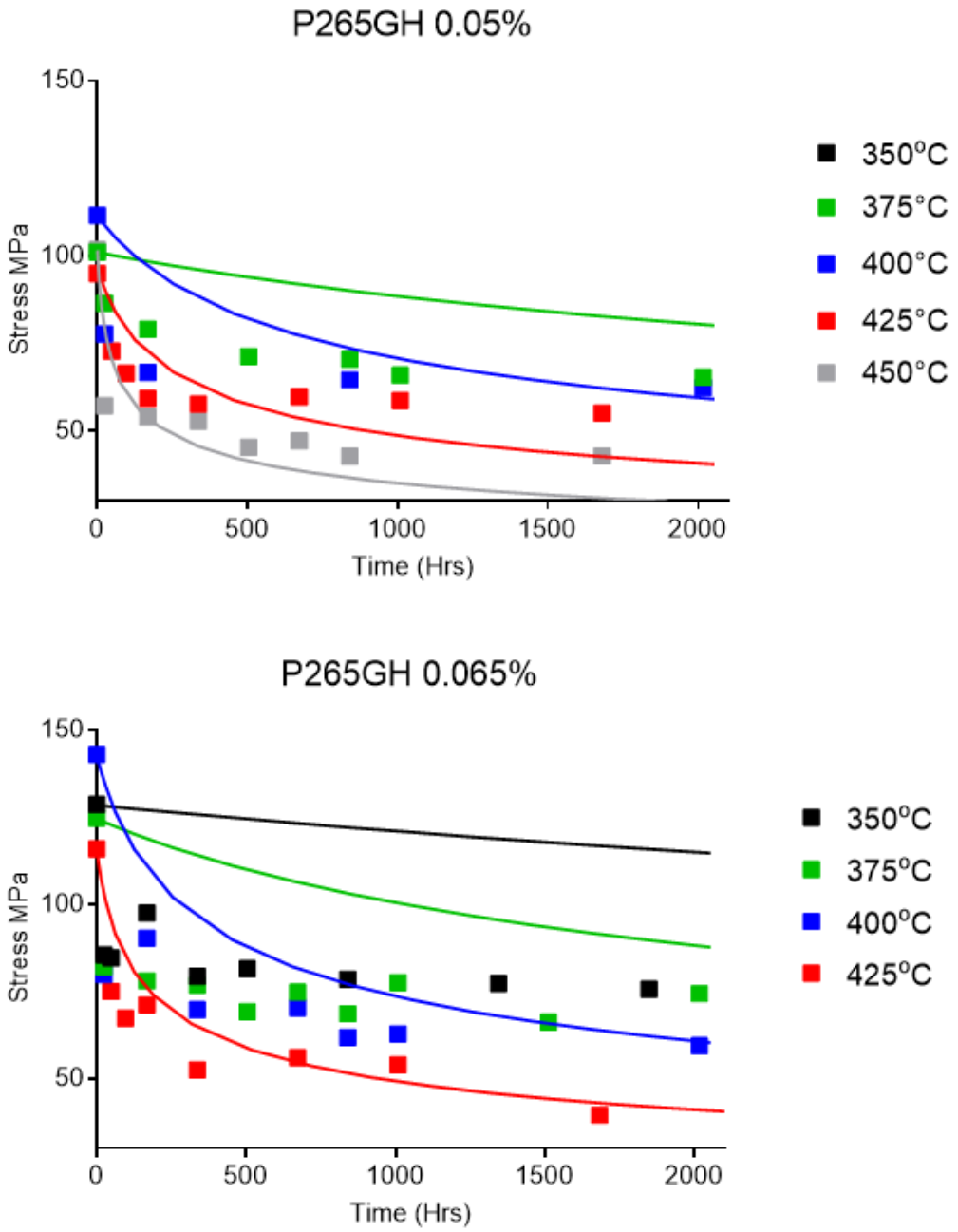

Figure 6.19: P265GH COMSOL result (solid line) & modified model bolt test results.

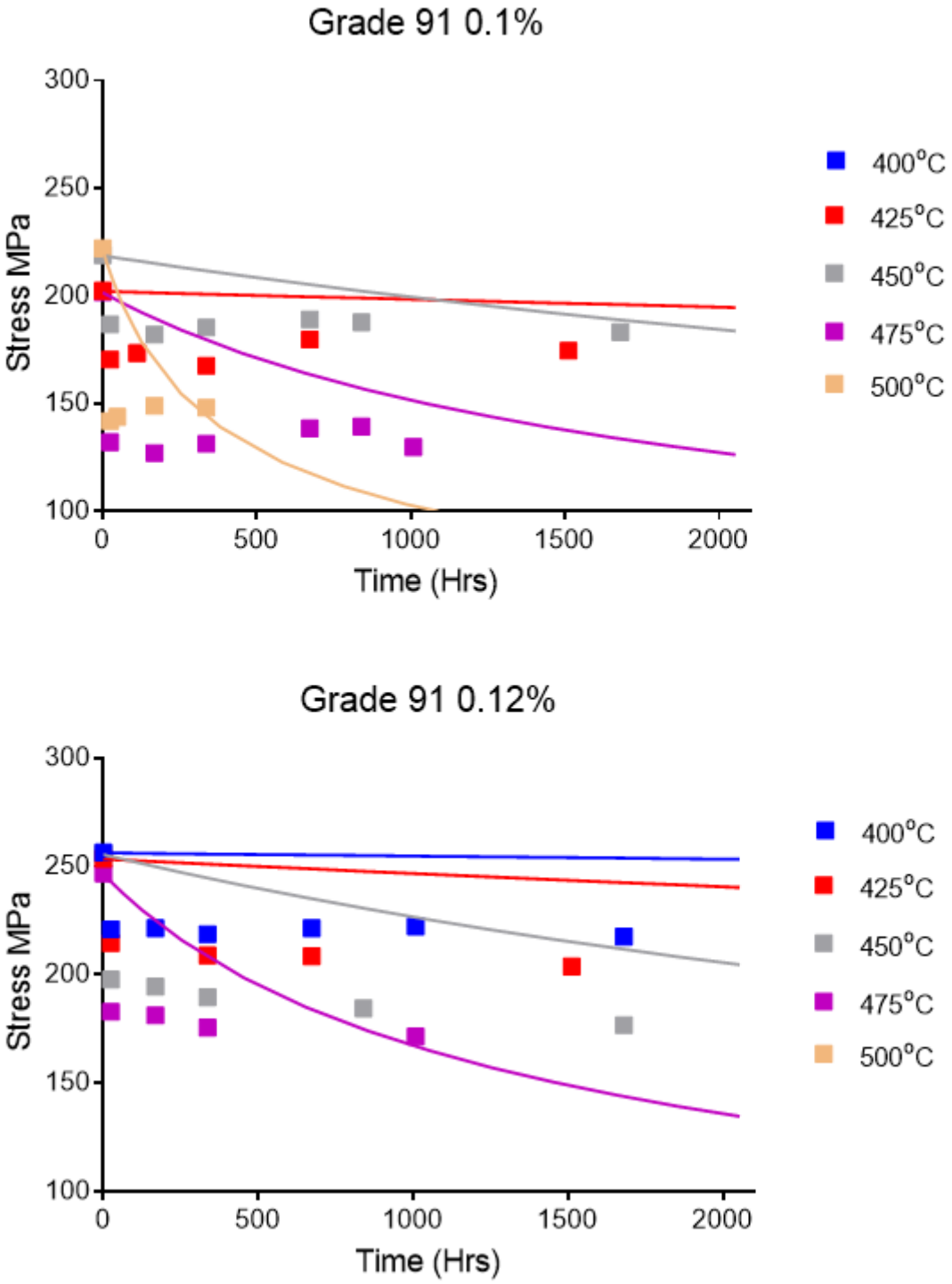

Figure 6.20: Grade 91 X10CrMoVNb9-1 COMSOL result (solid line) & modified model bolt test results.

In general, the Norton model FEA stress relaxation simulation does not show good agreement with the modified model bolt experimental results. In particular, the model is under-relaxed in the early stages for the Grade 91 material. With the limited data, the general

shapes of the curves appear better represented at $\leq$ 425°C. For the P265GH material, the model appears a better representation of the early stress drop at $\geq$425°C when the creep curves are sufficiently progressed compared to those below this.

6.6 Concluding Remarks

The P265GH data indicates the method can be used to provide an estimate of the stress relaxation curve though the method is restricted in the range of stress and requires further validation with standard step-down relaxation methods. The initial stresses allowable to obtain a linear portion and the stress rates within the initial 24 hour period did not allow a calculation of a useful stress rate. This turned into an exercise of applying the method rather than deriving a stress rate for comparison with the creep data.

The variability in measuring individual data points requires the use of a suitable SR model. The alternative higher initial strain measured by bolt extensions then using the MMB tensile test method may be the best combination for this method. Tests carried out at 1 or 2 hourly intervals over the initial 24hrs before the longer durations carried out here should provide the stress rate data required. At these times the concern would change from oxidation effects to disturbance and particularly loosening of the nuts during the tensile test stage. Eventually, loading to the established load limit, one of these tests would provide a sufficient linear portion of the displacement plot from where the retained stress can be calculated and a stress relaxation curve produced from that time on. Whether the method will provide a suitable curve can be assessed from the load limit at temperature based on tensile tests yield limits and shape. This may form a suitable test program for future applications of the method but needs a comprehensive comparison with a traditional stress relaxation method. The possible effects of a varying anelastic contribution as the stress is relaxed require further work. The technique works better in materials that show little or no oxidation (e.g. Ni-based bolting alloys)

Chapter 7

Conclusions Recommendations for Further Work

7.1 Conclusions

In applying a negligible limit of 0.2% creep strain at 200kh recent work within European Standards has found the traditional 'rule-of-thumb' that ferritic martensitic (F/M) materials do not creep below 375 ° C, and austenitic materials below 425 ° C may not be the case. Moreover, the findings indicate many F/M grades are creeping well below this limit potentially without creep design consideration or monitoring requirements whilst others that easily exceed it may be required to implement expensive surveillance and creep damage monitoring. Establishing a temperature below which creep strain exceeds this limit, or any other is challenging in that creep tests are normally performed well above this temperature range. There is simply no experimental evidence of creep behaviour at temperatures around the limit with little to justify expensive long-term creep testing.

The broad aims of this research were to address this gap in the data around the temperatures of interest, review the models and techniques available and develop methodologies to define the limits from short-term uniaxial creep and stress relaxation tests. The broad aims and objectives outlined in Chapter 1 have been achieved with this research work and thesis.

Throughout the emphasis has been on practical models, methods and techniques to advance the development of defining a material no-creep, T_{NC} and negligible creep temperatures, T_{NEC} and providing experimental evidence. The review of the models available has also provided a number of recommendations for their use and provided some insight into

how their resulting estimates might be viewed in practice. This is often the first time many of these methods, models and techniques have been used to derive the no-creep temperature which has until now has been limited to the Wilshire models and equations.

Chapter 2 utilised the German VDEh data to provide estimates of the no-creep temperatures based on two recognised creep models - the Manson-Haferd and Wilshire models which will extrapolate in temperature to the area of interest. While these extrapolations broadly agreed that some of the low alloy steels are likely exceeding these limits well below 375°C they also highlighted differences between the models and variation in the application of the proposed Wilshire model and equations to define the temperatures.

Chapter 3 reviewed the Wilshire model. There are several examples of the use of the Wilshire model and equations in the open literature. The methods adopted for fitting are often obscure and as pointed out by others could vary between authors. A fundamental problem with the method is the arbitrary choice of apparent activation energy, Qc*. It is evident from the simple rearrangement of the model the calculation of a no-creep temperature from data is directly proportional to the value of Qc* and the subjective selection of a value is the cause of some unease. A review of the model indicates it is often used without reference to the Monkman-Grant relation for the material and its suitability. The original model with a floating activation energy does appear to be conservative in all cases to the point where the estimates can be lower than the classical limit. The establishing of the Monkman-Grant relation for a material should be the starting point. This has been acknowledged by Evans who has provided a modified form of the Wilshire model to address the MG relations variability and the choice of Qc*. There appear no further examples of its use in the open literature other than its introduction. The chapter includes a practical application of the Evans modified form of the Wilshire model to identify regions within the data and derive a no-creep temperature without selecting an arbitrary value of Qc*. The model appears to provide a plausible estimate of the T_{NC} in agreement with others around 410°C (rounded down nearest decade) for the NIMS Grade 91 data. The original method with a fixed Q_{SD} also appears to provide a conservative estimate for NIMS Grade 91 compared to the modified form. A standard method of identifying kinks in the data is required not least to identify and cull data with an excessive IPS the technique is described and used to compare the technique to the IMechE method for culling data.

Chapter 4 explores the use of artificial neural networks to extrapolate the data and provide

and a no-creep temperature. The methodology is mainstream and is relatively straightforward with software packages. There are, however, a number of issues to be considered with creep data with a view to establishing the temperature limits. Not least is that historical creep data is accelerated to varying degrees. The techniques adopted provide no-creep temperatures based on creep data and total strain to account for the often significant IPS in the accelerated data. The method adopted provides values in broad agreement with the modified model in Chapter 3 for the NIMS Grade 91 data. Anelastic effects will have varying contributions to the creep curves and particularly the lower strains with accelerated testing and typical design stress curves are required for training e.g. the NIMS data is limited to $\geq$500°C for Grade 91.

The experimental section of this work then looked at two methods that could potentially provide the T_{NC} and T_{NEC} by the extrapolation of short-term uniaxial creep data and stress relaxation.

Chapter 5 describes the isostress creep method with the results presented for P265GH, Grade 91 and 316L(N) materials. The data was limited to <3k hours and the 316L(N) data was substantially limited. The P265GH extrapolation does appear to provide a plausible estimate of the temperatures in agreement with the extrapolation of the VDEh data in Chapter 2 at 330°C which is significantly lower than the 'classical' limit and adds some support for historical failures for this material below the limit. There also appears some justification for this being a marginal material and using it as the basis for the grade as a whole. The limit appears to be supported by historical failures outside the creep range. Any use of the material above this temperature should be designed and monitored for creep. Fitting the original Wilshire model to the test data for times to 0.2% strain provides a non-conservative estimate compared to the isostress linear extrapolation, highlighting it cannot be relied upon to provide a conservative estimate with an arbitrary Qc* of 300 kJ/mol. The isostress extrapolation for the Grade 91 material at around 440°C contains some uncertainty in the extrapolation without parallel isostress lines. Ideally, the tests would have been progressed sufficiently. This value appears to be higher than the value for this X10CrMoVNb9-1 material derived using the modified Wilshire model and the NIMS Grade 91 material at around 410°C. Other models and data sources are explored with the ANN to extrapolate the data with the results provided. It is only by this application of various models and techniques that an informed value can be derived when such a long-term extrapolation is required. The experimental data

for the 316L(N) was inconclusive but raised some issues for the austenitics. The Rieth *et al.* data indicates a value of 490°C may be appropriate for that material from data gathered at design stress levels.

The experimental isostress method is easy to apply and offers an experimental technique to derive the T_{NC} and T_{NEC}, the method can also provide an interim value while tests progress and provide times to specific strains data for the Wilshire and other models. The method has been proposed as an experimental method to provide the temperature limits for an individual heat in a revision to EN13445-3. The results indicate tests of >10k hours might be required if the isostress lines are not parallel to reduce uncertainty in the extrapolation. Details and recommendations for the practical implementation of an isostress program to establish the limits are included.

A model to establish the primary/secondary regime with some flexibility for an upturn with the accelerated tests is still an objective. The Gray & Whittaker model may prove useful if extended data to >0.5% is available, or provide the basis for a hybrid model artificial neural network. The ANN described appears to be a useful tool to extrapolate creep curves to the no-creep temperature threshold.

The Modified model bolt method has been developed to where it can be used to provide an approximate stress relaxation curve, the measurement variation and oxide build-up make the method more appropriate to higher preloads and materials with limited oxidation e.g. nickel superalloys.

7.2 Recommendations for Future Work

Establishing the limits for complete grades of material requires further work which can only be from the experience of deriving individual heat values and might include identifying a 'marginal' heat for the material though Chapter 4 indicates this is more complex than a simple yield strength relation. Both the spread and level can provide insight into the creep ductility. The spread of the T_{NC} needs further work to investigate how this is related to the propensity for creep cracking and whether the temperature/ reference normalised stress design limits should include a limit on this spread of total strain. This would be an alternative approach to controlled composition relying instead on an ANN or other methods of extrapolation of curve data from isostress type test arrays beyond x3. Further development of the

ANN and other methods could provide a more accurate extrapolation of the creep curves.

Further development of the modified model bolt method is required to validate the stress relaxation in comparison to the standard step-down method. This would include establishing the initial prestrain from the overall bolt length extension.

Appendix 1:

Extrapolation Model

The time to specific strains was calculated using the DIN 50 118 linear interpolation method. For each target strain data point the log strain value is linearly interpolated between successive experimentally measured data points. For multiple time values, the Excel GEOMEAN function is used which is the nth root of the product of all values and recommended practice to identify a time to a specific strain. In most creep tests the creep strain-time data can be represented as

$$\log(t) = m \cdot \left(- \left(\log \left(\frac{\varepsilon_u}{0.80 A_5} \right) \right) \right)^{\frac{1}{n}} + C \tag{7.1}$$

where εu is the creep strain and to is the fitted value of the rupture life (for discontinued, its estimated value) obtained from its logarithm as the intercept, A5 is the measured rupture elongation, t is the measured time, n is the exponent of the strain function and m is the gradient. The divisor term to normalise to plastic strain 0.8A5 is based on the rupture strain have a contribution from necking strain. Immediately before failure, the strain is ~80% of the strain measured on putting the two specimens together i.e. only a portion of the rupture elongation is included in the fitting. The value can be adjusted if it does not fit the tertiary region well e.g. for unfailed tests the value reduces with reducing stress and 0.5 may be more appropriate — the model is insensitive to the value of A5. It is herein referred to as an exponential plastic strain model. The simple model is intended to extrapolate data to 0.2% strain i.e. it is required to fit a decreasing strain rate and be flexible enough to curve upwards. The model is fitted using the SLOPE and INTERCEPT functions of EXCEL with the value of n optimised using the SOLVER non-linear optimisation routine and maximising the correlation coefficient. There is some scope within the model to refer to total strain when there is IPS or just creep strain with the total strain being preferable.

Bibliography

[1] Rieth M. Falkenstein A. Graf P. Heger S. Jaentsch U. Klimiankou M. Materna-Morris E. Zimmermann H. Creep of the austenitic steel AISI 316 L(N): Experiments and models. Technical Report FZKA-7065, Forschungszentrum Karlsruhe GmbH Technik und Umwelt (Germany). Inst. fuer Materialforschung - Programm Kernfusion, 2004.

[2] Manfred Schirra. Creep rupture strength and creep tests on the EFR structural material 316L(N), DIN 1.4909. *Nuclear Engineering and Design*, 147(1):63–78, jan 1994.

[3] NIMS. Nims Atlas of Creep Deformation Property. No. D-1, Creep deformation properties of 9Cr1MoVNb steel for boiler and heat exchangers. Technical report, National Institute of Materials Science, 2007.

[4] NIMS. Nims Atlas of Creep Deformation Property No. D-2, Creep deformation properties of 9Cr1MoVNb steel for boiler and heat exchanger. Technical report, 2008.

[5] E. N. da C. Andrade. The flow in metals under large constant stresses. *Proceedings of the Royal Society of London Series A*, 90:329, 1914.

[6] George E. Dieter. *Mechanical metallurgy*. McGraw-Hill, London, si metric ed. / adapted by david bacon.. edition, 1988.

[7] R.W. Evans and B. Wilshire. *Introduction to Creep*. Institute of Materials, 1993.

[8] Michael E. Kassner and Maria-Teresa Perez-Prado. *Fundamentals of Creep in Metals and Alloys*. Elsevier Science, 2004.

[9] Fujio Abe, Torsten-Ulf Kern, R. Viswanathan, Minerals Institute of Materials, and Mining. *Creep-resistant steels*. Woodhead Publishing : Maney Publishing : CRC Press, Cambridge, England; Boca Raton, FL, 2008.

[10] Jun-jie Shen, Ken-ichi Ikeda, Satoshi Hata, and Hideharu Nakashima. Primary-transient creep and anelastic backflow of pure copper deformed at low temperatures and ultra-low strain rates. *Transactions of Nonferrous Metals Society of China*, 26(7):1729–1735, 2016.

[11] K. Maruyama. *Fundamental aspects of creep deformation and deformation mechanism map*, pages 265–278. 2008.

[12] R.K. Penny and D.L. Marriott. *Design for Creep*. Springer Netherlands, 1995.

[13] K. Murty, Srikant Gollapudi, K. Ramaswamy, M. D. Mathew, and Indrajit Charit. *Creep deformation of materials in light water reactors (LWRs)*, pages 81–148. 2013.

[14] V. Gray and M. Whittaker. Development and assessment of a new empirical model for predicting full creep curves. *Materials (Basel)*, 8(7):4582–4592, 2015.

[15] M. W. Spindler and S. L. Spindler. Creep deformation, rupture and ductility of Esshete 1250. *International Journal of Pressure Vessels and Piping*, 85(1-2):89–98, 2008.

[16] Stuart Holdsworth. The european creep collaborative committee (ECCC) approach to creep data assessment. *Journal of Pressure Vessel Technology*, 130(2), 2008.

[17] S. Holdsworth. *Constitutive equations for creep curves and predicting service life*, chapter 14, pages 403–420. Woodhead Publishing, 2008.

[18] Frederick Harwood Norton. *The creep of steel at high temperatures*. McGraw-Hill Book Company, Incorporated, 1929.

[19] Henry Eyring. Viscosity, plasticity, and diffusion as examples of absolute reaction rates. *The Journal of Chemical Physics*, 4(4):283–291, 1936.

[20] Viswanathan R. *Damage Mechanisms and Life Assessment of High-Temperature Components*. ASM International, Metals Park, Ohio, 1993.

[21] R. L. Sherby O.D., Orr and Dorn J. E. Creep correlations of metals at elevated temperatures. *JOM*, 6(1):71–80, 1954.

[22] Sherby O. D. and Miller A. K. Combining phenomenology and physics in describing the high temperature mechanical behavior of crystalline solids. 101:387–395, 1979.

[23] Kassnner M.E. *Fundamentals of Creep in Metals and Alloys*, chapter Five-Power Law Creep, pages 7–102. 2015.

[24] A. M. Brown and M. F. Ashby. On the power-law creep equation. *Scripta Metallurgica*, 14(12):1297–1302, 1980.

[25] Dorn J.E. Mukherjee A.K, Bird J.E. Experimental correlations for high temperature creep. 62:155–179, 1969.

[26] Phillips P. The slow stretch in india rubber, glass and metal wire when subjected to a constant pull. *The London and Edinburgh Philisophical Magazine*, pages 513–531, 1905.

[27] A. H. Cottrell. Logarithmic and Andrade creep. *Philosophical Magazine Letters*, 75(5):301–308, 1997.

[28] Duval P. Louchet F. Andrade Creep Revisited. *International Journal of Materials Research*, 100:1433–1439, 2009.

[29] R.W. Evans, B. Wilshire, Institute of Metals, and Metals Society. *Creep of Metals and Alloys*. Institute of Metals, 1985.

[30] A Graham and KFA Walles. Relationships between long and short time creep and tensile properties of a commercial alloy. *Journal of the Iron and Steel Institute*, 179:104–121, 1955.

[31] McVetty P.G. Factors affecting the choice of working stresses for high temperature service. *Trans. ASME*, 55:99–109, 1933.

[32] M.J. Conway, J.B. Mullikin. An Evaluation of Various First Stage Creep Equations. *Journal Of Metals*, 17:1020, 1965.

[33] A Nadai. The influence of time upon creep, the hyperbolic sine creep law. *Stephen Timoshenko Anniversary*, 1938, 1938.

[34] McHenry. A newaspect of creep in concrete and its application to design. In *Proceedings ASTM*, volume 40, pages 1069–1084, 1943.

[35] Kachanov L. Rupture time under creep conditions. *Izvestiia Akademii Nauk SSSR, Otdelenie Teckhnicheskikh Nauk,*, 8:26–31, 1958.

[36] Rabotnov Y.N. Creep problems in structural members. 1969.

[37] Prager M. Development of the MPC Omega method for life assessment in the creep range. *ASME Journal of Pressure Vessel Technology*, 117:95–103, 1995.

[38] Stuart Holdsworth, Martin Askins, A. Baker, Elisabetta Gariboldi, Stefan Holmström, Andreas Klenk, M. Ringel, Gunther Merckling, R. Sandstrom, M. Schwienheer, and Stefano Spigarelli. Factors influencing creep model equation selection. *International Journal of Pressure Vessels and Piping*, 85:80–88, 2008.

[39] Dyson B.F. and McLean M. *Microstructural evolution and its effects on the creep performance of high-temperature alloys*. Institute of Materials, London, 1998.

[40] McLean M. and Dyson B.F. Modeling the effects of damage and microstructural evolution on the creep behavior of engineering alloys. 122:273–278, 2000.

[41] Lubhan J.D. and Felgar R.P. *Plasticity and Creep of Metals*. John Wiley and Sons, New York, 1961.

[42] Davies C.M. Li D.F., O'Dowd N.P. and Nikbin K.M. A review of the effect of prior inelastic deformation on high temperature mechanical response of engineering alloys. *International Journal of Pressure Vessels and Piping*, 87:531–542, 2010.

[43] IMechE. High temperature design data for ferritic pressure vessel steels : Creep of Steels Working Party, 1983.

[44] Ashby M.F. A first report on deformation-mechanism maps. *Acta Metallurgica*, 20:887, 1972.

[45] Frost H.J. and Ashby M.F. *Deformation Mechanism Maps*. Elsevier Science, london, 1982.

[46] Frost H.J. Transient deformation mechanism maps. in flow and fracture at elevated temperatures. 1985. American Society of Metals, Ohio.

[47] Raghubir Singh. Remaining life assessment of high temperature components using threshold stress concept. *Sadhana*, 20(1):87–101, 1995.

[48] M. T. Whittaker and B. Wilshire. Long term creep life prediction for Grade 22 (2.25Cr-1Mo) steels. *Materials Science and Technology*, 27(3):642–647, 2011.

[49] Z. Abdallah, K. Perkins, and S. Williams. Advances in the wilshire extrapolation technique - full creep curve representation for the aerospace alloy titanium 834. *Materials Science and Engineering: A*, 550:176–182, 2012.

[50] F. Vakili-Tahami, M. Sajjadpour, and P. Attari. Experimental study of the creep lifetime of the 1.25Cr0.5Mo steel pipes. *Strain*, 47(5):414–420, 2011.

[51] Goldoff R.M. Development of a standard methodology for the correlation and extrapolation of elevated temperature creep and rupture data. Technical report, Metals Properties Council, 1979.

[52] K. Maruyama, J. Nakamura, and K. Yoshimi. Assessment of long-term creep rupture strength of T91 steel by multiregion rupture data analysis. *Journal of Pressure Vessel Technology*, 138(3), 2016.

[53] IA Shibli, SR Holdsworth, and G Merckling. *Creep and fracture in high temperature components: design and life assessment issues*. DEStech Publications, Inc, 2005.

[54] B. Wilshire and P. J. Scharning. Extrapolation of creep life data for 1Cr-0.5Mo steel. *International Journal of Pressure Vessels and Piping*, 85(10):739–743, 2008.

[55] DIN. Din 50118:1982 Testing of Metallic Materials: Stress-rupture Test, Creep Test with Tensile stress, 1982.

[56] K. N. Melton. The isostress extrapolation of creep rupture data. *Materials Science and Engineering*, 59(2):143–149, 1983.

[57] Worley N.G. Hayhurst D.R., Lavender D.A. and Salim A. An assessment of the Îž-projection method for the representation and extrapolation of creep data for 1 *International Journal of Pressure Vessels and Piping*, 20(4):289–317, 1985.

[58] K. Maruyama and H. Oikawa. An extrapolation procedure of creep data for the determination: With special reference to Cr-Mo-V steel. *Journal of Pressure Vessel Technology*, 109(1):142–146, 1987.

[59] S. G. R. Brown, R. W. Evans, and B. Wilshire. A comparison of extrapolation techniques for long-term creep strain and creep life prediction based on equations designed to represent creep curve shape. *International Journal of Pressure Vessels and Piping*, 24(3):251–268, 1986.

[60] F.R. Larson and J. Miller. *A Time-temperature Relationship for Rupture and Creep Stresses*. 1952.

[61] Auerkari P. Holmström S. and Holdsworth S. Predicting creep strain response from rupture data and a robust creep curve model. In *Holdsworth S.*, pages 185–195, 2007.

[62] Goldoff R. Towards standardization of time-temperature parameter useage in elevated temperature data analysis. *Journal of Testing and Evaluation JTEVA*, 2(5):387–424, 1974.

[63] Manson S.S. and Haferd A.M. A linear time-temperature relation for extrapolation of creep and stress rupture data. Technical report, Lewis Flight Propulsion Laboratory NACA, 1953.

[64] Dr Amitava Ghatak and P. Robi. Modification of the Larson-Miller parameter technique for predicting creep life of materials. *Transactions of the Indian Institute of Metals*, 69, 2015.

[65] Chang M. K. and Lin Yu-Sheng. Creep Life Prediction of 9Cr-1Mo ferritic steel with Larson-Miller and Manson-Haferd Parameter. *Advanced Science Letters*, 15:53–57, 2012.

[66] S. S. Manson. Design considerations for long life at elevated temperatures. *Proceedings of the Institution of Mechanical Engineers, Conference Proceedings*, 178(1):D–29–D–55, 1963.

[67] Perkins K. Abdallah Z. and Arnold C. *Creep*, chapter Creep Lifing Models. IntechOpen, 2018.

[68] II Trunin, NG Golobova, and EA Loginov. New method of extrapolation of creep test and long time strength results. In *Proceedings of the 4th International Symposium on Heat-Resistant Metallic Materials, Mala Fatra, Czechoslovakia*, pages 168–176, 1971.

[69] Manson S.S. and Muralidharan U. Analysis of creep rupture data for five multiheat alloys by the minimum committment method using double heat term centring technique. *Progress in Analysis of Fatigue and Stress Rupture*, pages 1–46, 1984.

[70] BSI. BS EN 13445-3:2009+ A1:2012(e) Unfired Pressure Vessels, Part 3: Design, Issue 5 (2013-07) Annex R, 2013.

[71] Holdsworth S. Advances in the assessment of creep data. In *Proceedings of 9th Liege Conference: Materials for Advanced Power Engineering*, pages 946–957, 2010.

[72] Bullough C. Smith W. Holmström S. Provision of materials creep properties for design of high temperature plant to EN13445-3. In *1ST EPERC INTERNATIONAL CONFERENCE PRESSURE EQUIPMENT INNOVATION AND SAFETY*, pages 84–104, 2019.

[73] S. G. R. Brown, R. W. Evans, and B. Wilshire. Exponential descriptions of normal creep curves. *Scripta Metallurgica*, 20(6):855–860, 1986.

[74] R. W. Evans. The Îž projection method and low creep ductility materials. *Materials Science and Technology*, 16(1):6–8, 2000.

[75] S. Holmström and Auerkari P. Robust prediction of full creep curves from minimal data and time to rupture model. *Energy materials*, 1(4):249–255, 2006.

[76] B. Wilshire, P. J. Scharning, and R. Hurst. A new approach to creep data assessment. *Materials Science and Engineering: A*, 510-511:3–6, 2009.

[77] M. Evans. Sensitivity of the theta projection technique to the functional form of the theta interpolation/extrapolation function. *Journal of Materials Science*, 37(14):2871–2884, 2002.

[78] M. Evans. Predicting times to low strain for a 1CrMoV rotor steel using a 6-Îž projection technique. *Journal of Materials Science*, 35(12):2937–2948, 2000.

[79] R. W. Evans and P. J. Scharning. The Îž projection method applied to small strain creep of commercial aluminum alloy. *Materials Science and Technology*, 17(5):487–493, 2001.

[80] F. C. Monkman and N. J Grant. An empirical relationship between rupture life and minimum creep rate in creep rupture tests. In *proc. ASTM*, volume 56, pages 91–103, 1956.

[81] Stefan Holmström. Defining a negligible creep temperature curve for Gr. 91 steel. *International Journal of Pressure Vessels and Piping*, 146:198–202, 2016.

[82] Stefan Holmström. *Negligible creep temperature curve verification for steels 10CrMoV9-10 and X2CrMoNiMo17-12-2*. Luxembourg : Publications Office, Luxembourg], deliverable 2015-8 edition, 2016.

[83] Stefan Holmström. A study of negligible creep criteria based on EN-10028 standard creep strength and yield properties. Report EUR 27783 EN, European Union, 2016.

[84] S. Chen J.C. Holmström. Recommendation for the negligible creep domain for P91. Report EUR 27782, EC Joint Research Centre Institute for Energy and Transport, 2016.

[85] S Holmström. Negligible creep temperature curves for EN-13445. 2017.

[86] NIMS. National institute of materials science of japan. creep datasheets in MatNavi database., December 2020.

[87] VDEh. Ergebnisse deutscher zeitstandversuche langer dauer, prepared by the 'verein deutscher eisenhuttenleute' in association with the 'arbeitsgemeinschaft fur warnfeste stahle' and the 'arbeitsgemeinschaft fur hochtemperature werkstoffe' pub verlag stahleisen mbh dusseldorf 1969 (translation -results of german creep tests of long duration). Technical report, German Steel Institute, 1969.

[88] BSCC. High temperature data - british long-term creep rupture an elevated temperature tensile data on steels for high temperature service. Technical report, British Steelmakers Creep Committee, The Iron and Steel Institute, 1978.

[89] Wilshire B. and Burt H. Yield stress rationalization of creep and creep fracture properties. *Scripta Materialia*, 53(8):909–914, 2005.

[90] BSI. BS EN 10028 Flat Products made of Steels for Pressure Purposes Part 2: Non-alloy and Alloy Steels with Specified Elevated Temperature Properties, 2017.

[91] Gooch D.J. The effect of microstructure on creep crack growth in a C-Mn steel at 360C. *Materials Science and Engineering*, 83(1):17–27, 1986.

[92] D. J. Gooch. The effect of anisotrophy on creep and creep crack growth in cold-worked C-Mn steel at 360C. *Materials Science and Engineering*, 91:45–54, 1987.

[93] Neate G.J. Creep crack growth in cold formed steel at 360C. *Materials Science and Technology*, 3(1):14–22, 1987.

[94] Shibli I.A. Creep crack growth characteristics of prestrained C-Mn steels at 360C. *Materials Science and Technology*, 3(2):110–117, 1987.

[95] Bache M.R. Williams S.J. and Wilshire B. 25 year perspective recent developments in analysis of high temperature creep and creep fracture behaviour. *Materials Science and Technology*, 26(11):1332, 2010.

[96] Whittaker M. Abdallah Z., Gray V. and Perkins K. A critical analysis of the conventially employed creep lifing methods. *Materials*, 7(5):3371–3398, 2014.

[97] Bolton J. A critical examination of a wilshire model for creep rupture. *https://www.researchgate.net/publication/279495306*, 2015.

[98] Wilshire B and Scharning P.J. Rationalization and extrapolation of creep and creep fracture data for Grade 91 steel. *Materials at High Temperature*, 25(2):55–65, 2008.

[99] Wilshire B. and Scharning P.J. Creep ductilities of 9-12 *Scripta Materialia*, 56(12):1023–1026, 2007.

[100] Wilshire B. and Scharning P. Creep and creep fracture of commercial aluminium alloys. *Journal of Materials Science*, 43:3992–4000, 2008.

[101] Wilshire B. and Scharning P.J. Theoretical and practical approach to creep of Waspalloy. *Materials Science and Technology*, 25(2):242–248, 2009.

[102] Whittaker M.T. and Evans M. Long-term creep data prediction for Type 316H stainless steel. *Materials Science and Technology*, 552:145–150, 2012.

[103] Wilshire B. and Scharning P.J. Prediction of long-term creep data for forged 1Cr-1Mo-0.25V steel. *Materials Science and Technology*, 24(1):1–9, 2008.

[104] Evans M. Formalisation of wilshire-scharning methodology to creep life prediction with application to 1Cr-1Mo-0.25V rotor steel. *Materials Science and Technology*, 26(3):309–317, 2010.

[105] William Harrison, Mark Whittaker, and Steve Williams. Recent advances in Creep modelling of the Nickel Base Superalloy, Alloy 720Li. *Materials*, 6(3):1118–1137, mar 2013.

[106] Cedro lii V. Garcia C. and Render M. Use of the Wilshire equations to correlate and extrapolate creep data of Inconel 617 and Nimonic 105. *Materials (Basel)*, 11(12), 2018.

[107] Cedro lii V. Garcia C. and Render M. Use of the Wilshire equation to correlate and extrapolate creep rupture data of Incoloy 800 and 304h stainless steel. *Materials at High Temperatures*, 36(6):511–530, 2019.

[108] ISO. ISO 6303:1981 Method of Extrapolation used in the Analysis of Creep Rupture Data, 1981.

[109] Cipolla L. and Gabrel J. New creep rupture assessment of Grade 91. In *ETD Conference Industry and Research Experience in the Use of P/T91 in HRSGS/Boilers*. Institute of Materials, 2005.

[110] Holmström S. Pohja R. Auerkari P. Friedman V. Klenk A. Leibling B. Spindler M. and Riva A. Long term stress relaxation modelling. In *3rd International ECCC Conference, Creep and Fracture in High Temperature Components, Design and Life Assessment*, 2014.

[111] Tonti A. Ciuffa F. Lega D. Baylac G. Gelineau O. and Pagano S. RCC-MR Application of negligible creep clauses to EN10028 and EN13445. In *International Conference High Temperature Materials*, 2011.

[112] Abe F. *Coal Power Plant Materials and Life Assessment*, chapter Grade 91 heat-resistant martensitic steel. Woodhead publishing, 2014.

[113] Wilshire B. and Battenbough A.J. Creep and creep fracture of polycrystalline copper. *Materials Science and Engineerinf*, 443(1-2):156–166, 2007.

[114] Deen C. Rae C. Whittaker M. Harrison W. and Williams S. Creep deformation by dislocation movement in Waspalloy. *Materials (Basel)*, 10(1), 2017.

[115] Whittaker M.T. and Harrison W.J. Evolution of Wilshire equations for creep life prediction. *Materials at High Temperature*, 31(3):233–238, 2014.

[116] Evans M. A statistical test for identifying the number of creep regimes when using the Wilshire equations for creep property predictions. *Metallurical and Materials trans A*, 47(12):6593–6607, 2016.

[117] Evans M. Semi-parametric estimation of the wilshire creep life prediction model: An application to 2.25Cr-1Mo steel. *Materials Science and Technology*, 35(16):1977–1987, 2019.

[118] Gray V. and Whittaker. The changing constants of creep: A letter on region splitting in creep lifing. *materials Science and Engineering: A*, 632:96–102, 2015.

[119] Evans M. Constraints imposed by the Wilshire methodology on creep rupture data and procedures for testing the validity of such constraints: Illustration using 1Cr-1Mo-0.25V steel. *Metallurgical and Materials Transactions A*, 46(2):937–947, 2014.

[120] Evans M. A re-evaluation of the causes of deformation in 1Cr-1Mo-0.25V steel for turbine rotors and shafts. *Materials*, 10(6):575, 2017.

[121] Cedro lii V. Garcia C. and Render M. Use of the Wilshire equations to correlate and extrapolate creep data of HR6W and Sanicro 25. *Materials*, 11(9), 2018.

[122] Sundarajan G. The Monkman-Grant relationship. *Materials Science and Engineering A*, 112:205–214, 1989.

[123] Davies P. and Wilshire B. An interpretation of the relationship between creep and fracture. The Iron and Steel Institute, 1960.

[124] Evans M. The importance of creep strain in linking together the Wilshire equations for minimum creep rates and times to various strains (including the rupture strain): an illustration using 1CrMoV rotor steel. *Journal of Material Science*, 49(1):329–339, 2014.

[125] Dobe F. and Milicka K. The relation between minimum creep rate and time to fracture. *Metal Science*, 10(11):382–384, 1976.

[126] Povolo F. Comments on the Monkman-Grant and the modified Monkman-Grant relationships. *Journal of Material Science*, 20(6):2005–2010, 1985.

[127] Maruyama K. Sekido N. and Yoshimi K. Changes in Monkman-Grant relation among four creep regions of modified 9Cr-1Mo steel. *Materials Science and Engineering: A*, 749:223–234, 2019.

[128] Abe F. Creep Behaviour,Deformation Mechanisms, and Creep life of Mod. (Cr-1Mo Steel. *Metallurgical and Materials Transactions A*, 46(12):5610–5625, 2015.

[129] Holmström S. Bullough C. Tonti A. Baylac G. Forot C. and Smith W. New approaches to determine negligible creep of steels to EN 13445 CEN/TC 54. Technical report, BSI Secretariat, 2021.

[130] Bhadeshia H.K.D.H. Neural networks in materials science. *ISIJ International*, 39(10):966–979, 1999.

[131] Hong H. Cai Z. Wang H. Wang W. and Liu Y. A model guided neural network for the prediction of creep behaviour under in-service conditions. *Journal of Engineering for Gas Turbines and Power*, 142(7), 2020.

[132] Mathew M.D. Srinivasan V.S., Choudhary B.K. and Jayakumar T. Long-term creep rupture prediction for modified 9Cr-1Mo ferritic steel and type 316L(N) austenitic stainless steels. *Materials at High Temperature*, 29(1), 2012.

[133] Evans M. Method for improving parametric creep rupture life of 2.25Cr-1Mo steel using artificial neural networks. *Materials Science and Technology*, 15(6):647–658, 1999.

[134] Liang T. Liu X. Fan P. Zhu L. Bi Y. and Zhang Y. Prediction of long-termcreep life of 9Cr-1Mo-V-Nb steel using artificial neural network. *International Journal of Pressure Vessels and piping*, 179, 2020.

[135] P. Feltham. Creep and stress relaxation in alpha-brass at low temperatures. *Philosophical Magazine*, 6(62):259–270, feb 1961.

[136] A. Sarkar, S.K. Sinha, J.K. Chakravartty, and R.K. Sinha. Artificial neural network modelling of in-reactor diametral creep of Zr2.5%Nb pressure tubes of indian PHWRs. *Annals of Nuclear Energy*, 69:246–251, jul 2014.

[137] Amitava Ghatak and P. S. Robi. Prediction of creep curve of HP40Nb steel using artificial neural network. *Neural Computing and Applications*, 30(9):2953–2964, feb 2017.

[138] Fujio Abe. Heat-to-heat variation in long-term creep strength of some ferritic steels. *International Journal of Pressure Vessels and Piping*, 87(6):310–318, jun 2010.

[139] Jonathan Parker and John Siefert. Metallurgical and stress state factors which affect the creep and fracture behavior of 9% Cr steels. *Advances in Materials Science and Engineering*, 2018:1–15, 2018.

[140] Weiju Ren and Totemeier Terry. Assessment of negligible creep, off-normal welding and heat treatment of Gr.91 steel for nuclear reactor pressure vessel application. Technical report, oct 2006.

[141] Voorhees H.R Prager M. Assessment and use of creep-rupture properties. In *Mechanical Testing and Evaluation*, volume 8, pages 383–397. ASM International, 2000.

[142] Smith W. Bullough C and Gill S. Determination of no-creep and negligible creep temperatures using accelerated testing methods. In Tonti A. and Faidy C., editors, *1st EPERC International Conference Pressure Equipment Innovation and Safety*, pages 105–116, 2019.

[143] Timmins R. and Smith J.J. Creep Extrapolation Programme - Final Assessment Report 2A/1498/93/M3. Technical report, ERA Technology, 1993.

[144] C K Bullough. An assessment of the constant stress extrapolation method: Phase 1, A comparison of linear and recipricol temperature models. ERA Technology Project 2021, Creep of Steels BPNMP/171/91. Technical report, 1991.

[145] ISO. BS EN ISO 6892-2:2018 Metallic Materials - Tensile Testing. Part 2: Method of Test at Elevated Temperature (ISO 6892-2:2018), 2018. 978 0 539 02150 9.

[146] Möller M. Robust structural verification of pressurized nuclear components subjected to ratcheting, Part 2 -. Technical report, Swedish Radiation Authority Safety Authority, SSM, 2017.

[147] A H Cottrell and B A Bilby. Dislocation Theory of Yielding and Strain Ageing of Iron. *Proceedings of the Physical Society. Section A*, 62(1):49–62, jan 1949.

[148] P Rodriguez. Serrated plastic flow. *Bulletin of Materials Science*, 6(4):653–663, sep 1984.

[149] G Schoeck. The Portevin-le Chatelier effect. A kinetic theory. *Acta Metallurgica*, 32(8):1229–1234, aug 1984.

[150] Robert A Elliot, Egon Orowan, Teruyoshi Udoguchi, and Ali S Argon. Absence of yield points in iron on strain reversal after aging, and the bauschinger overshoot. *Mechanics of Materials*, 36(11):1143–1153, nov 2004.

[151] Osamu Kanemaru, Masaru Shimizu, Toshio Ohba, Koichi Yagi, Yuhei Kato, and Kenji Hattori. Life prediction by the iso-stress method of boiler tubes after prolonged service. *International Journal of Pressure Vessels and Piping*, 48(2):167–182, jan 1991.

[152] Moon Sik Han and Oh Geon Kwon. Free nitrogen effect on creep failure and creep crack growth of C-Mn steel. *Journal of Materials Science*, 39(21):6555–6559, nov 2004.

[153] Jonathan Parker. In-service behavior of creep strength enhanced ferritic steels Grade 91 and Grade 92 Part 1 Parent Metal. *International Journal of Pressure Vessels and Piping*, 101:30–36, jan 2013.

[154] B. Fournier, F. Dalle, M. Sauzay, J. Longour, M. Salvi, C. Caës, I. Tournié, P.-F. Giroux, and S.-H. Kim. Comparison of various 9–12%Cr steels under fatigue and

creep-fatigue loadings at high temperature. *Materials Science and Engineering: A*, 528(22-23):6934–6945, August 2011.

[155] Parker J. Siefert J. An informed perspective on the recent reduction in the allowable stress values for Grade 91. Technical report, EPRI, 2021.

[156] S.J. Brett. The impression creep Monkman-Grant relationship. *Ubiquity Proceedings*, 1(S1):7, sep 2018.

[157] API. Use of 9Cr-1Mo-V (Grade 91) Steel in the Oil Refinig Industry Technical Report TR 938-B. Technical report, American Petroleum Institute, 2008.

[158] Q. Auzoux, L. Allais, C. CaÃ«s, I. Monnet, A.F. Gourgues, and A. Pineau. Effect of pre-strain on creep of three AISI 316 austenitic stainless steels in relation to reheat cracking of weld-affected zones. *Journal of Nuclear Materials*, 400(2):127–137, may 2010.

[159] B.K. Choudhary. Activation energy for serrated flow in type 316L(N) austenitic stainless steel. *Materials Science and Engineering: A*, 603:160–168, May 2014.

[160] Ronald Lesley Plaut, Clara Herrera, Doris Maribel Escriba, Paulo Rangel Rios, and Angelo Fernando Padilha. A short review on wrought austenitic stainless steels at high temperatures: processing, microstructure, properties and performance. *Materials Research*, 10(4):453–460, dec 2007.

[161] ISO. BS EN ISO 204:2018 Metallic Materials - Uniaxial Creep Testing in Tension - Method of Test, 2018.

[162] T.O. Erinosho, K. Abburi Venkata, M. Mostafavi, D.M. Knowles, and C.E. Truman. Influence of prior cyclic plasticity on creep deformation using crystal plasticity modelling. *International Journal of Solids and Structures*, 139-140:129–137, may 2018.

[163] Swindeman R. A Review of Current Operating Conditions Allowable Stresses in ASME Section iii Substection NH. Technical report, ASME/DOE Gen-IV Materials Project Task 6, 2009.

[164] Woo Gon Kim, Sung Ho Kim, and Woo Seog Ryu. Evaluation of Monkman-Grant parameters for type 316LN and modified 9Cr-Mo stainless steels. *KSME International Journal*, 16(11):1420–1427, nov 2002.

[165] Q. Auzoux L. Allais A.F. Gourgues A. Pineau. Reheat cracking in austenitic stainless steels. In *14th European Conference on Fracture: Fracture Mechanics Beyond 2000,*, pages 137–144. EMAS, 2002.

[166] V. Ganesan, K. Laha, and M.D. Mathew. Influence of nitrogen content on the evolution of creep damage in 316 LN stainless steel. *Procedia Engineering*, 86:58–65, 2014.

[167] BSI. BS EN ISO 9513:2012 Metallic Materials - Calibration of Extensometers used in Uniaxial Testing, 2012.

[168] A. Shibli. Remaining life assessment issues in high Cr martensitic steels and development of new innovative tools for damage monitoring and integrity assessment. *Transactions of the Indian Institute of Metals*, 63(2-3):339–348, apr 2010.

[169] J. Hald. Microstructure and long-term creep properties of 9–12% Cr steels. *International Journal of Pressure Vessels and Piping*, 85(1-2):30–37, jan 2008.

[170] K. Sawada, H. Kushima, M. Tabuchi, and K. Kimura. Microstructural degradation of Gr.91 steel during creep under low stress. *Materials Science and Engineering: A*, 528(16-17):5511–5518, jun 2011.

[171] Manjoine M.J. Voorhees H.R. Compilation of stress-relaxation data for engineering alloys. Technical Report DS 60, ASTM, 1982.

[172] P. J. Ennis and A. Czyrska-Filemonowicz. Recent advances in creep-resistant steels for power plant applications. *Sadhana*, 28(3-4):709–730, jun 2003.

[173] Guguloth K. Jaganathan S. Ghosh R. Creep life prediction of P91 steel from stress relaxation tests. In *3rd International ECCC Creep and Fracture Conference 2014, Rome*, 2014.

[174] S.C. Bose, Kulvir Singh, J. Swaminathan, and D.S. Sarma. Prediction of creep life of X10CrMoVNbN-91 (P-91) steel through short term stress relaxation test methodology. *Materials Science and Technology*, 20(10):1290–1296, oct 2004.

[175] David A. Woodford. Evolution of a modern mechanical testing and design standard for high temperature materials. *Materials Research Innovations*, 20(5):379–389, apr 2016.

[176] J Beddoes and T Mohammadi. Comparison of stress relaxation and creep strain rates for the superalloy IN738LC. *The Journal of Strain Analysis for Engineering Design*, 45(8):587–592, nov 2010.

[177] BSI. BS EN 10319-1:2003 Metallic Materials. Tensile Stress Relaxation Testing. Procedure for Testing Machines, 2003.

[178] Guest J.C. Standards in elevated temperature tensile and uniaxial creep testing. In *Measurement of High Temperature Mechanical Properties of Materials, Proceedings of Symposium held from 3-5 June, 1981 at the National Physical Laboratory, Teddington*, pages 23–31. HMSO, 1982. ISBN 0114800499.

[179] Strang A. Review of current international stress relaxation testing standards. In *Performance of Bolting Materials in High Temperature Plant Applications: Conference Proceedings, 16-17 June, 1994, York, UK*. Institue of Materials, 1994.

[180] DR Petersen, RE Link, SC Bose, K Singh, and G Jayaraman. Application of stress relaxation test methodology for predicting creep life of a large steam turbine rotor steel (1CrMoV). *Journal of Testing and Evaluation*, 31(3):19074, 2003.

[181] Woo-Gon Kim, Jae-Young Park, Min-Gu Won, Hyeong-Yeon Lee, and Nam-Su Huh. Non-linear modeling of stress relaxation curves for Grade 91 steel. *Journal of Mechanical Science and Technology*, 32(3):1143–1151, mar 2018.

[182] Stefan Holmström, Frits De Haan, Ulrich FÃŒhrer, Rami Pohja, and Jaromir Janousek. Engineering models for softening and relaxation of Gr. 91 steel in creep-fatigue conditions. *International Journal of Structural Integrity*, 8(6):670–682, dec 2017.

[183] Staf Huysmans Evy De Bruycker, Jean-Pierre Keustermans. Stress relaxation testing as an alternative to conventional creep rupture testing. In *2nd International ECCC Creep Conference, 21-23 April 2009*, Zurich, 2009.

[184] Krishna Guguloth, J. Swaminathan, Nilima Roy, and R.N. Ghosh. Uniaxial creep and stress relaxation behavior of modified 9Cr-1Mo steel. *Materials Science and Engineering: A*, 684:683–696, jan 2017.

[185] David A. Woodford. Stress relaxation testing of service exposed IN738 for creep strength evaluation. *Journal of Engineering for Gas Turbines and Power*, 122(3):451–456, may 2000.

[186] BSI. BS EN 10319-2:2006 Metallic Materials - Tensile Stress Relaxation Testing - Part 2: Procedure for Bolted Joint Models., 2006.

[187] Stefan Weihe, Matthias Oechsner, and Heft. Issue R594 . relaxationsverhalten stress relaxation behaviour no 1326 zwischenbericht interim report (ZB),. Technical report, 2020.

[188] M. PELEG. Considerations of a general rheological model for the mechanical behavior of viscoelastic solid food materials. *Journal of Texture Studies*, 7(2):243–255, sep 1976.

[189] Jakobiet W. Keienburg K.H. Mayer K.H. Gulden H. Schmidt W. Huchtemann B. Relaxationsverhalten warmfester stahle fur schrauben EUR 6458. Technical report, Technische forschung stahl. VDEh Dusseldorf, 1980.